

**NIPER-634
(DE93000130)**

**Integration of the Geological/Engineering Model with Production
Performance for Patrick Draw Field, Wyoming**

Topical Report

**By
Susan Jackson et al.**

March 1993

Performed Under Cooperative Agreement No. FC22-83FE60149

**IIT Research Institute
National Institute for Petroleum and Energy Research
Bartlesville, Oklahoma**



**Bartlesville Project Office
U. S. DEPARTMENT OF ENERGY
Bartlesville, Oklahoma**

DISCLAIMER

This report was prepared as an account of work sponsored by an agency of the United States Government. Neither the United States Government nor any agency thereof, nor any of their employees, makes any warranty, express or implied, or assumes any legal liability or responsibility for the accuracy, completeness, or usefulness of any information, apparatus, product, or process disclosed, or represents that its use would not infringe privately owned rights. Reference herein to any specific commercial product, process, or service by trade name, trademark, manufacturer, or otherwise does not necessarily constitute or imply its endorsement, recommendation, or favoring by the United States Government or any agency thereof. The views and opinions of authors expressed herein do not necessarily state or reflect those of the United States Government or any agency thereof.

This report has been reproduced directly from the best available copy.

Available to DOE and DOE contractors from the Office of Scientific and Technical Information, P.O. Box 62, Oak Ridge, TN 37831; prices available from (615)576-8401, FTS 626-8401.

Available to the public from the National Technical Information Service, U.S. Department of Commerce, 5285 Port Royal Rd., Springfield, VA 22161.

Integration of the Geological/Engineering Model with Production
Performance for Patrick Draw Field, Wyoming

Topical Report

By
Susan Jackson et al.

March 1993

Work Performed Under Cooperative Agreement No. DE-FC22-83FE60149

Prepared for
U.S. Department of Energy
Assistant Secretary for Fossil Energy

Edith Allison, Project Manager
Bartlesville Project Office
P. O. Box 1398
Bartlesville, OK 74005

Prepared by
IIT Research Institute
National Institute for Petroleum and Energy Research
P.O. Box 2128
Bartlesville, OK 74005

TABLE OF CONTENTS

	<u>Page</u>
ABSTRACT.....	1
EXECUTIVE SUMMARY.....	1
ACKNOWLEDGMENTS.....	2
 CHAPTER 1. Introduction.....	 3
Background.....	3
End Member Models of Shoreline Barrier Deposition.....	4
Data Collected For Almond Formation.....	4
References.....	5
 CHAPTER 2—The Importance and Application of Hydrogeochemical Techniques to Reservoir Characteristics.....	 13
Chapter Summary.....	13
Introduction.....	13
Outline of the Petroleum Hydrogeochemistry, Principles, Techniques, and Practical Applications.....	14
Capability of Quantitative Hydrogeochemical Reservoir Analysis.....	14
Principles, Techniques, and Economy of Hydrogeochemical Investigation of Formation Fluids in Oil Reservoirs.....	15
Handling of Formation Water Geochemical Analyses.....	15
Geochemical Detection of Flow Discontinuities, Stratification, Compartment Boundaries, Fluid Mixing in Open Systems, and Impairment of Sweep Efficiency Between Reservoir Compartments.....	16
Geochemistry of Formation Waters in Patrick Draw Field, Wyoming.....	17
Data Source and Quantity.....	17
Formation Water Characteristics; Salinity, Chemical Composition.....	18
Fluid Compartmentalization.....	18
Production Relationships and Anomalies in Arch Unit of Patrick Draw Field.....	20
Geochemistry of Formation Waters in Bell Creek Field.....	21
Data Source and Quality.....	21
Formation Water Characteristics; Salinity, Chemical Composition.....	21
Conclusions.....	22
References.....	22
 CHAPTER 3—The Effect of Salinity Variations on Oil Saturation Calculations From Wireline Logs at Patrick Draw Field.....	 41
Chapter Summary.....	41
Introduction.....	41
Water Saturation Calculations in Patrick Draw Field.....	41
The Effect of Salinity and Clay Content on Various Log Analysis Methods.....	42
Conclusion.....	44
References.....	44
 CHAPTER 4—Structural and Sedimentological Features That Control Fluid Distribution and Movement.....	 53
Chapter Summary.....	53
Tectonic Framework at Patrick Draw Field.....	53
Introduction.....	53
Faults Identified and Mapped Using Log Cross Sections.....	54
Mapping of Faults With Seismic and Wireline Log Data.....	54
Introduction.....	54
The Technique of Fault Mapping and its Limitations.....	54
Nature of Faulting at Patrick Draw Field.....	55

TABLE OF CONTENTS (continued)

	<u>Page</u>
Comparison of Fault Map with Other Parameters	55
Comparison of "Old" and "Updated" Structure Maps	55
Lineament Study Performed in the Patrick Draw Field From Satellite Image Data	56
Distribution of Coquina	56
Comparison of Lithology and Petrographical Features With Petrophysical Properties	58
Introduction	58
Coquina, Petrographic Features and Calcite Cement	58
Clay Content Determination	59
Pore Throat Size Distribution	59
Rock Texture and Petrophysical Properties	59
Conclusions	60
References	61
 CHAPTER 5—Analysis of Reservoir and Production/Injection Data	 85
Chapter Summary	85
Petrophysical Properties	85
Production/Injection Analysis	85
Petrophysical Properties and Oil Recovery	86
Introduction	86
Rock Permeability	86
Porosity, Pay and Saturation	86
Porosity and Pay	86
Permeability and Primary Recovery	87
Permeability and Waterflood Recovery	87
Reservoir Volume Balance Calculations	88
Introduction	88
Reservoir Volume Balance Calculations	88
Production Analysis	88
Introduction	88
Primary Production	89
Arch Unit	89
Monell Unit	89
Water Flood Production	90
Arch Unit	90
Monell Unit	90
Recovery Efficiency and Residual Oil Saturation	91
Arch Unit	91
Monell Unit	91
Enhanced Oil Recovery Potential	92
Arch Unit	92
Monell Unit	92
Hall Plot Analysis	92
Introduction	92
Hall Plot Technique	92
Three Periods of Hall Plot	93
Numerical Simulations	93
Drainage Volume	94
Simulation Studies	94
Single-Phase Simulations	94
Analytical Calculations	94
Field Data	95

TABLE OF CONTENTS (continued)

	<u>Page</u>
Conclusions	95
Petrophysical Properties and Oil Recovery.....	95
Reservoir Volume Balance Calculations.....	95
Production Analysis.....	95
Enhanced Oil Recovery Potential.....	96
Hall Plot Analysis.....	96
References.....	96

TABLES

	<u>Page</u>
1.1 Some general geomorphological differences between microtidal and mesotidal barrier islands. After Hayes and Kana, 1976.	7
2.1 Salinity (TDS), ionic composition (in milligrams per liter=mg/l), reacting values (in milliequivalent=meq), chemical types based on percentage of milliequivalents (% meq), and resistivities (in ohm-m) of selected formation waters co-produced with oil from the Upper Cretaceous Almond Formation in Monell (M) and Arch (A) production units of Patrick Draw Field, Wyoming.	24
2.2 Salinity (TDS), ionic composition (in milligrams per liter=mg/l), reacting values (in milliequivalent=meq), chemical types based on percentage of milliequivalent (%meq), and resistivities (in ohm-m) of selected formation waters co-produced with oil from the Lower Cretaceous Muddy Formation in production units A, B, C, and D of Bell Creek Field, Montana.	25
3.1 Measured Water Resistivity (R_w) at Different Salinity (TDS) in Patrick Draw Field.....	45
3.2 Reservoir Parameters Used in the Computation of Porosity and V_{sh} in S_w Calculations from Density and Gamma Ray Logs in Well Arch 120, Patrick Draw Field, WY.....	46
3.3 Average water saturations for UA-5B sandstone in well Arch 120 calculated by different methods for three different water resistivities of formation water	46
4.1 Reservoir Parameters Used in the Computation of Porosity and V_{sh} in S_w Calculations From Density and Gamma Ray Logs in Well Arch 120, Patrick Draw Field, WY.....	80
4.2 Average Water Saturations for UA-5B Sandstone in Well Arch 120 Calculated by Different Methods for Three Different Water Resistivities of Formation Water	80
5.1 Statistics of Petrophysical Properties and Productions in Arch and Monell Unit Wells.....	97
5.2 Comparison of reservoir parameters of Monell Unit, Patrick Draw field with EOR screening criteria.....	98

ILLUSTRATIONS

	<u>Page</u>
1.1. Location of oil fields studied. Note the location of Bell Creek Field, Powder River Basin, MT and Patrick Draw Field, Washakie Basin, WY.....	8
1.2. Morphological models for microtidal, and mesatidal barrier shoreline with medium wave energy.....	9
1.3. Base map of Patrick Draw Field well locations.....	10

ILLUSTRATIONS—Continued

	<u>Page</u>
1.4 Stratigraphic cross section showing the vertical arrangement of reservoir sands and the lateral variability of sand thickness in Patrick Draw Field, WY.....	11
1.5 Map of the east flank of the Rock Springs Uplift, Sweetwater Co., WY.....	12
2.1. Isosalinity map of formation waters in the Almond Formation of Patrick Draw Field (in g/l).....	26
2.2 Composition and salinity of selected formation waters in the Almond Formation of Monell Unit shown on the trilinear diagram.....	27
2.3. Composition of selected formation waters in the Almond Formation of Monell Unit, Patrick Draw Field shown on the Stiff diagram.....	28
2.4. Formation water composition and salinity monitored in 1961, 1962, and 1989 shown on the trilinear diagram; well 44-35, Arch Unit, Patrick Draw Field.....	29
2.5. Formation water composition monitored in 1961, 1962, and 1989 shown on the Stiff diagrams; well 44-35, Arch Unit, Patrick Draw Field.....	29
2.6. Formation water salinities (TDS), resistivities (R_w), and chemical formulas in two productive sandstone units (UA-8A and UA-8B) interpreted as tidal delta facies with 70% and 85 confidence level respectively; well 80, East Arch Unit, Patrick Draw Field.....	30
2.7. Composition and salinity of formation waters in UA-8A and U8A-B sandstone units in well 80 shown on the trilinear diagram; Almond Formation, East Arch Unit, Patrick Draw Field.....	31
2.8 Composition of formation waters in UA-8A and U8A-B sandstone units in well 80; Almond Formation, East Arch Unit, Patrick Draw Field shown on the Stiff diagrams.....	31
2.9. Composition and salinity of formation water in UA-8 sandstone unit in well 84; Almond Formation, East Arch Unit, Patrick Draw Field shown on the trilinear diagram.....	32
2.10. Composition of formation waters in UA-8 sandstone unit in well 84; Almond Formation, East Arch Unit, Patrick Draw Field shown on the Stiff diagrams.....	32
2.11. Composition and salinity of formation water in the Fox Hill Formation sandstone overlying the Almond Formation; Monell Unit, Patrick Draw Field shown on the trilinear diagram.....	33
2.12. Composition of formation water in the Fox Hill Formation sandstone overlying the Almond Formation shown on the Stiff diagrams; Monell Unit, Patrick Draw Field.....	33
2.13. Relationship between initial production (IP) and cumulative production (CP) in wells of Arch Unit, Patrick Draw Field. General trend for most wells is quite clear although a group of wells departs from this trend.....	34
2.14. Relationship between initial production and product of permeability, porosity, and oil saturation in wells of Arch Unit, Patrick Draw Field.....	34
2.15. Relationship between cumulative production and product of permeability, porosity, and oil saturation in wells of Arch Unit, Patrick Draw Field.....	35
2.16. Relationship between initial production and thickness of net pay in wells of Arch Unit, Patrick Draw Field.....	35
2.17. Relationship between cumulative production and thickness of the net pay in wells of Arch Unit, Patrick Draw Field.....	35

ILLUSTRATIONS—Continued

	<u>Page</u>
2.18. Location of formation water data points in the Muddy Formation of Bell Creek Field, Montana.....	36
2.19. Composition and salinity of formation waters (set 1) in the Muddy Formation shoreline barrier sandstones shown on the trilinear diagram; Bell Creek Field, Montana.....	37
2.20. Composition of formation waters (set 1) in the Muddy Formation shoreline barrier sandstones shown on the Stiff diagrams; Bell Creek Field, Montana.....	37
2.21. Composition and salinity of formation waters (set 2) in the Muddy Formation shoreline barrier sandstones shown on the trilinear diagram; Bell Creek Field, Montana.....	38
2.22. Composition of formation waters (set 2) in the Muddy Formation shoreline barrier sandstones shown on the Stiff diagrams; Bell Creek Field, Montana.....	38
2.23. Composition and salinity of formation waters (set 3) in the Muddy Formation shoreline barrier sandstones shown on the trilinear diagram; Bell Creek Field, Montana.....	39
2.24. Composition of formation waters (set 3) in the Muddy Formation shoreline barrier sandstones shown on the Stiff diagrams; Bell Creek Field, Montana.....	39
2.25. Comparison of composition and salinity of "typical" formation water in Bell Creek Field with composition and salinity of average present sea water shown on the trilinear diagram.....	40
2.26. Comparison of composition and salinity of "typical" formation water in Bell Creek Field with composition and salinity of average present sea water shown on the Stiff diagram.....	40
3.1. Relationship of resistivities (R_w) and total dissolved solid contents (TDS) in formation waters of Patrick Draw Field.....	47
3.2. Water saturation profiles of well Arch 46, calculations based on four different water resistivity values.....	47
3.3. Water saturation map of Patrick Draw Field, calculations based on a constant water resistivity value of 0.2 ohm-meter.....	48
3.4. Water saturation map of Patrick Draw Field, calculations based on salinity map in Fig. 2.1.....	49
3.5. Difference of water saturation interpretations by subtracting S_w values in Fig. 3.4 from those in Fig. 3.3.....	50
3.6. Calculation of water saturations in the producing UA-5B sandstones in well Arch 120 for a resistivity of formation water, $R_w = 0.1907$ ohm-meters.....	51
3.7. Calculation of water saturations in the producing UA-5B sandstones in well Arch 120 for a resistivity of formation water, $R_w = 0.25$ ohm-meters.....	51
3.8. Calculation of water saturations in the producing UA-5B sandstones in well Arch 120 for a resistivity of formation water, $R_w = 0.35$ ohm-meters.....	52
3.9. The calculated water saturation values by Archie's and Simandoux's methods in Arch 120 compared with the deviation of clay value at each point from the mean.....	52
4.1. Base map of Patrick Draw Field showing location of structural log cross sections. Faults identified on cross sections are indicated by symbols.....	63

ILLUSTRATIONS—Continued

	<u>Page</u>
4.2. Updated structure map of top of UA-5B sandstone, Almond Formation at Patrick Draw Field showing locations of fault zones identified from structural log cross sections and those published previously.....	64
4.3. Fault map for Patrick Draw Field derived from combined seismic and log interpretations.....	65
4.4. Locations of seismic lines and log cross-sections used in mapping faults at Patrick Draw Field, Wyoming.....	66
4.5. Two-way reflection times from the top of Almond Formation along seismic line AA-6.	67
4.6. Elevations above sea level on the top of UA-5B sandstones obtained from interpretations of core and log data.	67
4.7. Overlay of the isosalinity map of Patrick Draw area (based on Fig. 2.1) and the location of faults as determined by seismic and wireline log correlations.	68
4.8. Overlay of major fault zones indicated by electric log correlations compared with the areas of greater than 25 ft thickness of permeable sandstone in Patrick Draw Field.	69
4.9. Historical structure map of top of Almond Formation at Patrick Draw Field.	70
4.10. Surface lineaments in the Patrick Draw area.	71
4.11. Rose diagram showing the comparison of fault and lineament orientations at Patrick Draw Field. A. Faults include only those identified during construction of log cross sections. B. Faults determined from combined log and seismic cross sections.	72
4.12. Relationship of log signatures and facies for UA-5 sand, Almond Formation, in well Arch 120.	73
4.13. Correspondence between log signatures and facies for UA-5 and UA-6 sands, Almond Formation, in well Arch 106.	74
4.14. Isopach map showing the distribution of the high resistivity marker at the top of UA-5B.	75
4.15. Comparison of formation water salinity and the high resistivity marker at the top of UA-5B.	76
4.16. Comparison of the distribution of the high resistivity marker at the top of Almond Formation stratigraphic interval UA-5B and the distribution of UA-5A sands.	77
4.17. Base map showing the location of resistivity stratigraphic cross sections A-A', B-B', C-C', D-D', and E-E'.	78
4.18. Resistivity stratigraphic cross section A-A', which runs along the length of the permeable sand thin between the eastern and western bars in Arch Unit.	79
4.19. Resistivity stratigraphic cross section B-B'.	79
4.20. Resistivity stratigraphic cross section C-C'.	80
4.21. Resistivity stratigraphic cross section D-D'.	80
4.22. Resistivity stratigraphic cross section E-E'.	81
4.23. Cross plot of natural logarithm permeability versus log-derived clay content (V_{cl}).	82
4.24. Cross plot of total clay versus porosity.	82

ILLUSTRATIONS—Continued

	<u>Page</u>
4.25. Cross plot of bulk volume porosity versus oil saturation for 6 samples from wells Arch 120 and Arch 7-18-1.....	83
4.26. Cross plot of permeability versus oil saturation for same samples as in Fig. 4.25.....	83
4.27. Cross plot of microporosity versus oil saturation for same samples as in Fig. 4.25.....	84
4.28. Cross plot showing relationship between feldspar content of thin sections from well Arch 120 and microporosity.....	84
5.1. Histogram of sand permeability in Arch Unit, Patrick Draw Field.....	99
5.2. Histogram of sand permeability in Monell Unit, Patrick Draw Field.....	99
5.3. Histogram of mean permeability for 70 wells in the Arch Unit, Patrick Draw Field.....	99
5.4. Histogram of mean permeability for 38 wells in the Monell Unit, Patrick Draw Field.....	99
5.5. Map of geometrically-averaged mean permeability for wells in Patrick Draw Field.....	100
5.6. Histograms of Dykstra-Parsons coefficient in 70 Arch Unit wells Patrick Draw Field.....	101
5.7. Histogram of Dykstra-Parsons coefficient in 38 Monell Unit wells, Patrick Draw Field.....	101
5.8. Map of Dykstra-Parsons coefficient values for 108 wells in Patrick Draw Field.....	102
5.9. Histogram of sand porosity in Arch Unit, Patrick Draw Field.....	103
5.10. Histogram of sand porosity in Monell Unit, Patrick Draw Field.....	103
5.11. Map of average log-derived porosity in Patrick Draw Field.....	104
5.12. Histogram of pay thickness in the Arch Unit, Patrick Draw Field.....	105
5.13. Histogram of pay thickness in Monell Unit, Patrick Draw Field.....	105
5.14. Histogram of product of porosity, pay, and oil saturation in Arch Unit, Patrick Draw Field.....	105
5.15. Histogram of product of porosity, pay, and oil saturation in Monell Unit, Patrick Draw Field.....	105
5.16. Crossplot of primary recovery efficiency and Dykstra-Parsons coefficient in Arch Unit, Patrick Draw Field..	106
5.17. Crossplot of primary recovery efficiency and mean permeability in Arch Unit, Patrick Draw Field.....	106
5.18. Crossplot of primary recovery efficiency and Dykstra-Parsons coefficient in Monell Unit, Patrick Draw Field.....	106
5.19. Crossplot of primary recovery efficiency and mean permeability in Monell Unit, Patrick Draw Field.....	106
5.20. Crossplot of waterflood recovery efficiency and mean permeability in Monell Unit, Patrick Draw Field.....	107
5.21. Crossplot of waterflood recovery efficiency and Dykstra-Parsons coefficient in Arch Unit, Patrick Draw Field.....	107
5.22. Crossplot of waterflood recovery efficiency and Dykstra-Parsons coefficient in Monell Unit, Patrick Draw Field.....	107

ILLUSTRATIONS—Continued

Page

5.23. Pre-waterflood oil production map of UA-5 sands in Patrick Draw Field.....	108
5.24. Pre-waterflood oil production map of UA-6 sands in Arch Unit, Patrick Draw Field.....	109
5.25. Production history for Monell well 62. Production started in July, 1960.	109
5.26. Distribution of recovery efficiency in Monell Unit, Patrick Draw Field for primary production.....	110
5.27. Production history for well Monell 38. Production started in September, 1960.....	111
5.28. Production history for well Monell 147. Production started in September, 1968.	111
5.29. Three regions with different producing characteristics in Arch Unit, Patrick Draw Field.....	112
5.30. Distribution of oil bank period (months) during waterflood in Patrick Draw Field.	113
5.31. Distribution of water breakthrough time (months) in Patrick Draw Field.....	114
5.32. Distribution of cumulative oil production during waterflood from UA-5 sands in Patrick Draw Field.	115
5.33. Distribution of recovery efficiency in Monell Unit, Patrick Draw Field for waterflood production.....	116
5.34. Distribution of recovery efficiency in Monell Unit, Patrick Draw Field for both primary and waterflood productions.....	116
5.35. Distribution of cumulative water injection in pore volumes in Patrick Draw Field.	117
5.36. Distribution of ultimate recovery efficiency in Patrick Draw Field.....	118
5.37. Distribution of remaining oil saturation in Patrick Draw Field.....	119
5.38. Hall plot from Arch well 8. The shut-in of offset production wells shown by arrows, well number and dates, correspond with an increase in Hall plot slope.....	120
5.39. Simulation results of Hall plots with and without shut-in of offset production wells.	120
5.40. Two-phase simulation results of Hall plots with and without nearby permeability barriers.	120
5.41. Single-phase simulation results of Hall plots with and without nearby permeability barriers.	120
5.42. Influence of barrier distance on injection pressure.....	121
5.43. Influence of intersection angle between barrier and injector-producer line on injection pressure.....	121
5.44. Hall plot slope vs. reciprocal of pay thickness (h) times permeability (k).	121
5.45. Map showing Hall plot slope values, net pay thickness, and fault locations.....	122

INTEGRATION OF THE GEOLOGICAL/ENGINEERING MODEL WITH PRODUCTION PERFORMANCE FOR PATRICK DRAW FIELD, WYOMING

ABSTRACT

The NIPER Reservoir Assessment and Characterization Research Program incorporates elements of the near-term, mid-term and long-term objectives of the National Energy Strategy-Advanced Oil Recovery Program. The interdisciplinary NIPER team focuses on barrier island reservoirs, a high priority class of reservoirs, that contains large amounts of remaining oil in place located in mature fields with a high number of shut-in and abandoned wells. The analysis and model developed in the course of the research will directly benefit the operators of the fields, as well as those companies operating in similar types of reservoirs.

The project objectives are to: (1) identify heterogeneities that influence the movement and trapping of reservoir fluids in two examples of shoreline barrier reservoirs (Patrick Draw Field, WY and Bell Creek Field, MT); (2) develop geological and engineering reservoir characterization methods to quantify reservoir architecture and predict mobile oil saturation distribution for application of targeted infill drilling and enhanced oil recovery (EOR) processes; and (3) summarize reservoir and production characteristics of shoreline barrier reservoirs to determine similarities and differences.

This report covers the work conducted in FY92 and includes the following topics: (1) the application of hydrogeochemical techniques to reservoir characterization; (2) the effect of salinity variations in the determination of oil saturation by wireline logs; (3) structural and sedimentological features that control fluid distribution and movement; and (4) analysis of lateral variations in production performance.

The major findings of the research include: (1) hydrogeochemical analytical techniques were demonstrated to be an inexpensive reservoir characterization tool that provides information on reservoir architecture and compartmentalization; (2) the formation water salinity in Patrick Draw Field varies widely across the field and can result in a 5 to 12% error in saturation values calculated from wireline logs if the salinity variations and corresponding resistivity values are not accounted for; and (3) an analysis of the enhanced oil recovery (EOR) potential of Patrick Draw Field indicates that CO₂ flooding in the Monell Unit and horizontal drilling in the Arch Unit are potential methods to recover additional oil from the field.

EXECUTIVE SUMMARY

NIPER's Reservoir Assessment and Characterization Research Program incorporates elements of the near-, mid-, and long-term objectives of the National Strategy-Advanced Oil Recovery Program. The reservoirs studied, shoreline barrier reservoirs, represent a class of reservoirs with large amounts of remaining oil in place (ROIP) located in mature fields with a high number of shut-in and abandoned wells. The analysis and models developed in the course of the research will directly benefit the operators of the fields, as well as those companies operating in similar types of reservoirs in the near term.

Near- to mid-term applications of the results of this research comprise a methodology to quantify the effects of heterogeneities and to construct accurate reservoir models. Long-term results of the research will be the determination of the transferability of reservoir and production characteristics among reservoirs of similar depositional histories. Identification of similar heterogeneities will allow application of similar reservoir management strategies and advanced recovery methods to maximize recovery efficiency.

The research program at NIPER employs an interdisciplinary approach that focuses on the high-priority reservoir class of shoreline barrier deposits to (1) determine the problems specific to this class of reservoirs by identifying the reservoir heterogeneities that influence the movement and trapping of fluids and (2) develop methods to characterize effectively this class of reservoirs to predict residual oil saturation (ROS) on interwell scales and to improve prediction of the flow patterns of injected and produced fluids.

Accurate descriptions of the spatial distribution of critical reservoir parameters (e.g. permeability, porosity, pore geometry, mineralogy, and oil saturation) are essential for designing and implementing processes to improve sweep efficiency and thereby increase oil recovery. Most of FY92 was devoted to integrating the previously developed geological and engineering model for the mesotidal shoreline barrier reservoir at Patrick Draw Field, WY with reservoir production performance, and testing previously identified reservoir characterization methods. The scope of the work for FY92 may be subdivided into four main areas, each represented by chapters in this report: (1) the application of hydrogeochemical techniques to reservoir characterization; (2) the effect of salinity variations in the determination of oil saturations by wireline logs; (3) structural and sedimentological features that control fluid distribution and movement; and (4) analysis of lateral variations of reservoirs properties and production/injection performance.

The first area of research (Chapter 2) investigated the

principles and practical applications of hydrogeochemical analytical techniques. Distribution of salinity and the chemical composition of formation waters that coexist with oils within reservoirs can provide important information on reservoir compartmentalization. Interpretation of log signatures and calculation of accurate saturation values from wireline logs is particularly dependent on the variation and spatial distribution of formation water salinity, composition, and consequent resistivity.

The second area of investigation (Chapter 3) is the effect of salinity variations on oil saturation calculations from wireline logs at Patrick Draw Field. Calculation of water saturation profiles based on water resistivity values ranging from 0.1 to 0.5 ohm-meter resulted in a range of average water saturations from 34% to 76%, the difference between a good oil reservoir and a residual oil reservoir. A constant value of water resistivity based on an assumption of a homogeneous distribution of salinity is often used in interpreting oil reserves from resistivity logs. This work shows that comparison of oil saturation distribution based on a single R_w value for the entire field, and that based on R_w values from accurate salinity data resulted in a 5 to 12% difference in saturation values in the Patrick Draw Field. Comparison of various log analysis methods to determine the effect of salinity and clay content indicated that in moderately low clay filled sandstones (<8%) with relatively small amounts of clays that have high cation exchange capacities (<1%), the Simandoux's method gives reliable estimates of S_w .

In the third area (Chapter 4), the structural and sedimentological controls on fluid distribution and movement were investigated. Structural cross-sections based on wireline log correlations and seismic data were used to identify numerous, previously unreported structural faults within the production limits of Patrick Draw Field. The fault directions are consistent with lineaments identified in the region and were determined to have a subtle effect on sand depositional patterns, which had previously been correlated with production. Additional controls on fluid distribution and movement at Patrick Draw were related to the areal distribution of an impermeable (coquina) deposit as well as petrophysical properties, some of which are controlled by diagenetic processes such as compaction, cementation, and the creation of secondary porosity and microporosity.

The fourth broad area of research (Chapter 5) consisted of an evaluation of the lateral variations in production performance. Determination of the effectiveness of primary and waterflood recovery operations at Patrick Draw Field requires precise estimation of water saturations of the producing sandstones during different stages of production from the field. Efficiency of waterflood recovery was found to increase with average permeability. This relationship is believed to exist due to the relatively high ratio of oil relative permeability to water relative permeability (k_{ro}/k_{rw}) for the rocks of higher permeability values in this strongly water wet system. No correlation was found between oil recovery efficiencies and Dykstra-Parsons coefficients in either Arch Unit or Monell Unit. In

addition to reservoir pressure and petrophysical properties, the importance of the lateral distribution of oil saturation in the reservoir at different phases of recovery is demonstrated.

The best production at Patrick Draw Field lies primarily in the area of good oil reserves with a thick pay and high oil saturation. Water injection and expansion of the gas cap contributed to successful production of reserves from the southwestern area of Arch Unit and the northwestern area of Monell Unit.

Waterflood production from Monell Unit is comparable to that from primary recovery, and equivalent to recovery of approximately 23% OOIP. Monell wells have recovery efficiencies ranging from 20% to more than 50% indicating a good oil recovery. Arch Unit has a relatively poor recovery efficiency except for the area immediately west of the mapped low-permeability flow barrier.

A high degree of heterogeneity in Arch Unit is evidenced by sand discontinuities (compartments) reflected by gross changes in pay thickness and fluid saturations, by poor sweep efficiency and low waterflood recovery compared to Monell Unit, and by the large contrast in water breakthrough times.

No significant wellbore damage was identified by Hall plots analysis for most injection wells in Arch Unit. Some sharp increases in Hall plot slopes during late injection stages were caused by shut-in of surrounding wells.

Reservoir volume balance calculations in three regions of Arch Unit show no evidence of loss of injection water to sands other than UA-5 and UA-6 sands. This indicates that no major conduits connect the upper Almond Formation sands to other sands within the area studied.

An analysis of the enhanced oil recovery (EOR) potential of Patrick Draw Field indicates that the northwestern and central parts of the Monell Unit are recommended project areas because of the relatively high ROS and uniform pay. CO₂ flooding is a candidate EOR process because the reservoir pressure in the Monell Unit is higher than the minimum miscible pressure and a nearby source of CO₂ is available.

ACKNOWLEDGMENTS

The research team for Project BE1 gratefully acknowledges Tom Burchfield, Mike Madden, Min Tham, and Bill Linville for their continued guidance throughout this project. The efforts of Viola Rawn-Schatzinger, Djaun Grissom, Kathy Bertus, and Dwight Haney helped to improve the manuscript. The support of Edith Allison, Project Manager, Bartlesville Project Office, U. S. Department of Energy is greatly appreciated. We appreciate the financial support of this research by the U. S. Department of Energy through Cooperative Agreement DE-FC22-83FE60149. Special thanks are due to Frank Lim, Senior Staff Engineer, Union Pacific Resources Co., Fort Worth, TX for providing core material, core measurements, and other reservoir data. This manuscript was word processed by Edna Hatcher.

CHAPTER 1

INTRODUCTION

by Susan R. Jackson, Project Leader

Background

The broad objectives of the Department of Energy's program for geoscience research are to develop methods for locating residual oil saturation distribution in oil reservoirs and to evaluate suitable methods for recovering the oil. The objectives of the NIPER BE1 program fit within those of the Department of Energy's geoscience program by providing a methodology for the effective characterization of shoreline barrier reservoirs and increasing the understanding of the heterogeneities that influence movement and trapping of fluids within this class of reservoirs. Two reservoirs were selected for study: Bell Creek Field, MT and the Patrick Draw Field, WY (Fig 1.1).

At first, a microtidal system at Bell Creek (MT) Field was selected for reservoir assessment and characterization research (FY86-FY89) (Fig. 1.2). A combined quantified geological/engineering model was developed and used to identify the types and scales of heterogeneities in the shoreline barrier system at Bell Creek. From this basis, the influence of various heterogeneities on fluid flow and hydrocarbon trapping was investigated (Honarpour, et al., 1989).

To broaden the geological and engineering understanding of comparative aspects of shoreline barrier reservoirs, a mesotidal shoreline barrier example, Patrick Draw Field, was selected during FY90 (Figs. 1.2 and 1.3). The cross section presented in figure 1.4 illustrates the vertical arrangement of producing sands in the Patrick Draw Field and the lateral variations in sand thickness. The relatively rapid lateral changes in thickness are characteristic of mesotidal shoreline barrier deposits.

The work during FY90 consisted of three main areas. First, a mesotidal, tide-dominated shoreline barrier/barrier island reservoir, (Patrick Draw Field) was selected. The second area of work focused on determining the fundamental relationships between geological, petrophysical, and reservoir production/injection characteristics. The third area of investigation consisted of determining more efficient and economical methods for shoreline barrier/barrier island reservoir description and simulation (methodology).

During FY91, characterization of the mesotidal system at Patrick Draw Field continued primarily through work in four areas. First was continued improvement and quantification of the geological shoreline barrier model for Patrick Draw Field. The second area included construction of the engineering model for Patrick Draw Field through improved reservoir description and its integration with the geological model. The third area included geostatistical

analysis in order to estimate interwell reservoir properties in Patrick Draw Field. This activity provided an opportunity to investigate the strengths and weaknesses of different geostatistical techniques. The final area of work during FY91 was to continue to improve and generalize the methodology for characterizing shoreline barrier reservoirs.

The work during FY92 consisted of continued development of reservoir characterization methods and a reservoir model for Patrick Draw Field. Four general areas were addressed and the advances in each of these areas are described in this report. The first involved the application of hydrogeochemical techniques to reservoir characterization. The second area of work focused on structural and sedimentological features that control fluid distribution and movement. Also included in the second area of work was a comparison of lithology and diagenetic processes and their effect on petrophysical properties, pore types, and pore system continuity. The third major area of work included geophysical investigations of Patrick Draw Field emphasizing the structural setting as interpreted from seismic lines. The fourth area of work included an analysis of lateral variations in production performance; an investigation of the effect of petrophysical properties on oil recovery; and the development and application of the Hall Plot technique in identifying reservoir compartments.

The data collected and generated during the interdisciplinary research and model development of Patrick Draw Field has been compiled in electronic spreadsheets and documented and has been submitted in a separate report (Jackson and Rawn-Schatzinger, 1992). The data compiled consists of 319 files and includes: production data from 256 wells in both Arch and Monell Units of Patrick Draw Field; petrophysical and saturation data from routine core analysis; petrographic analyses including grain size data (300 point counts for over 75 thin sections); digitized well log data for 38 wells; and formation water composition. Data collected from outcrop exposures of the Almond Formation include: 80 permeability and porosity values measured from outcrop samples; petrographic data, and 923 fracture azimuths. The compilation and documentation of the data generated in this study will allow other researchers to benefit from our data collection and analysis and to utilize it for other purposes such as geostatistical studies, developing mapping algorithms, compiling general characteristics of this class of reservoirs and providing analog information for other reservoirs.

In a separate report, the data requirements and acquisition for reservoir characterization was addressed (Jackson, et al., 1992). This report outlines the types of data, data sources

and measurement tools required for effective reservoir characterization, the data required for specific enhanced oil recovery (EOR) processes, and a discussion on the determination of the optimum data density for reservoir characterization and reservoir modeling.

Significant technology transfer efforts were made during FY 92 to transfer the information generated from this research project to oil companies and other organizations. Research results were presented at technical society meetings, research forums, and during visits to oil companies, universities and other organizations. Geologic field trips were conducted for both domestic and foreign oil companies as well as government contractors. These efforts will continue in FY93 where a workshop will be organized and conducted to transfer the information generated through this research to independent producers of the Rocky Mountain region.

End Member Models Of Shoreline Barrier Deposition

Our studies have shown that reservoir characteristics of shoreline barrier depositional systems vary widely and cannot collectively be described by a single model. The morphology of shoreline barrier sand deposits is related to a number of processes including tidal range, tidal currents, wave conditions, and storm action (Hayes, 1975), sediment supply rate and the direction and rate of relative sea level changes. After several years of studying tidal deltas under different conditions of wave and tidal regimes, Hayes (1975), Hayes and Kana (1976), and Hayes and Sexton (1989) concluded that tidal range has the principal control over the distribution and form (facies architecture) of shoreline barrier sand deposits. Davies (1964) recognized the importance of tidal range and suggested that coasts with tidal fluctuations less than 2 m be classified as microtidal; those from 2 to 4 m, mesotidal; and when greater than 4 m, macrotidal. Microtidal and mesotidal shoreline barriers are common along modern shorelines and may form adjacent to one another over distances of a mile. Shoreline barriers are generally not developed under macrotidal conditions.

Processes that dominate microtidal barrier shorelines are created by wind and wave effects. Wind tidal flats are commonly associated with microtidal shoreline barriers, as are aligned beaches and recurved and cusped spits. Tidal currents are generally important only at the mouths of inlets (Hayes, 1975), so that flood tidal deltas are usually small, but larger than ebb tidal deltas (Hayes and Sexton, 1989). Another characteristic deposit of microtidal shoreline barriers includes washover fans deposited during storm surge floods that push fan-shaped sand accumulations onto the lagoonal side of the barrier. Wave-dominated, or microtidal barrier islands tend to be long and continuous with few inlets (Fig. 1.2).

Mesotidal barriers differ in that sediments deposited by tidal currents predominate. The barrier islands tend to be short and "drumstick" shaped deposits (Fig. 1.2) with abundant breaks between islands occupied by inlets, and on the lagoonal side, large, conspicuous tidal deltas.

Important loci of sand deposition in mesotidal shoreline barriers are behind the barrier on the tidal deltas and within the tidal channels. Although flood tidal deltas are prominent on mesotidal barriers, they are often smaller than associated ebb tidal deltas. Comparison of microtidal and mesotidal barrier island geomorphological characteristics is given in Table 1.1.

The ultimate control of barrier morphology is related to the ratio of wave energy flux to tidal energy flux (hydrologic regime) as previously described (Hayes, 1979). However, barrier morphology is also a function of the direction and rates of sea level movement of sequence stratigraphic context. Landward migrating (transgressive) barriers have different vertical sequences and often have different morphologies than seaward prograding (regressive) barriers. Transgressive barriers are similar morphologically (Hayes and Sexton, 1989), regardless of hydrodynamic regime. They are generally composed of straight washover terraces whose lengths are determined by the hydrographic regime. Regressive barriers, in contrast, show great morphological differences depending on the hydrographic regime.

Preservation potential of reservoir quality sand deposits is higher on the sheltered lagoonal side of the barrier. The facies with the greatest potential for preservation include those deposited in depositional lows such as tidal channels and inlet fill deposits, and those associated with the lobes of tidal deltas. Downdrift migration (and occasionally updrift migration) of tidal inlets also has a significant impact on the preserved sequence and architecture of mesotidal barrier sandbodies. Inlets migrate in response to preferential addition of sediment by longshore transport to one side of the inlet (FitzGerald, 1976). As the inlet migrates so do the associated flood and ebb-tidal deltas. On the lagoonal side of the barrier, the result is often a laterally continuous, interconnected accumulation of sands which are dominated by tidal delta and tidal channel facies. The lateral extent of these potential reservoir quality sands is controlled by the distance between inlets, the size of flood tidal deltas, the rate of inlet migration, rate of transgression or regression, syndepositional and post depositional erosion, and the preservation of non-reservoir facies associated with the tidal delta and tidal channel sands.

Permanent tidal inlets may also be fixed relative to their lateral position along the coastline. Fixed inlets are generally related to preexisting depressions such as flooded river valleys cut into semiconsolidated marine clays (FitzGerald, 1976; Morton and Donaldson, 1973). At fixed inlets, constructional processes include shoreline progradation due to landward marine bar migration, and spit accretion welding the newly emergent bar to the existing beach. Sediment capture is also created by transport reversal as waves refract around the ebb delta reintroducing downdrift migrating sand to the inlet or inlet marginal shoals.

Data Collected For Almond Formation

The basis for understanding the architecture of reservoir

quality sandstones and ultimately production/injection behavior is the analysis of geological data and its integration with the production/injection records at Patrick Draw Field. Fifteen cores from the Almond Formation housed in the U. S. Geological Survey core collection (Denver) were correlated with wireline logs and subjected to sedimentological analysis. From these cores 33 one-inch diameter plugs were taken from six cores for petrophysical measurements and thin sections.

Additionally, two cores taken from locations near the outcrops of Almond stratigraphic intervals UA-1, UA-2, and UA-3 were examined, and the locations of the two coreholes were visited during a field reconnaissance (see Fig. 1.5).

Confidence of certain facies identifications may be dramatically increased through outcrop studies where directional features can be identified and types and scales of identified heterogeneities can be traced laterally. During the field reconnaissance, it was determined that the depositional facies observed in the outcrop exposures were similar to those encountered in subsurface cores from Patrick Draw Field and that the depositional environments were hydrodynamically similar. At that time, it was found that some of the outcrops extend laterally for thousands of feet and provide three-dimensional exposure of the facies.

The presence of good outcrops which are depositionally similar to the setting at Patrick Draw Field that can provide useful information about subsurface reservoir performance suggested that further outcrop investigation was warranted. Therefore, a second geological field trip to the outcrop exposures of the Almond Formation along the Rock Springs Uplift was conducted in June, 1991. Geological field work during this trip included selection of the best outcrops for geological measurement and detailed future sampling, detailed sedimentological characterization of three selected outcrop profiles, drilling of approximately 80 one inch plugs for petrophysical measurements and the petrographic study, and documentation of fracture orientation, density, continuity, and fracture filling.

Outcrops RG and RH, which were previously described by Roehler (1988), are located about 2 miles apart and were selected for detailed section measuring and drilling of core plugs (Fig. 1.5). One 257-ft-thick section was measured at the northern outcrop (RG) and two sections (145 and 140 ft thick) located 1200 feet apart were measured at the southern outcrop (RH). Cross-sections of these described profiles were constructed to determine lateral facies continuity and changes. Because the lateral extent of some of the facies were less than 1200 feet, correlations of some of the facies in the RH profiles were not possible. In FY 92, limited field work consisted of checking and correcting descriptions, interpretations, and correlations of the previously described profiles. A third described profile located between the previously described profiles in outcrop RH increased the resolution of the cross-sections and allowed documentation of the lateral extent of the facies.

Information about heterogeneity of formation fluids and their chemical characteristics at different locations and producing horizons is crucial for correct interpretation of

certain log responses and for estimation of rock-fluid interaction processes and products which may affect rock permeability. Strong anomalies in water salinity and chemical composition were documented earlier in some Almond Formation wells at Patrick Draw Field (Szapkiewicz and Collins, 1985; Szpakiewicz, et al., 1991). Variations in fluid chemistry have also been used to identify compartmentalization within the reservoir. Advances in these areas are also described in this report.

Because of the importance of fluid heterogeneities, it was decided to check the wellheads of about 20 selected wells in Patrick Draw Field with the cooperation of Union Pacific Resources Co. (UPRC) personnel from Rock Springs, WY, to determine sampling techniques for future sampling of formation fluids. During the June, 1991 field trip updated chemical analyses of natural gas and co-produced formation waters were also acquired from UPRC. In FY92, the Patrick Draw Field formation water composition data from UPRC files were augmented with those from the Petroleum Data System BRIN file. These data were screened based on analytical accuracy and the date of the sampling to assure that the original reservoir conditions were obtained. Wide variations in formation water salinity found in Patrick Draw Field indicate that the oil saturations calculated from wireline logs may be in error if only one resistivity value is assumed for the whole field.

References

- Davies, J. L., 1964, A Morphogenetic Approach to World Shorelines: *Zeits. fur Geomorph.* v. 8, p. 127-142.
- FitzGerald, D. M. 1976, Ebb-tidal delta of Price Inlet, South Carolina: Geomorphology, physical processes, and associated inlet shoreline changes: *in* Hayes, M. O., and T. W. Kana, eds., Terrigenous Clastic Depositional Environments. Coastal Research Division, Dept. of Geology, Univ. of South Carolina, p. II-143-II-157.
- Hayes, M. O. 1975, Morphology of sand accumulation in estuaries: An introduction to the symposium: *in* Cronin, L. E., ed., Estuarine Research, v. 2, Geology and Engineering, p. 3-22.
- Hayes, M. O. 1979, Barrier island morphology as a function of tidal and wave regime: *in* Leatherman, S.P., ed., Barrier Islands from the Gulf of St. Lawrence to the Gulf of Mexico, Academic Press, N.Y., p. 1-27.
- Hayes, M. O. and T. W. Kana. 1976, Terrigenous Clastic Depositional Environments- Some Modern Examples. AAPG Field Course Guidebook and Lecture Notes. Tech. Rept. No. 11-CRD, Coastal Res. Div., Dept. of Geology, Univ. of S. Carolina, Columbia, Part I, 131 p., Part II, 184 p.

- Hayes, M. O. and W. J. Sexton. 1989, Modern Clastic Depositional Environments, South Carolina. Field Trip Guidebook T371. 28th Intern. Geol. Congress. Amer. Geophysical Union, Washington, D. C., 85 p.
- Honarpour, M., et al., 1989, Integrated Reservoir Assessment and Characterization Covering the Period October 1, 1985 - September 30, 1988. Final Report. DOE Report NIPER-390, 336 p.
- Jackson, S. R., M. M. Chang, and M. K. Tham, 1992. Data Requirements and Acquisition for Reservoir Characterization. DOE Report NIPER-615, 26 p.
- Jackson, S. R. and V. Rawn-Schatzinger, 1992. Reservoir and Outcrop Data From the Almond Formation, Patrick Draw Field, WY, and the Muddy Formation, Bell Creek Field, MT. DOE Report NIPER-662, 11 p.
- Morton, R. A., and Donaldson, A. C. 1973, Sediment Distribution and Evolution of Tidal Deltas Along a Tide-Dominated Shoreline, Wachapreague, Virginia. Sed. Geol. v. 10, pp. 285-299.
- Roehler, H. W. 1988, The Pintail Coal Bed and Barrier Bar G - A Model for Coal of Barrier Bar-Lagoon Origin, Upper Cretaceous Almond Formation, Rock Springs Coal Field, Wyoming. USGS Prof. Paper 1398, 60 p.
- Szpakiewicz, M. J., and A. G. Collins. 1985, Hydrochemical Study of the Upper Cretaceous and Lower Tertiary Formations in the Uinta, Piceance and Greater green River Basins; Implications for Oil and Gas Related Problems. DOE Report NIPER-95, 70 p.
- Szpakiewicz, M. J., R. Schatzinger, S. Jackson, B. Sharma, A. Cheng, and M. Honarpour. 1991, Selection and Initial Characterization of a Second Barrier Island Reservoir System and Refining of Methodology for Characterization of Shoreline Barrier Reservoirs. DOE Report NIPER-484, 170 p.

TABLE 1.1 - Some General Geomorphological Differences Between Microtidal And Mesotidal Barrier Islands. After Hayes and Kana, 1976

Barrier type	Length	Washover features	Tidal inlets	Flood-tidal deltas	Ebb-tidal deltas
Microtidal	long (30-100 km)	abundant; washover terraces and washover fans numerous	infrequent	large; commonly coupled with washovers	small to absent
Mesotidal	stunted (3-20 km)	minor; beach ridges or washover terraces; washover fans rare	numerous	moderate size to absent	large with strong wave refraction effects

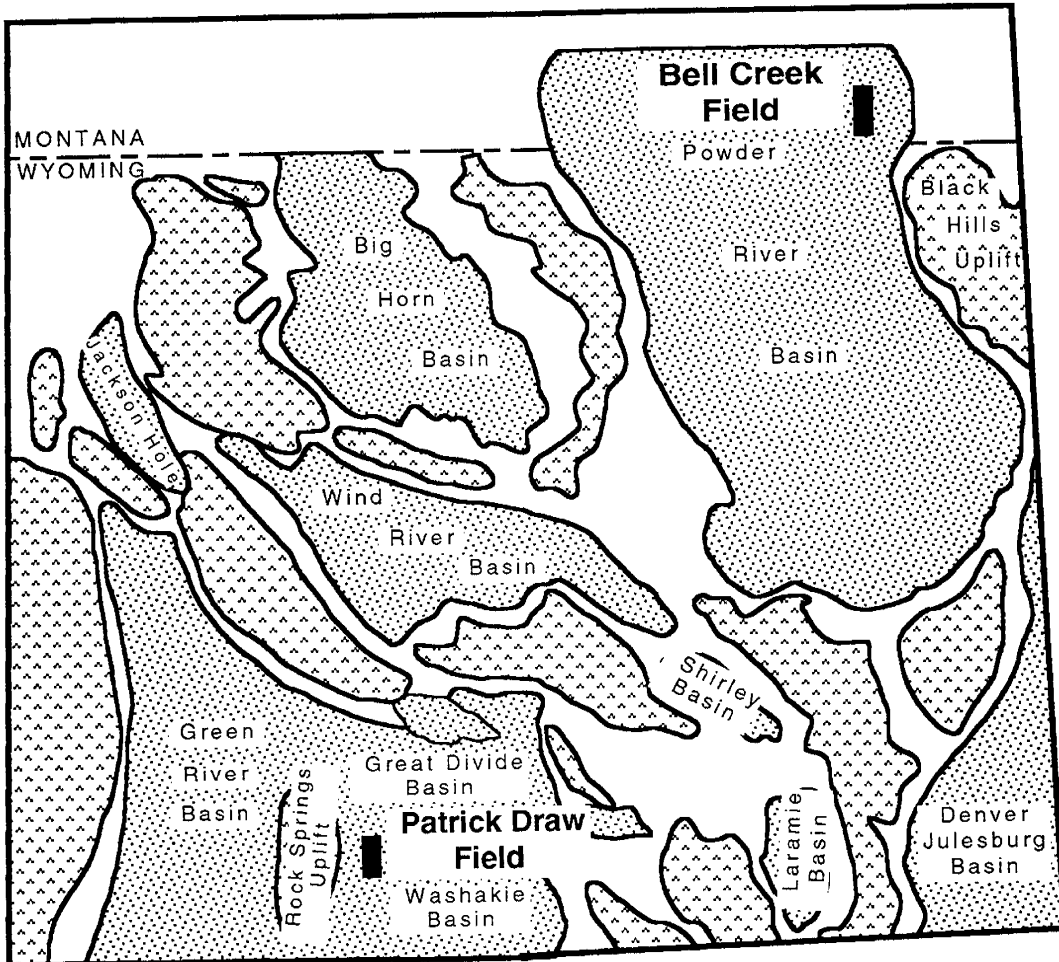


Fig. 1.1. Location of oil fields studied. Note the location of Bell Creek Field, Powder River Basin, MT and Patrick Draw Field, Washakie Basin, WY.

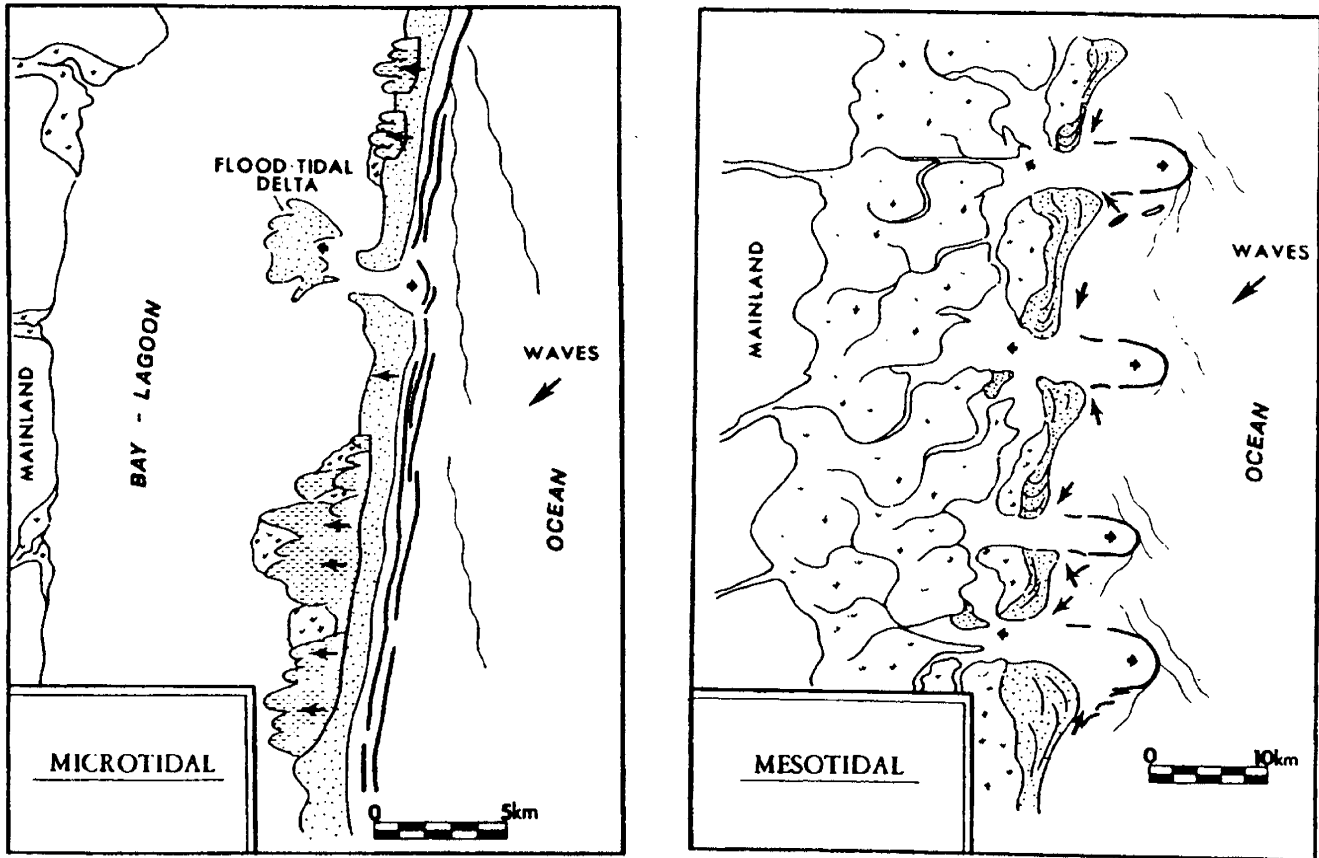


Fig. 1.2. Morphological models for microtidal, and mesotidal barrier shoreline with medium wave energy. Note that in microtidal barrier shorelines flood-tidal deltas tend to be considerable larger than ebb-tidal deltas. Also note the abundance of inlet in the meso-tidal model. After Hayes (1979).

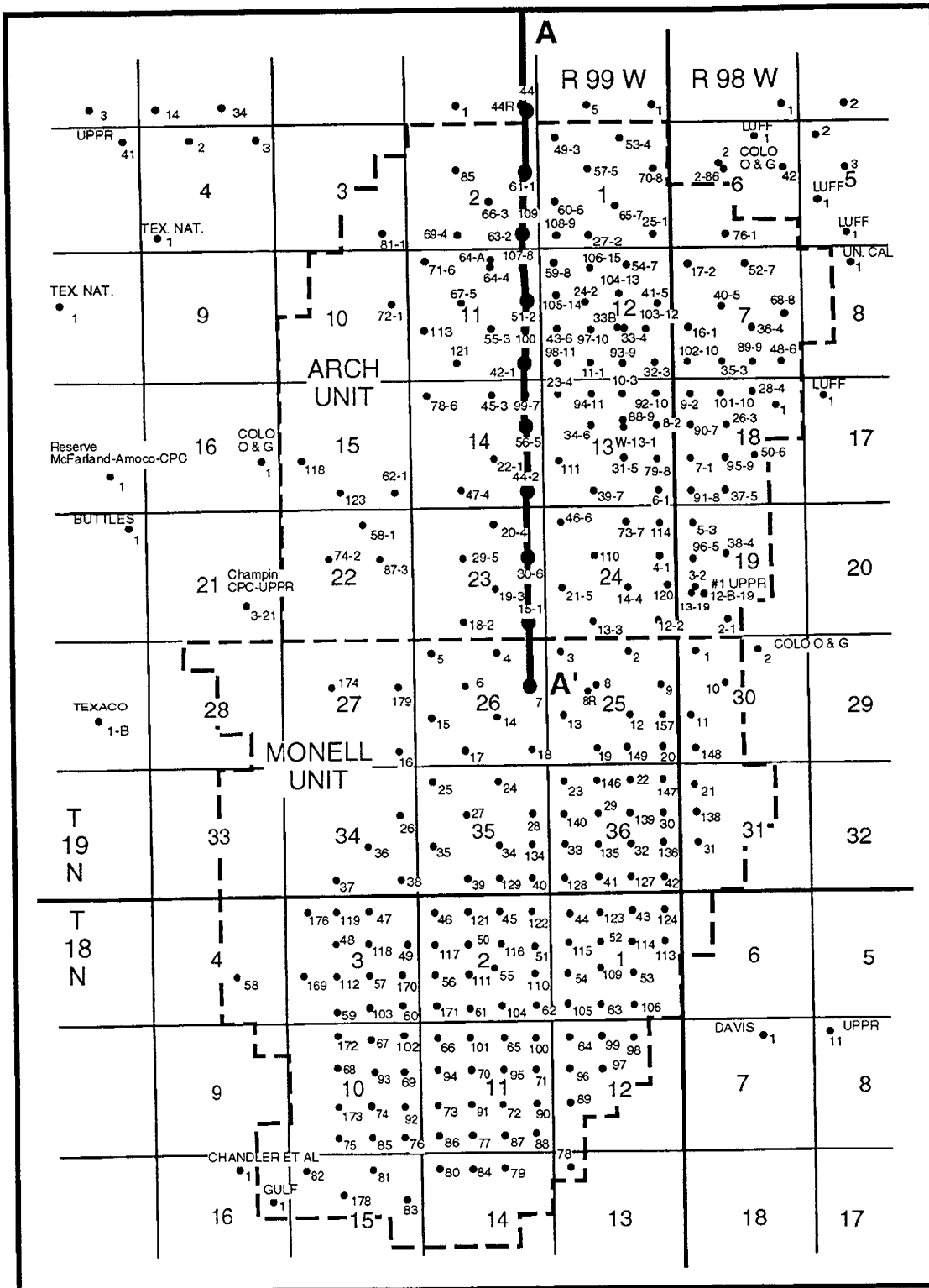


Fig. 1.3. Base map of Patrick Draw Field well locations. Stratigraphic cross section A-A' is shown in figure 1.4.

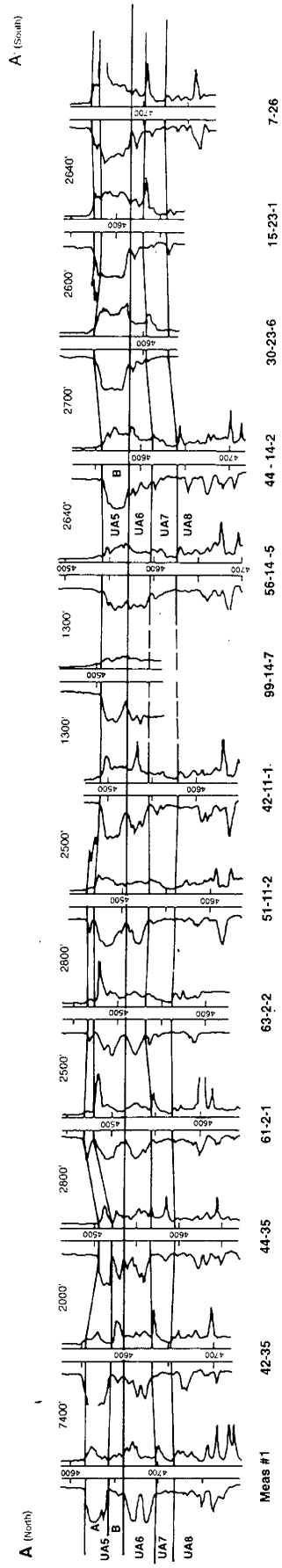


Fig. 1.4. Stratigraphic cross section showing the vertical arrangement of reservoir sands and the lateral variability of sand thickness in Patrick Draw Field, WY. Datum is top of stratigraphic interval UA6-A. Location of cross section is indicated in figure I.3. (after Irwin, 1976)

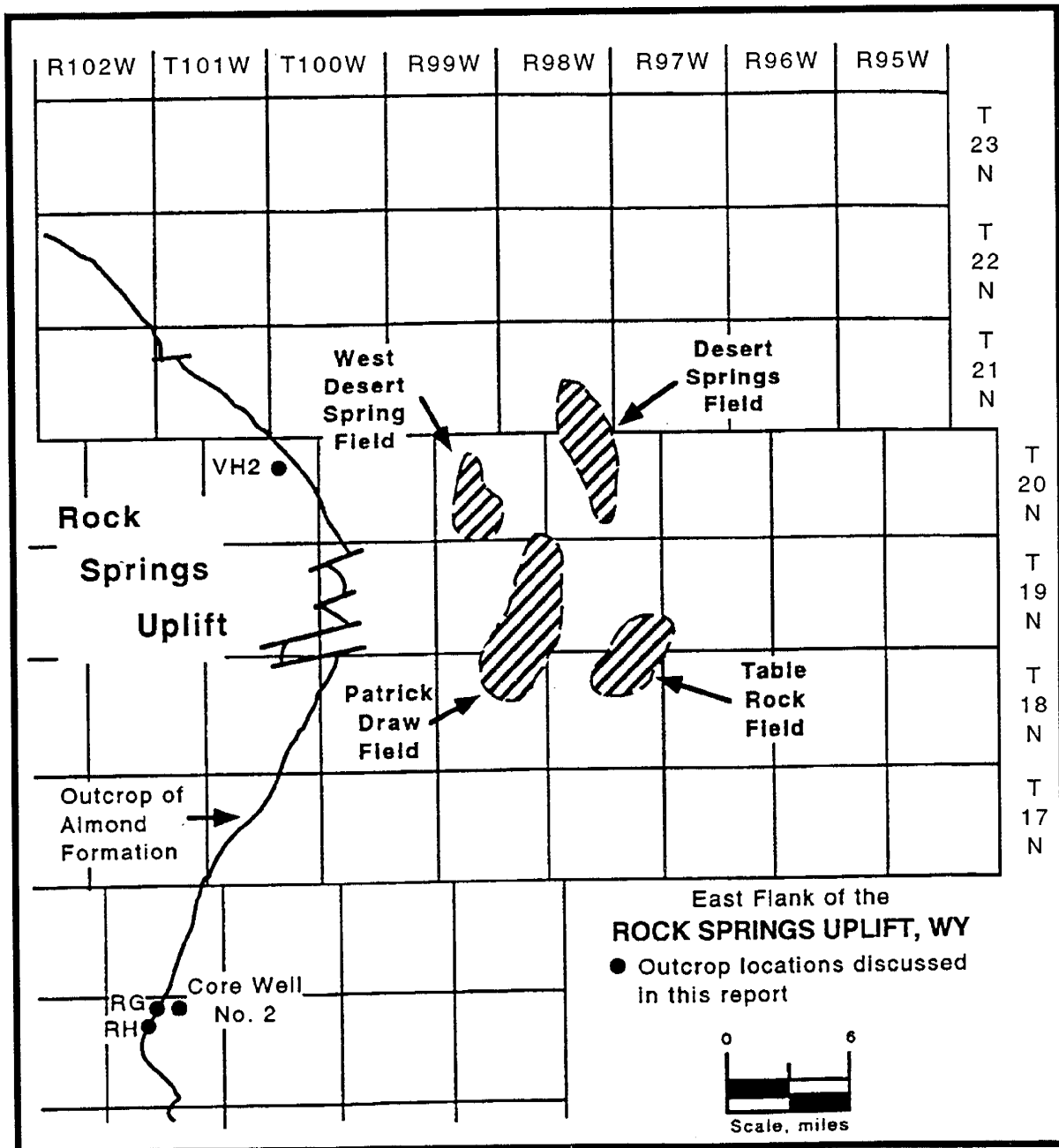


Fig. 1.5. Map of the east flank of the Rock Springs Uplift, Sweetwater Co., WY. Note locations of Almond outcrop exposures (RH, RG, VH2) and Patrick Draw Field.

CHAPTER 2

THE IMPORTANCE AND APPLICATION OF HYDROGEOCHEMICAL TECHNIQUES TO RESERVOIR CHARACTERIZATION

by M.Szpakiewicz

Chapter Summary

The applicability of the comprehensive and quantitative hydrogeochemical techniques to hydrocarbon reservoirs are outlined. It is exemplified by the case study of Patrick Draw Field, WY. and Bell Creek Field, MT.

Identification of the origin and the distribution of salinity and chemical composition of the formation waters coexisting with oil in productive systems has been proven useful to assist managerial decisions in a number of petroleum reservoirs. The effective and affordable hydrogeochemical techniques are not yet commonly used by field operators, although the recommended monitoring of produced fluids can be highly profitable. Interpretation of log signatures and calculation of realistic values of oil saturation from wireline logs is particularly dependent on interpretation of salinity, composition, and resistivity of the formation waters.

In many cases, however, the inexpensive methods cannot be used to the fullest for characterization of oil reservoirs because the formation water data acquired by oil producers and stored in national files are scarce, unreliable, incomplete, or constrained to only one stage of reservoir development. Recommendations for collecting better quality hydrogeochemical data are provided. However, even data of limited quality such as those used in this study may reveal important practical aspects of reservoir characteristics and significantly improve understanding of reservoir hydrodynamics.

Introduction

A study of Patrick Draw Field illustrates the high potential for application of simple hydrogeochemical indicators for improved reservoir development. Mapped salinity contrasts provided the basis for recalculation of original oil-in-place and provided a guide for improved enhanced oil recovery (EOR) tactics. Identification of fluid compartments may be used to improve flood patterns and may aid in selection of the most prospective sites for infill drilling. Compartments with distinct fluid salinity and composition have been shown to have a strong effect on calculation of oil saturation. In addition, compartments with contrasting fluid types may adversely affect some EOR processes because the processes are sensitive to salinity, and the presence of divalent cations and major anions such as bicarbonates and sulfates. Hydrogeochemical data strongly indicate that individual compartments within the Almond Formation could have

been in communication with multiple allochthonous (originating elsewhere) sources of formation waters.

Approximate boundaries of several square miles size mega-compartments and much smaller sub-compartments have been identified in the Patrick Draw Field, Wyoming on the basis of mapped salinity contrasts of original (pre-waterflood) formation waters and heterogeneity of hydrochemical facies. Reservoir compartments were also indicated by the salinity and composition of in situ formation water which remained unchanged after long term waterflooding of the surrounding area.

In the Arch Unit of Patrick Draw Field most wells of superior productivity are concentrated in the southwest section of the unit where the formation water salinity is highest while wells of inferior productivity are predominantly located within the zone of low salinity. High hydrochemical gradient zone between the two areas reflects a position of barrier to flow where drainage conditions are impaired.

Approximate oil saturation calculations based on mapped distribution of water salinities and corresponding resistivities indicate up to 12% more original oil in place in the area of highly saline formation waters generally updip, and up to 5% less oil in the much lower salinity sections of Patrick Draw Field near the oil-water contact. Recommendation for further improvement of the calculations is provided based on resistivity values corrected for non-Na-Cl formation waters in identified areas of the field.

In Bell Creek Field, Montana, compartmentalization of productive units within the Muddy Formation is evident based on earlier geological studies conducted by NIPER. Deep valley incisions into the oil productive shoreline barrier deposits provide barriers to lateral communication of fluids. A potential for vertical communication of fluids through conductive faults between the compartmentalized Muddy Formation and an unidentified aquifer is indicated by anomalously low salinities in the Muddy Formation and by the nearly complete homogenization of water composition across the field. In the case of Bell Creek Field, the available formation water data do not indicate lateral barriers to flow within the Muddy Formation probably because vertical intercommunication with a single dynamic aquifer dominates the chemical composition of fluids in the entire vertical system. More comprehensive analysis of fluid dynamics including the stable isotope ratios is needed for solving the puzzling problem of fluid origins, anomalously low salinities and relatively uniform composition of formation waters identified in several geologically separated production units of the Muddy Formation in Bell Creek Field.

Outline of the Petroleum Hydrogeochemistry; Principles, Techniques, and Practical Applications

Capability of Quantitative Hydro-geochemical Reservoir Analysis

Monitoring the distribution of salinities and chemical and isotopic composition of formation waters hosted in hydrocarbon-bearing reservoirs provides unique information regarding differentiation of fluid regimes. The spatial characteristics of geochemical fluid facies provides information about the actual state of thermodynamic rock-fluid equilibrium (a potential for precipitation or dissolution) in a reservoir system. These fluid characteristics also indicate a degree of hydrodynamic continuity of reservoir flow units at any stage of reservoir development. The in-situ chemical interaction between reservoir rock and liquids results in natural and man-induced diagenetic alterations such as mineral transformation, recrystallization, dissolution, and precipitation. It can be demonstrated that reliable, comprehensive water analyses can be used to quantitatively reconstruct geochemical conditions in a reservoir.

Hydrochemical and isotopic heterogeneity of many oil-bearing systems have been well documented worldwide (Moldovanyi and Walter, 1992; Morton and Land, 1987; Glasmann, et al., 1989; Smith, 1989; Szpakiewicz and Collins, 1985)). Geochemical anomalies of oil-associated formation waters at both regional and field scale are quite common. The anomalies are often manifested by the inversion of salinity gradient (decrease with depth) and by differentiation of hydrochemical facies. Barriers to flow prevent mixing of fluids and often manifest themselves by the spatial distribution of chemical and isotopic species in water. Also, a characteristic relationship between geochemically diagnostic ions and diversification of minor and trace components in liquids result from geochemical processes of water-rock interaction in separated fluid compartments. Geochemical information about the continuity of flow units can minimize the cost of engineering operations in a reservoir and eliminate some expensive interwell tests.

Reliable information on the distribution of resistivity, formation water salinity, and composition allows accurate interpretation of some wireline logs and provides a basis for more realistic estimation of oil saturations in reservoir systems. In addition, the often unrealistic assumption of uniform water salinity and composition in the calculation of oil reserves will lead to an error. Salts other than NaCl are present in variable concentrations in formation liquids where they affect resistivity. Highly bicarbonate-rich or sulfate-rich waters are very common in Rocky Mountain oil reservoirs (Szpakiewicz and Collins, 1985). Also, the conversion of measured water resistivity (at ambient temperature) to the actual resistivity at reservoir temperature will not be correct for hydrochemically heterogeneous systems. The conversion charts provide correct resistivity values only for sodium-chloride

solutions. As will be discussed more specifically later in this text, none of the Muddy Formation waters in Bell Creek Field and only some of the Almond Formation waters in Patrick Draw Field are of simple chloride-sodium type. Thus, oil resources calculated using the Archie equation are not correct in these reservoirs.

Hydrochemical and isotopic data collected at different production stages may facilitate estimation of sweep efficiency during waterflood and tertiary stimulation. This is done by calculation of mixing ratios between the injectors and producers. Distribution of monitored changes in produced fluid chemistry and isotopic composition will indicate preferential directions of propagation of the injection fluids. Dissolution and precipitation potential at different stages of reservoir development can be modeled on the basis of precise measurements of changing ionic composition, pH, and temperature of the involved fluids. The complete set of geochemical data necessary for computation of saturation indices are, however, rarely available.

Effectiveness of EOR chemicals such as surfactant, alkali, and polymer injected into the formation also depends to a large degree on the salinity, pH, and composition of the in situ formation waters (Jackson, et al., 1992). Significant alterations of formation mineralogy, porosity, and permeability may take place due to natural and man-induced water-rock geochemical interactions (Szpakiewicz, et al., 1987). Recent experimental studies provide excellent quantitative examples of the man-induced rock-fluid interaction products observed after exposure to high temperature and to injected foreign fluids. For example, the Lower Cretaceous Clearwater Formation sandstone (Western Canada Sedimentary Basin) is mineralogically classified as the feldspathic litharenite that contains up to 14 authigenic minerals including silicates and carbonates. After 21 days of experimental steam flooding of sandstone core the following dramatic alterations were observed by Kirk, et al. (1987):

- dolomite decreased by 70% plus
- calcite increased by up to 200%
- kaolinite decreased by 50%
- smectite increased by up to 100%

A partial dissolution of K-feldspar overgrowths and the formation of albite and certain zeolites (phillipsite?) was also observed. The man-induced geochemical alterations resulted in 85% decrease in permeability of the Clearwater Formation samples from 6 D to 900 mD. Recently reported numerical simulation (Dudley and Moore, 1992 a and b), including kinetics and fluid transport, matched the experimental results of Kirk, et al. (1987) reasonably well.

Similar geochemical processes may leave their distinct mineralogic signatures and effects on permeability during the post-depositional history of oil-bearing formations subjected to natural hot saline fluids ascending through conductive faults. A positive geothermal anomaly indicated by enhanced thermal maturity within a few thousand feet thick sequence of rocks below the productive horizons in Patrick Draw Field was documented by Law

(1992). Several thousand feet deep faults clearly show up on the seismic profiles in Patrick Draw Field area (this study). The faults were the most probable pathways for ascensions of fluids, heat, and possibly migrating hydrocarbons into the shoreline barrier sandstones of the Almond Formation. There is a good possibility that the hydrothermal processes are responsible for very poor permeability of the oil-bearing Almond Formation shoreline barrier sandstones in Patrick Draw Field.

Regional geochemical analysis of the origin, dynamics, and physico-chemical properties of the present day formation waters in the Washakie Basin, including the Almond Formation reservoir system in Patrick Draw Field, seems to be an imperative for understanding the distribution of hydrocarbons, reservoir petrophysical properties, and the potential for formation damage. Comprehensive geochemical investigation should address the distribution of in situ pressures, temperatures, salinities, resistivities, and chemical and isotopic composition of fluids.

Principles, Techniques, and Economy of Hydrogeochemical Investigation of Formation Fluids in Oil Reservoirs

The most comprehensive analysis of the petroleum hydrogeochemistry can be found in "Geochemistry of Oilfield Waters" by G. A. Collins (1975) and "Chemical Hydrogeology" by Back and Freeze (1983). Specialty journals such as *Geochimica et Cosmochimica Acta*, *Chemical Geology*, and *Applied Geochemistry* provide updated information on the theory and practical application of the hydrochemical techniques to the petroleum industry. For the purpose of this report only a few practical aspects of petroleum inorganic geochemistry will be emphasized in the context of the problems encountered during analyses of reservoir performance in Bell Creek Field, MT and Patrick Draw Field, WY.

For optimum characterization of reservoir performance representative fluid samples should be taken from all hydrocarbon-bearing reservoir horizons and monitored at different stages of reservoir development. Downhole sampling provides the best hydrochemical information. However, samples taken at the wellhead are sufficient if the well has been properly purged or had been long enough on production. The following 6 major ions should be measured because they represent the minimum geochemical information required for interpretation: sodium, calcium, magnesium, chloride, sulfate, and bicarbonate. The minor dissociated and undissociated species of potassium, strontium, manganese, barium, iron, carbonate, iodide, bromide, boron, and silica should also be analyzed in order to provide optimum geochemical information. Mineral pattern analyses (so called "short analysis") of oilfield waters are relatively inexpensive (\$100 per sample) and include; specific gravity, pH, resistivity, total dissolved solid content (TDS), sodium, calcium, magnesium, iron, chlorides, bicarbonates, carbonates, and sulfates. The cost of expanded geochemical analysis should not exceed \$200. This analysis includes the major species and properties

typically measured at the water analytical laboratory, field measurements of unstable constituents, and laboratory measurements of the most indicative minor species. Unstable constituents such as the content of dissolved and free gases, alkalinity, pH, Eh, and water temperature must be measured at the wellhead during or immediately after sample collection. Measurement of unstable parameters within an isolated flowline system (flow chamber) is preferred. Fluid separation and filtration precedes the measurement of total alkalinity which is done by titration of water samples to the inflection point of pH 3.5. This technique insures inclusion of bicarbonates and weak organic (aliphatic) acids, which sometime may dominate the alkalinity of deep-seated oil-associated formation waters (Carothers and Kharaka, 1978). Collected water samples need to be acidified and preserved before transportation to the analytical laboratory. In addition to samples taken for chemical analyses, samples of uncontaminated formation water, gas, and oil may be taken at the well site for a more sophisticated geochemical interpretation based on the stable isotope content present in all fluid phases. Samples for stable isotope ratios of the oxygen, hydrogen, carbon, sulfur, and strontium primarily should be considered because of their highly diagnostic value in the isotope geochemistry of oil reservoirs (Szipkiewicz, 1990 and 1991). An approximate cost of measuring stable isotope ratios of oxygen and hydrogen in water molecules is \$85 per sample, of oxygen and carbon in carbonates—\$45, of deuterium and carbon isotopes in methane and other gases—\$150, of sulfur in sulfates—\$65, and of strontium between \$75 and \$250 depending on the precision (interpretation costs are not included).

Sampling procedure at the wellhead and wellsite measurements of unstable constituents are inexpensive and relatively simple for the skilled hydrogeochemist. Typically, fluid sampling does not interfere with production. However, it needs to be strongly emphasized that the diagnostic value of chemical and isotopic analyses depends highly on the representativeness of the acquired samples from the horizon of interest and on the fulfillment of rigorous requirements of geochemical sampling, sample preservation, and analytical procedures.

Handling of Formation Water Geochemical Analyses

Quantitative interpretation of formation water composition enables definition of chemical water types based on the proportions of ions in the solution which exceed 20% of milliequivalents (% meq/l). For example, simple chloride-sodium type waters (Na-Cl) would contain the two major ions in excess of 90% meq/l and none of other major anions or cations exceeds 10% meq/l. The symbol Na-Cl-HCO₃ means that the formation water contains at least 20% milliequivalents of sodium, chloride, and bicarbonate, while chloride prevails over bicarbonate. In a case where bicarbonate prevails over chloride, the formula Na-HCO₃-Cl would be used. The ions present in significant reactive amounts above 10% meq/l, but below 20% meq/l are included into the chemical formula in

parentheses. For example, the formula Na-Cl-(SO₄)-(HCO₃) indicates that sulfate and bicarbonate content is significantly enhanced in the four component formation water (above 10% meq/l) while sodium must exceed 90% meq/l and chloride 60% meq/l. One should keep in mind, however, that the hydrogeochemical classification used here only depicts the reactive proportions of major water constituents and does not reflect their total concentration. Comparison of numerous tabulated water analyses data is tedious and time-consuming; therefore, different graphical methods are commonly used in hydrogeochemistry for their positive and rapid identification. For description of the methods refer to Collins, (1975); Freeze and Cherry, (1979); and Back and Freeze, (1983). Each graphical system has its merit; however, omissions of important information are unavoidable. Multiple-trilinear diagrams and Stiff diagrams have been used in this study for quantitative comparative visualization of chemical composition and salinity for several dissimilar water types encountered in the two Rocky Mountain oil reservoirs studied. Projection of analytical points from the anion and cation triangles (expressed in % meq/l) into the diamond-shaped diagram enables definition of hydrochemical facies according to the domain in which the points occur on the diagram segments. The diameter of scaled circles plotted around the point in the upper (diamond-shaped) field of the trilinear diagram indicates the total dissolved solid content of the samples. For detailed description of the graphic procedure and for additional capabilities of the methods refer to the original publications by Piper (1944), and Stiff (1951).

A rigorous approach based on quantification of water composition in an oil-bearing system allows distinction of hydrochemical facies (a paraphrase of the definition as used by sedimentologists). The geochemical analysis becomes a starting point for calculation of mineral equilibria in an oil-bearing system. Saturation indices under reservoir-specific conditions such as the pressure, temperature, pH, and chemical composition of pore-filling fluids can be calculated. Thermodynamic calculations allow fairly quantitative estimation of natural and man-induced trends of geochemical interactions between reservoir rock, formation fluids, and injected chemicals. The information obtained can be used for making reservoir management decisions regarding selection of an optimum stimulation process.

Isotopic techniques complement the information obtained by other subsurface geochemical methods. In many cases these data provide unique and inexpensive information about the reservoir system in contrast to expensive interwell testing. Isotopic data provide valuable information regarding continuity of flow units, advective transport of fluids between formations, origin of fluids encountered in reservoir, and degree of reservoir confinement. If the isotopic composition of reservoir water is chemically compatible but isotopically different than the injected water, the preferential migration paths can be detected by monitoring the isotopic composition of produced waters. Presence of short-lived isotopes such as Tritium and Carbon-14 in water samples and fluids extracted from fresh core would indicate contamination with

drilling mud. More specific information on the applicability of natural isotopes to characterization of complex reservoirs was provided earlier (Szapakiewicz, 1990; 1991).

Geochemical Detection of Flow Discontinuities, Stratification, Compartment Boundaries, Fluid Mixing in Open Systems, and Impairment of Sweep Efficiency Between Reservoir Compartments

Formation water advection, dispersion, mixing, and water-rock interaction processes govern the distribution and characteristics (hydrogeochemical facies) of fluids in a dynamic system. Monitoring salinity contrasts and variations in chemical and/or isotopic composition of the oil-associated formation waters enables identification of and provides unique information about the presence and nature of local or regional baffles/barriers to fluid flow and about the hydraulic discontinuity (compartmentalization) of reservoir flow units. On the other hand, lateral continuity of reservoir flow units or existence of vertical communication pathways between leaking horizons can be inferred when a chemical and isotopic equilibration of fluid composition in a monitored system has been achieved.

A number of recent hydrogeochemical studies provide evidence for large scale interformational flow in sedimentary basins (Szapakiewicz, 1990). In the Alberta Basin the isotopic measurements of strontium, oxygen, and deuterium combined with chemical compositional trends give evidence for two distinct water regimes in Devonian-Lower Cretaceous reservoirs and in Upper Cretaceous and younger sedimentary rocks (Connolly, et. al., 1990). The two regimes are separated by a regional transgressive shale in the Colorado Group. Cross-formational upward migration, superimposed on lateral fluid flow, was required to explain the geochemistry and isotopic systematics in the brines from Devonian—Lower Cretaceous reservoirs. Deuterium values indicated post-Laramide flushing of Tertiary waters throughout the basin, with subsequent hydrochemical isolation of the older system from the invasion of more modern waters. At the reservoir scale, the existence of untapped reservoir compartments was indicated by the detailed field studies of Stratton Field reservoirs in South Texas (Burnett, 1992). The primary reservoir compartment size averages 40 acres in Stratton Field. The compartments seem to be significantly smaller than the current completion spacing in many parts of the field. Conventional development practice will leave these compartments only partially drained (Burnett, 1992). Another case of smaller than field scale compartmentalization was reported from the Cherokee Group fluvial-dominated deltaic sandstones in the Midcontinent Region. Heavy oil occurs in discontinuous compartments of depositional and diagenetic origin which are commonly smaller than 1 acre in size (Olsen and Johnson, 1991). The compartmentalization was documented in a number of cases by ineffective

waterflooding within current completion spacing and by nearly original reservoir pressure encountered in some newly drilled infill wells (Olsen, 1992). Geochemical data which could indicate the lateral isolation of flow units at the early stage of a reservoirs' development were not collected from the Cherokee Sandstones before implementation of subsequent expensive reservoir development techniques. Equilibration of fluids with the reservoir rock-forming minerals in isolated or semi-isolated systems (compartments) should lead to a detectable differentiation of their chemical and isotopic composition.

In the Muddy Formation of Bell Creek Field, Montana an anomalously low original formation water salinity has been recorded (usually between 4,000 and 7,000 mg/l TDS at depth of 4,500 to 5,000 ft). Despite the evident lateral compartmentalization of fluids between and within production units created by the erosional, depositional, and structural features (Szpakiewicz, et al., 1989) the salinity and composition of the formation waters co-produced with oil from the Muddy Formation is relatively uniform. One hypothetical explanation of the apparently paradoxical situation is that an active vertical migration of low salinity water from a dynamic and hydrochemically uniform aquifer is still taking place through numerous conductive faults probably into all the megacompartments of the Muddy Formation. The active water flow from an unknown source into individual compartmentalized productive units A,B,C,D,E, and Ranch Creek of Bell Creek Field may be responsible for equalization of water composition. Bell Creek Field is a good candidate for genetic study of the formation waters that could lead to explanation of regional hydrodynamics and resulting hydrochemical anomalies. The case of Bell Creek Field is elaborated more specifically in succeeding sections.

In the Almond Formation of Patrick Draw Field, in contrast to Bell Creek Field, the well documented original formation water salinities vary significantly (between less than 20,000 to more than 70,000 mg/l TDS) within and between the major oil productive sandstones. The salinity and compositional contrasts, documented within the same sandstone unit and at the same time, strongly indicate lateral hydraulic discontinuity of major flow units.

There is a possibility that still active interformational supply of fluids from different sources is responsible for the documented heterogeneity. The origin of these fluids cannot be identified based on the existing geochemical data of limited quality which are discussed in the next paragraph. Without these data, however, we wouldn't even know that such a heterogeneity exists and we would not have been aware of its impact on diagenesis and oil saturation in the system.

Geochemical information on the lateral distribution of original water salinities (TDS) and resistivities (R_w) analyzed for this study in the hydrochemically heterogeneous system of Patrick Draw Field enabled re-interpretation of original water saturations (S_w) from log responses (Chapter 3). Gross error in oil saturations may still result; however, from estimation of true water resistivity at reservoir temperature where non-chlorine anions are present or dominant in a solution (Computalog

Ltd.) and this is the case in Patrick Draw and Bell Creek fields.

The distribution and geochemical characteristics of oil-associated formation waters in Bell Creek Field and Patrick Draw Field is elaborated in more detail later on in this report.

Complete hydrochemical data, if collected at different production stages, would facilitate calculation of rates of fluid advection based on mixing ratios between a network of injection and production wells. Degree of sweep efficiency during the waterflood and tertiary stimulation processes can be estimated for individual well patterns using the mixing ratios of the in situ formation water and the injected water. Unproduced reservoir compartments may be detected which provide candidate locations for infill drilling. Also, in a geochemically well documented system an original and man-induced dissolution/precipitation potential could be modeled on the basis of monitored changes in water composition, pH, and temperature.

Postulated cost-effective techniques based on monitoring of complete hydrogeochemical information holds promise for identification of larger fluid compartments and for predicting the distribution of flow units, their stratification, and reservoir response to the hydrodynamic conditions imposed by stimulation processes. However, currently even the identification of hydrochemical facies and their distribution in a developed reservoir is not commonly used by field operators for solving practical problems.

Geochemistry of Formation Waters in Patrick Draw Field, Wyoming

Data Source and Quality

The distribution of the quantity, salinity, and ionic composition of formation waters produced with hydrocarbons during the primary production stage in Monell and Arch Units, Patrick Draw Field has been analyzed and mapped on the basis of hydrochemical information stored in the Petroleum Data System - BRIN file, and in the UPRC data file. Some of the more recent water analyses were also collected from the UPRC field office in Rock Springs, WY. Distribution of documentary data points used in this study is shown on the isosalinity map (Fig. 2.1). Thirteen out of about 35 analyses available from an area larger than Patrick Draw Field were tabulated (Table 2.1). About 20 analyses come from the production area, although not all of them passed the selection criteria for analytical accuracy or for representativeness based on sampling with regard to stage of production.

Most of the available water analyses provide only basic information on the content of eight major anions and cations. Data are not available on the geochemically important divalent cations such as barium, strontium, and iron which are quite common in many oil field waters. There is no information on the content of minor and trace elements including such diagnostic geochemical indicators as iodide, bromide, and boron. There is no indication of field measurements of the unstable constituents at the

wellhead. Water resistivities were measured at ambient temperature and may not reflect the actual resistivity of liquids in subsurface where log responses were recorded. In most cases the sampling intervals are large and may include more than one sandstone layer in the Upper Almond rock suite. There are virtually no data on the isotopic composition of the originally produced liquids (before waterflood). Few water analyses postdate the primary recovery stage.

Generally, most of the available hydrochemical data from Patrick Draw Field is of limited quality and therefore the geochemical interpretation is also limited. Some water analyses had to be eliminated from consideration because either the date of sampling was not specified or the samples may have been contaminated with drilling mud. In some other water analyses, the calculated reacting values were not properly balanced between the negative and positive species. Given the incompleteness of data available it is difficult to make conclusions about the origin of formation water in the Almond Formation system. The origin of analyzed fluids (water, oil, and gas) is extremely important for answering a number of practical questions in the Patrick Draw and Bell Creek reservoirs. The differentiation of hydrochemical characteristics in Patrick Draw Field combined with thermal maturation data indicates a strong possibility of local invasions of fluids from other formations.

However, despite these limitations some general information on water composition such as the total dissolved solid content (TDS) and the major ionic composition is still of some value for practical consideration. The most reliable water analyses from Arch, East Arch, and Monell production units in Patrick Draw Field were tabulated and the reactive proportions of major ions (meq/l and % meq/l) were calculated (Table 2.1). Chemical water types were defined according to the method described above.

It was expected that comparison of water characteristics sampled during the primary production stage from different parts of the shoreline barrier reservoir would indicate the regions where hydraulic communication of liquids could be impaired or even completely disrupted.

Formation Water Characteristics: Salinity and Chemical Composition

The original formation water salinities vary significantly within the principal oil productive sandstones across Patrick Draw Field. This variation is from less than 20,000 mg/l (down dip) to more than 70,000 mg/l (up dip) sometimes within a distance of about 2 miles (Fig. 2.1). In addition to field-wide contrasts in salinity a high gradient has been monitored within the UA-5 sandstone in the area of closely spaced wells 60, 61, and 66 located in sections 3, 2, and 11 (T18N, R99W) respectively. The salinity gradient in this area is as great as 60,000 mg/l per mile. The salinity contrasts documented within the same sandstone unit before the waterflood had started strongly indicate lateral hydraulic discontinuity. If continuity of flow unit and good hydraulic communication had been

maintained, the formation fluids would have equalized their salinity and composition due to advection, convection, and gravity mixing. The location of heavier waters in the updip portion of the reservoir supports the presence of discontinuity.

Sampling information and computed results of selected high confidence water analyses are shown in Table 2.1. Geochemical water types and water resistivities also are shown. In most cases sodium and chloride ions predominate in the formation waters encountered in Arch, East Arch, and Monell production units. However, bicarbonates are typically high (usually between 2,000 and 5,000 mg/l) and in most cases they strongly influence the formation water formula. In some cases, however, the bicarbonate content exceeds 8,000 mg/l; namely, in well 61 in Monell unit and in well 80 in East Arch Unit where HCO₃ anion content reached 8,479 mg/l (17% meq/l) and 8,296 mg/l (62% meq/l) respectively. In well 80, bicarbonate amounts are much greater than chloride.

Calcium, magnesium, and sulfates can occur in amounts greater than 10% meq/l or even 20% meq/l. It is very symptomatic, in the context of fluid isolation, that in closely spaced wells such as 60 and 61 in Monell Unit (less than 0.5 a mile apart) the composition and salinity of the formation water in UA-5 sandstone was found to be very different. For example, water in well 60 contains 1,620 mg/l (11% meq/l) magnesium and 3,790 mg/l (15% meq/l) calcium while water in well 61 contains only 129 mg/l (1% meq/l) magnesium and 22 mg/l (0% meq/l) calcium. Salinity decreases 20,000 mg/l between the two wells and resistivity increases from 0.120 ohm-m to 0.168 ohm-m (at ambient temperature). Considering the drastic difference in proportion of major components in these two waters (relative to simple chloride-sodium solutions for which temperature correction charts are constructed) conversion of their resistivity from ambient to reservoir temperature conditions will involve gross corrections. Additional errors from measuring bicarbonate content and resistivity in the laboratory instead of at the wellhead are also anticipated because these parameters (as well as some others) are highly unstable. Therefore, a serious error may result when oil saturation is being calculated.

Fluid Compartmentalization

The general position of postulated barriers to flow and the location of fluid compartments in the shoreline barrier oil-bearing deposits of Patrick Draw Field was indicated in an earlier report on the "composite map" (Fig. 2.52 in Schatzinger, et al., 1992). The map was partially based on the distribution of wells producing single hydrocarbon phase (oil only) versus those producing oil and gas during initial production (IP). The timing of IP data for individual wells was not available when the map was constructed and the distribution shown depicted different (non-comparable) stages of reservoir development. This led to misinterpretation of the distribution of fluid phases during primary production stage. However the three remaining independent lines of evidence of fluid compartmentalization i.e. (1) shift of the original oil-water and oil-gas contacts,

(2) distribution of formation water salinities and variations in chemical composition, and (3) pattern of pressure depletion (drawdown) still hold true in Patrick Draw Field.

The different position of oil-water and oil-gas contacts on both sides of the northwest/southeast trending poorly-productive or non-productive zone within Arch Unit indicates effective disruption of fluid communication which is probably caused by presence of tight coquina beds and the fine grained (silty and shaley) lithologies documented in the examined cores and logs from this area. Another barrier to lateral communication of formation fluids, that trends southwest-northeast seems to exist in the Monell Unit. The hydrochemical anomaly expressed downdip by a significant decrease of formation water salinities in the Almond Formation within Monell Unit corresponds with a postulated hydrodynamic barrier. Evidence supporting the existence of such a barrier in Patrick Draw Field also includes the presence of two distinct areas of significant formation pressure drop which developed at the early stage of hydrocarbon production between April-May, 1961 and June, 1966 shown on the isobaric maps (UPRC, 1965). The areas of high pressure drawdown are located in the downdip portions of the Arch and Monell productive units, close to the oil-water contacts. During the 5-year production period, the pressure dropped at least 800 to 1,000 psi below the original formation pressure, down to 700 psi in both areas. In Monell Unit the area of maximum pressure drop is located just southeast of the high geochemical gradient zone. The 900 psi isobar curves around the 700 psi isobar in Arch and Monell units forming pressure "sinkholes" indicate potential for the presence of a flow barrier between the well drained areas (where the formation pressure dropped significantly) and the rest of the field. The pressure anomalies provide a third line of evidence for disrupted hydrodynamic communication between large portions of Patrick Draw Field. Exact boundaries of the compartments still cannot be defined due to the scarcity of reliable hydrochemical data. However, comparing Fig. 2.1 and Fig. 2.52 in Schatzinger et al., (1992) one can easily observe that (1) general orientation of the highest salinity gradient zones corresponds with boundaries of the major earlier postulated compartments, and (2) position of pressure sinkholes tends to correspond to the areas of lower salinity waters located on the downdip side of high geochemical gradient zone.

In addition to the mega-compartments smaller sub-compartments are strongly indicated by geochemical data. In Monell Unit some wells located much above the oil-water contact and structurally updip (within the oil column) co-produced with oil significant amounts of formation water while most of the other wells produced mostly oil and very limited amounts of water. For example, well 66 produced about 3,000 bbls of water before waterflood began in the area in 1968. The relatively high water production combined with the distinct variation of salinities and water composition strongly indicate lateral isolation of formation fluids trapped in the reservoir sub-compartments. Documented Na-(Ca)-(Mg)-Cl water type in the well 60 versus Na-(HCO₃)-Cl type in the nearby well 61 and simple Na-Cl type in well 66 with corresponding values of

the TDS of 72.8 g/l, 51.3 g/l, and 55.1 g/l respectively (Table 2.1 and Figs. 2.2 and 2.3) provide evidence for lack of lateral hydraulic communication between these wells.

In Arch Unit two water samples taken from well 44-35 (SE 1/4 sec.35, T20N, R99W) in March 1961 and June 1962 (Table 2.1) and a third sample taken in August 1989 revealed almost identical salinity, resistivity, and chemical composition of Na-Cl-HCO₃ type water. TDS contents were 30.7 g/l, 30.8 g/l, and 30.7 g/l respectively (Figs. 2.4 and 2.5). The hydrogeochemical data clearly indicate that about 25 years of waterflood in the area had no effect on this well; indicating that an unidentified portion of reservoir around well 44-35 is isolated.

In East Arch Unit where reliable geochemical and geological data are available, a thin impermeable swamp and marsh sequence effectively separated formation fluids contained by two sandstone units (UA-8A and UA-8B). The two sandstone units were interpreted as tidal delta facies. Vertical hydraulic isolation between the two productive horizons has been documented in well 80 located in East Arch Unit (NW1/4 sec.10, T19N, R98W). Fluid isolation is reflected by a significant difference in the produced water salinity, and bicarbonate, chloride, and sulfate ionic composition (Figs. 2.6, 2.7, and 2.8). The upper horizon (UA-8A) in well 80 contained waters of Na-Cl-(HCO₃) type and TDS content 16.2 g/l while the lower horizon contained water of Na-HCO₃-SO₄-(Cl) type and TDS content 5.7 g/l. In the lower horizon (UA-8B) sulfate content reached 1,177 mg/l (33% meq/l) and bicarbonates reached 2,123 mg/l (46% meq/l) while in the upper horizon (UA-8A) sulfates were virtually absent (in trace amount) and bicarbonate content was much higher (8,296 mg/l and 62% meq/l). Clearly, the two superimposed horizons were not in hydraulic communication. In 1990 (26 years after waters in well 80 were analyzed) the UA-8 sandstones in well 84 located less than one mile northwest of well 80 produced the formation water of much higher salinity (45.7 g/l) and different chemical composition (Na-Cl type) (Table 2.1 and Figs. 2.9 and 2.10). This clearly indicates an impairment or disruption of hydrodynamic communication between the stratigraphically equivalent sandstones in wells 80 and 84. An alternative interpretation is also possible; well 84 could be naturally "supplied" with waters from a different source while both UA-8 horizons in well 80 were isolated from this source (and from each other). There is also a slight possibility that in well 84 communication was established between different horizons during engineering activity. The water is very similar in composition to the Fox Hills Formation water (Table 2.1 and Figs. 2.11 and 2.12). The problem cannot be solved at this point without stable isotope analyses of waters (and gases) in different formations.

Migration of foreign fluids into some of these mega-compartments and sub-compartments from distant sources at a certain time of reservoir evolution is highly possible, mostly because of the anomalous geochemical characteristics of the original (pre-waterflood) reservoir waters identified in the updip portions of the oil column. Their high salinity (twice as great as an average ocean water) and ionic composition cannot be explained by

interaction processes of autochthonous (in situ) waters with the Almond Formation rocks. Carbonate cement is common in cores from Patrick Draw Field. Vertical fractures filled with layers of calcium-magnesium carbonates are also observed. However, the oyster shells in coquina layers which are commonly observed in outcrops and cores of the Upper Almond Formation are macroscopically in good condition i.e. without obvious indication of leaching. Therefore, it is concluded that fluids from which the cement and fracture fill precipitated had to be allochthonous (of foreign source and origin). In contrast to the Muddy Formation, where carbonate shells were not found (because they must have been dissolved), the formation waters flushing the Almond Formation sediments since the time of their deposition obviously had to be oversaturated with respect to carbonates. Stylolite seams observed under microscope in some shells (Chapter 4) were formed by the process of pressure solution. However, stylolitization could provide probably limited amounts of calcite and not the dolomite which is also observed in fractured cores and must be allochthonous.

Impaired horizontal communication between the compartments prevented lateral chemical equilibration of water composition within the Almond Formation. Conductive faults could provide pathways for the inferred cross-formational (vertical) flow or seepage of allochthonous waters into the Almond Formation. Contrasts in salinity and chemical composition between compartments indicate different sources and probably origins of liquids migrating into individual compartments of the Almond Formation. Voluminous active (present day) natural flood of ascending deep-seated fluids seems to be unlikely primarily because there is no obvious indication of foreign water influx to the producing wells and there are no signs of pressure maintenance due to natural water drive within the compartments. However, although they may not show up in quantity during reservoir development, even small volumes of the ascending waters are significant in geologic time because they introduce significant alterations to local formation fluids and minerals. Only advanced geochemical methods such as spectral analysis of diagnostic minor and trace elements and the isotopic techniques are capable of identifying the processes involved and their origin.

Production Relationships and Anomalies in Arch Unit of Patrick Draw Field

Some major trends and anomalies in well productivity within the Almond Formation in Arch Unit, Patrick Draw Field were identified in this study:

- Initial Production (IP) vs. Cumulative Production (CP)
- IP vs. product of k, phi, and oil saturation
- CP vs. product of k, phi, and oil saturation
- IP vs. sandstone thickness
- CP vs. sandstone thickness

The plots (Figs. 2.13 through 2.17) indicate a fairly distinctive positive relationship between productivity (IP

and CP) and the fundamental reservoir parameters. A number of wells, however, significantly depart from the relationships, i.e. the oil production is not directly related to either sandstone thickness, or the product of rock petrophysical properties and oil saturation, or both. For example, wells 16, 20, 21, and 44 in Arch Unit produce much more oil than indicated by all of the general trends, while some other wells perform below expectations with respect to either sandstone thickness or the product of k, phi, oil sat., or both. Well 18 is an example where the initial production (IP) was lower than indicated by productivity trend for most of the wells in Arch Unit with respect to the sandstone thickness and the product of k, phi, and oil saturation. However, well 18 performed above expectation as the indicated by relationship between cumulative production and the product of k, phi, and oil saturation seen in the general productivity trend.

A geologic reason for the anomalies is not clear based on depositional and structural analysis. However, there seems to be a straightforward relationship between productivity and reservoir compartmentalization indicated by the hydrogeochemical analysis. Almost all superior producers in Arch Unit, i.e. wells 20, 21, and 44 and the very good producers (well 3 and 4) in Arch Unit are located within a megacompartiment where the highest formation water salinity of 70 g/l TDS and more prevails, while a group of inferior producers (performing much below expectation defined by general production trends) such as the wells 2, 10, 13, 34, 42, and 54 are located within the narrow zone of the highest hydrochemical gradient where salinity decreases from 70 g/l to 20 g/l (Fig. 2.1). As noted earlier the zone of salinity decrease is interpreted as a boundary between major compartments in Patrick Draw Field where flow conditions are impaired. Well 18 where IP was lower than expected but cumulative production versus product of k, phi, and oil saturation was above expectation is located near the 70 g/l isosalinity contour on the updip side of the highest hydrochemical gradient and the postulated barrier.

Another group of wells of poor productivity (41, 94, 27, and 70) is located on or in close proximity to the NE-SW trending barrier zone shown earlier on the "composite map" (Fig. 2.52 in Schatzinger, et al., 1992). The barrier was indicated by reservoir pressure drawdown which developed between 1961 and 1966 and was discussed above in more detail. Poorly-productive wells 42 and 54 are located in SE 1/4 sec.11 and NE sec.14, respectively, where the two postulated barriers to flow meet each other.

In summary, the general location of earlier postulated NW-SE trending barrier in Arch Unit of Patrick Draw Field and the location of superior and inferior oil producing wells correspond to the high hydrochemical gradient zone defined by the largest contrasts in formation water salinity which separates major fluid compartments. Position of postulated NW-SE and NE-SW barriers in Arch Unit of Patrick Draw Field and the location of inferior producers corresponds fairly well with trends of minimum thickness (less than 10 ft) of the UA-5B sandstone, shown earlier on the isopach map (Fig 2.11 in Schatzinger, et al., 1992). The latter barriers outline the area of maximum pressure decrease in Arch Unit. There is little doubt that the documented

hydrochemical contrasts, pressure depletion areas, thickness of major producing sandstone (UA-5B), and oil productivity are interrelated in Arch Unit. Less is known at this point about their relationships and their geological explanation in Monell Unit.

Geochemistry of Formation Waters in Bell Creek Field

Data Source and Quality

The source of hydrochemical data collected from the Muddy Formation in Bell Creek Field and their quality is analogous to that of Patrick Draw Field. Most of the work at NIPER in Bell Creek Field was done in 1986-1989. At that time attention was focused predominantly on the sedimentological, structural, and engineering aspects of the reservoir. Geochemical data related to productivity of the Muddy system were not acquired. Basic hydrochemical data available from the former field operator were not systematically collected.

Thirty water analyses available from Petroleum Data System (PDS) files were collected for this study from all 6 production units and from the surrounding aquifer in the Muddy Formation of Bell Creek Field (Fig. 2.18). The field was discovered in 1967 and most of the water sampling took place in 1968 before the waterflood was implemented. The formation water was sampled from wells located both updip and downdip of the oil producing reservoir. For comprehensive information on the geology and structural characteristics of the Muddy Formation in Bell Creek Field the reader may refer to Szpakiewicz, et al., (1989). Nine of the analyses were selected on the basis of similar quality criteria to those applied in Patrick Draw Field. The analyses were re-calculated according to geochemical standards and results tabulated (Table 2.2). Selected data points are located in production units A, B, C, D, and in the aquifer southeast of unit A and northwest of unit B (Fig. 2.18).

Formation Water Characteristics: Salinity and Chemical Composition

Salinity and chemical characteristics of the formation waters co-produced with oil from the Muddy Formation in Bell Creek Field are surprisingly uniform and do not seem to be depth related. Total dissolved solid content (TDS) is much lower than in the Almond Formation of Patrick Draw Field. TDS content varies in Bell Creek Field between about 4.0 g/l and 7.5 g/l (the average sea water has 35.0 g/l TDS) while the variation in Patrick Draw Field is between less than 20g/l to more than 70 g/l. Both reservoirs are at similar depth between 4,500 and 5,000 ft.

Chemical composition of water varies in Bell Creek Field only slightly and mostly due to changing relative reacting proportions of bicarbonates in the solution (Table 2.2 and Figs. 2.19 through 2.26). Average sea water salinity and composition also has been shown on the trilinear and Stiff diagrams for comparison. The formation

waters in the Muddy Formation of Bell Creek Field are predominantly of Na-Cl-HCO₃ type. In all cases, however, chloride definitely predominates over bicarbonates (59% meq/l to 83% meq/l vs. 14% meq/l to 39% meq/l respectively). Calcium, magnesium, and sulfates occur in negligible proportions of major ions (between 0% meq/l and 2% meq/l). Reported water resistivities (measured at ambient temperature) vary in narrow range between 1.05 ohm-m to 1.34 ohm-m.

The anomalously low salinity at reservoir depth (4,600 ft.), stable chemical composition, and the origin of bicarbonates which are common in the present formation waters of Bell Creek Field is puzzling. Calcite cement is quite common in cores and outcrops of the Muddy Formation sandstones. The cement precipitated from formation waters oversaturated with respect to carbonates. In contrast to the Almond Formation, traces of surviving marine shells can not be found either in outcrop sections or in subsurface cores of the Muddy Formation. This indicates that at some time after sedimentation of the shoreline barrier sandstones waters extremely undersaturated with respect to carbonates penetrated the system dissolving the previously—deposited carbonate (marine shells). Present formation waters in Bell Creek reservoir do not contain much calcium or magnesium in solution while bicarbonate content is high. This composition indicates that previously dissolved material was flushed out of the system and new fluids entered the system. Reconstruction of the dynamic conditions would provide a chance for predicting diagenetic pattern of the field.

However, even the present hydrodynamics and hydrogeochemistry of the system between outcrops of the Muddy Formation in NE Wyoming and Bell Creek reservoir at 4,600 ft is poorly understood. Few systematic studies on the subject have been reported. Regional hydrodynamic study in the northern Powder River Basin (Smith, 1988) indicates general groundwater flow downdip into the basin center. Bell Creek Field is located in a low potentiometric gradient area while significant pressure differences (high gradients) occur just updip from the producing field and further southeast between outcrops and the field. This indicates an impairment or disruption of hydrodynamic communication of meteoric waters with formation waters within the oil field. Therefore, desalinization of formation waters at reservoir depth by descending meteoric waters is unlikely.

A potential for mixing of fluids between the Muddy and another formation cannot be positively estimated without stable isotope data. It is quite remarkable that fresh waters do occur below the Muddy Formation in the Powder River Basin. In Bell Creek Field water from the Pennsylvanian Madison Formation aquifer is used for injection. The water is nearly fresh (1.2 g/l TDS) and is high in calcium and fairly high in magnesium. The hypothetical concept of possible active migration through faults of allochthonous waters derived from a dynamic aquifer is rather intuitive than based on solid facts. It is conceivable, however, that waters from a strong aquifer may ascend or descend and equilibrate the chemical characteristics of waters in laterally disconnected hydraulic units within the Muddy Formation

in Bell Creek Field. At this point, however, there is probably no other reasonable explanation of the observed phenomenon.

Conclusions

1. Successful enhanced oil recovery depends much on prediction of the actual distribution of water and hydrocarbons in a productive system and on the distribution of petrophysical properties resulting from water-rock interaction processes. A recommendation is provided for the broader use of effective and economical hydrogeochemical techniques as an assistance in predicting reservoir performance. The recommendations can be easily applied by field operators to their advantage.
2. Typically, the available data for hydrogeochemical analysis are of limited quality and allow only a limited interpretation. It is recommended that a more comprehensive approach to geochemical characteristics of formation fluids in productive reservoirs be obtained by monitoring changes in fluid composition with time and by including more sophisticated tools in the analysis such as measuring stable isotope ratios.
3. Based on available hydrogeochemical data of limited quality, a strong hydrogeochemical anomaly has been identified and mapped in the Almond Formation of the Washakie Basin where Patrick Draw Field is located. High salinity formation waters (more than 70 g/l TDS) occur in the updip portions of Arch and Monell production units while brackish waters (20 g/l TDS and less) are found downdip, closer to the oil-water contact.
4. Distinctly different fluid regimes were identified in portions of Patrick Draw Field by quantitative determination of hydrogeochemical facies of reservoir waters. High salinity gradient zones indicate positions of barriers to lateral flow. Major reservoir compartments and local subcompartments were inferred within the Almond Formation on the basis of salinity gradients and differences in chemical composition of the formation waters.
5. High salinity and sometimes unique composition of formation waters in the updip portion of Patrick Draw reservoir cannot be explained by autochthonous (in situ) processes of water-rock interaction. Contrasts in salinity and chemical composition between compartments indicate that allochthonous (of different source and probably origin) fluids migrated into individual compartments of the Almond Formation.
6. Faults are the most probable pathways for interformational migration of fluids from which the fracture fill and matrix cement precipitated. Therefore, the most diagenetically affected parts of reservoir should be sought in the neighbourhood of structural disturbances indicated by well log and seismic analyses (Chapter 2 and 3).
7. The strong hydrogeochemical indication of fluid compartments within the Almond Formation and a probability of vertical migration of fluids through faults provide a guidance for enhanced oil recovery tactics, contributes to an improvement of flood patterns, and may be useful to guide selection of the best prospective sites for

infill drilling within untapped compartments.

8. In the Arch Unit of Patrick Draw Field most wells of superior productivity (producing more oil than the general trends) are concentrated in the high salinity megacompartments while the wells of inferior productivity (performing below expectation) are predominantly located within the zone of highest hydrochemical gradient which indicates the position of barrier to lateral flow. It indicates a relationship between oil productivity and reservoir compartmentalization.

9. There is little doubt that the salinity contrast zones, heterogeneity of water composition, pressure depletion zones, thickness of the major producing sandstone, and productivity of wells are interrelated in Arch Unit. Less is known at this point about the relationships and their geologic reason in Monell Unit.

In Bell Creek Field, Montana lateral compartmentalization of productive units within the Muddy Formation is evident based on earlier geological and engineering analysis.

10. A potential for vertical communication of fluids through conductive faults between the Muddy Formation and an unidentified aquifer is indicated by strong hydrogeochemical anomalies that include low salinities and nearly complete homogenization of water composition across the Bell Creek Field despite the presence of barriers to lateral flow.

11. In contrast to Patrick Draw Field, probably a single, dynamic, allochthonous source of water is involved in the inferred mixing process between formations because relatively uniform salinities and composition of formation waters were documented in all four horizontally separated productive units of the Muddy Formation in Bell Creek Field.

References

- Back, W., and R. A., Freeze, 1983, *Chemical Hydrogeology: Benchmark Papers in Geology*. v. 73, Hutchinson Ross Publishing Company, 416 p.
- Burnett, W., 1992, GRI R&D Highlights for the First Quarter of 1992: GRI, pages unnumbered.
- Carothers, W., and Y. Kharaka, 1978, Aliphatic acid anions in oil-field waters—Implication for origin of natural gas: *AAPG Bull.*, v. 62, no. 12, p. 2441-2453.
- Collins, A. G., 1975, *Geochemistry of oilfield waters, developments in petroleum science*: v. 1, Elsevier Scientific Publishing Company, 496 p.
- Computalog Ltd., Chart Book, no date, Computalog Ltd., pages unnumbered.
- Connolly, C. A., L. M. Walter, H. Baadsgard, and F. J. Longstaff, 1990, *Applied Geochemistry*: v. 5 no. 4, p. 397-413.

- Dudley, J. S., and C.H. Moore, 1992a; Coupled reaction transport modeling of oil steam stimulation (Abs.): 1992 AAPG Annual Convention Program, Calgary, Alberta, p. abstract 33.
- Dudley, J. S., and C. H. Moore, 1992b, Computer modeling of steam flood experiments: Preprint 7th International Symposium on Water-Rock Interaction, Park City, Utah, 5 p.
- Glasmann, J. R., R. A. Clark, S. Larter, N. A. Briedis, and P. D. Lundegard, 1989, Diagenesis and hydrocarbon accumulation, Brent Sandstone (Jurassic), Bergen High Area, North Sea: AAPG Bull. v. 73, no. 11, p.1341-1360.
- Freeze, R. A., and J. A. Cherry, 1979, Groundwater: Prentice-Hall, Inc., 604 p.
- Jackson, S., M. M. Chang, and M. Tham, 1992, Data requirements and acquisition for reservoir characterization: DOE Report NIPER-615, 25 p.
- Kirk, J. S., G. W. Bird, and F. J. Longstaffe, 1987, Laboratory study of the effects of steam-condensate flooding in the Clearwater Formation: high temperature flow experiments: Bull. Canadian Petroleum Geology, v. 35, no.1, p 34-47.
- Law, B. E., 1992, Paleofluid flow paths—Evidence from thermal maturity mapping, Greater Green River Basin, Wyoming and Utah: (Abs.) 1992 AAPG Annual Convention Program, Calgary, Alberta, abstract 73.
- Moldovanyi, E. P., and L. M. Walter, 1982, Regional trends in water chemistry, Smackover Formation, Southwest Arkansas: geochemical and physical controls: AAPG Bull. v. 76, no. 6, p. 864-894.
- Morton, R. A., and L. S. Land, 1987, Regional variations in formation water chemistry, Frio Formation (Oligocene), Texas Gulf Coast: AAPG Bull., v.71, no. 2, p.191-206.
- Olsen, D., and W. Johnson, 1991, Feasibility study of heavy oil recovery in the Midcontinent region (Oklahoma, Kansas, Missouri): Quarterly Technical Report, January-March; DOE Report NIPER-529, 62 p.
- Olsen, D., 1992, personal communication, NIPER.
- Piper, A. M., 1944, A graphic procedure in the geochemical interpretation of water analyses: American Geophys. Union Trans., v. 25, p. 914-923.
- Schatzinger, R. A., M. Szpakiewicz, S. R. Jackson, M. M. Chang, B. Sharma, and M. K. Tham, 1992, Integrated geological-engineering model of Patrick Draw Field and examples of similarities and differences among various shoreline barrier systems: DOE Report NIPER-575, 146 p.
- Smith, D. A., 1988, The integration of hydrodynamics and stratigraphy, Muddy Sandstone, northern Powder River Basin, Wyoming and Montana: Wyoming Geological Association Guidebook Diedrich, R. P., M. A. K. Dyka, W. R., Miller (Eds.), Thirty-ninth Field Conference, p.179-189.
- Smith, L. R., 1989, Regional variations in formation water salinity, Hollin and Napo formations (Cretaceous), Oriente Basin, Ecuador: AAPG Bull. v. 73, no. 6, p. 757-776.
- Stiff, H. A., Jr., 1951, The interpretation of chemical water analyses by mean of patterns: Jour. Petroleum Technology , v. 3, no.10, p.15-16.
- Szpakiewicz, M., 1990, Application of natural isotopes in groundwater for solving environmental problems: DOE Report NIPER-450, 70 p.
- Szpakiewicz, M., 1991, Identification of cross-formation flow in multireservoir systems using isotopic techniques (Phase 1): DOE Report NIPER-538, 38 p.
- Szpakiewicz, M., and A. G. Collins, 1985, Hydrochemical study of the Upper Cretaceous and Lower Tertiary Formations in the Uinta, Piceance, and Green River Basins: Implications for oil- and gas-related problems: DOE Report NIPER-95, 70 p.
- Szpakiewicz, M., K. McGee, and B. Sharma, 1987, Geological problems related to characterization of clastic reservoirs for enhanced oil recovery: SPE Formation Evaluation, v. 2, no. 4, December, p. 449-460.
- Szpakiewicz, M., R. Schatzinger, M. Honarpour, M. Tham, and R. Tillman, 1989, Geological and engineering evaluation of barrier island and valley-fill lithotypes in Muddy Formation, Bell Creek Field, Montana: in E. B. Coalson (Ed.) Petrogenesis and Petrophysics of Selected Sandstone Reservoirs of the Rocky Mountains Region, Rocky Mountain Association of Geologists, p. 159-182 and color plates p. 330-333.
- UPRC, 1965, Isobaric map of Patrick Draw Field.

Table 2.1. Salinity (TDS), Ionic Composition (milligrams per liter=mg/l), Reacting Values (milliequivalents per = meq), Chemical Types Based on Percentage of Milliequivalents (%meq), and Resistivities (ohm-m) of Selected Formation Waters Co-Produced with Oil from the Upper Cretaceous Almond Formation in Monell (M) and Arch (A) Production Units of Patrick Draw Field, Wyoming.

Prod unit	Well no	Sampled horizon, depth, ft	SS unit	Date of sample	TDS g/l	Na ⁺ mg/l meq % meq	K ⁺ mg/l meq % meq	Mg ²⁺ mg/l meq % meq	Ca ²⁺ mg/l meq % meq	ΣK meq % meq	Cl ⁻ mg/l meq % meq	HCO ₃ ⁻ mg/l meq % meq	CO ₂ ⁻ mg/l meq % meq	SO ₄ ²⁻ mg/l meq % meq	ΣA meq % meq	Ion balance	Chemical Water type determined by % meq	R _w ohm-m (68°F)
M	60	4,554 4,582	UA-5 A&B	4/64	72.8	21,223 924 74	150 4 0	1,620 133 11	3,790 189 15	-- 1,250 100	42,000 1,184 95	3,977 65 5	0 0 0	0 0 0	-- 1,249 100.0	-- 1.00	Na-(Ca, Mg)-Cl	0.120
M	61	4,740 4,774	UA-5 A&B	3/64	51.3	18,510 805 98	80 2 0	129 11 1	22 1 0	-- 819 99	24,000 677 83	8,479 139 17	108 4 0	0 0 0	-- 82.0 100.0	0.990	Na(HCO ₃)-Cl	0.168
M	66	4,695 4,725	UA-5 A&B	8/65	55.1	20,519 893 97	90 2 0	155 13 2	205 10 1	-- 918 100	30,400 857 93	3,697 61 7	0 0 0	0 0 0	-- 918 100.0	1.000	Na - Cl	0.150
M	31	5,218 5,242	UA-5B	8/65	17.9	6,192 269 100	35 1 0	2 0 0	11 0 0	-- 270 100	5,100 144 33	5,246 86 32	1,200 40 15	75 2 1	-- 2.70 101.0	--	Na-Cl-HCO ₃ -CO ₃	0.490
M	78	5,449 4,502	UA-5 UA-6	12/59	29.2	10,300 448 97	0 0 0	66 5 1	171 9 2	-- 462 100	13,200 372 81	5,441 89 32	1 0 0	16 0 0	-- 46.1 100.0	1.000	Na-Cl-HCO ₃	--
M	3	3,112 3,400	Fox Hills	4/62	56.2	21,462 934 97	-- -- --	131 11 1	336 17 2	-- 962 100	33,500 945 98	622 10 1	173 6 1	20 0 0	-- 96.2 100.0	1.000	Na-Cl	0.140
A	44-35	4,511 4,518	UA	6/62	29.0	11,158 485 97	-- -- --	90 7 1	202 10 2	-- 502 100	15,700 443 88	3,636 60 12	-- -- --	23 0 0	-- 503 100.0	1.000	Na-Cl-(HCO ₃)	0.261
A	44-35	4,552 4,562	UA	3/61	29.2	10,951 476 94	-- -- --	212 17 3	271 14 3	-- 507 100	16,200 457 90	3,001 49 10	-- -- --	58 1 0	-- 507 100.0	1.00	Na-Cl-(HCO ₃)	0.248
A	105	4,589 4,602	UA-6	10/67	23.0	8,807 383 96	70 2 0	40 3 1	178 9 3	-- 397 100	12,500 353 89	2,635 43 11	-- -- --	65 1 0	-- 397 100.0	100.0	Na-Cl-(HCO ₃)	0.320
A	80	5,956 5,968	UA-8A	6/64	16.2	4,888 213 96	66 2 1	63 5 2	14 1 0	-- 221 99	2,500 71 32	8,296 136 62	408 14 6	Tr 0 0	-- 221 100.0	0.990	NaHCO ₃ -Cl	0.650
A	80	5,956 5,996	UA-8B	5/64	5.7	1,544 67 87	105 3 4	14 1 1	112 6 8	-- 77 100	400 11 14	2,123 35 46	180 6 8	1,177 25 33	-- 77 101.0	0.990	Na-HCO ₃ -SO ₄ (Cl)	1.900
A	84	--	UA-8	1/90	42.6	16,197 705 99	0 0 0	54 4 0	120 6 1	-- 715 100	24,500 691 96	1,659 27 4	0 0 0	0 0 0	-- 718 100.0	1.000	Na-Cl	--
A	67	--	UA-6	5/63	45.7	17,400 757 98	-- -- --	98 8 1	140 7 1	-- 772 100	26,500 747 97	1,525 25 3	0 0 0	-- -- --	-- 772 100.0	-1.00	Na-Cl	--

Table 2.2 Salinity (TDS), Ionic Composition (milligrams per liter=mg/l), Reacting Values (milliequivalents=meq), Chemical Types Based on Percentage of Milliequivalents (% meq), and Resistivities (ohm-m) of Selected Formation Waters Co-Produced with Oil from the Lower Cretaceous Muddy Formation in Production Units A,B,C, and D of Bell Creek Field, Montana.

Prod unit	Well no.	Sampled horizon depth, ft	SS unit	Date of sample	TDS g/l	Na ⁺ mg/l meq % meq	K ⁺ mg/l meq % meq	Mg ²⁺ mg/l meq % meq	Ca ²⁺ mg/l meq % meq	ZK -- meq % meq	Cl ⁻ mg/l meq % meq	HCO ₃ ⁻ mg/l meq % meq	CO ₃ ²⁻ mg/l meq % meq	SO ₄ ²⁻ mg/l meq % meq	ΣA -- meq % meq	Ion balance	Chemical Water type determined by % meq	R _w ohm-m (68 F)	
A	22-5	--	Muddy	Oct-70	7.5	2,547	27	21	35	--	2,950	1,928	--	7	--	--	1.04	Na-Cl-HCO ₃	1.04
						111	1	2	2	116	83	32	--	0	115	1			
A	35-12	4,302-4,307	Muddy	Dec-68	7.2	2,090	565	8	19	--	2,800	1,635	36	1	107	1	1.08	Na-(K)-Cl-HCO ₃	1.08
						91	14	1	1	107	79	27	1	0	99	0.99			
A	15-7	4,640-4,648	Muddy	Dec-68	7.4	2,546	26	13	22	--	2,960	1,830	0	5	--	--	1.04	Na-Cl-HCO ₃	1.04
						111	1	1	1	114	83	30	0	0	113	1			
A	2-12	4,358-4,464	Muddy	N/A	5.0	1,739	17	6	25	--	2,100	1,135	0	1	--	--	--	Na-Cl-HCO ₃	--
						76	0	0	1	77	59	19	0	0	78	0.99			
B	29-1	4,472-4,496	Muddy	Dec-68	6.9	2,456	23	9	31	--	3,222	1,122	0	25	--	--	1.05	Na-Cl-(HCO ₃)	1.05
						107	0	1	2	110	91	18	0	0	109	1			
B	8-12	4,552-4,619	Muddy	Feb-70	6.7	2,321	20	3	18	--	2,640	1,684	0	26	--	--	1.22	Na-Cl-HCO ₃	1.22
						101	0	0	1	102	74	28	0	0	102	1			
C	9-4	4,470-4,600	Muddy	N/A	4.3	1,414	20	5	15	--	1,340	1,513	0	1	29	--	--	Na-Cl-HCO ₃	--
						62	1	0	1	64	38	25	0	1	64	1			
D	32-12	4,556-4,562	Muddy	Dec-68	6.0	2,006	25	11	222	--	2,080	1,769	60	10	--	--	1.34	Na-Cl-HCO ₃	1.34
						87	1	1	1	90	59	29	2	0	90	1			
D	1-15	4,347-?	Muddy	Jun-68	6.8	2,397	0	68	22	--	3,352	958	0	34	--	--	--	Na-Cl-(HCO ₃)	--
						104	0	6	1	111	95	16	0	1	111	1			
						94	0	5	1	100	86	14	0	1	101	0.99			

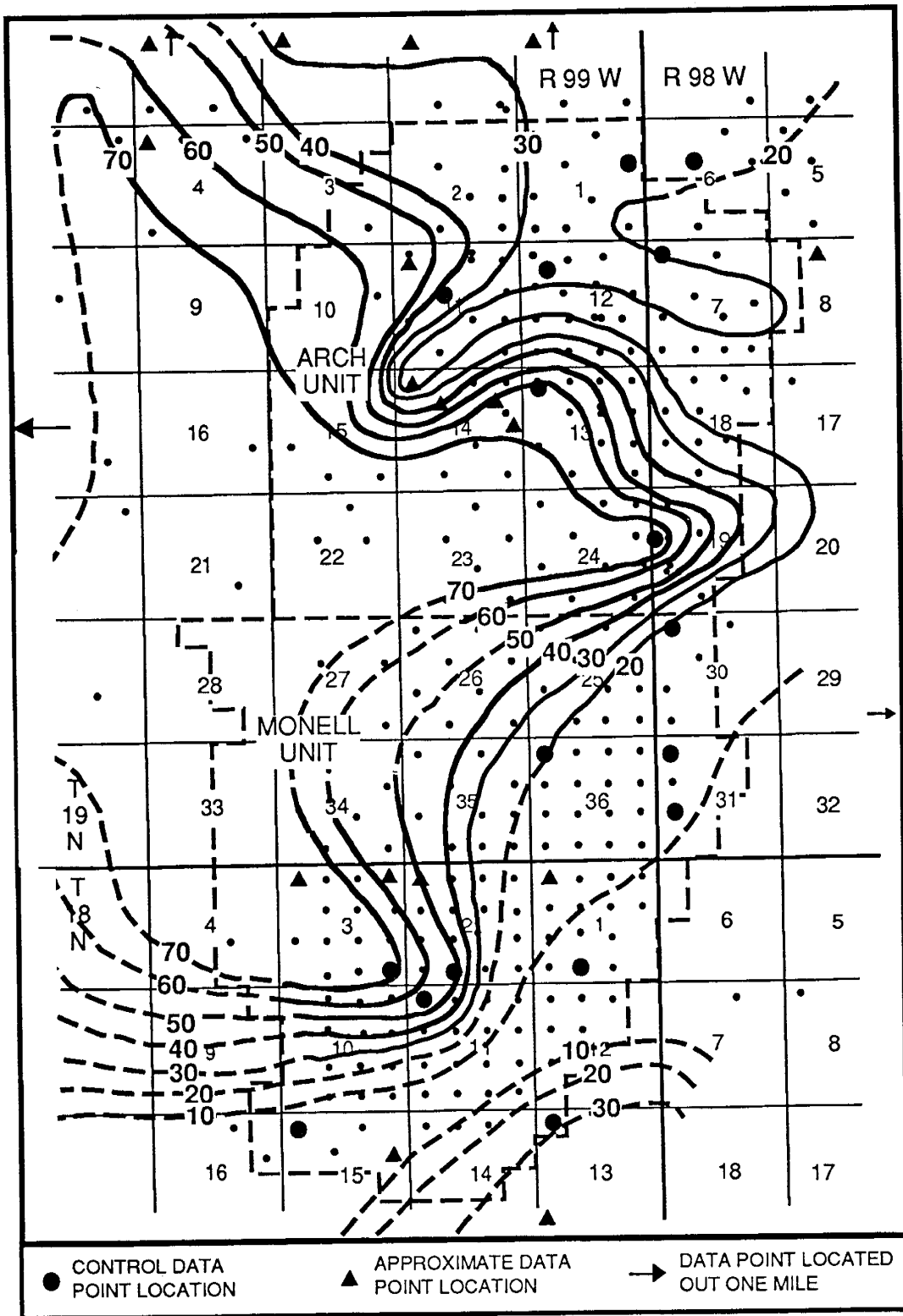


Fig. 2.1. Isosalinity map of formation waters in the Almond Formation of Patrick Draw Field (in g/l).

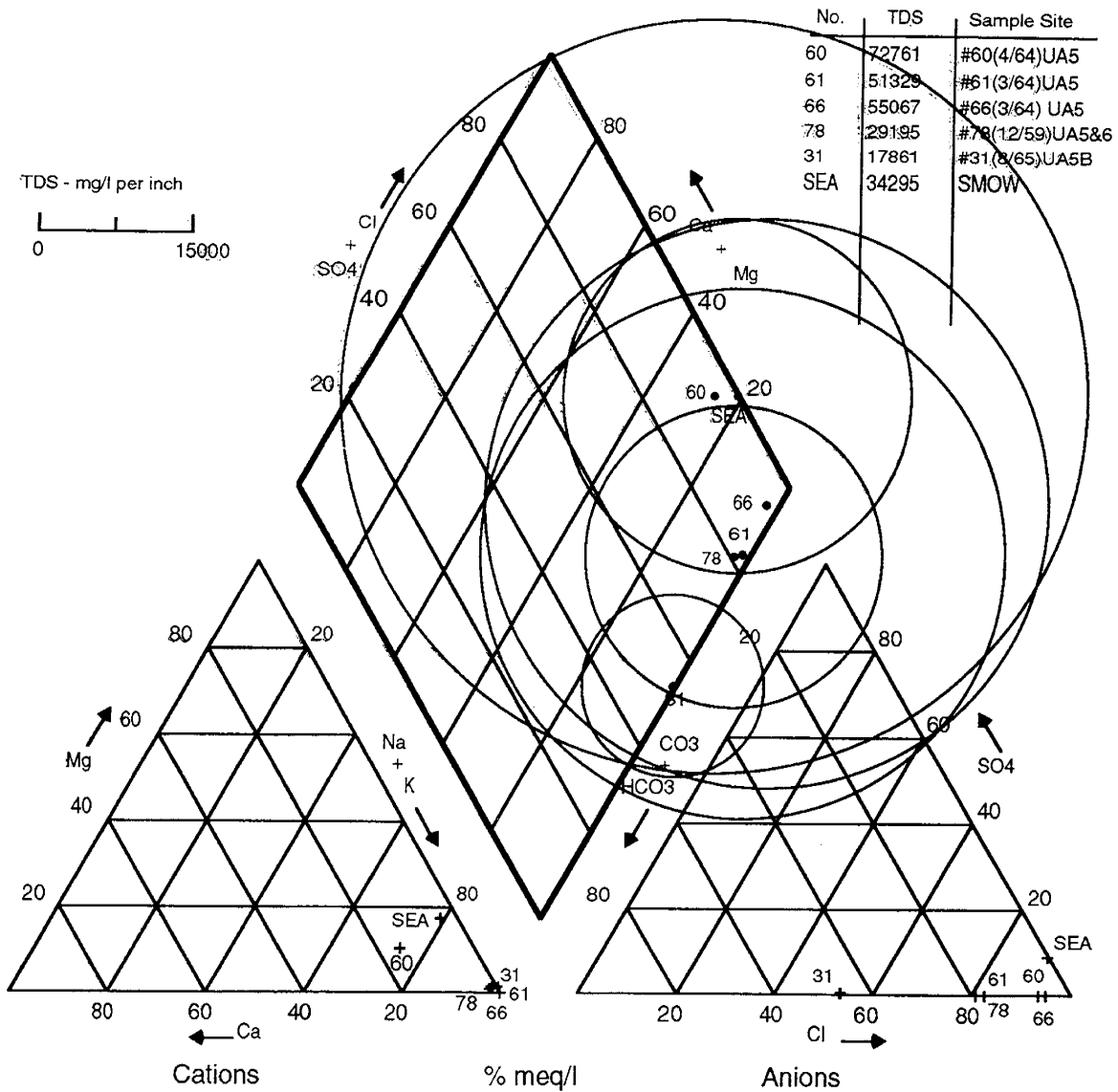


Fig. 2.2 Composition and salinity of selected formation waters in the Almond Formation of Monell Unit shown on the ternary diagram; Patrick Draw Field (for explanation refer to text). Standard Mean Ocean Water (SMOW).

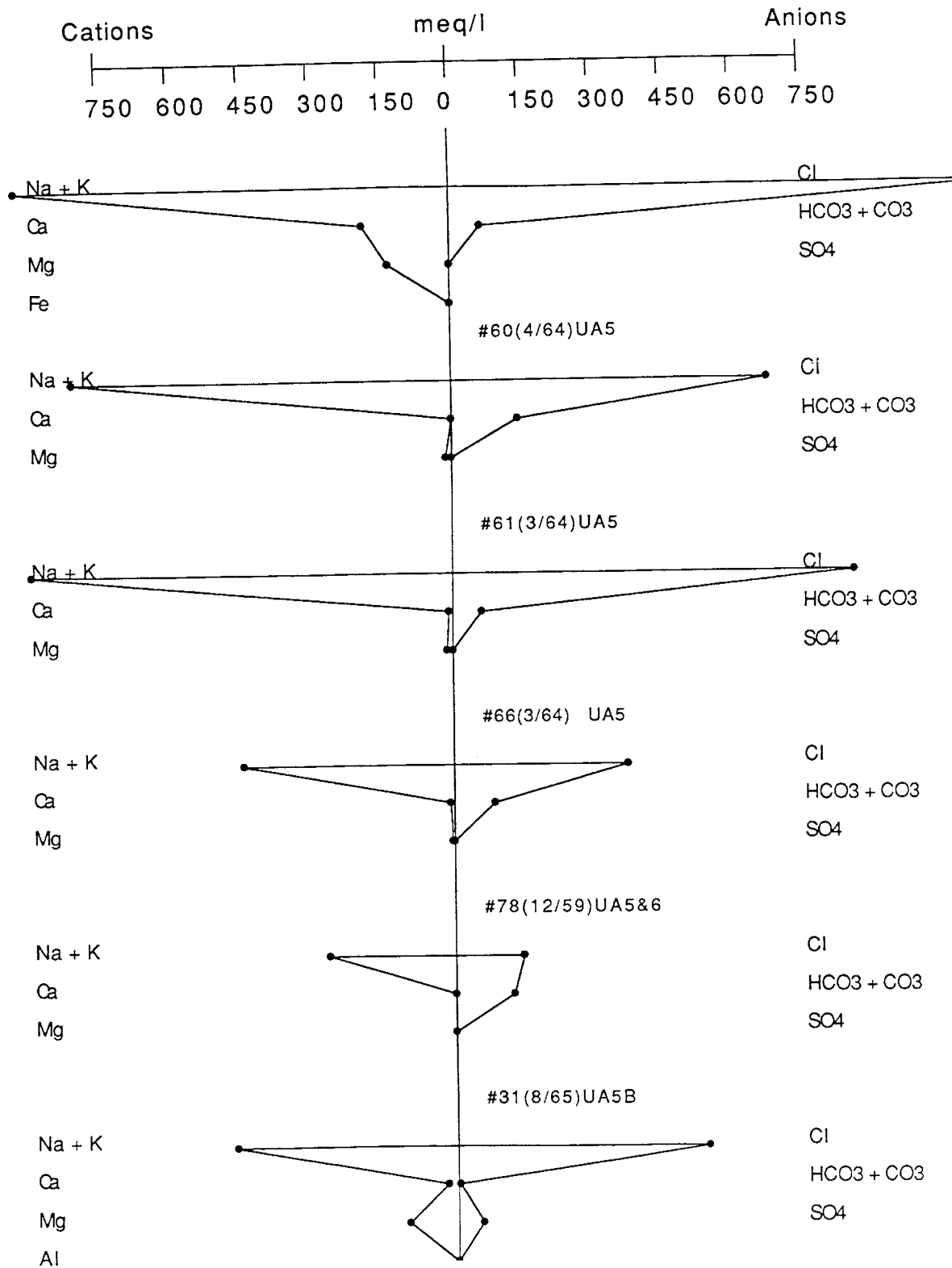


Fig. 2.3. Composition of selected formation waters in the Almond Formation of Monell Unit, Patrick Draw Field shown on the Stiff diagram (for explanation refer to text). The last Stiff diagram presents for comparison the average composition of present sea water. Well number (#), date, (month, year) and unit is indicated for each sample.

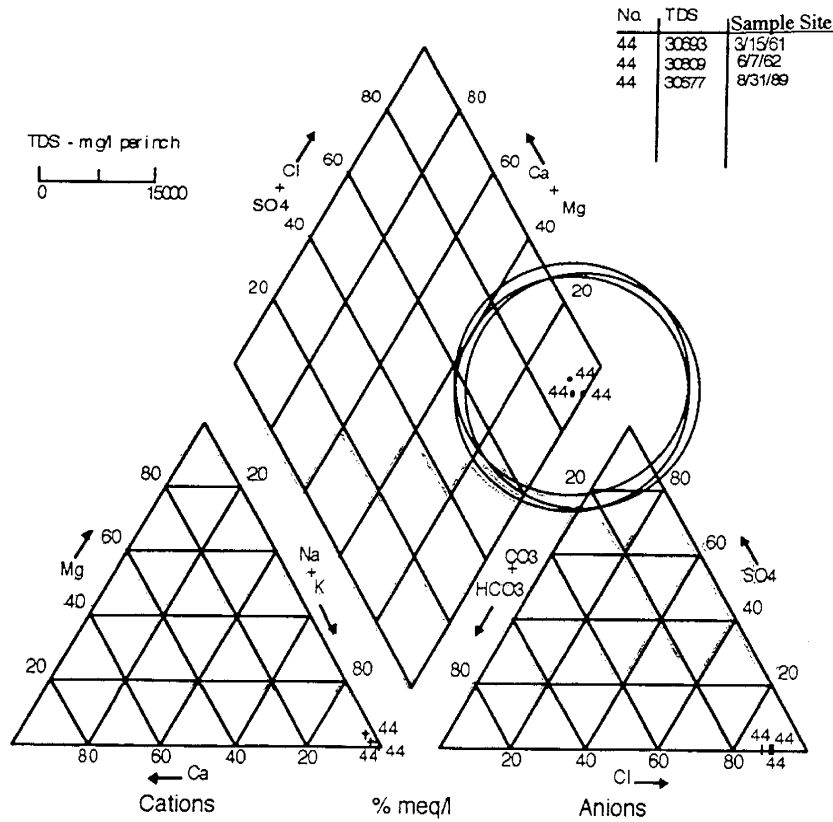


Fig. 2.4. Formation water composition and salinity monitored in 1961, 1962, and 1989 shown on the trilinear diagram; well 44-35, Arch Unit, Patrick Draw Field.

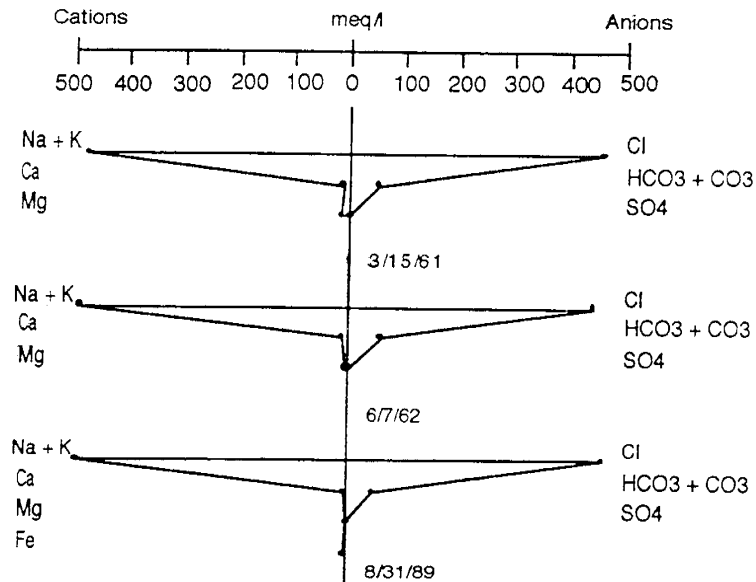


Fig. 2.5. Formation water composition monitored in 1961, 1962, and 1989 shown on the Stiff diagrams; well 44-35, Arch Unit, Patrick Draw Field. Composition of average sea water Standard Mean Ocean Water (SMOW) also is shown for comparison.

Measured Section
Well Arch Unit 80
SENW Sec. 10, R98W, T19N

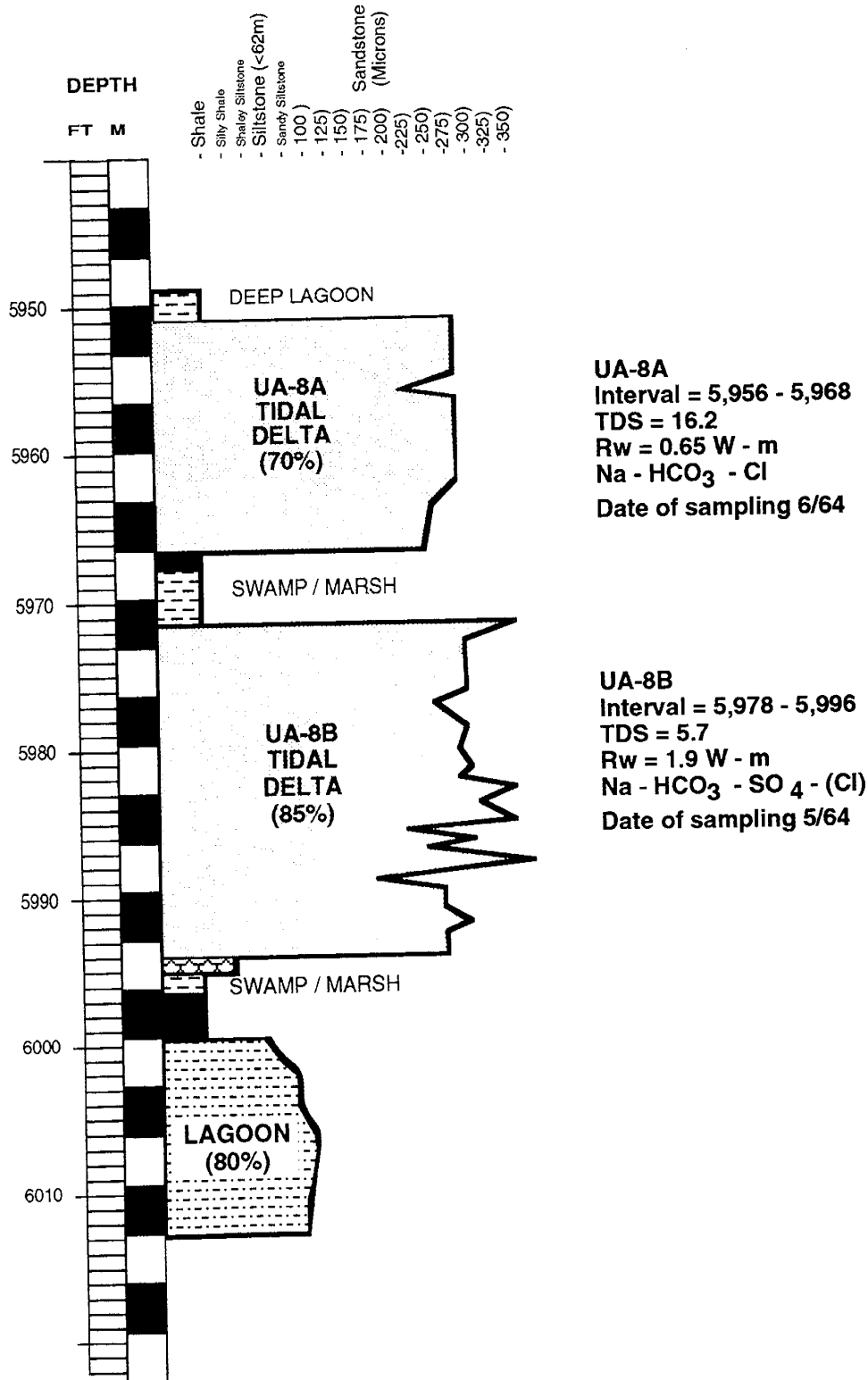


Fig. 2.6. Formation water salinities (TDS), resistivities (Rw), and chemical formulas in two productive sandstone units (UA-8A and UA-8B) interpreted as tidal delta facies with 70% and 85% confidence level respectively; well 80, East Arch Unit, Patrick Draw Field. Note separation of the two medium size grained sandstones by shaly and coaly swamp and marsh facies. For graphic illustration of the formation waters in the two horizons refer to figures 2.8 and 2.9.

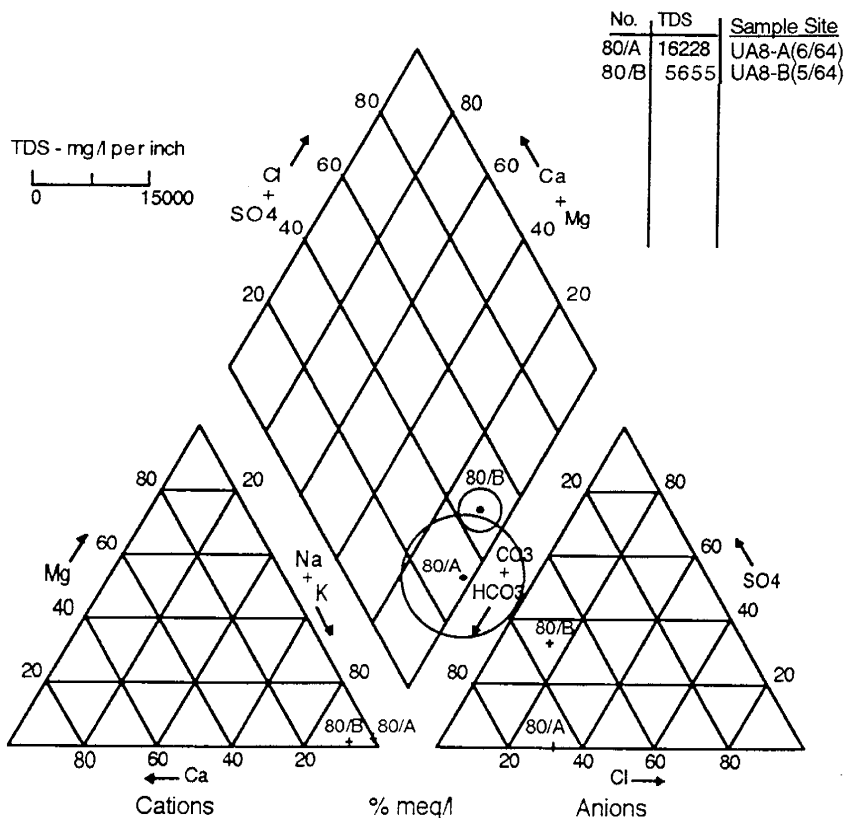


Fig. 2.7. Composition and salinity of formation waters in UA-8A and U8A-B sandstone units in well 80 shown on the trilinear diagram; Almond Formation, East Arch Unit, Patrick Draw Field.

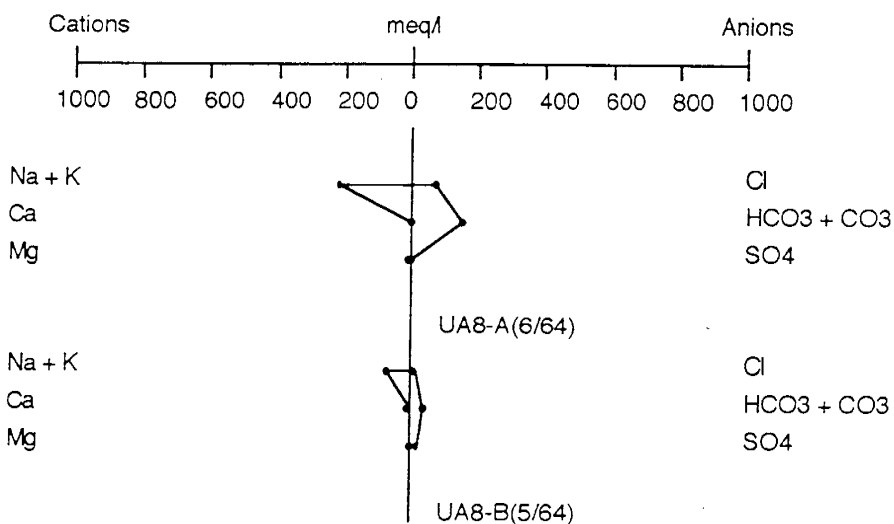


Fig. 2.8 Composition of formation waters in UA-8A and U8A-B sandstone units in well 80; Almond Formation, East Arch Unit, Patrick Draw Field shown on the Stiff diagrams. Unit and date (month and year) are indicated for each sample.

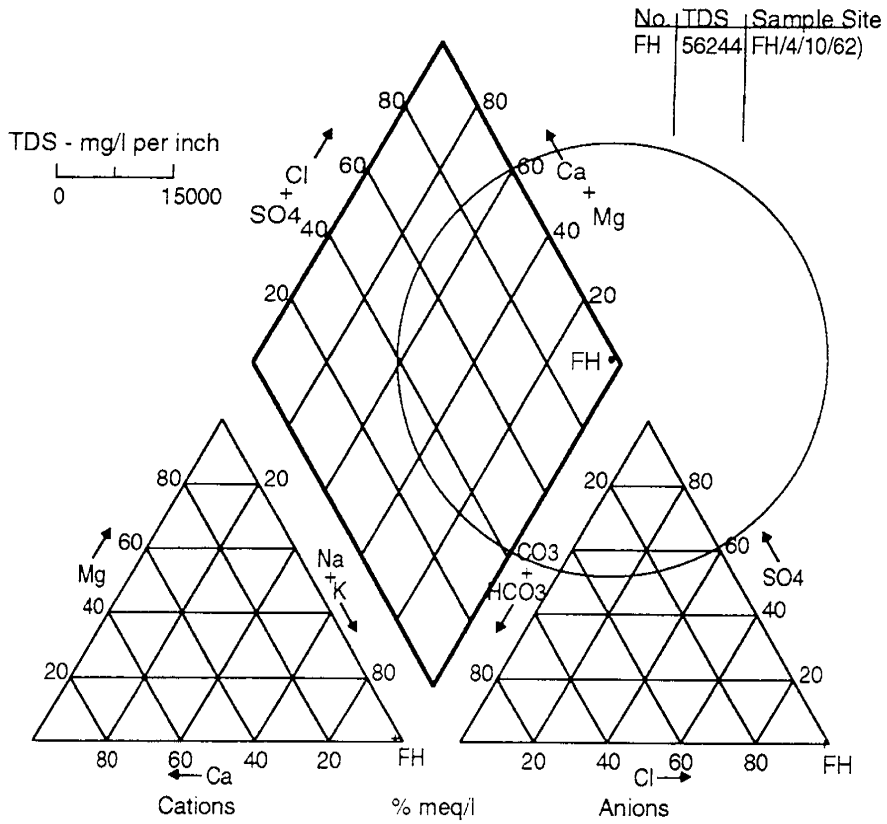


Fig. 2.11. Composition and salinity of formation water in the Fox Hill Formation sandstone overlying the Almond Formation; Monell Unit, Patrick Draw Field shown on the trilinear diagram.

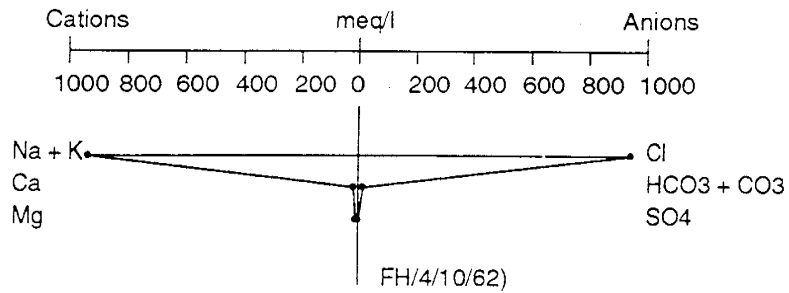


Fig. 2.12. Composition of formation water in the Fox Hill Formation sandstone overlying the Almond Formation shown on the Stiff diagrams; Monell Unit, Patrick Draw Field. Formation and date (month and year) are indicated for each sample.

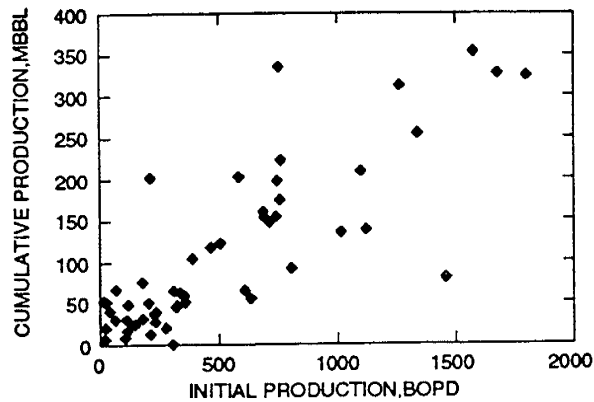


Fig. 2.13. Relationship between initial production (IP) and cumulative production (CP) in wells of Arch Unit, Patrick Draw Field. General trend for most wells is quite clear although a group of wells departs from this trend.

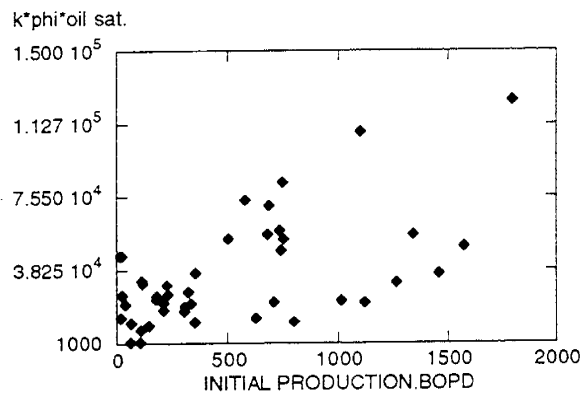


Fig. 2.14. Relationship between initial production and product of permeability, porosity, and oil saturation in wells of Arch Unit, Patrick Draw Field. Some wells initially produced more oil than indicated by the general trend.

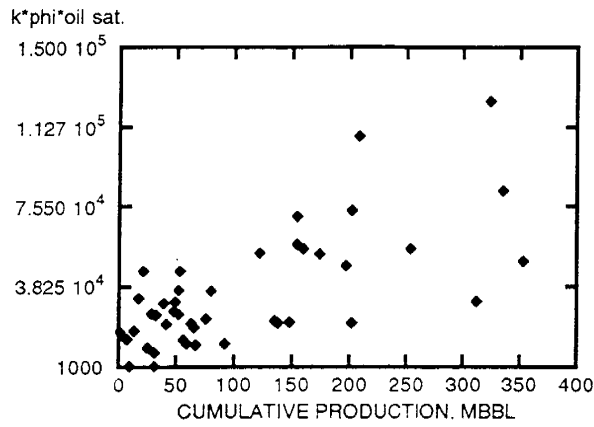


Fig. 2.15. Relationship between cumulative production and product of permeability, porosity, and oil saturation in wells of Arch Unit, Patrick Draw Field. A group of wells collectively produced more oil than indicated by the general trend.

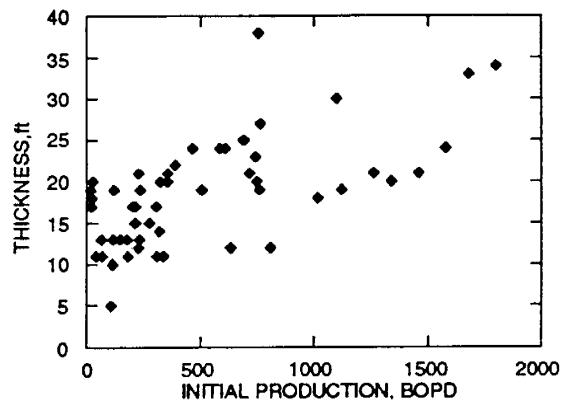


Fig. 2.16. Relationship between initial production and thickness of net pay in wells of Arch Unit, Patrick Draw Field. There is no clear trend in the relationship.

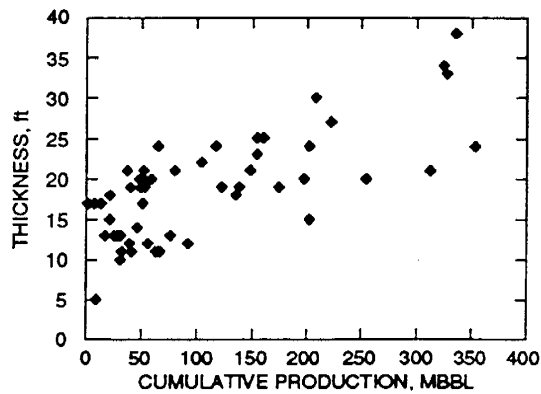


Fig. 2.17. Relationship between cumulative production and thickness of the net pay in wells of Arch Unit, Patrick Draw Field. A group of wells cumulatively produced more oil than indicated by the general trend.

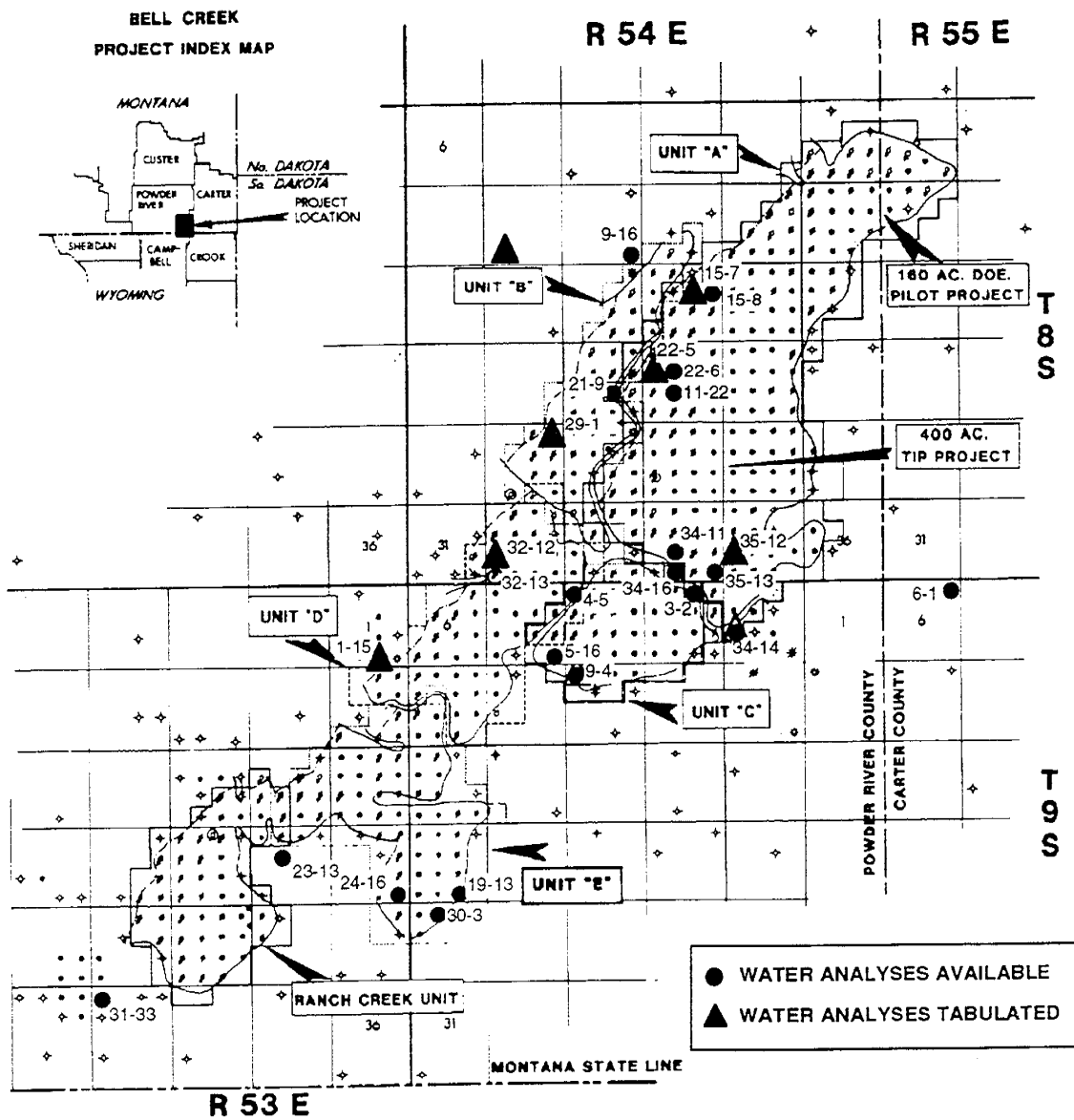


Fig. 2.18. Location of formation water data points in the Muddy Formation of Bell Creek Field, Montana. Analytical data from sample points shown in triangles were calculated and the chemical water types were interpreted in table 2.2.

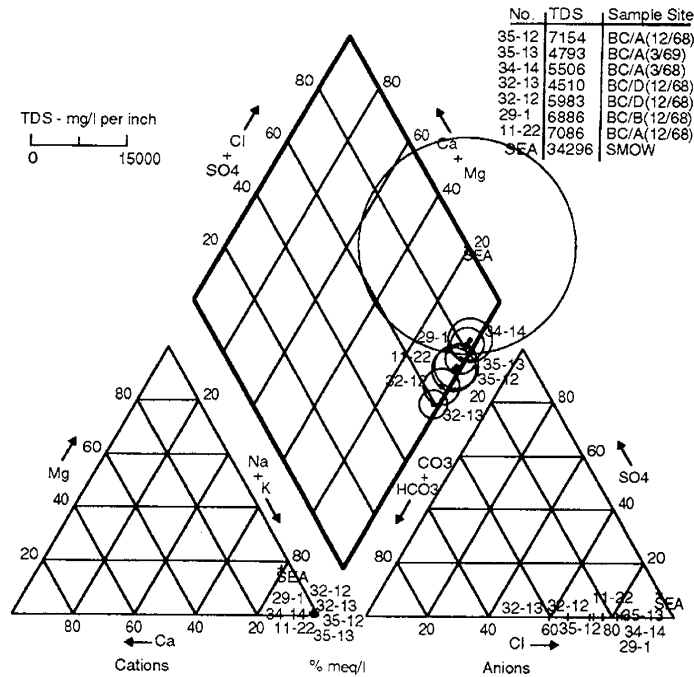


Fig. 2.19. Composition and salinity of formation waters (set 1) in the Muddy Formation shoreline barrier sandstones shown on the trilinear diagram; Bell Creek Field, Montana. Average sea water salinity and composition is shown for comparison.

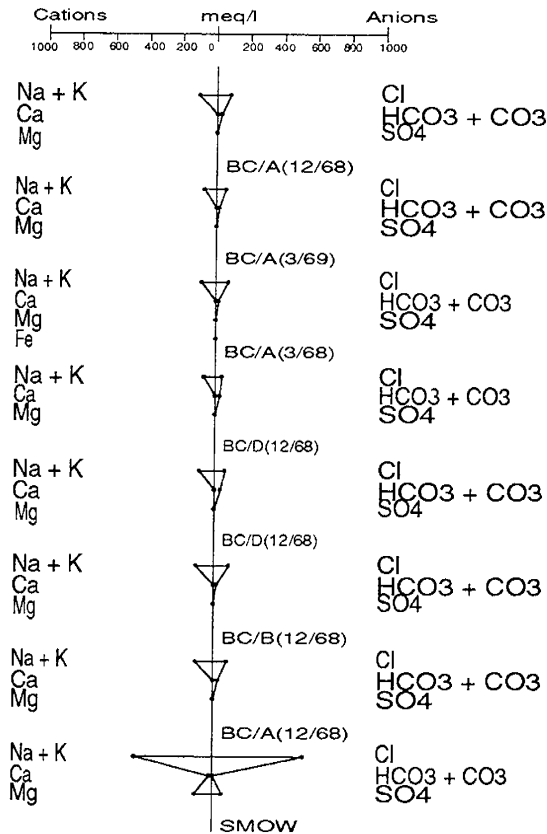


Fig. 2.20. Composition of formation waters (set 1) in the Muddy Formation shoreline barrier sandstones shown on the Stiff diagrams; Bell Creek Field, Montana. Field and date (month and year) are indicated for each sample.

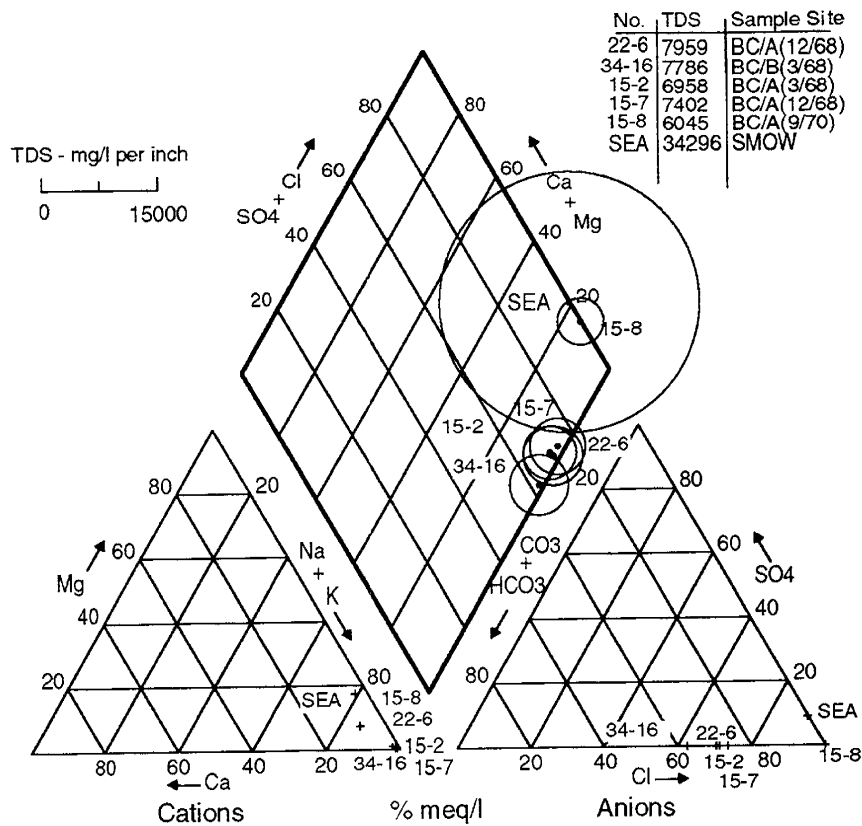


Fig. 2.21. Composition and salinity of formation waters (set 2) in the Muddy Formation shoreline barrier sandstones shown on the trilinear diagram; Bell Creek Field, Montana. Average sea water salinity and composition is shown for comparison.

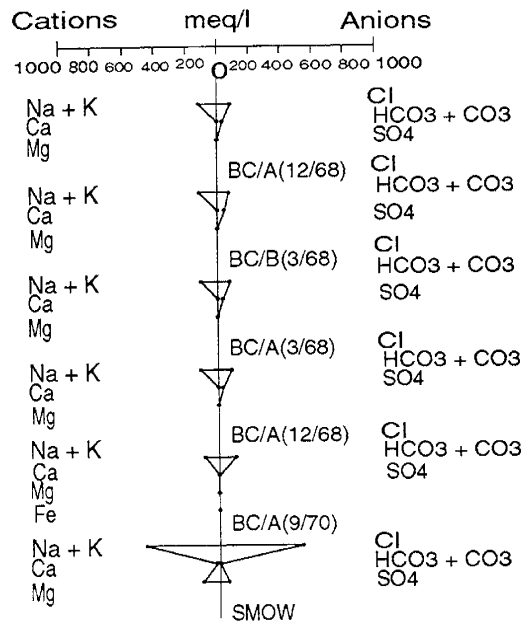


Fig. 2.22. Composition of formation waters (set 2) in the Muddy Formation shoreline barrier sandstones shown on the Stiff diagrams; Bell Creek Field, Montana. The last Stiff diagram illustrates for comparison the composition of present sea water. Formation and date (month and year) are indicated for each sample, Standard Mean Ocean Water (SMOW)

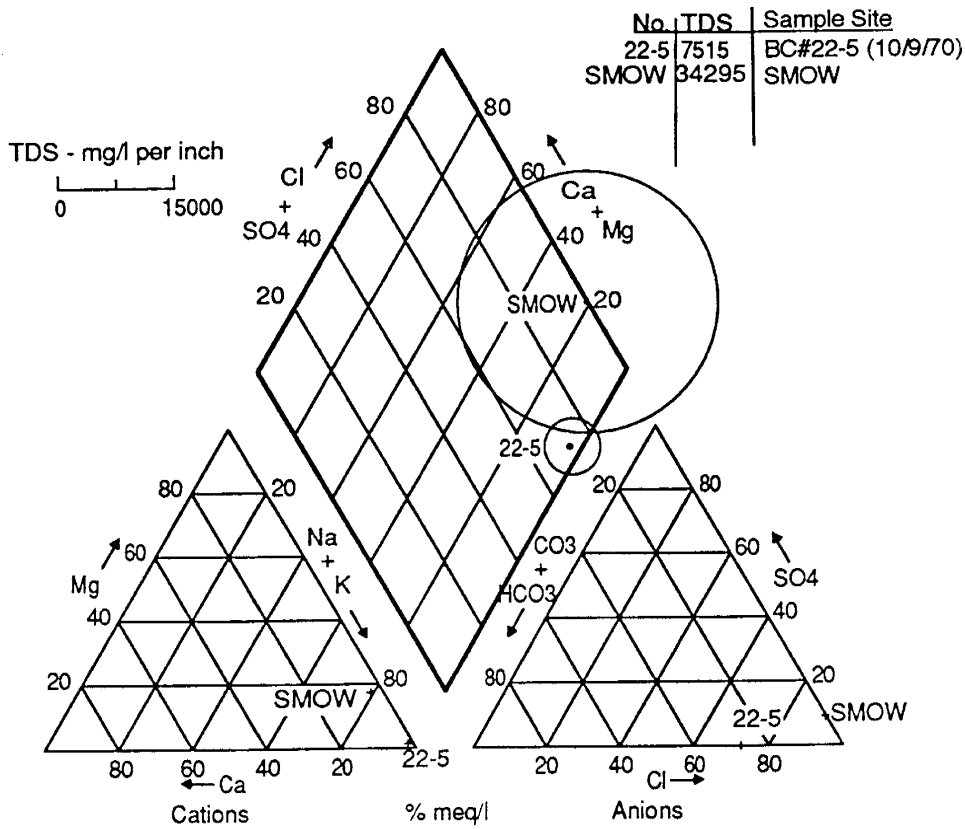


Fig. 2.25. Comparison of composition and salinity of "typical" formation water in Bell Creek Field with composition and salinity of average present sea water shown on the trilinear diagram.

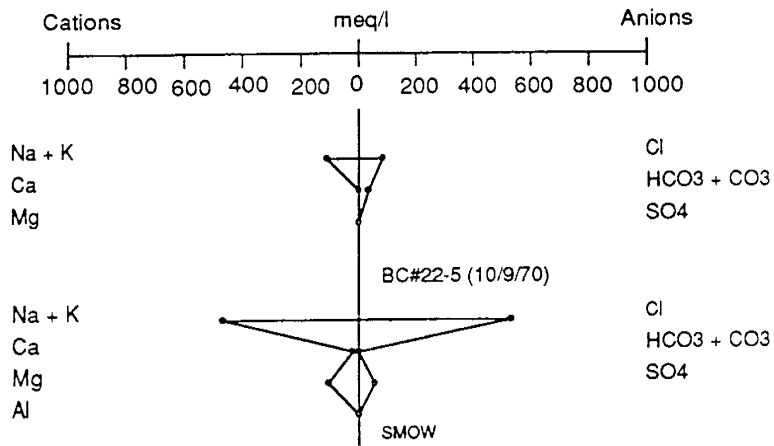


Fig. 2.26. Comparison of composition and salinity of "typical" formation water in Bell Creek Field with composition and salinity of average present sea water shown on the Stiff diagram. Field and date (month and year) are indicated for each sample, Standard Mean Ocean Water (SMOW)

CHAPTER 3

THE EFFECT OF SALINITY VARIATIONS ON OIL SATURATION CALCULATIONS FROM WIRELINE LOGS AT PATRICK DRAW FIELD

By B. Sharma, M. Chang, and M. Szpakiewicz

Chapter Summary

Accurate estimation of water saturation by wireline logs is strongly dependent upon the accuracy of formation water resistivity (R_w) values which has been shown to vary over a wide range in the UA-5B reservoir at Patrick Draw Field. Calculation of water saturation profiles based on water resistivity values ranging from 0.1 to 0.5 ohm-meter resulted in a range of average water saturations from 34% to 76%, the difference between a good oil reservoir and a residual oil reservoir. A constant value of water resistivity based on an assumption of a homogeneous distribution of salinity is often used in interpreting oil reserves from resistivity logs. Comparison of oil saturation distribution based on a constant R_w value and that based on Archie's equation and accurate salinity data resulted in a 5 to 12% difference in saturation values in the Patrick Draw Field.

Comparison of log analysis methods to determine the effect of salinity and clay content on various log analysis methods indicated that in moderately low (<8%) clay filled sandstones with relatively small amounts of clays (<1%) that have high cation exchange capacities, the Simandoux's method gives reliable estimates of S_w . The calculated S_w values by the Dual water model which indirectly computes the cation exchange capacity (CEC) from the V_{cl} data, were similar to those obtained from the Simandoux's method. This confirms that the high CEC clays probably had a negligible effect on the S_w calculations in Patrick Draw Field.

Introduction

Accurate estimates of oil saturation are important for calculation of hydrocarbon reserves, the determination of the effectiveness of primary and waterflood recovery processes, the distribution of oil saturation remaining after waterflood, and the evaluation and selection of EOR methods. Calculation of oil saturations from wireline logs require accurate water resistivity values. A constant value of water resistivity based on the assumption of a homogeneous distribution of salinity is often used to determine oil reserves from resistivity logs. However, the distribution of water salinity may not be homogeneous as is the case in Patrick Draw field.

The highly heterogeneous distribution of formation water salinities in Patrick Draw Field shown in figure 2.1 results in a corresponding broad range of water resistivities. Water resistivity values measured at 68° F vary from 0.12 ohm-m (for 72.8 g/l TDS in well Monell 60) to 1.02 ohm-m (for 7.6 g/l TDS in well East Arch 80) (Table 3.1). The

relationship between water salinities and resistivities presents a smooth curve with an exponential decrease in resistivity values between 5 and 15 g/l TDS (Fig. 3.1).

The sensitivity of log-derived water saturation calculations were investigated using the Archie equation, commonly used for open hole resistivity logs to evaluate oil and gas saturations in clean sands. The calculation shows that for relatively clay-free sandstones, the water saturation value will increase 41% from its initial value when the R_w value in Archie's equation is doubled and other parameters in Archie equation remain constant. When the R_w value in Archie's equation is reduced by one half, the calculated water saturation will decrease by 30% from its initial value. This difference in apparent water saturation could change the interpretation of an oil-producing reservoir to a water-producing reservoir or vice versa. It is obvious that we cannot afford this range of uncertainty in the evaluation of oil reserves.

To illustrate the effect of resistivity values on water saturation calculated from logs, the water saturation profiles of well 46 in the Arch Unit, Patrick Draw Field were calculated using different water resistivity values. Figure 3.2 shows interpretations of water saturation profiles based on water resistivity values ranging from 0.1 to 0.5 ohm-meter. This results in a range of average water saturations from 34% to 76%, the difference between a good oil reservoir and a residual oil reservoir.

Water Saturation Calculations in Patrick Draw Field

Based on the salinity map in figure 2.1 and resistivity measurements in figure 3.1, the initial water saturations using Archie's equation were calculated for each well in Patrick Draw Field. Although Archie's equation does not account for the effects of clay, it was used in this study because it is commonly used, and the X-ray diffraction measurements of UA-5 reservoir sandstone samples in Patrick Draw Field indicate relatively low amounts of clay (3-4% by weight) (Schatzinger et al., 1992). Even though log-derived clay values indicate higher clay content in some zones (V_{cl} values up to 25%) (Schatzinger, et al. 1992), the calculations using the Archie's equation will give an approximate idea about the effect of R_w variations on the distribution of oil saturation values in the relatively cleaner reservoir sandstones.

The water resistivity values were determined from figure 3.1 according to the corresponding salinity value of the well. The water resistivity value was then adjusted for the formation temperature of the studied well using the

Schlumberger resistivity chart (Schlumberger, 1972) to account for the temperature effect on the water resistivity values. The formation temperature of UA-5 sands ranges from 104°F up-dip on the western edge to 120°F down-dip on the eastern edge in Patrick Draw Field.

Different water distributions were obtained in Patrick Draw Field for different water salinity distributions. Figure 3.3 shows the distribution of initial water saturation in Patrick Draw Field based on a constant R_w value of 0.2 ohm-meter, originally used to evaluate oil resources in the field. Values of 0.62, 2.16, and 2 were substituted for a , m , and n , respectively, in Archie's equation for calculating S_w for each foot of pay in each well. The arithmetic average of S_w values of each well was used for preparing the saturation map.

Figure 3.4 shows the distribution of water saturations in Patrick Draw Field calculated using Archie's equation and resistivity values that correspond to the salinity map in figure 2.1. The same values of a , m , and n as those used in developing figure 3.3 were used. Figure 3.4 shows a significant difference from figure 3.3 in S_w values in both Arch and Monell Units. Because of high water salinity values in the southern part of Arch Unit, the calculated S_w values in figure 3.4 are lower than those in figure 3.3 in that area, thus a larger amount (more than 8%) of oil in place is indicated by the more accurate saturation calculations presented in figure 3.4. In contrast, less oil reserve is indicated in the northern part of Arch Unit. The difference in water saturation interpretations by subtracting S_w values in figure 3.4 from that in figure 3.3 is shown in figure 3.5.

Similar water saturation values were found in the eastern part of the Monell Unit in both figures 3.3 and 3.4. A lower S_w value is shown in the western part of the Monell Unit in figure 3.4 compared to that in figure 3.3. This is caused by relatively high TDS values ranging from 40,000 to 70,000 ppm in the western part of the Monell Unit. The low S_w values in the western part of Monell Unit add more than 8% to the oil resources in that area (Fig. 3.5). This suggests a higher potential resource than previously calculated in the western part of Monell Unit for the tertiary recovery even after successful production during primary and secondary stages.

An additional source of error in the oil saturations based on the distribution of salinities and corresponding resistivities comes from the assumption that the formation water composition is a simple sodium-chloride type. The conversion of resistivity values measured at ambient temperature to the resistivity at reservoir temperature is based on the graphic relationship between resistivity and temperature in NaCl solutions. However, the documented composition of formation waters in Patrick Draw Field based on geochemically defined water types (Table 2.1) reveals the common presence of bicarbonates and even domination of bicarbonates over chloride at certain locations. This is predominantly in waters of lower salinity. This means that the revised oil saturations are probably nearly correct in the high salinity portions of the Patrick Draw Field where Na-Cl, Na-(Ca)-(Mg)-Cl, and Na-

Cl-(HCO₃) waters dominate but may be overestimated in the low salinity sections where Na-HCO₃-Cl, Na-Cl-HCO₃ and Na-Cl-(HCO₃) waters tend to predominate.

The Effect of Salinity and Clay Content on Various Log Analysis Methods

Besides salinity of formation water, the other reservoir parameters, that have a strong effect on the estimation of water saturation are the porosity and the shale or clay content in the sandstone pore spaces (Asquith, 1989; Crain, 1986; Dewan, 1983). The clay content and porosity at Patrick Draw Field could be calculated very accurately from the available gamma ray and density or other porosity logs (Sharma, 1992; NIPER, 1991), respectively. Table 3.2 shows the reservoir parameters used in the determination of porosity and clay content in the producing UA-5B sandstone in Arch 120. Detailed examination of the core and XRD analysis (Sharma, 1992) indicate that the top 2-3 ft of the core from the studied interval in Table 3.2 is highly calcite cemented and since there is no gamma ray emission from calcite, the calculated clay content in this interval will indicate very low values (note that the depths in Table 3.2 is the log depth and a correction of +32.00' is necessary to convert it to the core depth).

Well Arch 120 from the Patrick Draw Field was selected to conduct investigations on the effect of variations in formation water salinity on the determination of oil (S_o) or water saturations (S_w) at Patrick Draw Field because of the availability of core and a nearly complete suite of wireline logs. This well was drilled in December, 1987 and no oil production was reported from this well.

In the absence of the direct measurement of salinity of the formation water in well Arch 120, spontaneous potential (SP) logs were used to estimate the salinity or for wireline applications, the resistivity (R_w) of the formation water. The average value of R_w for formation water from UA-5B sandstone from several computations was found to be 0.1907 ohm-meters. It should be mentioned that the best estimates of R_w from the SP log are obtained from thick, clay free zones where there is full development of the spontaneous potential (SP), (Asquith, 1989; Crain, 1986). The presence of hydrocarbons also depresses the SP and may result in the calculation of too high a value of R_w . Although all precautions were taken in the estimation of R_w , the actual value of R_w may be somewhat different due to the possible sources of errors discussed above. S_w values were calculated for well Arch 120 using the following R_w values: $R_w = 0.1907$, 0.25 and 0.35 ohm-meters, which are within the range of values based on the available salinity data discussed above ($R_w = 0.12$ to 1.02 ohm-m).

S_w calculations were made using five different formulae but results are shown for the Archie's method and Simandoux's method, which gives reliable S_w values when the clay content in the reservoir is relatively low (Dewan, 1983; Asquith, 1989; NIPER, 1991) and the amount of high cation-exchange clay (like montmorillonite) is also very

small. The formulas used for S_w calculations by the two methods are as follows (Asquith, 1989, Dewan, 1983):

From Archie's equation

$$S_w = \left(\frac{a}{\phi^m} \frac{R_w}{R_t} \right)^{1/n} \quad (1)$$

From Simandoux's equation

$$S_w = \sqrt{\frac{5\phi^2}{R_w R_t} \left(\frac{V_{cl}}{R_{sh}} \right) - \frac{V_{cl}}{R_{sh}}} \quad (2)$$

where:

R_w = resistivity of formation water

R_t = true resistivity of formation

ϕ = effective porosity

a = tortuosity

m = cementation exponent

n = saturation exponent

R_{sh} = resistivity of shale

V_{cl} = volume of clay

C = 0.40 for sandstones

From earlier studies (NIPER, 1991) the estimated values of the constants a , m and n for the UA-5B sandstone reservoir of 0.62, 2 and 2, respectively, were used for all the calculations. Figure 3.6 through 3.8 show the water saturation calculations for the UA-5B sandstone for the three different water resistivities.

From equation (1) above, the accuracy of calculation of S_w values will be strongly dependent upon the accuracy of the porosity and the water resistivity data. As explained earlier, porosity could be calculated with a good deal of confidence from the density log and therefore, the accuracy of water saturation calculations strongly depends on using a reliable value of water resistivity (R_w). Larger than the actual values of R_w will yield very high values of S_w . This appears to be partly the reason for the erroneously high water saturation values (>100%) calculated for $R_w = 0.35$ ohm-meters (Fig. 3.8) at shallower depths. On the other hand, the calculated values for $R_w = 0.25$ and $R_w = 0.1907$ ohm-meters are within acceptable limits.

Since the Archie's method does not take into account the effect of the extra conductivity provided by the clay layer, the calculated water saturation by this method will be higher, i.e. it will indicate more water saturation than is actually the case. The V_{cl} and R_{sh} terms in the Simandoux's equation attempt to make an approximate correction for the volume of clay encountered within the sandstone pore spaces. From figures 3.6 through 3.8 and Table 3.2 that shows the distribution of clays in the sandstone, it may be noted that the difference in S_w calculated by the two methods increases with an increase in formation water resistivity. The difference in the calculated values of S_w by the two methods also increases with clay content and this is illustrated in figure 3.9 where the water

saturation values calculated for $R_w = 0.35$ ohm-meter by the two methods and the deviation of the clay content values from the mean clay content are plotted as functions of depth. Disregarding the top 2-3 ft of the clay values because of carbonate rock content in the UA-5B sandstone, the difference in S_w values calculated by the two methods increases when the clay values are much higher than the mean and decreases when the clay values are lower than the mean.

If most reservoir parameters except the water resistivity have been judiciously selected in the water saturation calculations, then a reasonably correct R_w value may be obtained from the type of analyses shown in figures 3.6 through 3.8. For example, for $R_w = 0.35$ ohm-meters, the S_w values derived from the Simandoux's and Archie's (Fig. 3.8) methods are both higher than the values measured from core, which is unrealistic. For $R_w = 0.1907$ ohm-meters (Fig. 3.6) the S_w values from the Simandoux's method are significantly lower than the values measured from core and are slightly lower than the values calculated by the Archie's formula. For $R_w = 0.25$ ohm-meters, the difference between the core derived values and the Simandoux's values decreases and those between the Simandoux and the Archie's values increases. Considering that for $R_w = 0.25$ ohm-meters the water saturation values by the Simandoux's method and by core measurements are almost identical for certain depths and since saturation measurements from routine core analyses are typically higher than in-situ conditions due to drilling mud invasion of core, it may be argued that the actual value of R_w is closer to the lower value of 0.1907 than 0.25 ohm-meters.

In the 1980's a transformation in shaly sand analysis was initiated on the basis of use of the cation exchange capacity (CEC) instead of the volume of clays (V_{cl}) in shaly sand equations. Although cation exchange is a better measure of the clay's effect on the logs than is the V_{cl} , the main drawback of the CEC based model like the Waxman-Smiths model is that the CEC values must be measured in the laboratory and secondly that it predicts that water sands of constant R_w , but increasing shaliness, have decreasing effective water saturation (Hilchie, 1982). Clavier, et al. (1977) have found a good deal of evidence to the contrary. The Dual Water Model (also called Bulk Volume Water Model) proposed by Clavier et al. (1977) circumvents the problems in the Waxman-Smiths model. In this model, the pore water is partitioned into bound water (S_b) and free water (S_w) based indirectly on the cation exchange capacity. Both bound and free water contribute to the resistivity of the shaly sand, each having their own formation water resistivities (R_b and R_w). Clavier, et al. calculated the boundwater resistivity, R_b from the following equation:

$$R_b = R_{sh} \phi_{tsh}^2$$

where: ϕ_{tsh} - total porosity of shale

R_{sh} - resistivity of adjacent shale.

The water saturations by the Dual Water Model were computed using the same reservoir parameters as those used for the Archie's and the Simandoux's methods and the

average saturation values for the entire sandstone obtained by using the three methods of calculations are shown in Table 3.3. It may be noted that the values calculated by the Dual Water Model (Table 3.3) are slightly lower than those by the Simandoux's model implying that there is probably slightly more clay correction in the dual water model than in the Simandoux's model. Considering that the high CEC clays like the montmorillonite are negligibly small in the Almond Formation reservoir sandstone, it may be concluded that both the Dual Water Model and the Simandoux model are acceptable methods of water saturation calculations.

This study illustrates the implications of a heterogeneous distribution of formation water salinity and the resulting resistivity (R_w) values required for saturation calculations from resistivity logs. A small change in R_w can cause a relatively large change in the S_w values and result in inaccurate reserve calculations. In moderately low (less than 7-8%) clay filled sandstones with relatively small amounts of clays (<1%) that have high cation exchange capacities, this investigation indicates that the Simandoux's method gives reliable estimates of S_w .

Conclusions

1. Calculation of water saturation profiles based on water resistivity values ranging from 0.1 to 0.5 ohm-meter resulted in a range of average water saturations from 34% to 76%, the difference between a good oil reservoir and a residual oil reservoir.
2. The recalculation of oil resources based on the mapped distribution of water salinities and related resistivities reveals up to 12% more original oil in place in the area of highly saline formation waters in the updip portions of Patrick Draw Field, and up to 5% less oil in the much lower salinity portions. This investigation illustrates the importance of heterogeneous formation water salinity distributions in the estimation of oil resources.
3. A small change in R_w can cause a relatively large change in the S_w values. In the absence of actual R_w measurements careful computation of R_w from the SP log may yield acceptable values provided all precautions are taken to remedy the possible sources of errors in this method of calculation. In moderately low (<8%) clay filled sandstones with relatively small amounts of clays (<1%) that have high cation exchange capacities, the Simandoux's method should give reliable estimates of S_w . The calculated S_w values by the Dual water model which indirectly computes the CEC from the V_{cl} data, were similar to those obtained from the Simandoux's method. This confirms that the high CEC clays probably had a negligible effect on the S_w calculations in Patrick Draw Field.

References

- Asquith, G. B., 1989, Log evaluation of shaley sandstones: a practical guide: AAPG Continuing Education Series #31, Tulsa, OK, 59 p.
- Clavier, C., G. Coates, and J. Dumanoir, 1977, The theoretical and experimental bases for the 'dual water' model for the interpretation of shaly sands: Soc. of Professional Engineers of AIME, Denver, SPE paper 6859, p 1-18.
- Crain, E. R., 1986, The log analysis handbook: PennWell Books, Tulsa, OK, p. 115-247.
- Dewan, J. T. 1983, Essentials of modern open-hole log interpretation: PennWell Books, Tulsa, OK, p. 227-265.
- Hilchie, D. W., 1982, Advanced well log interpretation: Golden, Colorado, D. W. Hilchie Inc.
- National Institute for Petroleum and Energy Research, 1991, Quarterly Technical Report for October 1-December 31, 1990, Volume II, Energy Production Research: DOE Report NIPER-522, February 1991, p. 92-100.
- Schatzinger, R. A., M. J. Szpakiewicz, S. R. Jackson, M. M. Chang, B. Sharma and M. K. Tham, 1992, Integrated geological-engineering model of Patrick Draw Field and examples of similarities and differences among various shoreline barrier systems: DOE Report, NIPER-575, 146 p.
- Schlumberger, 1972, Log Interpretation, Vol. 1 - Principles: Schlumberger Limited, New York, N.Y., 113 p.
- Sharma, B., 1992, Petrographic correlations and mathematical analysis of log signatures for clay identification: DOE Report NIPER-589, February, 1992, p. 1-14.

TABLE 3.1. Measured Water Resistivity (R_w) at Different Salinity (TDS) in Patrick Draw Field.

Well no.	TDS, g/l	R_w (ohm-m) at 68° F
78	29.2	0.27
36	23.5	0.31
105	26.6	0.27
31	15.2	0.49
66	55.1	0.15
60	72.8	0.12
61	51.3	0.17
86	26.3	0.27
2	19.5	0.38
21	29.0	0.26
44	29.2	0.24
105	23.0	0.32
63	4.8	2.40
70	23.2	0.32
80	7.6	1.02
86	26.3	0.27
11	13.7	0.50
13	18.0	0.40

TABLE 3.2. Reservoir Parameters Used in the Computation of Porosity and V_{sh} in S_w Calculations From Density and Gamma Ray Logs in Well Arch 120, Patrick Draw Field, WY

Depth ft	Matrix density gms/cc	Fluid/density gms/cc	Blk density gms/cc	sh density gms/cc	Vsh %	Porosity %
4910	2.64	1.0	2.497	2.58	7.00	8.4634
4911	2.64	1.0	2.478	2.58	6.66	9.6344
4912	2.64	1.0	2.436	2.58	6.09	12.216
4913	2.64	1.0	2.373	2.58	8.36	15.974
4914	2.64	1.0	2.337	2.58	6.91	18.222
4915	2.64	1.0	2.332	2.58	7.28	13.514
4916	2.64	1.0	2.319	2.58	7.2	19.309
4917	2.64	1.0	2.309	2.58	7.34	19.914
4918	2.64	1.0	2.302	2.58	5.92	20.393
4919	2.64	1.0	2.314	2.58	5.34	19.682
4920	2.64	1.0	2.319	2.58	5.42	19.374
4921	2.64	1.0	1.312	2.58	6.02	19.779
4922	2.64	1.0	2.312	2.58	7.86	19.712
4923	2.64	1.0	2.312	2.58	9.44	19.654
4924	2.64	1.0	2.308	2.58	6.9	19.991
4925	2.64	1.0	2.316	2.58	5.44	19.557
4926	2.64	1.0	2.314	2.58	6.45	19.642
4927	2.64	1.0	s.317	2.58	8.04	19.400
4928	2.64	1.0	2.309	2.58	7.21	19.919
4929	2.64	1.0	2.301	2.58	7.13	20.409
4930	2.64	1.0	2.289	2.58	7.01	21.145
4931	2.64	1.0	2.288	2.58	5.72	21.254
4932	2.64	1.0	2.285	2.58	5.74	21.436

TABLE 3.3. Average water saturations for UA-5B sandstone in well Arch 120 calculated by different methods for three different water resistivities of formation water.

Method of S_w determination	$R_w = 0.1907$ ohm-meters, %	$R_w = 0.25$ ohm-meters, %	$R_w = 0.35$ ohm-meters, %
Archie (Asquith, 1989)	54.81	62.75	74.25
Simandoux (Asquith, 1989)	47.81	53.51	61.28
Dual water (Clavier, et al. 1977)	46.86	51.47	58.38
Core	60.19	60.19	60.19

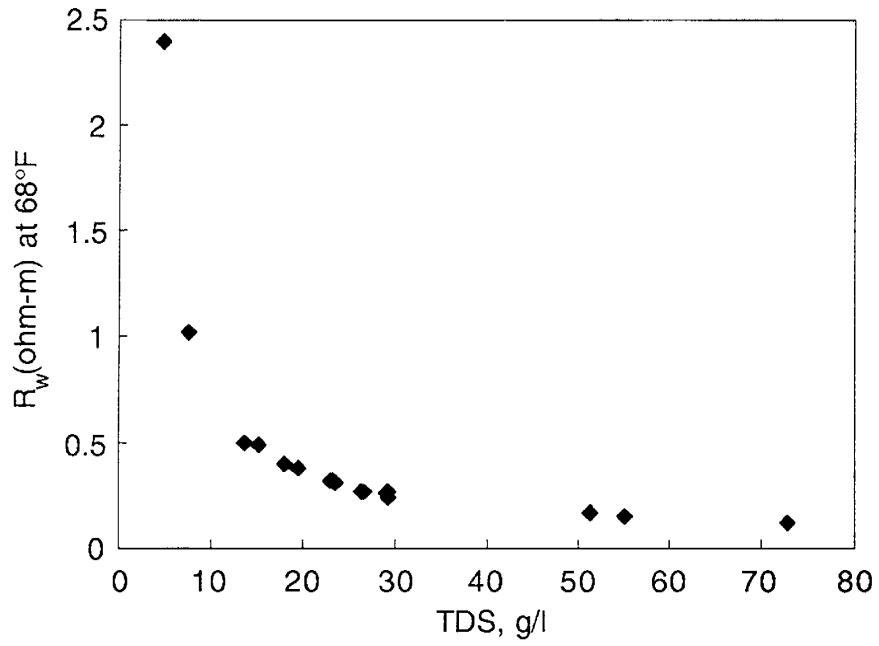


Fig. 3.1. Relationship of resistivities (R_w) and total dissolved solid contents (TDS) in formation waters of Patrick Draw Field.

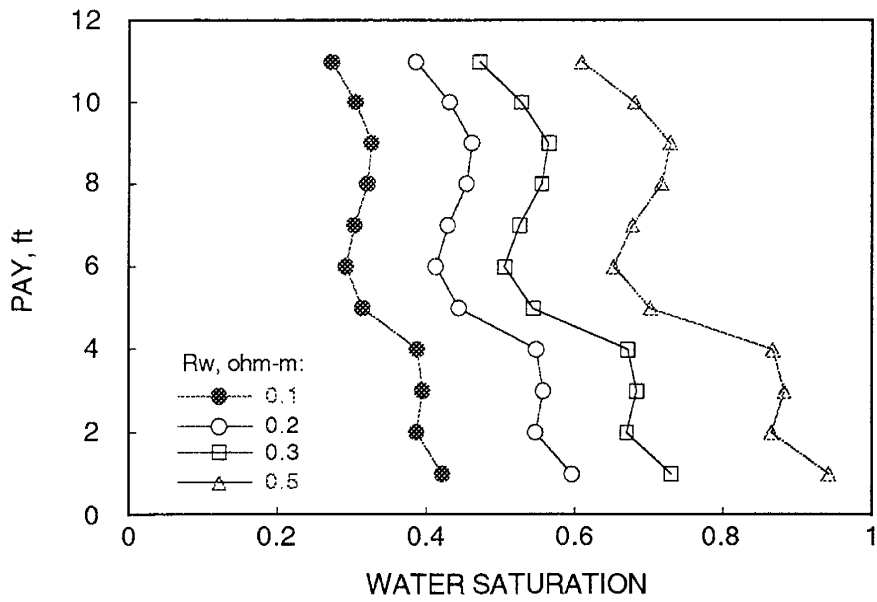


Fig. 3.2. Water saturation profiles of well Arch 46, calculations based on four different water resistivity values.

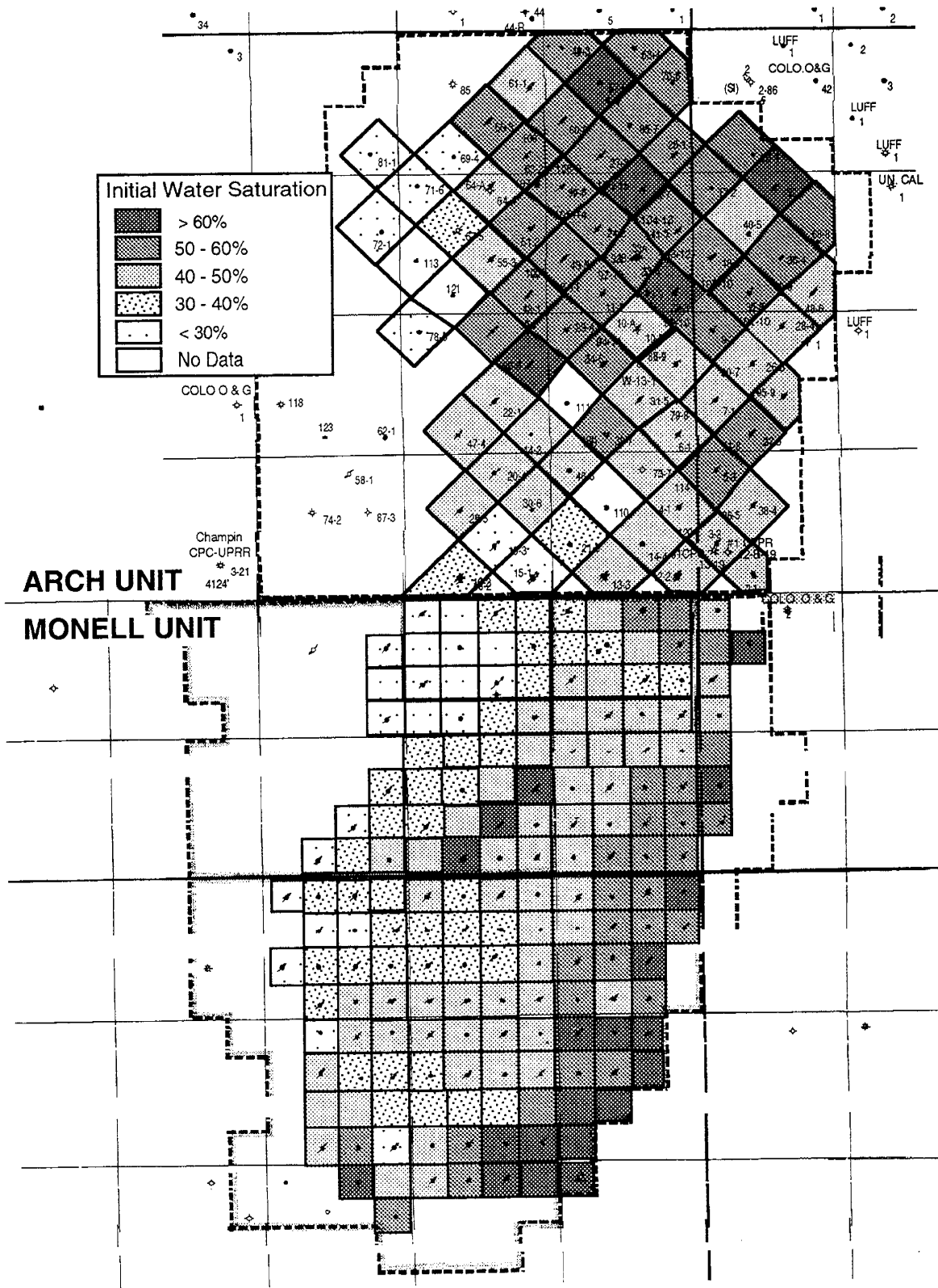


Fig. 3.3. Water saturation map of Patrick Draw Field, calculations based on a constant water resistivity value of 0.2 ohm-meter. For well numbers, see figure 1.3.

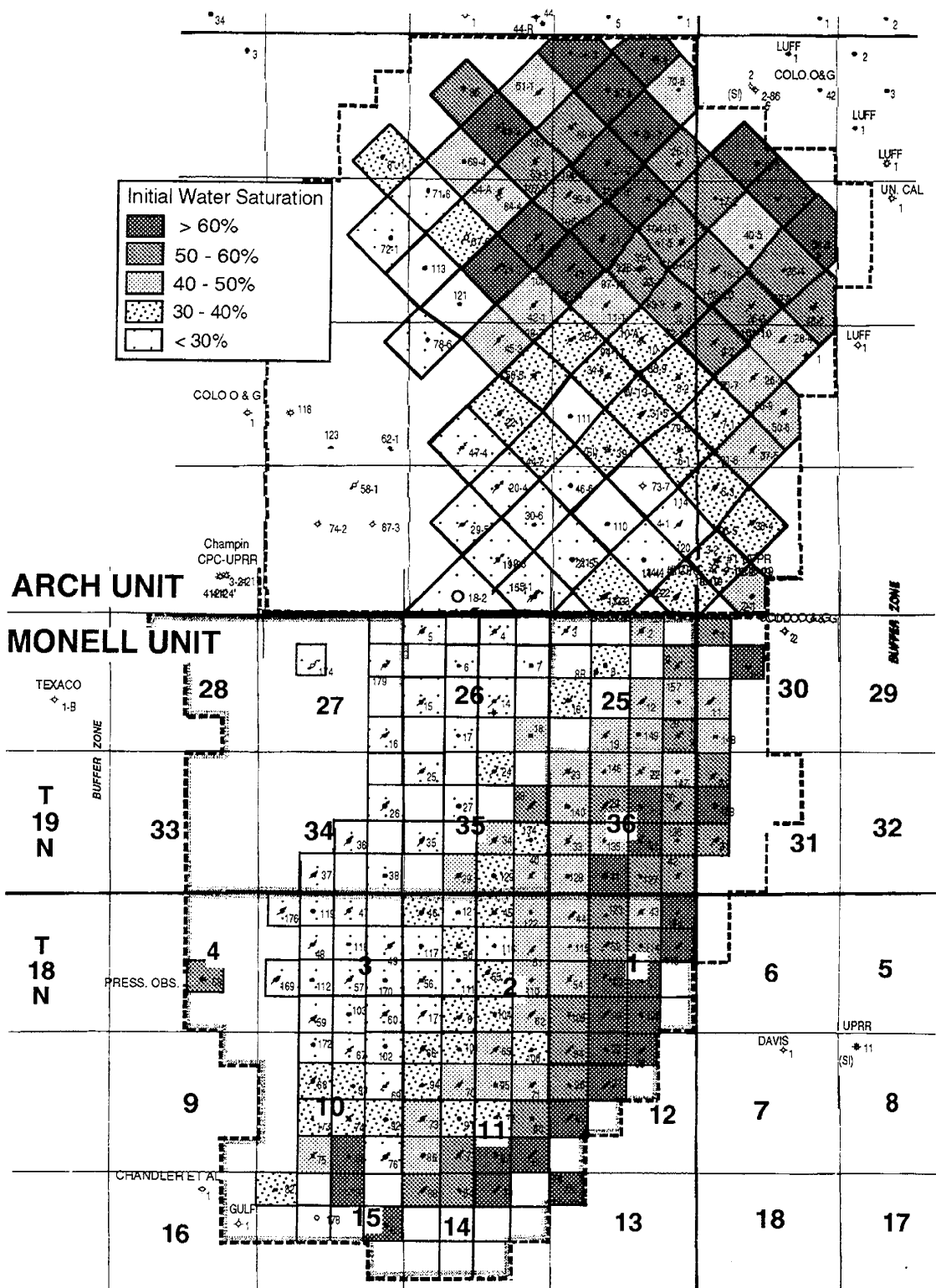


Fig. 3.4. Water saturation map of Patrick Draw Field, calculations based on salinity map in Fig. 2.1. For well numbers, see figure 1.3.

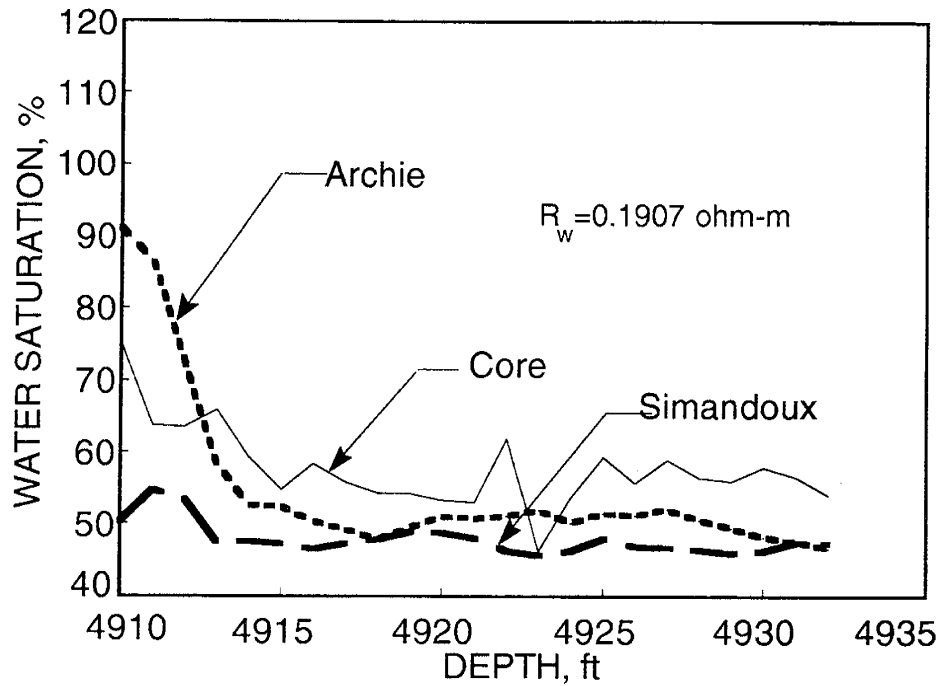


Fig 3.6 Calculation of water saturations in the producing UA-5B sandstones in well Arch 120 for a resistivity of formation water, $R_w = 0.1907$ ohm-meters. Values greater than 100% indicate errors in the calculation method.

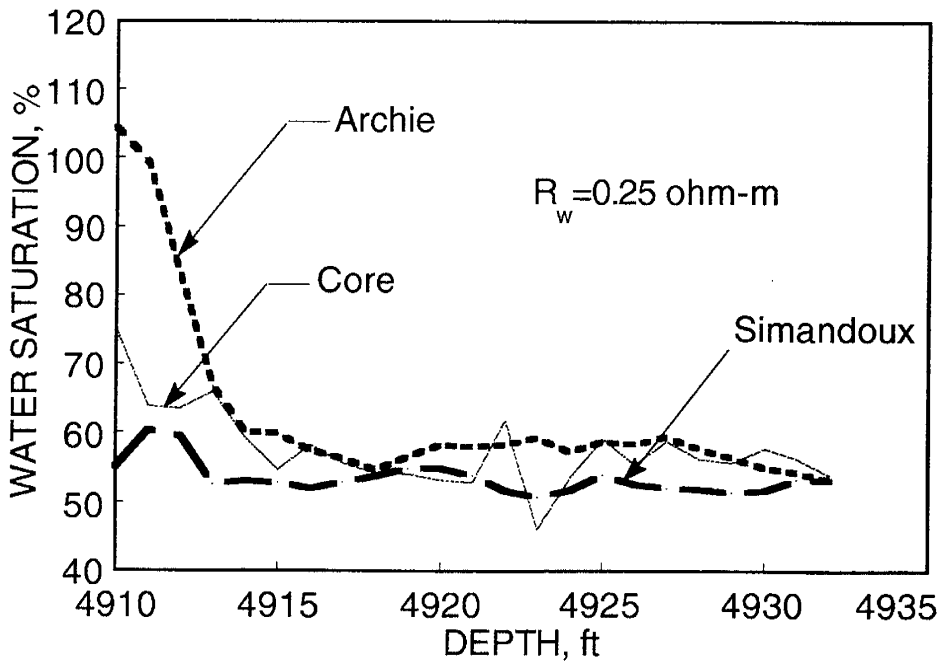


Fig 3.7. Calculation of water saturations in the producing UA-5B sandstones in well Arch 120 for a resistivity of formation water, $R_w = 0.25$ ohm-meters. Values greater than 100% indicate errors in the calculation method.

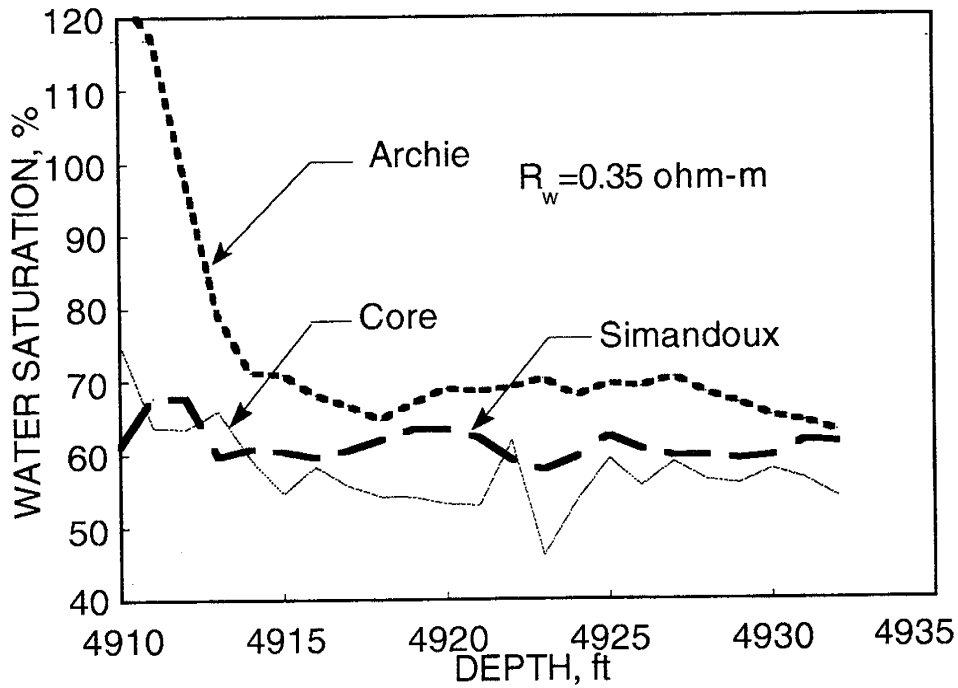


Fig 3.8 Calculation of water saturations in the producing UA-5B sandstones in well Arch 120 for a resistivity of formation water, $R_w = 0.35$ ohm-meters. Values greater than 100% indicate errors in the calculation method.

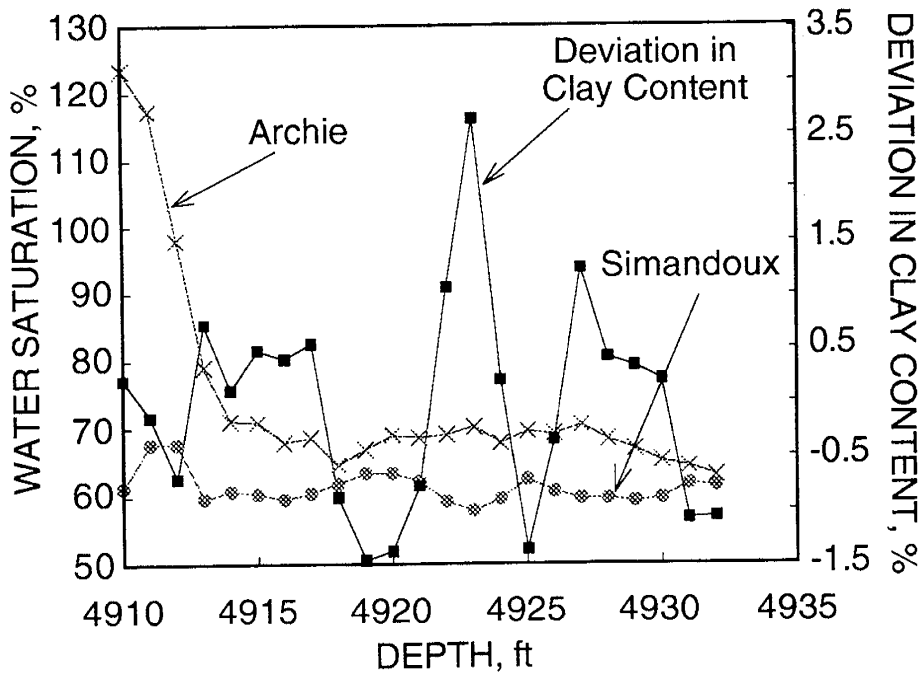


Fig. 3.9. The calculated water saturation values by Archie's and Simandoux's methods in Arch 120 compared with the deviation of clay value at each point from the mean. The water resistivity, R_w , for this calculation was assumed to be 0.35 ohm-m. Values greater than 100% indicate errors in the calculation method.

CHAPTER 4

STRUCTURAL AND SEDIMENTOLOGICAL FEATURES THAT CONTROL FLUID DISTRIBUTION AND MOVEMENT

By R. Schatzinger and B. Sharma

Chapter Summary

Large-scale features such as fracture and fault systems can have a significant effect on fluid distribution and movement within reservoirs. Twenty-three structural log cross sections were constructed, faults identified and mapped within Patrick Draw Field. Fault locations were honored during updating of the structure map of the top of Almond Formation sand interval UA-5B. Unlike previous published works the new structure map indicates that the upper Almond sand interval is cut by a number of fault zones. Further, the fault zones identified by log correlation appear to have had a subtle control on sand deposition, which had been previously correlated with production.

Five seismic lines and structural elevations from an additional fourteen wireline log cross-sections were used to improve the fault map in Patrick Draw Field beyond the version based on log cross sections alone.

A comparison was made of faulting directions obtained from this analysis with the direction of surface lineaments obtained from satellite images and with other studies in the general vicinity of Patrick Draw Field. Study showed that the major lineament directions within the bounds of Patrick Draw Field tend to be consistently offset from the mapped fault directions. The consistent offset of many of the lineaments strongly suggests that the surface lineaments are genetically related to the subsurface faults.

Faulting and fracturing at Patrick Draw Field could contribute to the uneven oil production rates observed in the different parts of the field. Partial control of fluid distribution and movement at Patrick Draw Field is also related to the areal distribution of coquina as well as to petrophysical properties, some of which are controlled by diagenetic processes such as compaction, cementation, and the creation of secondary porosity and microporosity.

Tectonic Framework at Patrick Draw Field

Introduction

Patrick Draw oil field is located in the Greater Green River Basin, east of the Rock Springs Uplift within the Washakie sub-basin and on the southern limb of the east-west trending Wamsutter Arch. The (northern) Arch Unit and (southern) Monell Unit combine to form a producing area approximately 8 1/2 miles long (n-s) by 4 miles wide (e-w). Structural strike trends south-west to north-east and the field dips eastward approximately 3-4°. Regional structure maps are available in Weimer (1966) and

McCubbin & Brady (1969).

Numerous east to northeast-trending normal faults have been documented in the outcrop belt of the Almond Formation on the Rock Springs Uplift (Weimer, 1966; Van Horn, 1979), however, few have been previously shown to cut through Patrick Draw Field. Although not emphasized in most reports, it has been known at least since 1961 that subsurface evidence in the northern part of the field indicates that faults traverse the producing sandstone within Patrick Draw Field (Burton, 1961).

A number of thrust or anticlinal structures were created in the general study area by compressive forces that prevailed in the area during the closing phases of Laramide orogeny (Dewey and Bird, 1970). The Table Rock anticline to the east of Patrick Draw Field is an example of such a structure.

Faulting that was syndepositional with the Almond Formation has been previously demonstrated (Van Horn, 1979). Van Horn concluded that movement on the faults of the eastern flank of the Rock Springs Uplift precluded their origin with the formation of the Rock Springs Uplift. He, however, noted that this did not preclude that most of the movement of these faults was associated with later Laramide tectonic events.

In describing crustal mechanics of Cordilleran foreland deformation Sales (1968) described a major northwest-oriented left lateral stress for the area between the Colorado Plateau block and the area south of the unyielding Canadian foreland and called this the "Wyoming couple". Sales (1968) modeling produced uplifts and thrusts very similar to those seen in central Wyoming, as well as northeast-trending tear faults (strike-slip faults oriented at a high angle to the structural "grain" of the deformed rocks) that are also similar to faults seen in the general area of the Rock Springs Uplift and surrounding area.

Such a configuration as suggested by Sales (1968) would account for the dominant northeast strike of the faults that cut through Patrick Draw Field, and are oriented at a high angle to the Almond Formation depositional trend. Van Horn (1979) also recognized that once formed, the "tear" faults could have absorbed new tectonic forces with resultant movement on their pre-defined fault planes producing the depositional and tectonic relationships now seen in faulted portions of the eastern flank of the Rock Springs Uplift and nearby areas.

Faults Identified and Mapped Using Log Cross Sections

In order to investigate the relationship between structure and other reservoir features, seven N-S oriented and 16 E-W oriented structural log cross sections were constructed (Fig. 4.1) in Arch and Monell Units. This field-wide, intersecting network of log-based structural cross sections was designed to provide a large scale view of the dominant fault zones or other structural complications within the Almond intervals UA-5, UA-6, UA-7 and the top of UA-8. Faults were suspected in the E-W log cross sections in Arch Unit when the dip between adjacent segments of the cross sections exceeded 4° or deviated to a great extent from the overall dip in that portion of the cross section. In the N-S oriented log cross sections, faults were more often indicated at inflections of otherwise straight profile segments. Slope of profiles increases considerably in the southernmost portion of Monell Unit and it is possible that there may be more faults in this area than are currently identified on the log cross sections.

Identified faults could lie anywhere between two wells on a given log cross section segment. For this reason, they were plotted at the midpoint between adjacent wells. Once all the structural cross sections were evaluated and the fault locations plotted, the resulting map was analyzed visually to determine the most probable location of major faulted zones (Fig. 4.2). Faults with little offset may not be identified by this technique and it is, therefore, probable that additional faults are present within the field.

Figure 4.2 compares the locations of major fault zones determined from structural log cross sections with fault zones reported in the literature. Fault zones identified in the log cross sections are numbered 1-6 on Figure 4.2. Zones 1, 2, 3, and 5 correspond very closely to previously reported fault zones. The relative motions of faults identified in zones 1 and 2 correspond with those which were previously published by White, et al., (1963), Weimer (1966), and McCubbin and Brady (1969). In addition, the relative motions of these faults indicate the presence of a nearly two mile-wide graben between fault zones 1 and 2 on figure 4.2.

The advantage of determining the location of faults by the technique of correlating wireline logs is that it is relatively quick and inexpensive, as it relies on materials that are already on hand. The drawbacks of this technique are that it often depends on prior experience in the area of study, it is subjective, the locations and directions of faults often cannot be definitively identified, and faults with minimal throw (less than about 10 ft) may be missed entirely. If diagenetic processes have modified the conductivity of the faults, even those with minimal throw may be critical avenues for or blockages to fluid flow. The conductivity of faults identified by log analysis is unknown. In addition, identification of fractures, whose conductivity can likewise be enhanced or reduced by diagenetic processes, are very difficult to identify using logs alone. In the absence of seismic data, however, log analysis of structure taken in concert with previously publications may provide a good basis for understanding

the spacing and direction of major fault zones within a given reservoir.

Mapping Of Faults With Seismic And Wireline Log Data

Introduction

A map showing the distribution of faults at the top of the UA-5B sandstone was generated in the Arch and Monell units of Patrick Draw Field, WY using seismic and wireline log data (Fig. 4.3). This was done to "upgrade" the fault distribution map for Patrick Draw Field created by log data alone (Fig. 4.2) and to demonstrate the advantage of adding seismic line information to the structural interpretation. The locations of five seismic lines and an additional fourteen log cross-sections used in this analysis are shown in figure 4.4. The seismic data were acquired from Union Pacific Resources Corporation (UPRC).

Since the widely spaced seismic lines did not provide adequate control for mapping of faults, the seismic data was supplemented by wireline log data. The "new" log cross-sections were selected at equal intervals perpendicular to the strike direction of the unfaulted (old) structure map on the top of the UA-5B sandstone obtained from UPRC.

The Technique of Fault Mapping and its Limitations

The following technique was used in the integration of seismic and log data for fault mapping. After accurately identifying the reflector at the top of the Almond Formation, the reflector was traced in all five seismic sections. Some of the criteria used in identifying faults on the seismic sections were as follows: (1) distinct displacement of beds along the fault plane, (2) disturbance along the fault plane in the seismic section generated by diffraction patterns along the fault plane, and (3) sudden termination of reflections at the fault. It should be noted that only the first of these three criteria provide evidence for the direction of throw on the faults. The faults mapped had very small throws (around 10-30 ft), so distinct displacements across the fault blocks could not always be seen. However, disturbances along the fault plane were clearly noticeable and led to identification of faults. The second difficulty in the precise mapping of faults at Patrick Draw Field was the lithological complexity of sediments. Because the sandstones (facies) are not continuous for long distances there are lateral variations in the reflection quality. Mineralogical variations of the sandstones also contributed to the variations in reflection quality. These depositional and diagenetic variations within the overall reservoir sandstone made reliable mapping of the reflector, precise location of the faults, and determination of throw quite difficult.

Out of the five seismic sections, processing of only two of the sections was of optimum quality for fault mapping. It is expected that with further processing and a more judicious selection of filters the quality of the sections

could be improved for fault mapping.

The locations of faults cutting the reflector at the top of the Almond Formation were traced on the seismic sections and these locations were then transferred to a log cross-section which was almost coincident with the seismic line. As an example, along seismic line AA-6 (Fig. 4.4) there are clear indications of four faults. The locations of these four faults were then transferred to the nearby log cross-section # 5 (Fig. 4.4). In figure 4.5 is shown the two-way seismic reflector times to the top of the Almond Formation along seismic line AA-6 and in figure 4.6 is shown the structural elevations at the top of UA-5B sandstone along the log cross-section. Distances along the log cross-section (Fig. 4.6) are measured from an arbitrary point X₅ located at the western end of this profile. The location of each fault was then traced on the adjacent log cross-section(s) if indication of faulting was present in these sections. Indications of faulting on the log cross-section consisted of a sudden change in structural elevation at the top of UA-5B sandstone that could not be explained by a change in the structural dip caused by thinning and thickening of the UA-5B sandstone interval. Other seismic lines available along the fault trace, provided further evidence for the extension of the fault up to the second seismic line. Finally, all of the fault traces identified during the original log study were incorporated with the seismic-based data. In this manner all the faults shown in figure 4.3 have been mapped.

A number of faults are indicated only from the seismic data, in areas where no offset has been recognized in the log cross sections. For example, on the log, cross section # 5 (Fig. 4.6), only four faults could be definitely identified, although seismic evidence and nearby log cross sections suggest that eight faults, some with practically no throw, have intersected section # 5.

Nature of Faulting at Patrick Draw Field

Most of the faults identified by the combined log and seismic evaluation of Patrick Draw Field were interpreted to have normal offsets. However, based on seismic sections AA-5 and AA-6 some faults could be interpreted to have reverse motions. Such motions are known on other faults nearby to Patrick Draw Field. For instance, Dewey and Bird (1970) determined that compressional forces gave rise to a thrust fault and anticlinal structure at Table Rock Field, east of Patrick Draw. However, compared to the Table Rock anticline, the flexures at Patrick Draw Field are of much smaller magnitude. Tight folding characteristic of reverse fault generated structures appears to be present though in the formations below the Almond Formation.

Comparison of Fault Map with Other Parameters

Comparison of the Patrick Draw fault map (Fig. 4.3) with the isosalinity map (Fig. 2.1) is presented as figure 4.7 and shows a number of relationships. First, there is a good correspondence between a pair of faults and the low

salinity embayment in sections 11 and 12 in Arch Unit. Low salinity formation waters probably used this fault zone as a conduit to invade a narrow area in sections 11 and 12. Second, the graben identified on the log (only) based fault map (Fig 4.2) between fault zones 1 and 2 approximates the eastward bulge in high salinity waters in southern Arch Unit. The updated fault map shown in figure 4.7, that takes seismic information into account, however, indicates that the eastward bulge of the high isosalinity is structurally fragmented by at least two additional faults (e.g. those in sections 22 and 23). The faults in sections 22 and 23 seem to have no (or minimal) effect on the isosalinity contours, however. In addition, fault zones are present at each major deflection of the isosalinity contours, possibly indicating a cause-effect relationship.

Knowing that a relationship exists between the location of the fault zones and the salinity of the initial formation waters could have been useful when calculating the original oil in place. Integrating limited original salinity data with the structure map could help delimit regions of similar initial salinity which is an important correction for when using log data to calculate reserves.

No obvious similarity exists when comparing the fault zone map (Fig. 4.3) with production maps for Arch and Monell primary production or cumulative waterflood production (See Figs. 5.23 and 5.32). However, the pattern of production for Patrick Draw Field generally agrees with the areas of thick sands for UA-5B sandstone (Schatzinger, et al., 1992). Areas of thick permeable sand thicks (>25 ft) are compared to the upgraded distribution map of fault zones within Patrick Draw Field in figure 4.8. It can be seen that the southern margin of thick permeable sandstone in Monell Unit is sub parallel with a fault zone. Other mapped faults are tangential to the northern and southern boundaries of thick net sandstone accumulations shown in figure 4.8. The coincidence of faults bounding the highly productive sand thick that straddles the Arch-Monell Unit boundary reinforces an earlier suggestion (Schatzinger, et al., 1992) that there may have been some synsedimentary structural control of sand accumulation. Therefore, although it is not obvious in the production maps, we suspect some linkage between tectonics and patterns of production within Arch and Monell units. The thick sand indicated in figure 4.8 along the eastern margin of Arch Unit was a poor producer because it lies on the oil-water contact. The small sand thick centered in section 7, T9N, R98W, was probably a poor producer due to abundant calcite cementation. The narrow sand thick extending through the eastern half of section 13, T19N, R99W, was a good producer during waterflood probably because, unlike the area surrounding it, calcite cementation was minimal.

Comparison of "Old" and "Updated" Structure Maps

The updated structure map (Fig. 4.2) may be compared to the previous structure map (Fig. 4.9) used in most earlier publications about Patrick Draw (Weimer, 1966;

Weimer, Porter, and Land, 1985) which did not take into account faults within Patrick Draw Field. Potential for tectonic segmentation of the field can be readily seen on figure 4.2, whereas the older structure map indicates a gradual, uninterrupted eastward-dipping monoclinical surface. Structural complications have been shown above to have an influence on the sand distribution, reservoir compartment size and number, and a bearing on primary and waterflood production. The structure map of a production unit should be continually upgraded as new wells are added to the pattern in order to provide successively more realistic appraisals of reservoir compartment size and connectivity.

Lineament Study Performed in the Patrick Draw Field From Satellite Image Data

The joint NASA/Geosat Test Case Project (Lang et al., 1984) recognized a large numbers of linear features (lineaments) that are generally regarded as some manifestation of topographic and vegetative enhancement of linear fracture traces.

However, while the lineaments are images of surface features, the structural features (faults, fractures, etc.) that presumably gave rise to the lineaments at Patrick Draw Field could occur at different depths and at different orientations below the surface. Depending upon several factors, including prevailing stresses, lithology of rock masses, structural configuration, density of subsurface data etc. the lineament locations may not be coincident with locations of subsurface faults or associated fractures. The topographic lineaments in the vicinity of Patrick Draw Field obtained from satellite imaging and shown in figure 4.10 is a combined interpretation from six different infrared wave lengths. A single lineament, therefore, has the potential of appearing six times in this illustration. While the location of actual lineament traces could be subjective and may vary depending upon the interpretation, what remains relatively constant and reproducible is the azimuth of the line drawn, rather than its precise location. Thus, in the investigation of topographic lineaments, trends rather than absolute locations of lineaments are emphasized.

Lang, et al., 1984, indicated that lineaments are generally regarded as some manifestation of topographic and vegetative enhancement of linear fracture traces. Comparison of the fault map (Fig. 4.2) with surface lineaments (linear features) from the same area (Fig. 4.10) shows a decided lack of agreement with respect to locations and directions. The data, however, fall into several distinct directional groups. Lineament directions (Lang, et al., 1984) were measured and an average for each group was plotted and can be compared with the directions of faults identified in this report based on log data alone or on log plus seismic data. The resulting display (Fig. 4.11) shows an approximate 30° offset between the major fault direction (determined by log correlations) and the two major lineament directions. The major fault direction determined by combined seismic and log data trends about 12° less than that from log data alone. The major fault direction

determined by logs alone is 32° offset from the dominant lineament direction and 34° offset from the second major lineament direction. In contrast, the major fault direction determined by combined seismic and log data is 20° offset from the primary lineament direction and 46° offset from the second major lineament direction. While there appears to be a consistent offset between the combined seismic plus log data and the major lineament directions, the log data alone (Fig. 4.2) provide the better evidence for a genetic relationship between the two parameters.

These observations suggest, but do not prove, that because of the consistent offset of dominant faults and lineaments, the surface lineaments are genetically related to the subsurface faults. The faults identified in the subsurface at Patrick Draw Field by log correlation may not be well represented at the surface, but several fracture sets are represented. Subsequent Laramide tectonic movements could have created stress fields at new orientations and thus created additional fracture sets that are also recognized at the surface as lineaments. Based on examination of cores it is certain that subsurface fractures exist and it is very probably that most subsurface fractures have not yet been identified. With additional work the subsurface fracture (and fault) orientations could be positively identified, analyzed, and compared with the orientation of surface lineaments in order to prove whether or not they are genetically related.

A statistical summary of 1860 topographic lineaments identified within the Rock Springs 1:250,000 quadrangle (a much larger area that includes (Fig. 4.10) was also presented by Lang, et al, (1984). Their cumulative frequency diagram indicates that the dominant direction for lineaments is 67°, which is 8° less than the dominant direction of faults identified at Patrick Draw by log analysis but only 3° offset from the major fault direction determined by combined seismic and log data. Given the amount of error inherent in plotting directions of faults within the field, the similarity of the dominant regional fault and lineament directions is most striking.

A number of NW-SE trending lineaments are indicated in figure 4.10 that are normal to the general direction of faulting (NE-SW) in the area. Faults with NW-SE azimuths were not mapped by the seismic and the log data (Fig. 4.11), probably because of small throws on the faults. In brief, therefore, it may be concluded that the general azimuths of the majority of topographic lineaments in the NE-SW quadrants are in good agreement with the average strike directions of the faults mapped.

Distribution of Coquina

Distribution of the coquina that acts as a barrier to fluid flow between the western and eastern portions of Arch Unit was determined by mapping its occurrence based on resistivity logs. It was found that there is good correspondence in general between log signatures and facies (once the facies are known) and an excellent correspondence between occurrence of coquina and the log signatures. Examples from two Arch wells (120 and 106) are presented in figures 4.12 and 4.13. Both figures show the

characteristically high resistivity "kick" for the coquina. Coquina is defined as an accumulation dominated by shell materials. In the upper Almond Formation coquina is created by accumulations of oyster shells. The accumulations are of two broad general types. First is whole and broken oyster shells in sparse, poorly sorted sandstone. The sand particles are commonly among the coarsest examined in UA-5B. Frequently this first type of coquina is massively bedded and very tight due to abundant carbonate cement. Often the first type of coquina is technically a carbonate rock. Calcite and dolomite-filled fractures have been examined from this type of coquina deposit. The other type of "coquina" typically consists of shell materials in a fine-grained matrix, usually silty sandstone, or mudstone, and is most common at the very top of the UA-5B interval. Both types of coquina have characteristically high resistivity which allows the unit to be traced laterally.

Because of the relatively limited amount of core control, resistivity logs were used to map the coquina. The high resistivity kick indicating the coquina was due primarily to high carbonate content. The excellent correspondence between log signatures and all cored coquina intervals minimizes the possibility that high resistivity is due to oil saturation or water salinity alone. Core descriptions supplied by UPRC as well as those by NIPER staff were used whenever possible to calibrate the core to log correlations. The resulting map could, therefore, be extended far beyond those parts of the field where cores were available. All available logs from Arch and Monell units were correlated and the distribution of the high resistivity zone near the top of UA-5B was determined (Fig. 4.14).

The distribution of the high resistivity marker (coquina) shown in figure 4.14 shows several unexpected features. First, the greatest thickness of coquina is indicated along the area permeable of thin sand in sections 13 and 24 (T19N, R99W) in southern Arch Unit. However the overall trend of the coquina thickness does not simply mirror the area of elongate thin sand. Instead, a second NW-SE trend is indicated by isolated thick areas coquina in sections 12 (T19N, R99W) and 7 and 18 (T19N, R98W). The two sub parallel coquina accumulations are probably genetically distinct based on this distribution. Secondly the coquina becomes markedly thinner at the southern margin of the thin sand area in Arch Unit (SE 1/4 section 24) but thickens on the eastern (seaward) margin of the buildup in section 30 (T18N, R98W) in northeastern Monell Unit. Thirdly, the more northerly buildup does not closely follow the thin permeable sand in sections 1 and 12. Both the core data and the high resistivity log data indicate that the coquina and calcite cemented sands are dominant only eastward of the prominent north-south oriented sand thin in Arch Unit. Based on these data it appears that the fluid barrier between eastern and western bars may be created by a combination of thin, calcite-cemented sand in the north and impermeable coquina in the south of Arch Unit. The isopach map showing the distribution of the high resistivity marker at the top of UA-5B (Fig. 4.14) also shows a small area (section 13)

lacking the resistivity kick in the area that lies between the thick coquina and corresponds to one of the better producing areas in eastern Arch Unit (see Fig. 5.32). The area is also a small but prominent sand thick in eastern Arch Unit.

Additional high resistivity thick areas are indicated in the southern portion of Monell Unit, however, as core control is entirely lacking in this area we cannot confirm if these represent coquina deposits or not.

Based on the examination of cores and analysis of thin sections within and adjacent to coquina deposits it is suggested that the broad thin area (0-5 ft thick interval) of higher resistivity on figure 4.14 represents areas with abundant calcite cement in contrast to the thicks (>5 ft) which mark the discontinuous, generally linear-trending coquina deposits.

When the distribution of the high resistivity deposits (coquina and calcite-cemented sandstone) in UA-5B are compared with the salinity map (Fig. 4.15) we can see a general tendency for the high resistivity zones to be located in regions of high salinity gradient (especially in Arch Unit). Thin section analysis shows that the oysters in the coquina deposits have been subjected to strong chemical compaction. Therefore, Ca^{+2} supplied by pressure solution could have been available to provide a local source for the calcite cement which is so common within the coquina deposits and which generally decreases vertically away from the coquina in overlying and underlying sands. Calcite cement which is abundant in the area outlined in figure 4.15 would tend to make the interval more brittle and thus susceptible to fracturing. Conductive fractures in an otherwise relatively low porosity/permeability zone (the high resistivity zone in eastern Arch Unit) could lead to relatively rapid breakthrough of waterflood waters, poor sweep efficiency, and generally low production in the area. Calcite and dolomite have been identified filling fractures in cores recovered from well Arch 120 which is located within the high resistivity zone indicated in figure 4.15. Only with additional petrographic analysis will it be possible to determine if the coarse-grained fracture filling calcite and the calcite cement that is found in the coquina and high resistivity sandstones reflect multiple diagenetic events.

The correspondence between the occurrence of carbonate cemented sands and the high gradient areas of the salinity map (Fig. 4.15) indicates that the carbonate precipitated along a geochemical rather than a lithological boundary with precipitation dominantly at the contact between the zone of high salinity and low salinity formation waters. The relative timing for carbonate cementation may have been very early because the zone of abundant carbonate cement (delimited by the boundary of the high resistivity zone in UA-5B) shows a generally negative relation to the area of deposition of UA-5A sands (Fig. 4.16). Only along the UA-5B sand thin between the eastern and western bars can we find overlapping UA-5A deposition with UA-5B carbonate-cemented sands. This arrangement suggests that generally the carbonate-cemented area may have remained topographically high during UA-5A deposition diverting those sands from the area, except in the

topographic low between the eastern and western UA-5B bars.

Vertical distribution of facies such as shown in figures 4.12 and 4.13 indicate that the coquina deposits are on the back or lagoonal side of the barrier. They are most commonly encountered in association with tidal channel or tidal delta sandstones. The general linearity of the coquina deposit "thicks" shown on figure 4.14 tends to support the concept of a channel-like morphology. In order to investigate the geometry of the deposits in eastern Arch Unit five stratigraphic resistivity cross sections (see Fig. 4.17) were constructed and detailed correlations were made. One stratigraphic cross section (A-A') runs down the axis of the permeable sand thin between the eastern and western bars (Fig. 4.18) and surprisingly showed the "coquina deposit" to actually consist of several successively offlapping deposits. Stratigraphic cross sections B-B', C-C', D-D', and E-E' (Figs. 4.19- 4.22) are oriented at high angles to section A-A'. These stratigraphic cross sections also show that the high resistivity marker (coquina) consists of numerous offlapping wedges, some of which overlap by one well spacing or slightly more (see cross section D-D', Fig. 4.21). The three dimensional geometry of the successive resistivity marker beds must therefore be interpreted as imbricated wedges of limited lateral extent rather than elongate channel shapes. The offlapping configuration of the coquina/resistivity markers presents a dilemma: it could have been brought about by lateral migration of the inlet/tidal delta complex or it could have been formed by overall seaward migration of the barrier system with little lateral (along strike) migration of the inlet/tidal delta complex. Additional facies interpretations and sequence stratigraphic work would be required to determine which scenario is correct.

The net result of the offlapping or imbricated coquina beds and carbonate cemented zones is to create within the overall UA-5B sandstone package a low permeable upper sandstone with complex geometry that partitions the UA-5B sandstone in eastern Arch Unit, creating highly variable petrophysical properties within the sandstone, and, except where the carbonate is absent in section 13, to degrade the reservoir quality and hinder lateral communication.

Comparison of Lithology and Petrographical Features With Petrophysical Properties

Introduction

Well Arch 120 was selected for detailed evaluation of UA-5B sandstone because information on mineralogy is available and a variety of petrophysical properties have already been analyzed to some degree (Szpakiewicz, et al., 1991; Schatzinger, et al., 1992). Petrographic analysis of 6 thin sections from UA-5B stratigraphic interval indicates that the flood tidal delta facies is remarkably consistent in lithology. Samples from the flood tidal delta comprise feldspathic litharenite with varying amounts of calcite and dolomite cement. Rock fragments comprise between 16-31% of the combined quartz-feldspar-rock fragment

component of the samples with rock fragment/feldspar ratios ranging from slightly greater than 1 to slightly less than 2. A broad spectrum of lithic fragments is present, including chalcedony, chert, metamorphic, volcanic, and fine-grained sedimentary types.

Coquina, Petrographic Features, and Calcite Cement

All samples from the "coquina" in Well Arch 120 as well as the flood tidal delta facies have been moderately to strongly compacted. As defined previously, coquina is a lithology dominated by fossil shells. Physical compaction indicated by the rotation and breakage of grains is common. Chemical compaction (solution-reprecipitation) is particularly noticeable as interlocking quartz overgrowths (2% of the rock volume), as solution seams with accumulations of insoluble components and clays, and as interpenetrating grains. Of particular interest is the strong embayment of oyster shells in the coquina by the sand fraction. Microstylolitic contacts are abundant. Chemical compaction along the length of single oyster valves was locally so strong that only discontinuous remnants are preserved. These observations provide strong petrographical evidence for a local source of calcite cement within the coquina beds and immediately subjacent portions of the flood tidal delta facies. In general, porosity increases downward away from the coquina layer in Well Arch 120 within UA-5B.

The compaction index for the six samples that were used in figure 4.23 ranges from 0.78 to 0.92 for Well Arch 120 and ranges from 0.78-0.82 for three of the four samples in well 7-18-1. The fourth sample from well 7-18-1 with 34.2% total cement (most of which is carbonate) has a compaction index of 0.36. Compaction index is the fractional ratio of the compactional porosity loss to the sum of compactional and cementational porosity loss since deposition (Lundegard, 1992). The compactional index equals 1.0 when all porosity loss is by compaction, and equals 0.0 when all porosity loss since deposition is by cementation. Thus 78-82% of the porosity loss since the time of deposition was due to compaction in the samples analysed. Only 18-22% of the porosity loss was due to all types of cementation. At this time it is not possible to distinguish the proportion of the porosity loss to compaction that may be due to pressure solution alone, however, based on the texture of the coquina and the high-resistivity calcite cemented sands of eastern Arch Unit, it is believed to be substantial.

The strong relative importance of compaction over cementation in the UA-5B Almond reservoir is reflected by and was probably controlled by the lithology and microtexture of the reservoir rocks. The reservoir sandstones are characteristically feldspathic litharenites (Schatzinger, et al., 1992) where lithic fragment to feldspar ratios are typically between 3:1 and 1:1. A preponderance of the lithic fragments are sedimentary rock fragments including siltstone and mudstone particles which are easily compressed. Crossplots of Almond data (NIPER, 1992) show that (with the exception of highly carbonate-

cemented samples) as lithic content increases the compaction index increases, and intergranular volume decreases. There is also some indication that as lithic content increases (NIPER, 1992), oil saturation (derived from core) increases, however, additional data will be required to verify this observation.

Clay Content Determination

One important property of reservoir sandstone is total clay content. X-ray diffraction analysis from the same intervals in well Arch 120 as thin sections were made from indicates a total clay content of about 4%, however, log-derived V_{cl} data indicate more variation in the clay content. V_{cl} data was compared with XRD-derived clay content (NIPER, 1992) from the same depth intervals in order to calibrate the V_{cl} data. Log-derived V_{cl} data from the tidal delta facies in Well Arch 120 indicate 6-8% clay, and significantly greater amounts of clay are reflected by higher V_{cl} values for the underlying bay/lagoonal facies as well as the overlying coquina bed. XRD samples within the tidal delta facies have total clay contents between 3 and 4% and show less variation in clay than do the log-derived data. A correction factor of V_{cl} minus 3% is proposed to calibrate this well.

Limiting factors that must be accounted for when using XRD-derived mineralogy to calibrate log-derived V_{cl} is the volume of the sample examined (an order of magnitude less for XRD), the variation in mineralogy due to layering (logs record an average reading for several cubic ft of rock), and the representative nature of the XRD sample. In addition, better correlation of petrophysical properties occurs within individual wells than between wells. Therefore, it is likely that calibration of log-derived V_{cl} may best be done with XRD samples from the same or nearby wells rather than applying a field wide correction based on one sample.

A plot of V_{cl} vs. natural logarithm of permeability from conventional core analyses for 26 data points in Well Arch 120 indicates a good correlation (coefficient $R=0.87$) when three outlying points are disregarded (Fig. 4.23). The outliers, identified on the plot, represent coquina or highly calcite cemented (22-37% calcite) samples based on XRD analyses and density log evaluation. The carbonate-rich samples all indicate lower clay content than expected from the main trend of the data, suggesting that this crossplot technique may provide a way to distinguish highly carbonate-cemented intervals within the pay sand. Data from additional wells are necessary to determine if similar trends of V_{cl} vs. natural logarithm permeability occur fieldwide or if values vary due to compartmentalization within the reservoir.

Pore Throat Size Distribution

Pittman (1992) recently developed a series of empirical equations for determining pore throat size distributions from porosity and air permeability that correspond to mercury saturation percentiles. This technique has been

applied to determine the median pore throat diameter for samples from Well Arch 120 and three additional wells from which petrographical analyses have been completed. Using Pittman's equations, the median throat radius may be calculated as

$$\log r_{50} = 0.778 + 0.625 \log K - 1.205 \log \phi$$

where r_{50} = radius of the median pore throat, K = permeability (mD), and ϕ = porosity in percent.

For well Arch 120, the calculated median throat diameter was found to have a correlation with permeability ($R = 0.83$), and would have been higher if the anomalous point that represents highly calcite-cemented coquina had been eliminated.

The relationships between calculated median pore throat diameter and permeability, log permeability, and porosity have correlation coefficients greater than 0.80 for data from combined Arch wells 120, 45-14-3, 7-18-1, and 49-1-3. Future mercury porosimetry will be necessary to test whether the high correlation coefficients between these parameters are real, or merely a function of the way the throat size is calculated.

The relationship between total carbonate content and porosity for nine points from well Arch 120 indicates a correlation coefficient of $R=0.95$. However, when the same relationship is examined for three other wells (10 samples) the correlation coefficient is $R=0.82$. When the data from all four wells are combined, the relationship between total carbonate and porosity has a correlation coefficient of only $R=0.70$, and the trend of the data from well 120 is not parallel to the best-fit line for the combined data. These relationships re-emphasize the better correlation of petrophysical properties on a single-well basis than for combined wells. This type of data distribution probably reflects the relatively great spatial variability (i.e. heterogeneity) of petrophysical properties inherent within this reservoir, and possibly within mesotidal shoreline barriers.

The crossplot of total clay percent versus porosity for four wells shows a wide scatter in the data (Fig. 4.24). However, the distribution of data may be useful to determine the maximum amount of clay to be expected given a certain porosity. For example, samples with 15% porosity would be expected to have no more than approximately 7% total clay, while samples with 20% porosity may contain up to 15% total clay. The positive relationship shown here between maximum clay content for a given porosity is not an expected relationship, because porosity generally decreases as clay content increases. However, the amount of microporosity (see Fig. 4.24) generally increases with porosity and clay content for the upper Almond Formation reservoir quality sandstones examined.

Rock Texture & Petrophysical Properties

Examination of thin sections confirms that more porous sands often contain increased proportions of microporosity within leached or altered feldspars or sedimentary rock

fragments. Feldspars were altered to clay, and many sedimentary rock fragments are dominated by microporous clay minerals. In addition, petrographical evidence indicates that more porous intervals tend to have proportionately more loosely associated books of kaolinite cement within interparticle pores where they often form a very poorly packed network of clay particles that partition rather than fill the interparticle pore volume. Therefore, sands with originally unstable grains now contain loose networks of interparticle kaolinite and have a tendency to have a greater proportion of microporosity.

The microporous texture of more porous UA-5 reservoir sandstones may be important in terms of waterflood or tertiary recovery because although the network of clay particles has a negligible effect on porosity (storage capacity), the micro-scale of many pores could lead to abundant dead-end pore configurations resulting in poor sweep efficiency. The texture of the pore system rather than the absolute amount of clay cement in the reservoir quality sands may be the reason that permeability in the Almond Formation UA-5 sandstones is generally low, and the geometry of the pore system could explain the tendency of these sands to have production problems often (incorrectly) attributed to mobile fines.

An example of the influence of rock texture may be seen when bulk volume porosity, permeability, microporosity and oil saturation (from core) are compared. Figure 4.25 shows the relationship between bulk volume porosity and oil saturation for 6 samples from two wells. Note that oil saturation is greatest for the samples with smallest bulk volume porosity. An exception is the point with only 11% porosity (well 7-18-1), however, the porosity in this sample is highly reduced by 31.8% dolomite. The relationship between permeability and oil saturation (Fig. 4.26) shows the same ranking of samples, that is those with the greatest bulk volume porosity have the greatest permeability. Well 7-18-1 was a primary production well, however, well Arch 120 was drilled and cored after waterflood had been in progress for many years. The data from figures 4.25 and 4.26 show that although the petrophysical properties of the samples from well 7-18-1 are generally better than those from Arch 120, the oil saturation is lower in the former well despite its being cored prior to waterflooding. Well 7-18-1 was a moderately good producer while Arch 120 was not. Reduced porosity and permeability in well Arch 120 is generally due to calcite cement which made it difficult to produce the oil in place, and may be associated with fractures that penetrated the water zone.

But why should samples from 7-18-1 be such a good producer despite the apparently low oil saturation values? First, the average log-derived oil saturation for samples from well 7-18-1 is 52.9%, considerably higher than the core-derived saturations. Secondly, the samples with porosity and permeability not reduced by dolomite cement contain abundant microporosity (see Fig. 4.27). Petrographic analysis (NIPER, 1992) of the samples from 7-18-1 indicate that the microporosity is located within leached unstable grains (feldspars, lithic fragments). Crossplots of data from well Arch 120 indicate that as

feldspar content increases so does microporosity ($R=0.80$) (Fig. 4.28). Such microporosity is characteristically not part of the effectively swept porosity, and is water saturated. This results in an underestimation of the efficiency of sweep from the main connected pore system. In other words, because of the averaging process a well with pay from a zone with this type of microporosity may produce even better than expected based on log estimates alone. In this case microporosity may lead to significant underestimation of the production from the well because of the texture of the pore system. Log analysis cannot determine the texture of the pore system and so the effect of irreducible water in the micropores would be overestimated. Petrographic or SEM analysis of cuttings provide the necessary information about texture.

Conclusions

1. In contrast to the work presented in this report, Patrick Draw Field has historically been considered structurally homogeneous, dipping monoclinally to the east. Previously unrecognized faults within UA-5 and UA-6 sands of the Almond Formation have been identified in this report by correlation of logs and construction of structural cross sections within Arch and Monell units at Patrick Draw Field. Because of the limitations of correlation it is probable that other faults with less than 10 ft of throw may also be present within the field.
2. Fault zones identified by analysis of structural cross sections are aligned parallel to several surface-mapped faults located immediately west of Patrick Draw Field. The fault zones identified by mapping fault locations identified on structural cross sections are dominantly oriented east-northeast and are offset approximately 30° to the two most dominant surface lineament directions. The dominant fault zones identified by combined seismic and log data are offset 20° and 46° from the major and second major lineament directions. A genetic relationship may exist between the regional surface and subsurface structural features. Carbonate-filled fractures within UA-5 sands have been recognized in cored intervals so there is reason to believe that other fractures may also be present within the field.
3. The documentation of fractures and faults, some of which are filled or partly filled with carbonate cement, within UA-5 sands of the Almond Formation at Patrick Draw Field suggest that tectonic forces may have played an important role in determining fluid migration and distribution within the reservoir. Additional work would have to be done to determine if specific fault or fracture sets are open or closed thereby creating baffles, channels for fluid flow, or reservoir compartments.
4. Production is generally best in the thickest reservoir sands and no obvious correlation exists between the distribution of faults and production maps for Arch and Monell units. However, the coincidence of faults bounding the highly productive sand thick that straddles the Arch-Monell Unit boundary provides an indication that some syndimentary structural control of sand accumulation probably exists.

5. The distribution of faults identified by analysis of log cross sections has a correlation with the distribution of some portions of the isosalinity map, particularly those areas marked by a strong gradient. The eastward projection of a tongue of high formation water salinity within a shallow graben (determined by log correlations) in the southern half of Arch Unit provides the strongest evidence for a relationship between at least some faults and formation water salinity distribution.

6. Faults mapped using the technique of log correlations were primarily of the normal type and the trend of the major identified fault zones are similar to those present west of Patrick Draw Field that have been reported in the literature. The aerial distribution of faults and their relative motions as determined by the technique of tying seismic lines together with log correlations is different. The presence of numerous previously unreported fault zones within Patrick Draw Field has been shown to exist.

7. The fault map constructed with seismic and wireline log data indicate a fairly large number of faults, some with very little vertical throws, criss-crossing Patrick Draw Field. The effect of these faults on primary oil production appears to be relatively minor but in certain parts of the Arch Unit where brittle, carbonate cemented rocks are encountered, the detrimental effect on sweep efficiency due to these faults appears to be significant. Fractures may be generated within the more brittle intervals by some of the faults that resulted in relatively fast breakthrough times in certain areas, particularly in the Arch Unit of the field.

8. The area of high isosalinity gradient located in the eastern part of Arch Unit generally coincides with the location of high resistivities, reflecting coquina development. Evidence for chemical compaction including microstylolitic grain contacts, solution seams, and embayed oyster shells points to a local source for the carbonate cement which is very abundant within the coquina interval.

The correspondence between the occurrence of carbonate-cemented sands and the high gradient areas of the salinity map of Patrick Draw Field indicate that carbonate cement precipitated along a geochemical rather than a lithological boundary.

9. Log-derived V_{cl} data indicate more variability in clay content within the UA-5 sand than do XRD samples. Because of the great variation in clay content encountered it is suggested that XRD samples be used to calibrate the V_{cl} . For one well, Arch 120, the correction factor is V_{cl} minus 3% equals true clay content.

10. The relatively great spatial variability of petrophysical properties within the reservoir, and possibly within mesotidal shoreline barrier reservoirs, results in better correlation of petrophysical properties on a single well basis than for combined wells. Empirically derived median pore throat diameters from four wells correlate with permeability; however, the correlation coefficient is higher on a single well basis. This is significant for field development because it means that relationships between petrophysical properties in a given well (e.g. permeability vs porosity) may not be the same, or may not be accurately predicted even in nearby wells.

11. It was found that the amount of microporosity generally increased with total porosity and clay content for samples tested. More porous reservoir sands often contain increased proportions of microporosity within leached or altered feldspars or lithic fragments. Also more porous intervals tend to have proportionately more loosely associated books of kaolinite cement within interparticle pores. Petrographic analysis indicates that sands with originally unstable grains have been leached and altered so that they have a tendency toward increased total porosity, microporosity, and clay content.

12. The microporous nature of the more porous UA-5 sands may be important to production in that although the micro-network of clay particles may have a negligible effect on porosity, the micro scale of many pores could lead to abundant dead-end pore configurations that result in poor sweep efficiency. Pore system texture then may be the reason for relatively low permeability within the reservoir and may explain the tendency of these sands to have production problems often incorrectly ascribed to mobile fines.

13. Distribution of the coquina that acts as a barrier to fluid flow between western and eastern portions of Arch unit was determined by mapping its occurrence. There is an excellent correspondence between coquina and log signatures. The greatest thickness of coquina is indicated along the sand thin that occurs between the western and eastern bars. However, the distribution of the coquina indicates more than one direction of isolated thicks. Two sub parallel accumulations formed that were probably genetically distinct. The fluid barrier between eastern and western bars may be created by a combination of thin, calcite-cemented sand in the north and impermeable coquina in the south of Arch Unit.

The carbonate-cemented areas may have formed relatively early and remained topographically high during UA-5A deposition, diverting UA-5A sands from the area except in the topographic low between the eastern and western UA-5B bars.

14. Vertical distribution of facies within cored wells indicates that the coquina deposits are on the back or lagoonal side of the barrier. They are most often in association with tidal channel or tidal delta sandstones. Stratigraphic cross sections show that the deposit consists of several successively offlapping thin wedges whose geometry could have formed by overall seaward migration of the barrier system with relatively little lateral (along strike) migration of the inlet/tidal delta complex.

References

- Arp, G. K., 1992, An integrated interpretation for the origin of the Patrick Draw oil field sage anomaly: AAPG Bull. 76 (3), p. 301-306.

Burton, G., 1961, Patrick Draw area Sweetwater Co., Wyoming: *in* Wiloth, G. J., ed., Wyoming Geological Association Symposium on Late Cretaceous Rocks, Wyoming and Adjacent Areas: Sixteenth Annual Field Conference-Green River, Washakie, Wind River and Powder River Basins: Wyoming Geological Association, p. 276-279.

Dewey, J. F., and J. M. Bird, 1970, Mountain belts and the new global tectonics: *Jour. Geophys. Res.*, v. 75, p. 1625-2645.

Lang, H. R., W. H. Alderman, and F. F. Sabins, Jr., 1984, Section 11- Patrick Draw, Wyoming, petroleum test case report: *in* Abrams, M. J., J. E. Conel, and H. R. Lang, eds., The Joint NASA/Geosat Test Case Project, Final Report: AAPG, Tulsa, p. 11-1 - 11-112.

Lundegard, P. D., 1992, Sandstone porosity loss-A "big picture" view of the importance of compaction: *Jour. Sed. Petrology*, v. 62, p. 250-260.

McCubbin, D. G., and M. J. Brady, 1969, Depositional environments of the Almond reservoirs, Patrick Draw Field, Wyoming: *The Mountain Geologist*, v. 6, p. 3-26.

NIPER, 1992, Open file report: Selected reservoir data from Patrick Draw Field: pages unnumbered.

Pittman, E. D., 1992, Relationship of porosity and permeability to various parameters derived from mercury injection-capillary pressure curves for sandstone: *AAPG Bulletin*, v. 76, p. 191-198.

Sales, J. K., 1968, Crustal mechanics of Cordilleran foreland deformation: A regional and scale model approach: *AAPG Bulletin*, v. 52, p. 2016-2044.

Schatzinger, R. A., M. J. Szpakiewicz, S. R. Jackson, M. M. Chang, B. Sharma, and M. K. Tham, 1992, Integrated geological-engineering model of Patrick Draw Field and examples of similarities and differences among various shoreline barrier systems: DOE Report NIPER-575, 146 p.

Szpakiewicz, M. J., R. Schatzinger, S. Jackson, B. Sharma, A. Cheng, and M. Honarpour, 1991, Selection and initial characterization of a second barrier island reservoir system and refining of methodology for characterization of shoreline barrier reservoirs: DOE Report NIPER-484, 170 p.

Van Horn, M. D., 1979, Stratigraphy of the Almond Formation, east-central flank of the Rock Springs Uplift, Sweetwater County, Wyoming: A mesotidal shoreline model for the Late Cretaceous: M.S. Thesis, Colorado School of Mines, 150 p.

Weimer, R. J., 1966, Time-stratigraphic analysis and petroleum accumulations, Patrick Draw Field, Sweetwater County, Wyoming: *AAPG Bulletin*, v. 50, p. 2150-2175.

Weimer, R. J., K. W. Porter, and C. B. Land, 1985, Depositional modeling of detrital rocks with emphasis on cored sequences of petroleum reservoirs: SEPM Core Workshop No. 8, Golden, Colo., 252 p.

White, E. J., O. C. Baptist, and C. S. Land, 1963, Physical properties of the Almond sands in the Patrick Draw area, Wyoming: U.S. Dept. of the Interior, Bureau of Mines, Report of Investigations, p. 1-19.

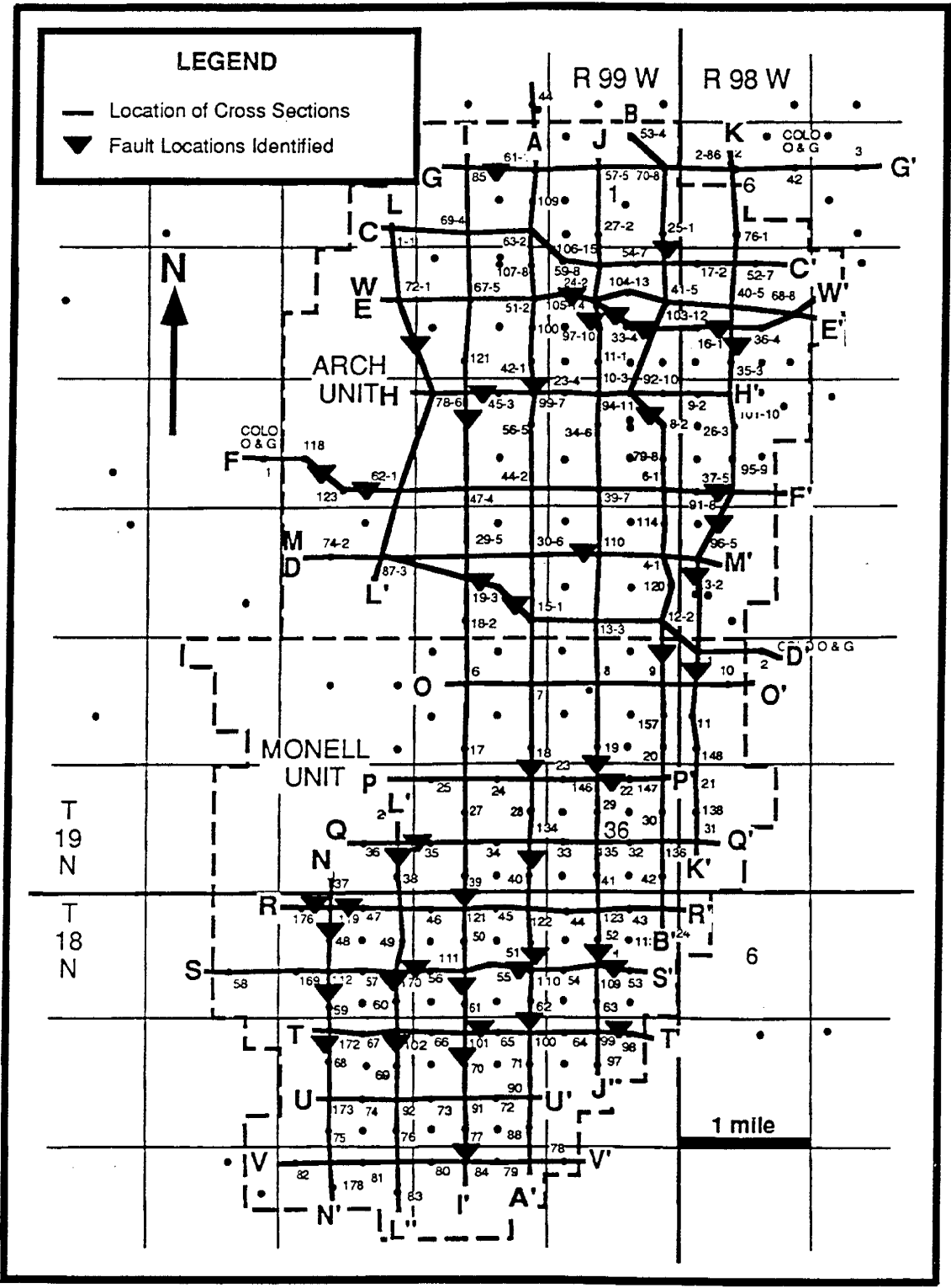


Fig. 4.1. Base map of Patrick Draw Field showing location of structural log cross sections. Faults identified on cross sections are indicated by symbols.

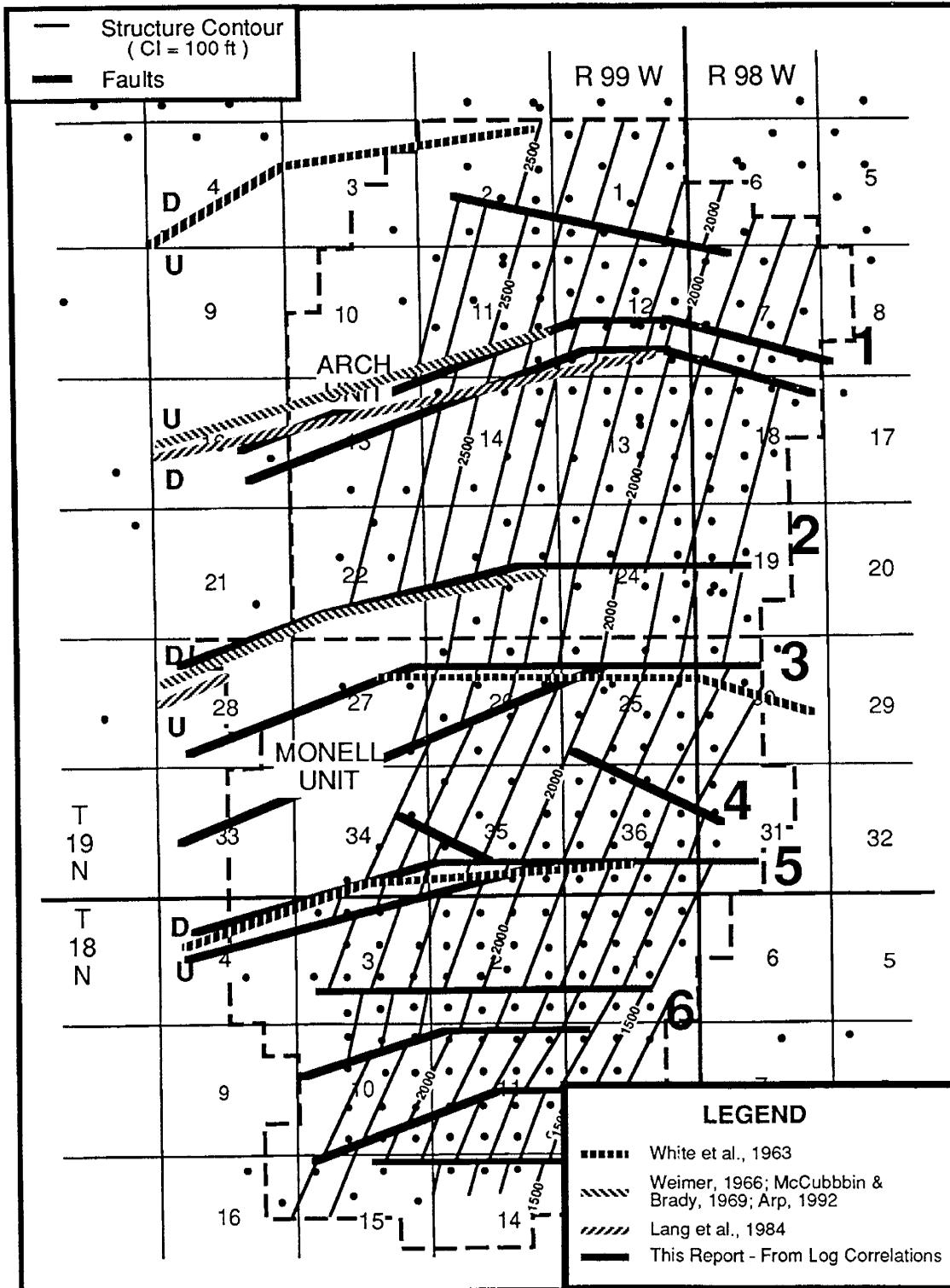


Fig. 4.2. Updated structure map of top of UA-5B sandstone, Almond Formation at Patrick Draw Field showing locations of fault zones identified from structural log cross sections and those published previously.

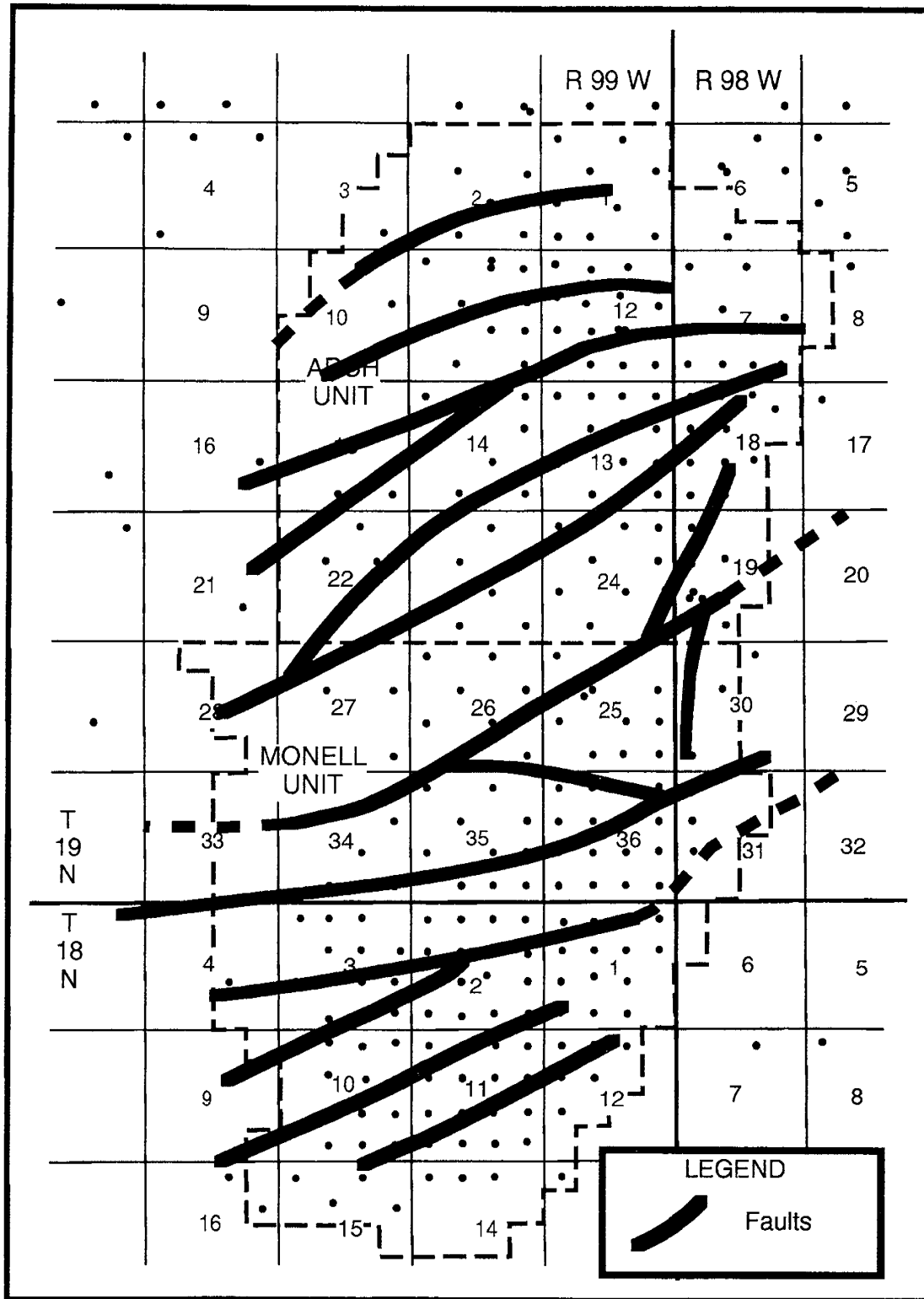


Fig. 4.3. Fault map for Patrick Draw Field derived from combined seismic and log interpretations.

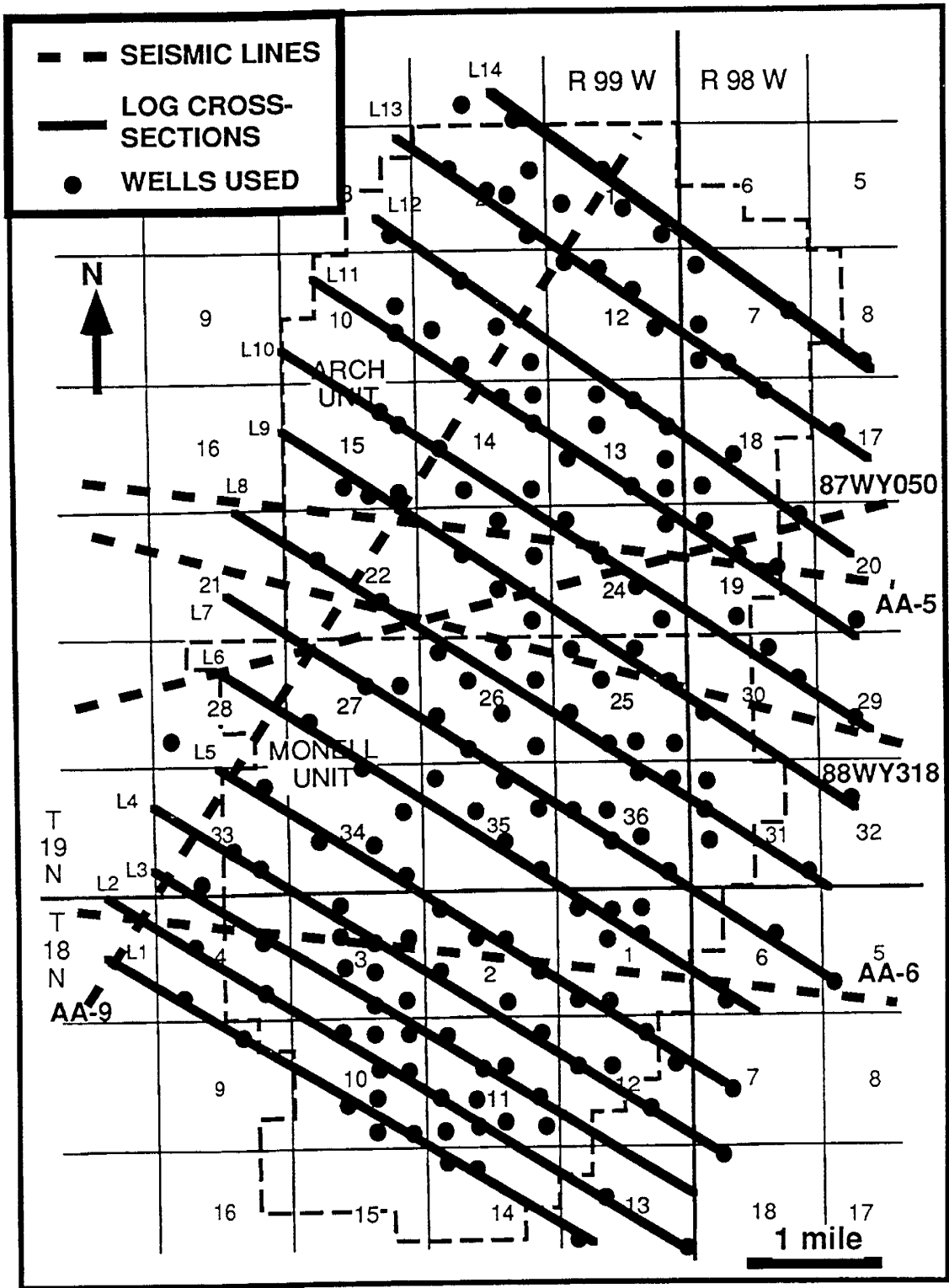


Fig. 4.4 Locations of seismic lines and log cross-sections used in mapping faults at Patrick Draw Field, Wyoming.

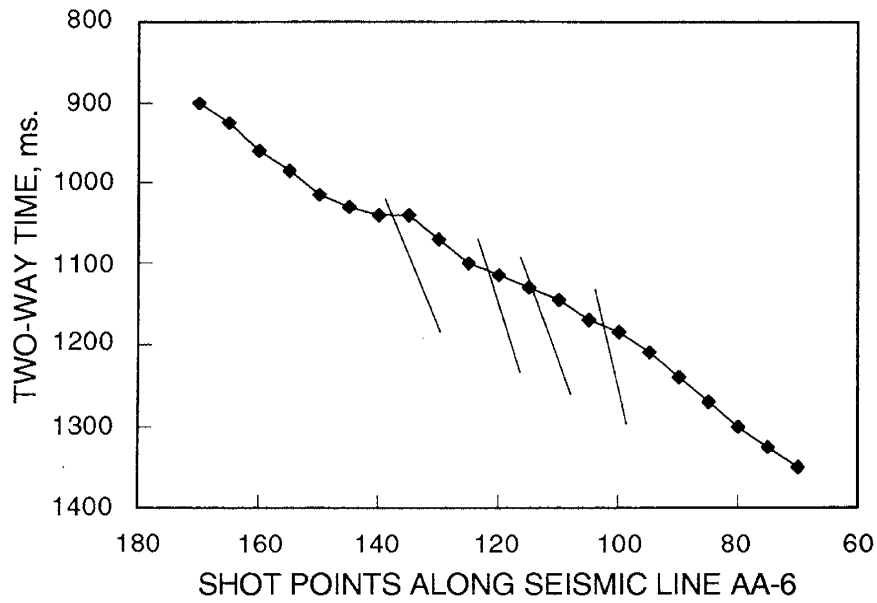


Fig 4.5. Two-way reflection times from the top of Almond Formation along seismic line AA-6. Locations of faults on the section are indicated.

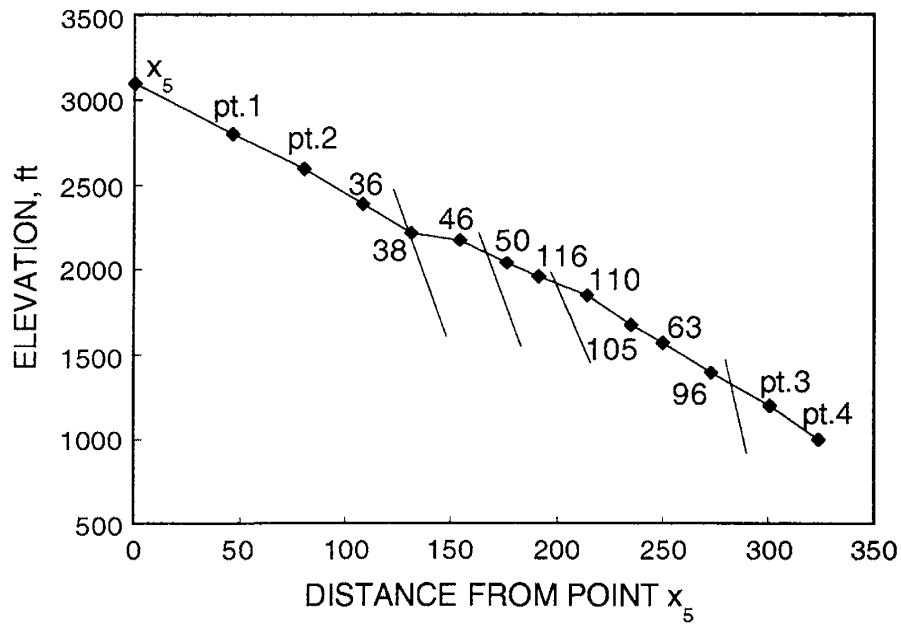


Fig 4.6. Elevations above sea level on the top of UA-5B sandstones obtained from interpretations of core and log data. Locations of wells and other points along the section are indicated. Distance along this profile is measured from an arbitrary point (X₅) located at the western end of this profile.

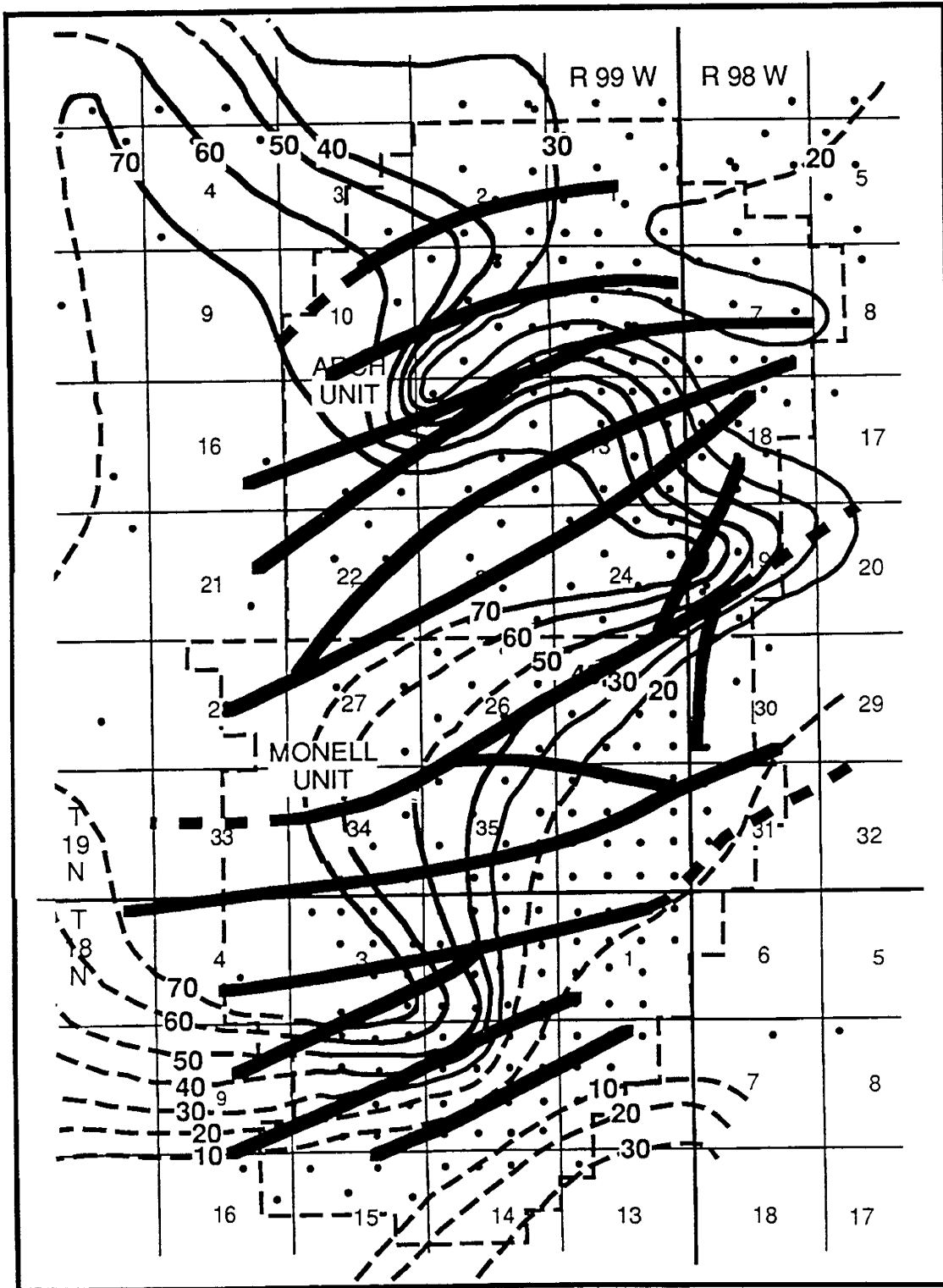


Fig. 4.7. Overlay of the isosalinity map of Patrick Draw area (based on Fig. 2.1) and the location of faults as determined by seismic and wireline log correlations.

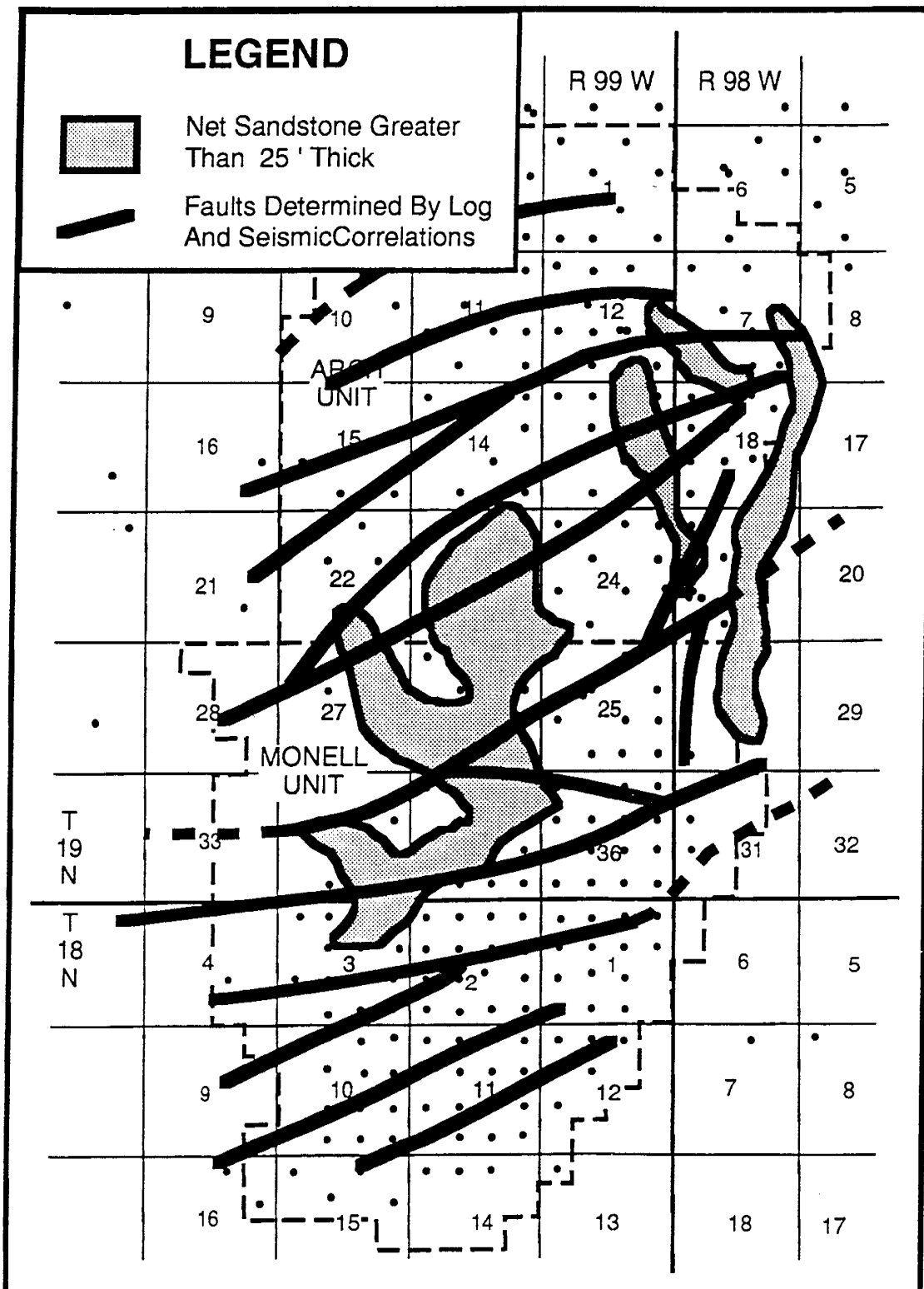


Fig. 4.8. Overlay of major fault zones indicated by electric log correlations compared with the areas of greater than 25 ft thickness of permeable sandstone in Patrick Draw Field.

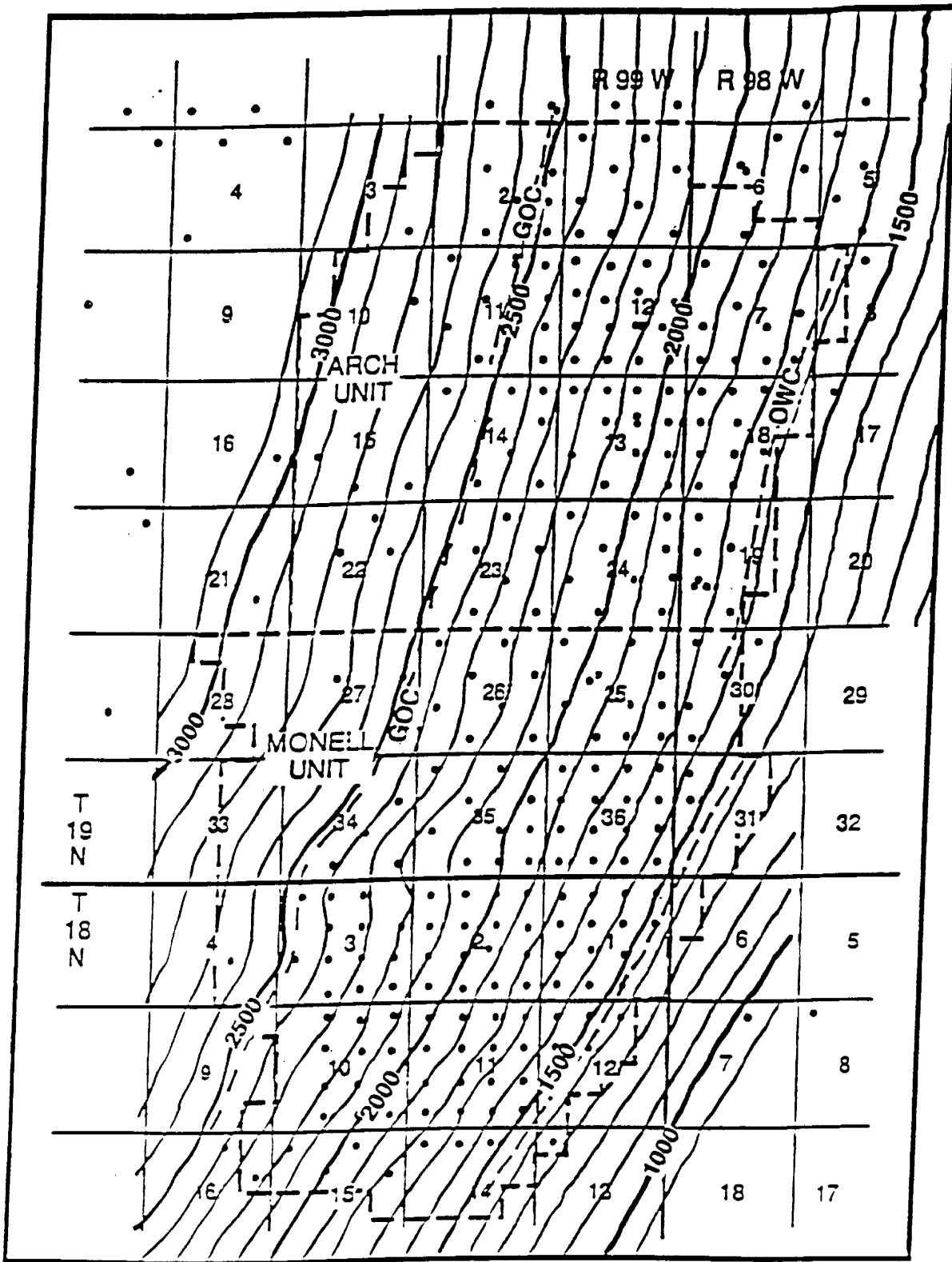


Fig. 4.9. Historical structure map of top of Almond Formation at Patrick Draw Field. Courtesy of UPRC.

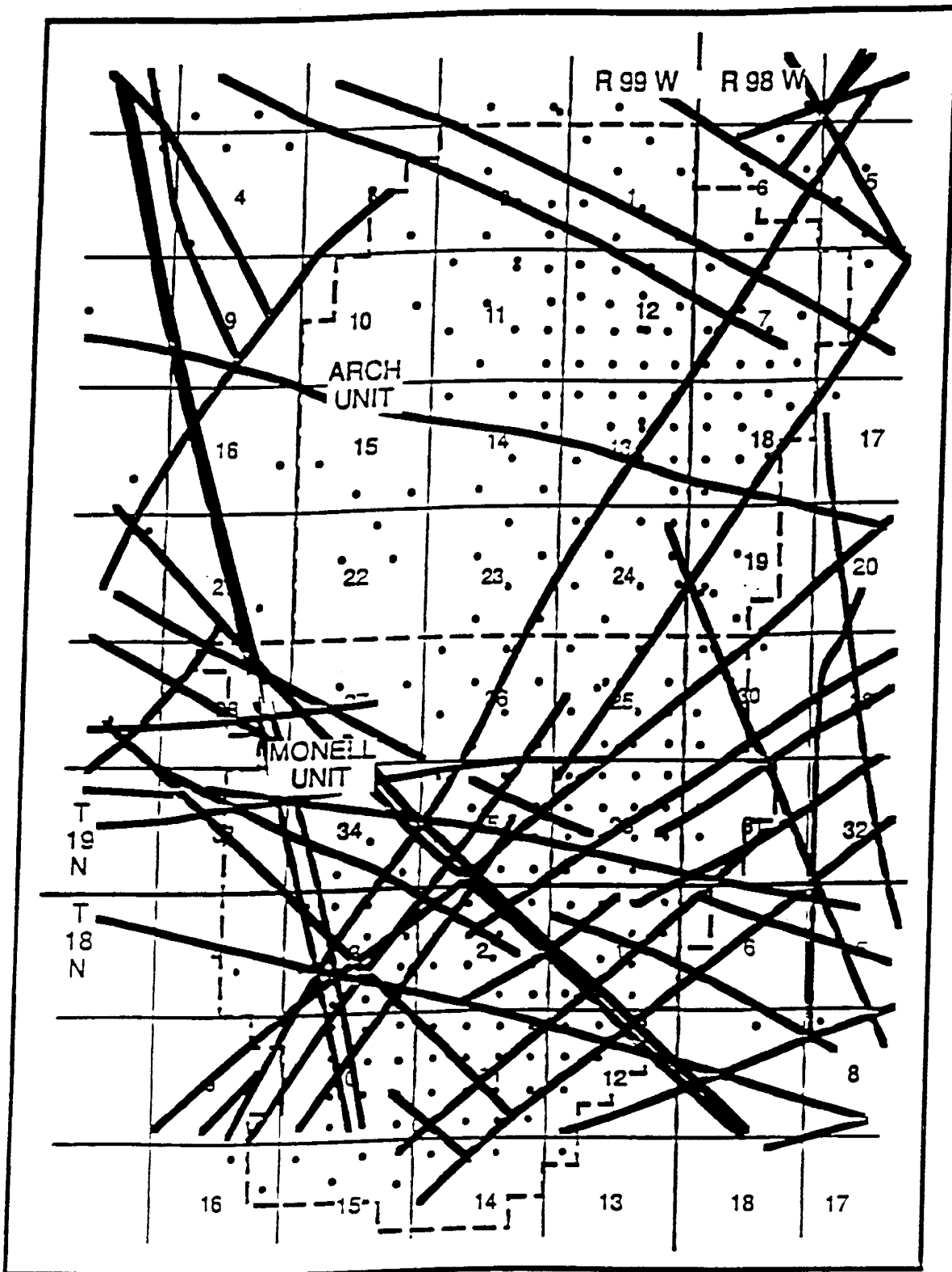


Fig. 4.10. Surface lineaments in the Patrick Draw area. After Lang, et al., 1984.

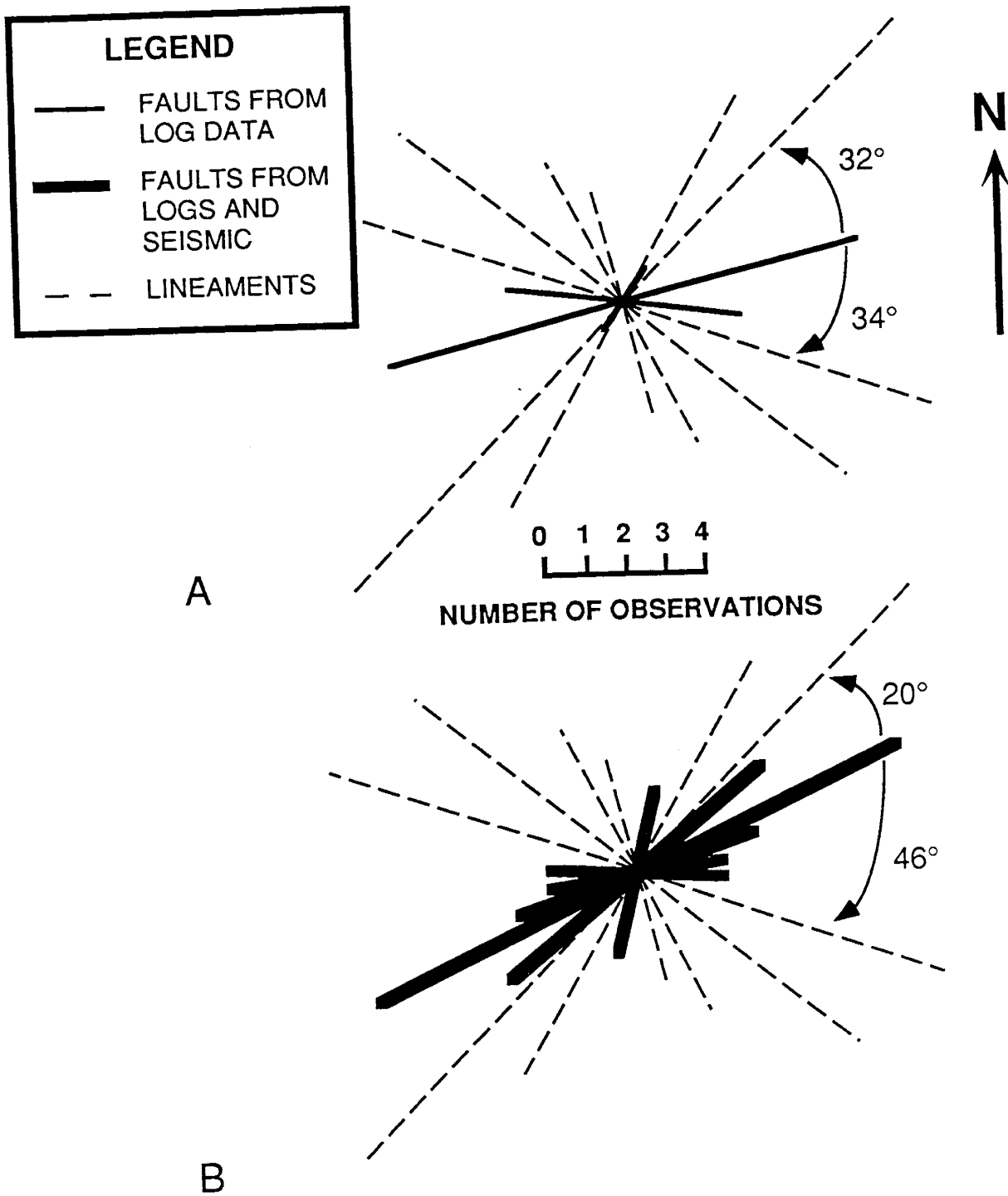


Fig. 4.11. Rose diagram showing the comparison of fault and lineament orientations at Patrick Draw Field. A. Faults include only those identified during construction of structural log cross sections. B. Faults determined from combined log and seismic cross sections. Average lineament orientations for each distinct group is shown. Lineament data taken from Lang, et al., 1984.

ARCH WELL 120

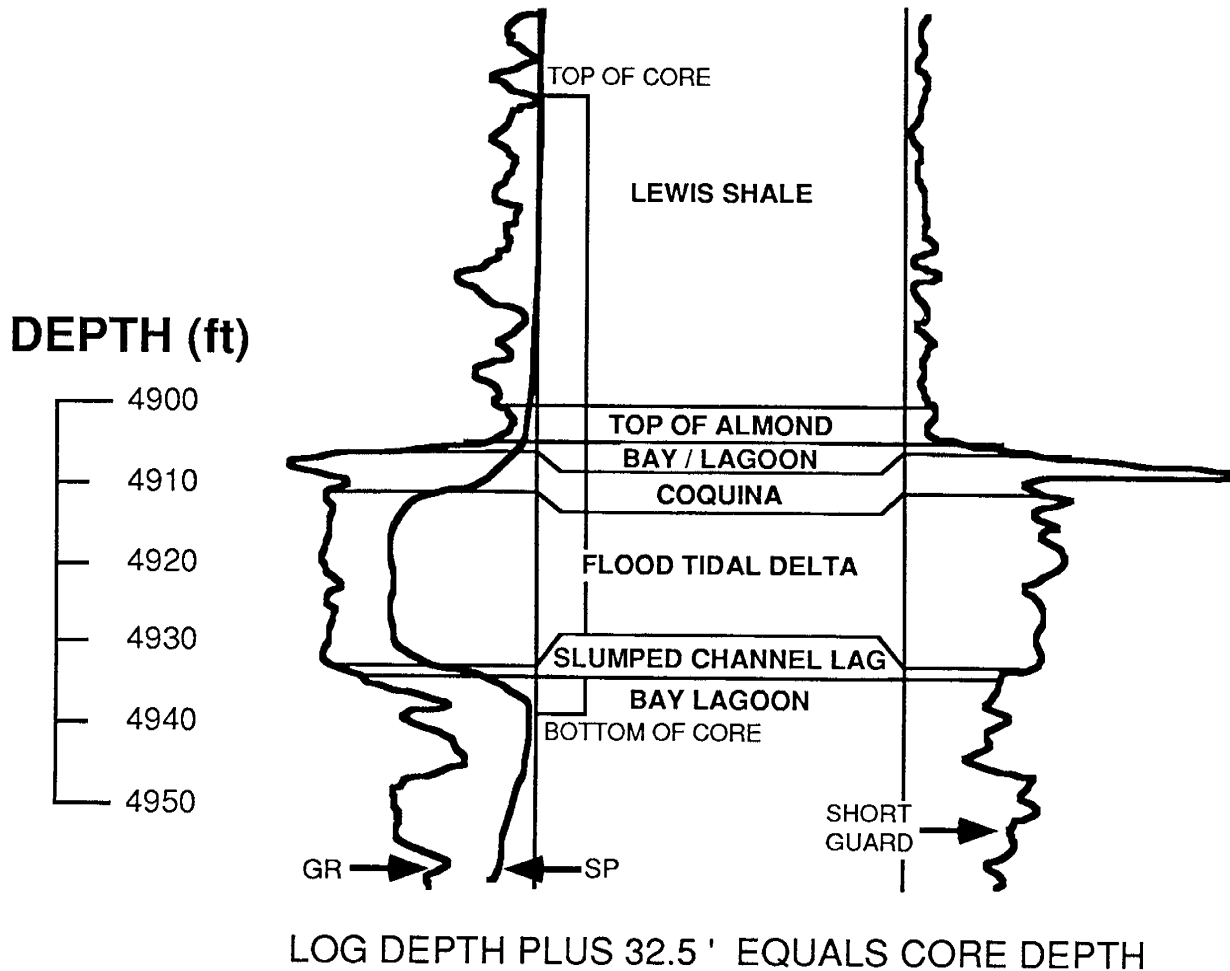


Fig. 4.12. Relationship of log signatures and facies for UA-5 sand, Almond Formation, in well Arch 120.

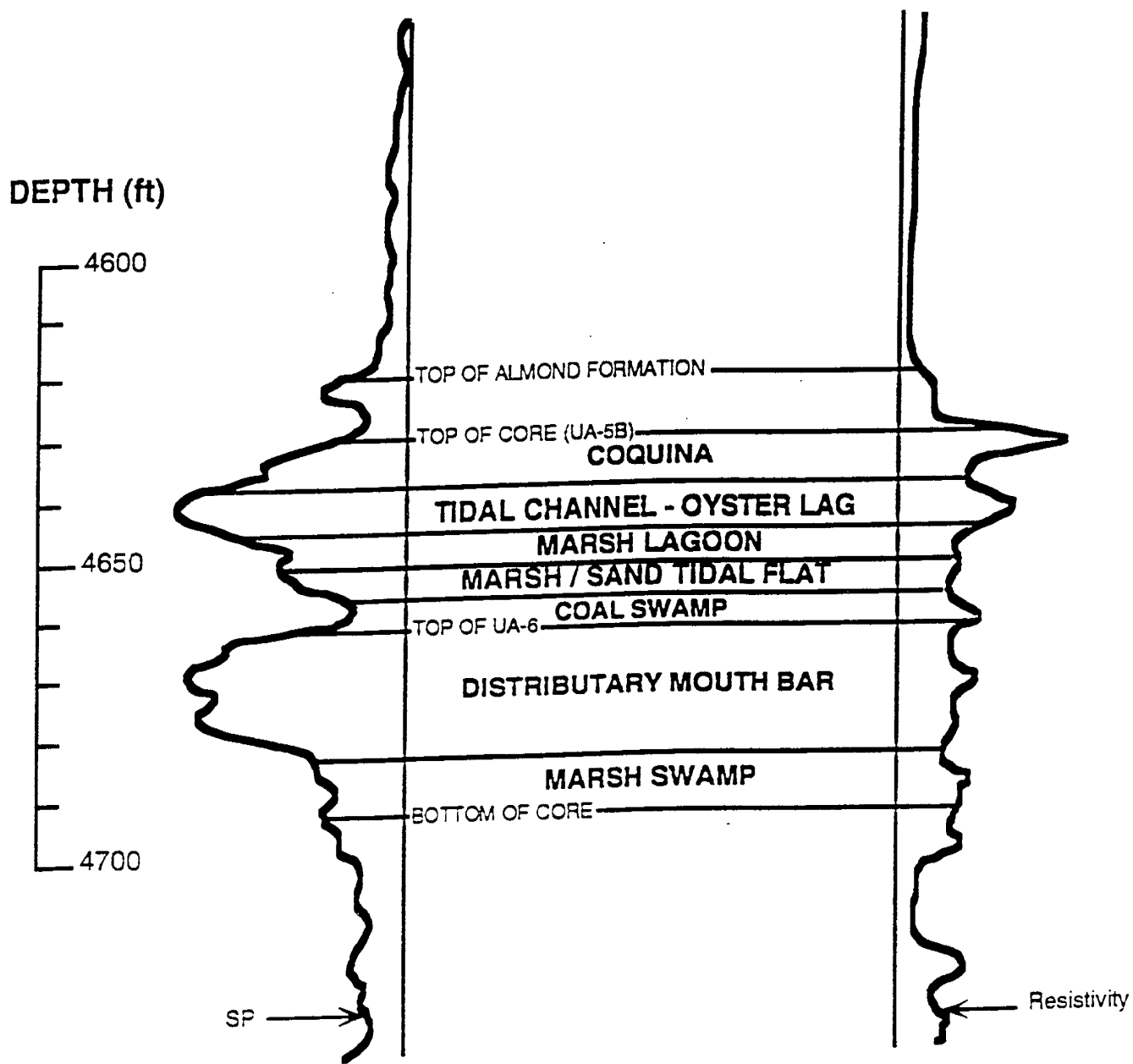


Fig. 4.13. Correspondence between log signatures and facies for UA-5 and UA-6 sands, Almond Formation, in well Arch 106.

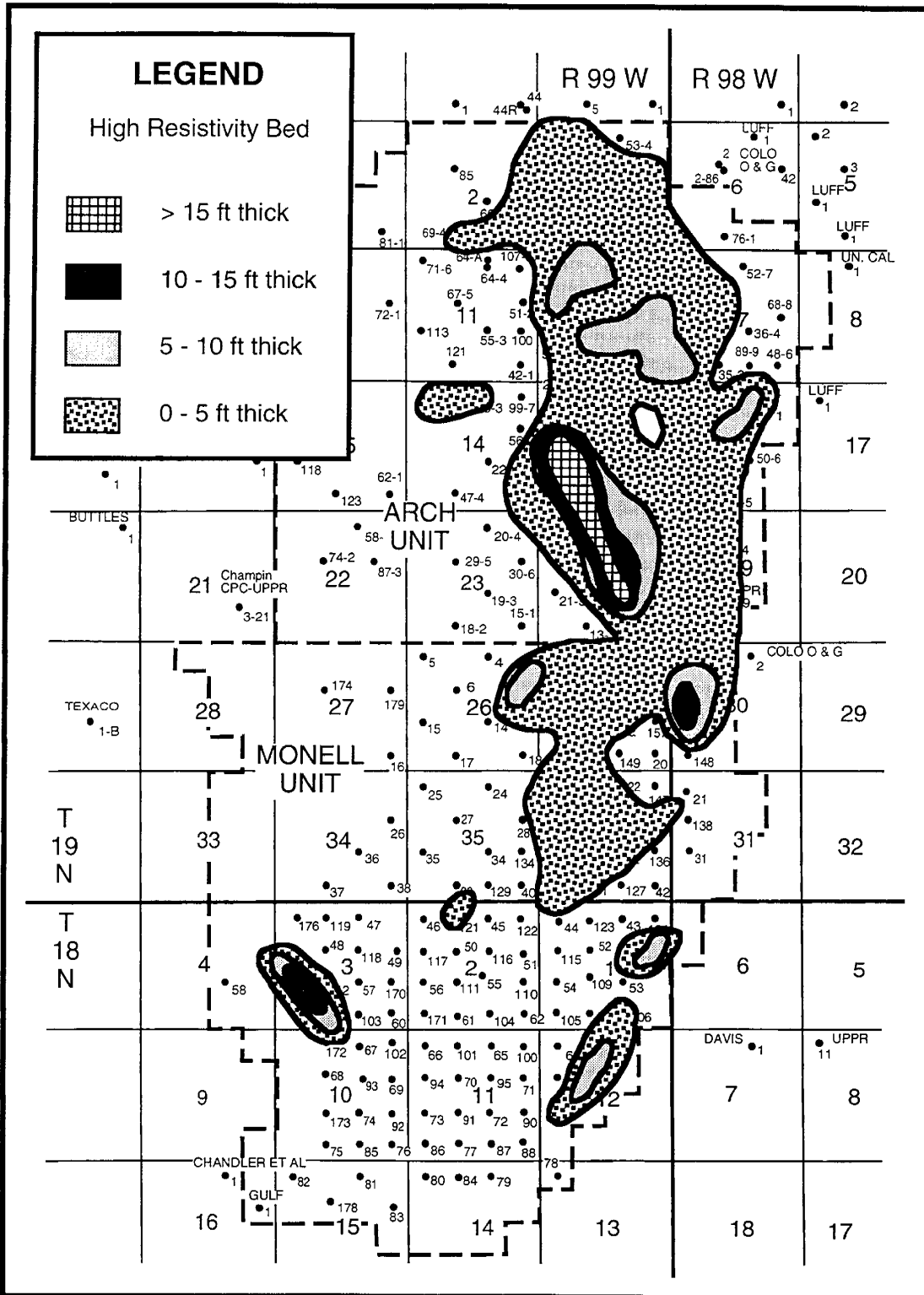


Fig. 4.14. Isopach map showing the distribution of the high resistivity marker at the top of UA-5B.

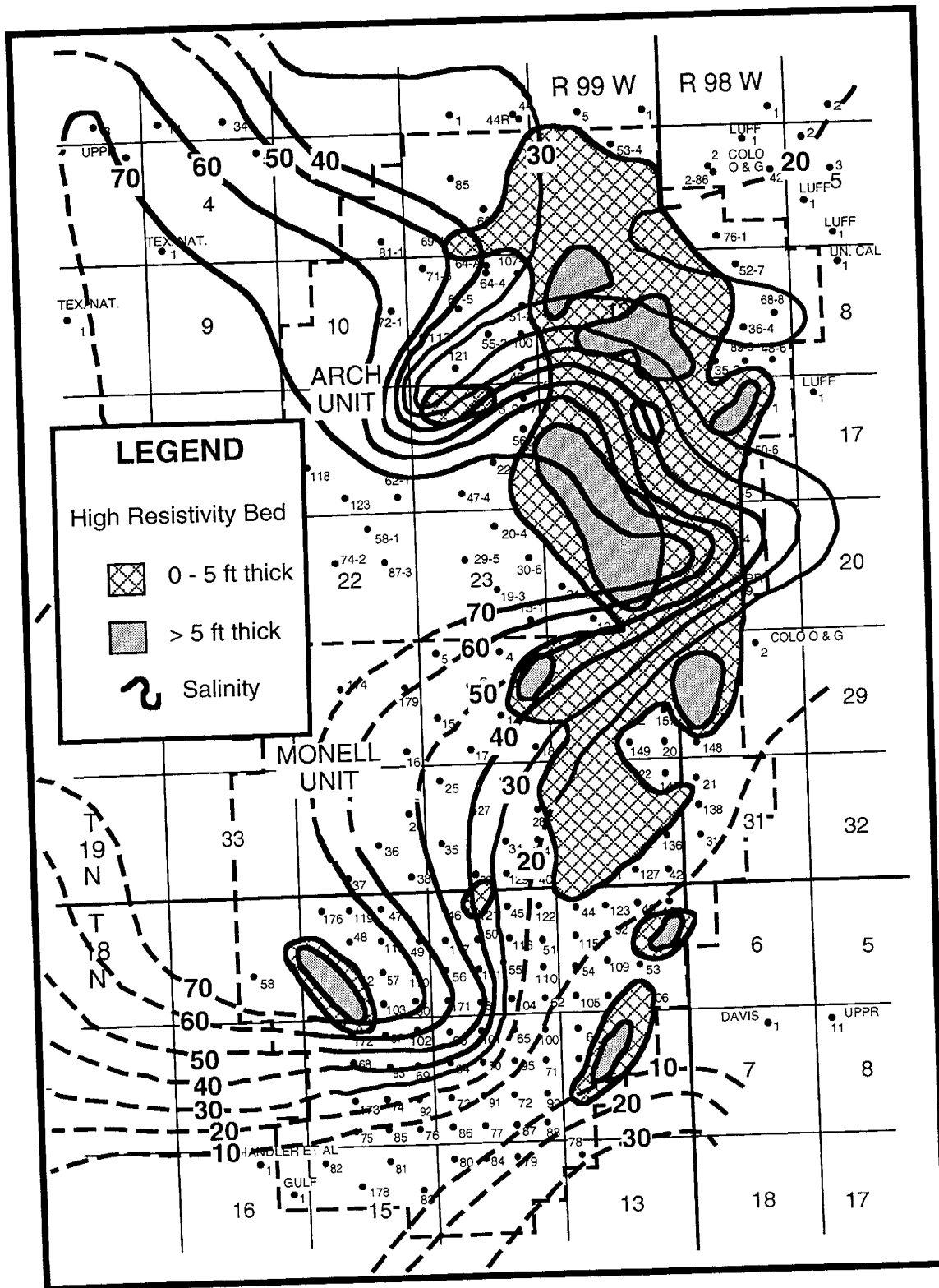


Fig. 4.15. Comparison of formation water salinity and the high resistivity marker at the top of UA-5B.

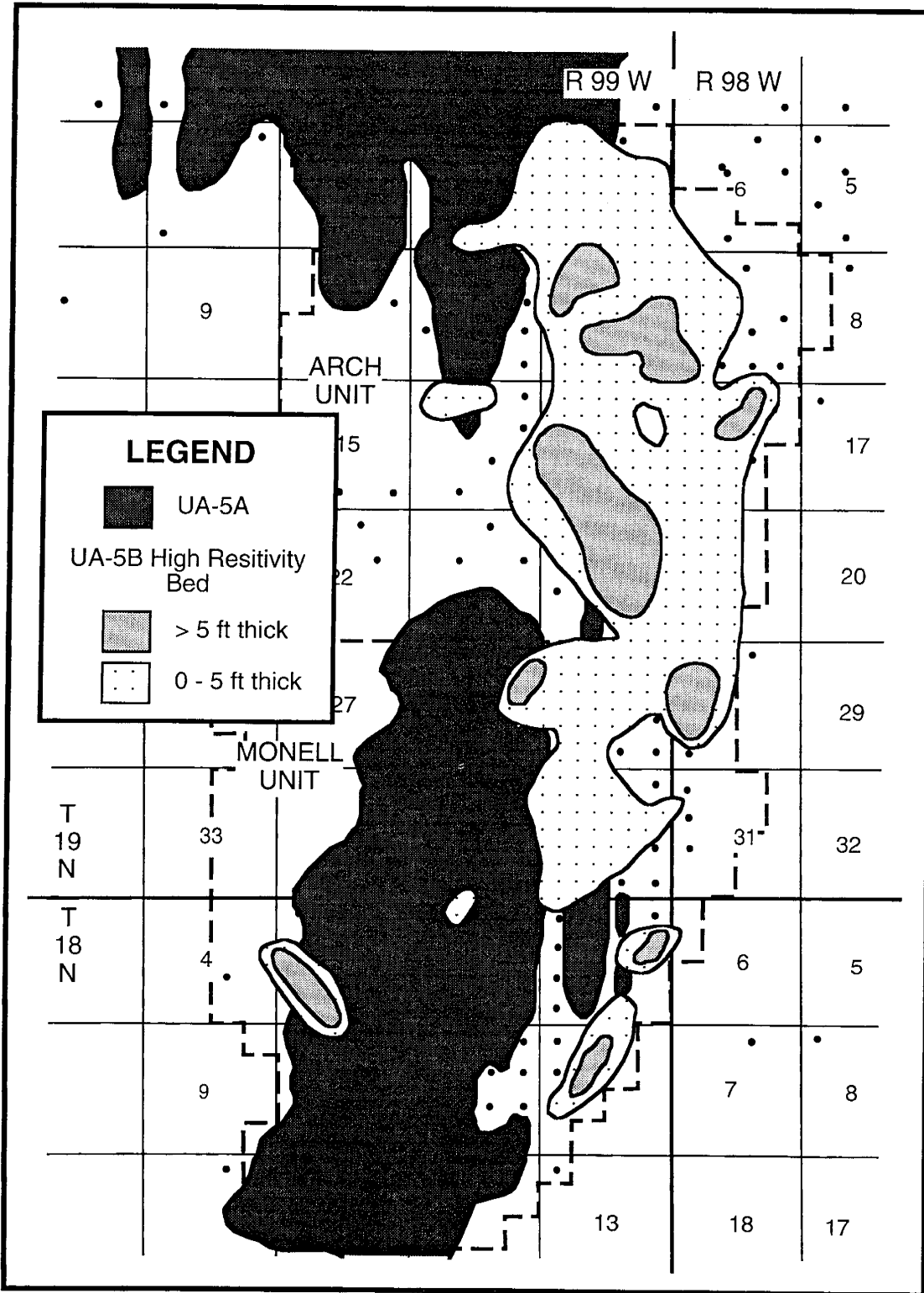


Fig. 4.16. Comparison of the distribution of the high resistivity marker at the top of Almond Formation stratigraphic interval UA-5B and the distribution of UA-5A sands.

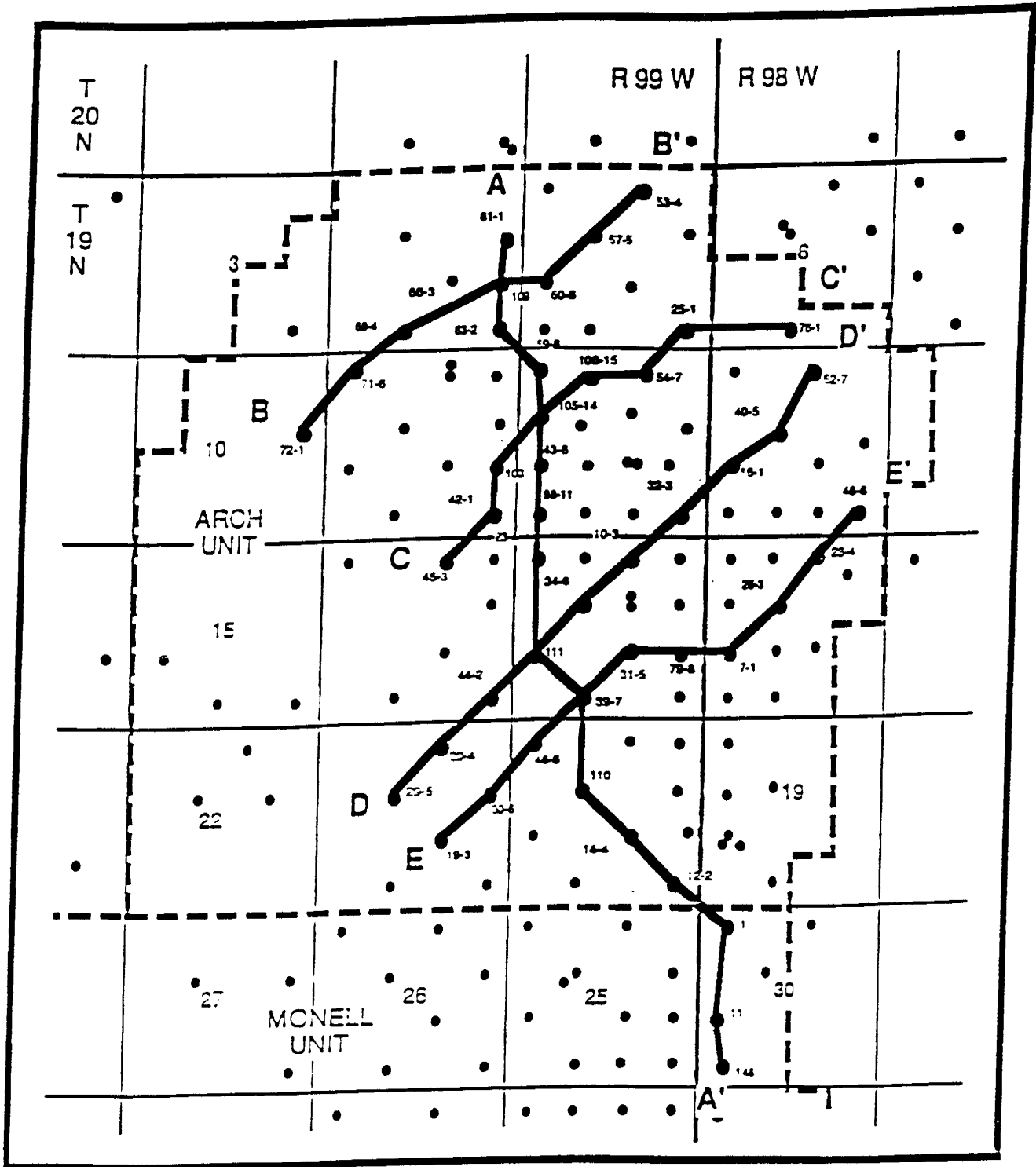
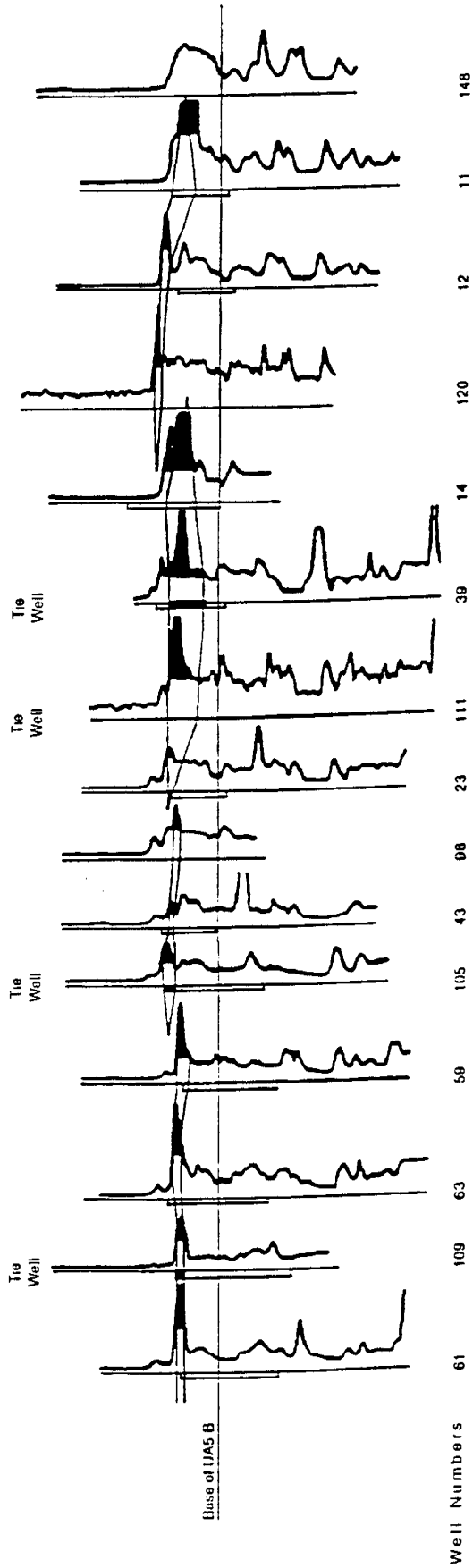


Fig. 4.17. Base map showing the location of resistivity stratigraphic cross sections A-A', B-B', C-C', D-D', and E-E'.

A'



A

Fig. 4.18. Resistivity stratigraphic cross section A-A', which runs along the length of the permeable sand thin between the eastern and western bars in Arch Unit. See Fig. 4.17 for location.

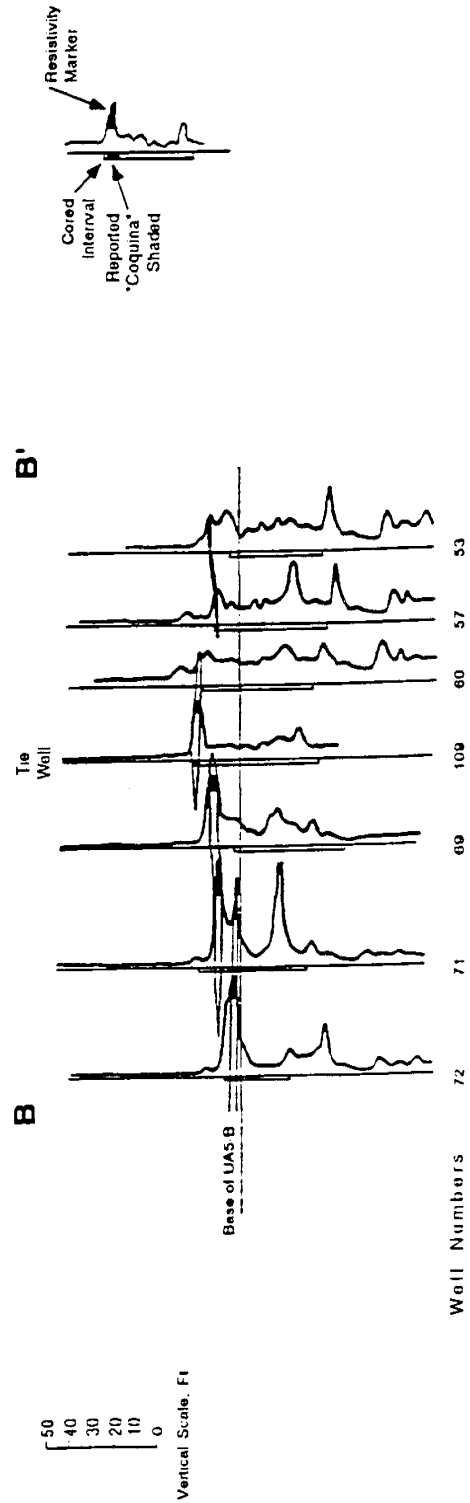


Fig.4.19. Resistivity stratigraphic cross section B-B'. See Fig. 4.17 for location.

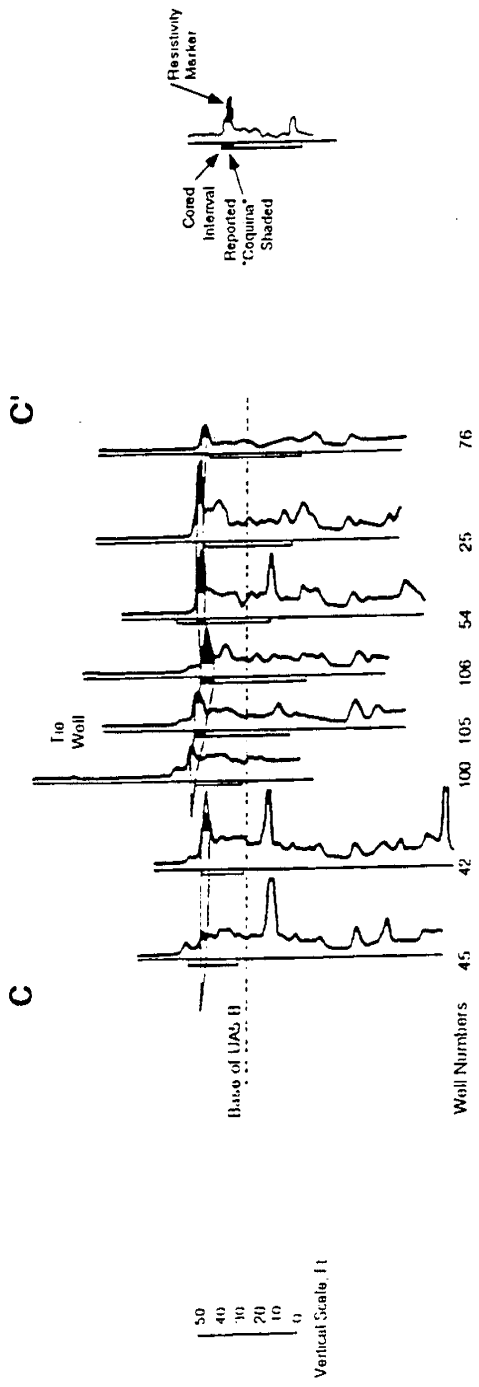


Fig. 4.20. Resistivity stratigraphic cross section C-C'. See Fig. 4.17 for location.

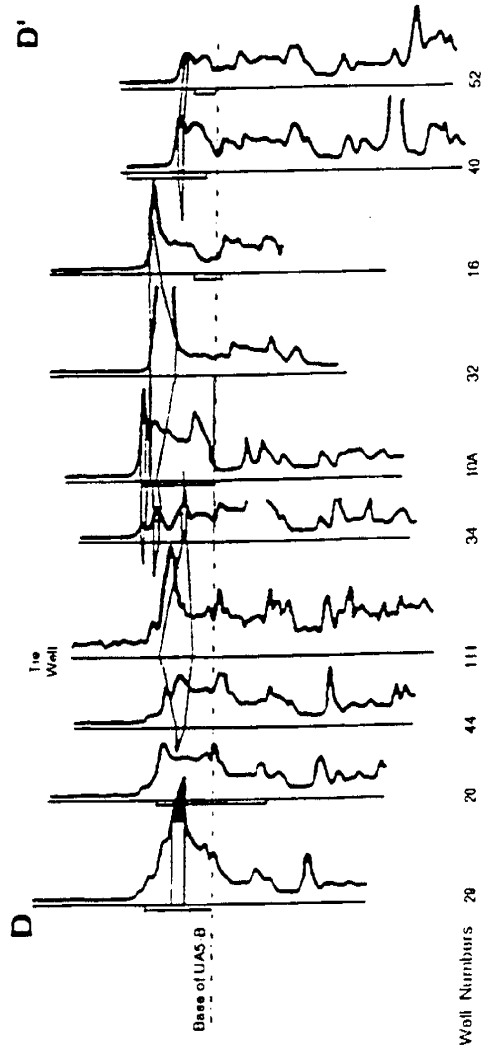


Fig. 4.21. Resistivity stratigraphic cross section D-D'. See Fig. 4.17 for location.

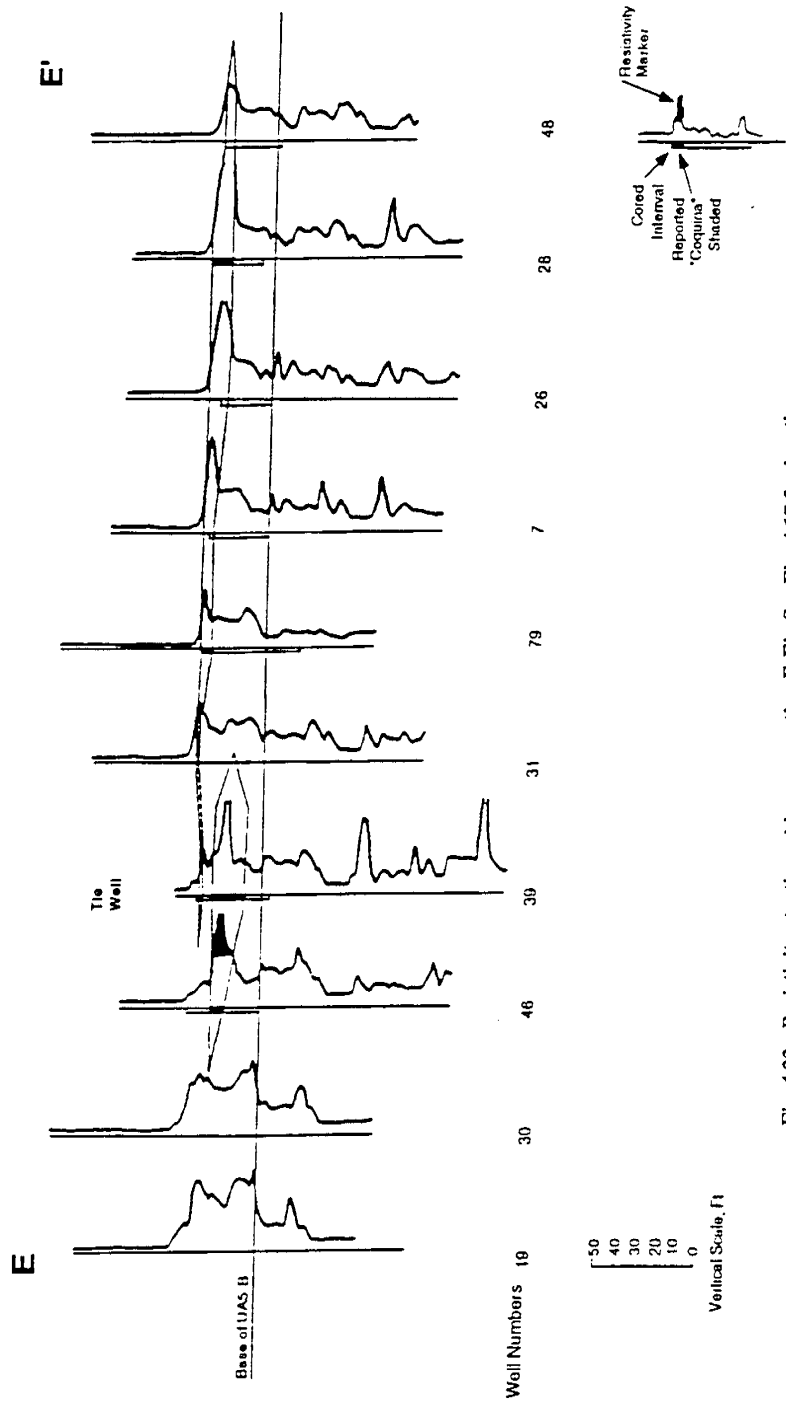


Fig. 4.22. Resistivity stratigraphic cross section E-E'. See Fig. 4.17 for location.

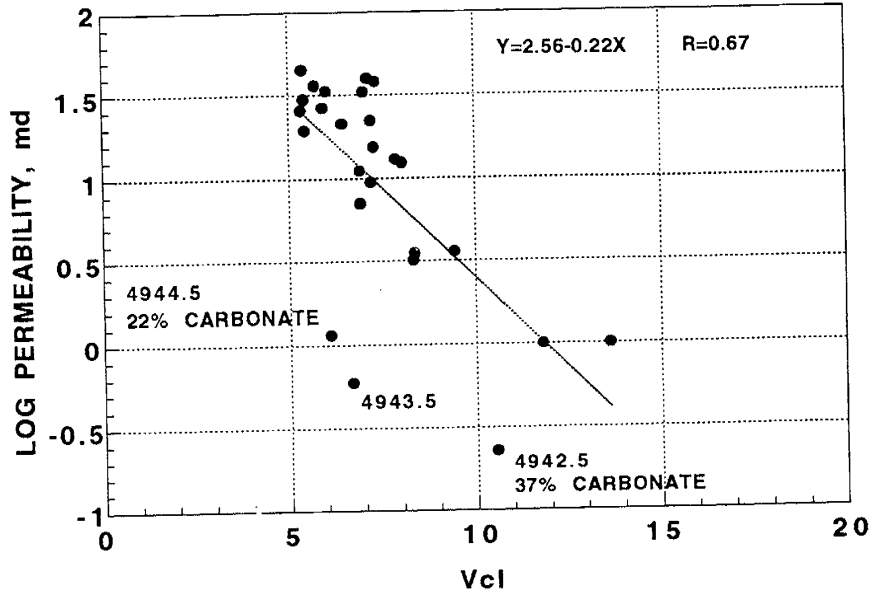


Fig. 4.23. Cross plot of natural logarithm permeability versus log-derived clay content (V_{cl}). Note that samples from 4942.5 ft and 4944.5 ft contain abundant carbonate based on XRD analyses. Density log indicates that the amount of carbonate in the sample from 4943.5 is very similar to that from 4942.5 ft. Other samples contain less than 5% carbonate.

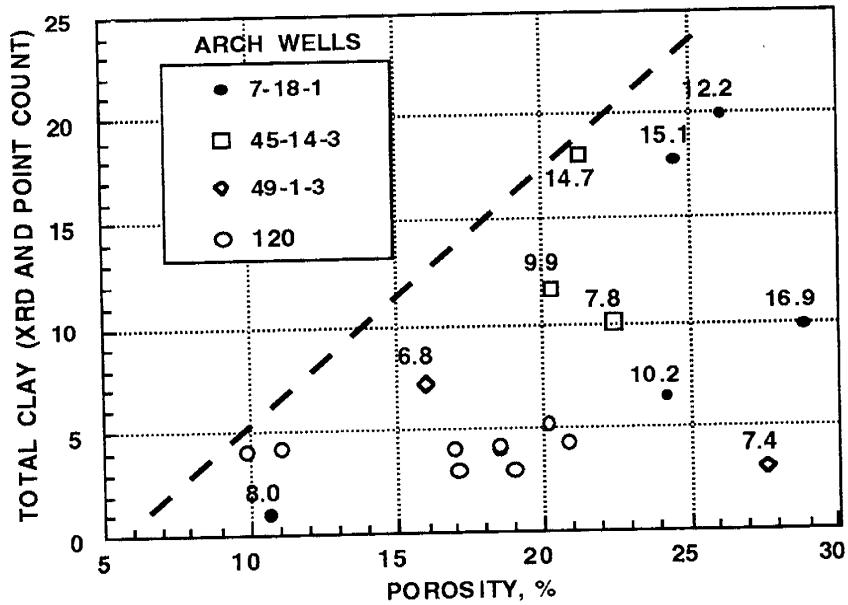


Fig. 4.24. Cross plot of total clay versus porosity. Numbers adjacent to data points represent the difference between bulk volume porosity and point counted porosity which is a measure of microporosity. Dashed line is a general indication of maximum clay content in reservoir quality sandstones for a given porosity.

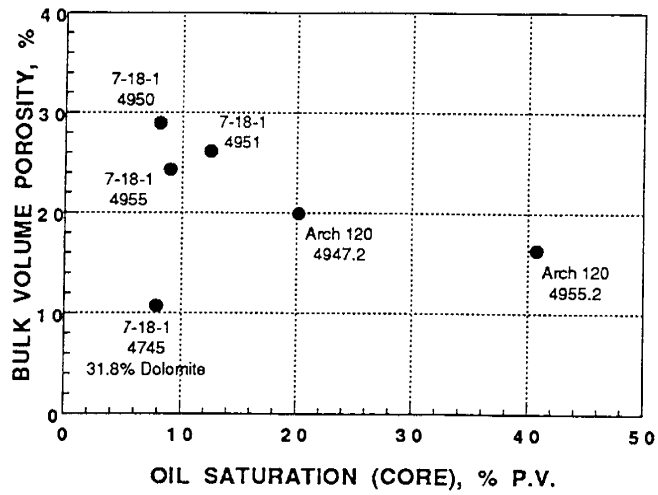


Fig. 4.25. Cross plot of bulk volume porosity versus oil saturation for 6 samples from wells Arch 120 and Arch 7-18-1.

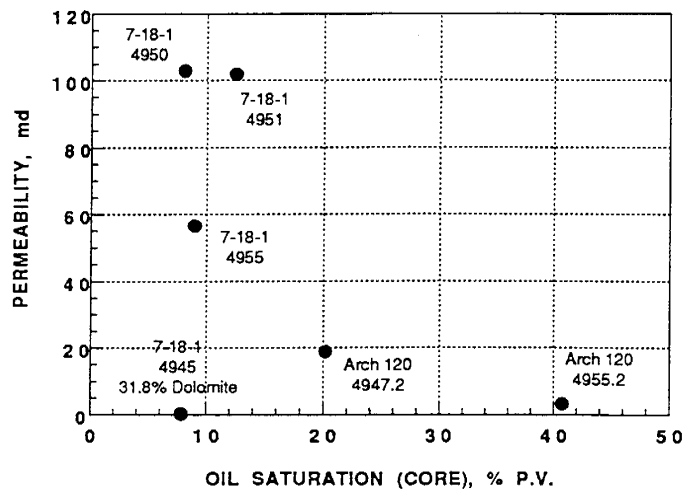


Fig. 4.26. Cross plot of permeability versus oil saturation for same samples as in Fig. 4.25.

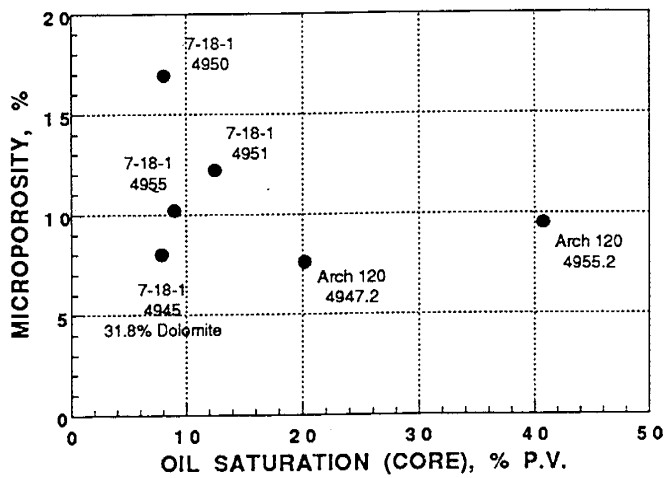


Fig. 4.27. Cross plot of microporosity versus oil saturation for same samples as in Fig. 4.25. Note that samples with greatest microporosity have lowest oil saturation.

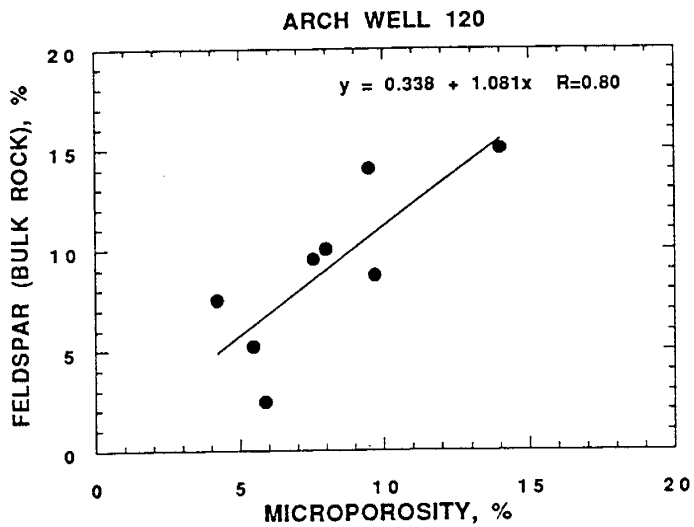


Fig. 4.28. Cross plot showing relationship between feldspar content of thin sections from well Arch 120 and microporosity.

CHAPTER 5

ANALYSIS OF RESERVOIR AND PRODUCTION/INJECTION DATA

By Ming-Ming Chang

Chapter Summary

Petrophysical Properties

The efficiency of waterflood recovery was found to increase with the average permeability of reservoir rock among 12 five-spot patterns in the Monell Unit. The reason for this correlation may be a high ratio of oil relative permeability to water relative permeability (k_{ro}/k_{rw}) for the rock of higher permeability values in this strongly water wet system as evidenced by relative permeability measurements. In contrast, no correlations were found between oil recovery efficiencies and Dykstra-Parsons coefficients in either Arch Unit or Monell Unit, suggesting that the Dykstra-Parsons coefficient is not a good indicator of production performance in Patrick Draw Field. In comparison to other Arch wells, well Arch 12 has poor primary recovery in spite of a high average permeability of 110 mD, indicating possible poor fluid continuity or a small drainage area for this well.

Production/Injection Analysis

The best production at Patrick Draw Field lies primarily in the area of good oil resource with a thick pay and a high oil saturation value. Water injection and the expansion of neighboring gas cap contributed to successful production from the southwestern area of Arch Unit and the northwestern area of Monell Unit. Decline of reservoir pressure and little water production before the initiation of waterflood suggests an inactive aquifer or poor lateral communication with the Almond Formation aquifer down dip at the oil-water contact.

In the investigation of lateral variation of cumulative and initial oil production from UA-5B sandstone along three east-west profiles it was observed that the production in the southwestern part of the Arch Unit (the well 44 area) was much higher compared to that in the central part of the unit (around well 88) although the latter area had greater pay thickness and better flow properties. Further analysis was conducted to document this distribution and to determine possible causes for the production differences.

Waterflood recovery is poor ranging from 7 to 288 MSTB per well in Arch Unit because of the fast water breakthrough and short periods of oil bank production. The mean and median of waterflood recovery from 39 Arch wells are 62.7 and 53.3 MBBL, respectively. This corresponds to about 15% OOIP and about one-half of primary recovery of Arch wells.

In Monell Unit, the waterflood production ranged from 50 to 1366 STB oil per well with a mean of 321.7 MBBL

and a median of 244.4 STB. This is comparable to the primary recovery (average 290.7 STB per well) and equivalent to a recovery of approximately 18% OOIP. Oil production decreases from the western part toward the eastern part of the field. The smooth change in oil production is caused by a gradual variation of oil-in-place.

Monell wells have ultimate recovery efficiencies ranging from 20% to more than 50% indicating a good oil recovery. Arch Unit has a relatively poor recovery efficiency except for the area immediately west of the low-permeability thin-pay area. The water injection volume in Monell Unit is proportional to its waterflood production of nearby producers. The water injected ranged from 15 to 60% pore volumes (PV) for most Monell wells and 10 to 40% PV for most Arch wells.

A high degree of heterogeneity in Arch Unit is evidenced by: a) sand discontinuity or compartments indicated by the drastic change in pay thickness and fluid saturations; b) a poor sweep efficiency and low waterflood recovery compared to that in Monell Unit; and c) the large contrast of water breakthrough times that ranged from less than 1 month to more than 100 months. The early breakthrough may be due to severe water channeling in the gas phase in high-permeability zones.

Reservoir volume balance calculations in three regions of the Arch Unit show no evidence of loss of injection water to sands other than UA-5 and UA-6 sands. This indicates that no major conduits connect the UA-5, UA-6 sands to other sands. Due to the large volume of gas production near the gas cap in the western edge of the field, the western region of Arch Unit showed a smaller ratio of injection to production volume than the eastern region.

No significant wellbore damages were identified in Hall plots for most injection wells in Arch Unit. This is evidenced by the constant slope of the Hall plots after the gas space in the reservoir was filled by water. The values of Hall plot slopes in Arch Unit is related to the presence of a thin pay or deterioration of the quality of pay sands. Some sharp increases in the Hall plot slope at the late injection stage were caused by shut-in of surrounding production wells.

Numerical simulations demonstrate that the slope of Hall plot increases with the number of nearby barriers and with the decrease of the distance between barriers and the injection well. Analytical calculations of injection pressures show a significant increase when one barrier is less than 200 ft away or two intersecting barriers are less than 400 ft away. The effect of the orientation of barriers on injection pressure; however, is not as significant as the distance of barriers from the injector.

An analysis of the enhanced oil recovery (EOR) potential

of Patrick Draw Field indicates that the northwestern and central parts of the Monell Unit are recommended project areas because of the relatively high ROS and uniform pay. CO₂ flooding is a candidate EOR process because of the reservoir pressure in the Monell Unit is higher than the minimum miscible pressure and a nearby source of CO₂ is available.

Petrophysical Properties and Oil Recovery

Introduction

Petrophysical properties such as permeability, porosity, pay thickness, and water saturation were analyzed foot-by-foot for wells in both Arch Unit and Monell Unit. Statistics of these petrophysical properties were compared between Arch and Monell Unit. Correlations of vertical profiles of well permeability with oil recovery in primary production and waterflood stages were made. Dykstra-Parsons coefficients were found to be a poor predictor of production in Patrick Draw Field. In contrast, rock permeability shows a positive relationship with both primary and waterflood production.

Rock Permeability

Permeability data provided by the UPRC from conventional core analyses were statistically analyzed for 70 Arch wells and 38 Monell wells. A total of 1,341 permeability measurements of UA-5 sand from 70 Arch wells shows an arithmetic mean permeability of 39.5 mD and a geometric mean of 16.5 mD. The permeability measurements show a somewhat log-normal distribution, skewed toward the low permeability values (Fig. 5.1). The whole set of permeability values has a Dykstra-Parsons coefficient (V_{DP}) of 0.825 and a coefficient of variation of 0.621. The logarithmic values of rock permeability were used in calculating this coefficient of variation.

A log-normal distribution (Fig. 5.2) was also found for 811 permeability measurements from 38 Monell wells. The foot-by-foot permeability values of Monell wells have an arithmetic mean of 27.7 mD and a geometric mean of 13.3 mD. The Dykstra-Parsons coefficient of Monell permeability distribution is 0.780, and the variation coefficient is 0.585. Comparison of the permeability distributions indicate that Monell wells have a lower mean permeability but a more homogeneous permeability distribution as evidenced by the lower value of Dykstra-Parsons and variation coefficients.

The mean value was calculated for the permeability profile of 70 wells in Arch Unit and 38 wells in Monell Unit. Histograms of mean permeability values for wells in these two units are shown, respectively, in figures 5.3 and 5.4. Arch Unit has a higher mean permeability per well than Monell Unit. Arch Unit has a permeability mode between 20 and 40 mD, whereas Monell Unit has a mode from 0 to 20 mD.

In Monell Unit, the low permeability values (<10 mD)

are found only in the northeastern and the southwestern edges of the arithmetic mean map and the geometric mean map (Fig. 5.5). The arithmetic and geometric mean values were calculated from the permeability profile of each well to derive the mean permeability for the arithmetic and geometric mean permeability maps, respectively. In the Arch Unit, the low permeability values (<10 mD) are found more in the northwestern region or the area near the low permeability thin pay (Fig. 5.5).

Histograms of Dykstra-Parsons coefficients (V_{DP}) are plotted for Arch wells (Fig. 5.6) and Monell wells (Fig. 5.7). These two histograms show similar statistics and cover a similar range (from less than 0.4 to approximately 0.9) of V_{DP} values. Arch Unit has 0.67, 0.66, and 0.13 for the mean, median, and standard deviation, respectively, of V_{DP} distribution. In comparison, Monell Unit has 0.65, 0.64, and 0.14 for the mean, median, and standard deviation, respectively. The V_{DP} values of most individual wells are lower than that calculated based on permeability values from the whole field or unit, indicating greater permeability variation on a field-scale than within individual wells.

Figure 5.8 shows the distribution of V_{DP} values in Patrick Draw Field. No patterns in the distribution of V_{DP} can be identified in either Unit except a slightly higher value of V_{DP} was found in the northern part of Arch Unit. The area of large V_{DP} values agrees well with that of low permeability value in Arch Unit. The small portion of high permeability facies found from wells with low permeability UA5 sands cause large contrasts in permeability profiles and therefore large V_{DP} values for these low permeability wells.

Porosity, Pay, and Saturation

The foot-by-foot measurements of porosity and pay thickness of Arch and Monell wells were examined using statistics. The water saturation values in Patrick Draw Field were investigated from resistivity logs based on the formation water salinity distribution mapped in Chapter 2 in this study.

Porosity and Pay The arithmetic mean of foot-by-foot log measurements of porosity, pay thickness, and water saturation was calculated for 100 Arch wells and 143 Monell wells. The statistics of these petrophysical properties including permeability values is listed in Table 5.1.

Porosity values show a normal distribution in both Arch Unit (Fig. 5.9) and Monell Unit (Fig. 5.10). Arch Unit has a higher porosity value (20.5% for both mean and median) than Monell Unit (18.9% for both mean and median). The standard deviation is also slightly higher for Arch Unit (1.68%) than that of Monell Unit (1.21%).

The map of mean porosity per well UA-5 (Fig. 5.11) presents an interesting comparison of porosity distributions in the Arch and Monell Unit. In the Monell Unit, the mean porosity value per well decreases gradually from more than 20% in the northwestern area near the gas

cap to less than 18% at the southeastern edge near the water-oil contact. In contrast, porosity values show a scattered distribution in Arch Unit. A well of low porosity value (<19%) can be found next to wells which have high porosity values (>22%) in several locations in Arch Unit, indicating a more heterogeneous environment than that in Monell Unit.

As illustrated in figures 5.12 and 5.13, pay thickness in Arch Unit (16 ft for mean and median) is less than that in Monell Unit (20.3 ft for mean and 22 ft for median). Both Arch and Monell Units have about the same range of pay thickness where Arch Unit has a mode ranging from 10 to 15 ft and Monell Unit from 20 to 25 ft. The relatively thinner pay in Arch Unit results in a lower mean value for OOIP in the Arch Unit (Fig. 5.14) than that for Monell Unit (Fig. 5.15). The pay thickness and OOIP per well show similar skewness in distribution curves because of normal distributions of porosity and saturation values. The OOIP per well in figure 5.15 is expressed as the product of porosity, pay, and oil saturation. The equivalent OOIP in a 40-acre spacing for an mean well is 549 MBBL in Arch Unit in comparison to 701 MBBL in Monell Unit.

Permeability and Primary Recovery

Dykstra-Parsons coefficients of Arch wells, calculated using a formula derived by Hirasaki (1985), range from less than 0.4 to more than 0.9 with an mean of 0.67. Monell wells show a similar distribution of Dykstra-Parsons coefficients.

Arch wells show no correlations between efficiency of primary oil recovery and Dykstra-Parsons coefficient (Fig. 5.16). A weak relationship exists between primary recovery efficiency and mean permeability (Fig. 5.17). The wells with good permeability values (above 40 mD) showed slightly better recovery than those wells with low permeability values (less than 40 mD). An exception was found for three wells (Arch 21, 44, and 46) which are located near the bottom of the oil column west of the low-permeability, thin pay in Arch Unit. Pressure maintenance due to gas cap expansion in the western region of Arch Unit resulted in a primary oil recovery greater than 50% for wells 21, 44, and 46 having an mean rock permeability less than 40 mD. Arch well 12 has a poor primary recovery in spite of a high permeability of 110 mD, indicating possible poor fluid continuity or a small drainage area for this well.

In Monell Unit, correlations were found neither between primary recovery efficiency and Dykstra-Parsons coefficient (Fig. 5.18) nor between primary recovery efficiency and mean rock permeability (Fig. 5.19). No Monell wells achieved a primary recovery above 40%, indicating that there may not be low-permeability thin-pay or barriers near the gas cap for maintaining gas expansion pressure as indicated in the Arch Unit. The flow barrier near the gas cap will reduce the reservoir volume for gas expansion and improve the maintenance of reservoir pressure during the primary production. Therefore, oil wells located between a gas cap and flow barriers can be benefited more than those

wells without nearby flow barriers.

Permeability and Waterflood Recovery

The efficiency of waterflood recovery was found to increase with the mean permeability of reservoir rock among 12 five-spot patterns in Monell Unit (Fig. 5.20). The reason for this correlation may be a relatively high ratio of oil relative permeability to water relative permeability (k_{ro}/k_{rw}) for the rock of higher permeability values in this strongly water wet system. The oil-water relative permeability data provided on samples in the Patrick Draw Field (Schatzinger, et al., 1992) indicates that the Almond Formation is strongly water wet.

The relationship between k_{ro}/k_{rw} and the rock permeability can be explained as follows. In the porous media, the nonwetting phase occurs in isolated globules several pore diameters in length that occupy the center of the pores. The trapping wetting phase, on the other hand, occupies the crevices between grains and coats the mineral surfaces. When the pore throats are large in the high-permeability rock the nonwetting phase is the mobile phase in the pore center. Because the pore throats are small in the low-permeability rock, the nonwetting phase becomes isolated islands and the wetting phase may become the mobile phase. As a result, k_{ro}/k_{rw} values are high for water-wet rock with high permeability values. It was reported (Wyllie, 1962) that in the drainage process k_{ro}/k_{rw} values are high for rocks with low values of initial water saturation, which usually occurs in rock of good permeability. Good waterflood recovery from rocks of relatively higher permeability in the Monell Unit suggests that the same relationship of k_{ro}/k_{rw} with permeability also holds for the imbibition process.

Dykstra-Parsons coefficients were calculated for wellbore permeability profiles of 70 wells in Arch Unit and 38 wells in Monell Unit. No correlations were found between oil recovery efficiencies from waterflood and Dykstra-Parsons coefficients in either Arch Unit (Fig. 5.21) or Monell Unit (Fig. 5.22), suggesting that the Dykstra-Parsons coefficient is not a good indicator of production performance in the Patrick Draw Field. Typically, low oil recoveries are associated with high values of V_{DP} , however, this assumption is based on the injection of large fluid volume (more than one pore volume) in a layer cake reservoir model and relative permeability values are not considered. The results of this study indicate that the relative permeability values of oil and water phases are much more important than V_{DP} for the waterflood recovery in Patrick Draw Field. Rock with 100 mD permeability has a larger value of k_{ro}/k_{rw} than rock with 10 mD in Patrick Draw Field. In contrast, a correlation was found between V_{DP} and the waterflood recovery in Bell Creek Field. This indicates that values of k_{ro}/k_{rw} do not vary much for rocks of high permeability in the range about 1 darcy (e.g. Bell Creek Field), where the permeability profile in the vertical direction became the controlling factor in waterflooding recovery. In conclusion, Dykstra-Parsons coefficient needs to be used carefully to predict

waterflood recovery. Low oil recoveries are associated with high values of V_{DP} only when a large pore volume of water is injected into a layer-cake type of reservoir and effects of relative permeability values are not important.

Reservoir Volume Balance Calculations

Introduction

A significant amount (33 MMSTB) of water was injected into the reservoir of Arch Unit, Patrick Draw Field in contrast to oil and water production volumes (20 MMSTB) during the waterflood operations. To investigate whether injected water was lost to sands other than the pay zone or channeled out of Arch Unit, reservoir volume balance calculations were conducted. The balance between injection and production volumes is important because the overinjection of water into the reservoir may imply that injection water was lost through fractures into sands other than pay zones.

Reservoir Volume Balance Calculations

The reservoir volume balance at the end of waterflood was estimated in Arch Unit in three different regions: eastern, northwestern, and southwestern regions. The three regions in Arch Unit were divided by elongate, sand-thin features (less than 10 ft) that restrict communication between the areas. While the northwestern and the southwestern area are in communication with a gas cap at the western edge of Arch Unit, the eastern region does not have a gas cap. Based on following reservoir volume balance calculations, none of these three regions indicated evidence of loss of injection water to sands other than UA-5 and UA-6 sands.

The production volume (Q_p) including oil, gas, and water is calculated as:

$$Q_p = B_o Q_o + B_g(Q_g - R_s Q_o) + B_w Q_w \quad (1)$$

where

B_o = oil formation volume factor = 1.22 bbl/STB

B_w = water formation volume factor = 1.0 bbl/STB

B_g = gas formation volume factor = 0.9 STB/MCF

R_s = solution gas-oil ratio = 450 SCF/STB

Q_o, Q_g, Q_w = cumulative production volume of oil, gas, and water, respectively.

Injection volume (Q_i) including water and gas is

$$Q_i = B_w Q_{wi} + B_g Q_{gi} \quad (2)$$

where

Q_{gi}, Q_{wi} = cumulative injection volume of gas and water, respectively.

The eastern region, which does not have a gas cap, has a ratio of cumulative water injection volume to cumulative production volume of 0.84. This indicates that the total injection volume is close to the total production volume, and that there is a good reservoir volume balance at the end of waterflood in the eastern region.

Equations 1 and 2 were also used to calculate Q_i/Q_p for northwestern and southwestern regions at the end of waterflood. Because of communication with the gas cap at the western edge of Arch Unit, northwestern and southwestern regions have Q_i/Q_p values of 0.48 and 0.76, respectively. In contrast to Q_i/Q_p value of 0.84 in the eastern region, volume balance ratios of 0.48 in the northwestern region and 0.76 in the southwestern region are lower. The low value of Q_i/Q_p indicates that the injection volume is much less than the production volume which leaves additional reservoir space for the continued water injection. The gas production from the gas cap in the western edge of Arch Unit appears to contribute most of the void space for water injection in northwestern and southwestern regions.

The different values of solution gas-oil ratio (R_s) were reported for oil produced in Arch Unit results in a range of volume balance calculations. In contrast to a R_s value of 450 SCF/STB reported by Union Pacific Resources Corp., R_s values of 446, 521, and 550 SCF/STB were reported by Core Laboratories, Inc. based on produced oil from wells Patrick Draw 1, Arch 60, and Arch 22, respectively. The Q_i/Q_p values based on R_s value of 600 SCF/STB (Wyoming Geol. Assoc., 1961) are 0.91, 0.84, and 0.51 for the eastern, northwestern, and southwestern region, respectively.

The calculated values of Q_i/Q_p are less than unity for all three regions in Arch Unit because of the high volume of gas production. This shows that the total injection volume is less than the total production volume for each of three regions. Therefore none of these three regions showed evidence of overinjection or loss of injection water to sands other than UA-5 and UA-6 sands. Furthermore, the reservoir volume balance calculations do not indicate that fractures have conducted injected water out of the UA-5 or UA-6 sands.

Production Analysis

Introduction

Patrick Draw Field is about 8.5 miles long and 3 miles wide with a dip of about 3.5° toward the east direction. The field is divided into a northern Arch Unit and a southern Monell Unit. Oil and gas were found in the upper part of the Almond Formation at depths ranging from 4,300 ft in the west to 5,300 ft in the east. The original oil-in-place (OOIP) was estimated to be about 40 MMSTB in Arch Unit and 83 MMSTB in Monell Unit from volumetric calculations.

Since Patrick Draw Field was discovered in 1959, more than 290 wells have been drilled and approximately one-

half of these wells are water injection wells. A total of approximately 58.2 MMSTB oil has been produced through primary and secondary operations. Compared with its primary production, waterflood recovery in Patrick Draw Field was low. The Arch Unit produced 13.1 MMSTB during primary production by 1967. An additional 5.1 MMSTB was produced since the initiation of waterflooding in 1967. The primary recovery for Monell Unit was 24 MMSTB and waterflood recovery was 15 MMSTB. Production performance was analyzed separately in this study for primary and secondary operations and compared between Arch Unit and Monell Unit.

Primary Production

The primary production mechanism in Patrick Draw Field was solution-gas drive. The main producing sand is the upper Almond UA-5 sand in both Arch and Monell Units and the upper Almond UA-6 sand in the northwestern part of Arch Unit. Patrick Draw Field is bounded by a gas cap on the western edge and a water-oil contact on the eastern and southern edges. Decline of reservoir pressure and little water production before the initiation of waterflood suggests an inactive aquifer or poor lateral communication with the Almond Formation aquifer down dip at the oil-water contact. The best production area lies primarily in the area of good OOIP with a thick pay and a high oil saturation. The expansion of a neighboring gas cap also contributed to the successful production in the area of good OOIP.

Arch Unit. Before water injection was implemented in 1967 and 1968, oil production rates decreased and producing gas-oil ratio increased with production time for all wells. The producing gas-oil ratio (GOR) was high for wells near the gas cap in the western edge of Arch Unit. The gas-oil ratio exceeded 10 MCF/STB for nine wells before being switched to water injectors. Among six of high GOR wells located in the southwestern region, Arch wells 18 and 20 produced at a GOR above 50 MCF/STB in the late production stage. The high producing GOR from wells in the southwestern region suggests a larger gas cap in this area than in the northwestern region.

The best production area is located in the southwestern part of the unit (Fig. 5.23) where it is isolated from the rest of Arch Unit by low-permeability, thin pay. Expansion of the nearby gas cap helped maintain the reservoir pressure and reduced the decline of oil production rate in this area. Arch well 46, located on the bottom of the oil column in this area, declined only two-thirds of its initial oil rate (4 MSTB/month to 1.3 MSTB/month) after production of 100 months. Because of the gas expansion the associated producing gas-oil ratio of Arch well 46 was kept between 2 to 3 MCF/bbl during the production period from 20 to 100 months.

Arch Unit shows a relatively poor primary production compared to Monell Unit. Out of 67 well patterns in Arch Unit in figure 5.23, 37 wells produced less than 150 MSTB of oil in comparison to 15 out of 73 wells in Monell Unit. The mean primary recovery per well is 190 and 291 MSTB for Arch and Monell Units, respectively.

The reason is primarily due to a larger mean OOIP for a Monell well (610 MSTB) than a Arch well (400 MSTB). Furthermore, good production wells, except those in the southwestern area, are scattered about in Arch Unit, reflecting a heterogeneity of reservoir. The reservoir heterogeneity in Arch Unit can be examined by analyzing the distribution of its petrophysical properties. Drastic changes in fluid saturations and pay thickness suggest sand discontinuity caused by structural complications or diagenetic changes discussed in Chapter 4. The thickness of UA-5 sand varies significantly from well to well. For example, Arch well 39, which produced gas from UA-8 sand, has no reservoir quality sand in the UA-5 interval. The water saturation (>80%) of Arch well 94 is significantly higher than water saturations ranging from 33 to 49% of the offset wells. This strongly indicates the discontinuity of fluid phase and petrophysical properties of sands.

Figure 5.24 shows the primary production from UA-6 sands located in the northwestern corner of Arch Unit. Arch wells 49 and 69 produced more than half a million barrels of oil from UA-6 sands whereas other eight UA-6 wells showed fair to poor productions.

Monell Unit. Primary production was initiated in 1960 in Monell Unit for a total of 73 wells. Primary production of Arch wells showed a similar decline behavior as those in Monell Unit. These wells were drilled in a 80-acre spacing except in the northwestern corner. The production history of Monell well 62 in figure 5.25 illustrated this decline in the primary production stage. After 78 months of production Monell well 62 decreased its oil rate by an order of magnitude from 10 MSTB/mo. to approximately 1 MSTB/mo. Monell well 38 is one of 7 wells in Monell Unit which produced through pressure depletion and waterflood stages. It showed a similar production decline until the producing gas-oil ratio was reduced by water injection 150 months later. The oil production rate of Monell well 38 declined to about one-third of its initial rate (20 MSTB/mo.) after 78 months production. In comparison to that of Monell well 62, the slower decline in oil rate for Monell well 38 was caused by pressure maintenance through the expansion of nearby gas cap.

Because of thick pay, high oil saturation, and pressure maintenance from gas cap expansion, the northwestern area shows a high cumulative oil production (Fig. 5.23) with 13 wells having produced more than half a million barrels per well. The best producer, Monell well 38, produced more than 2 million barrels of oil in total. Along with the decrease of pay and oil saturation, the cumulative oil production decreases gradually toward the southeastern part of Monell Unit. Except 15 wells immediately west of the water-oil contact at the eastern and southern edges of Monell Unit, all other wells produced more than 150 MSTB of oil during primary production. Variable pay thickness and the saturations appear to be responsible for the primary production performance in Monell Unit.

No distinct patterns of primary recovery efficiency (Fig. 5.26) can be identified in Monell Unit. Out of 73 well patterns for primary production, 28 wells recovered more

than 20%, 32 wells recovered from 10 to 20%, and 13 wells recovered less than 10% OOIP. Low recovery (<10%) wells are located either in the northern area or immediately next to the gas cap. The high producing gas-oil ratio associated with wells near the gas cap reduced oil recovery of such wells. Poor recovery in the northern area might be caused by reservoir heterogeneities. Close values in recovery efficiency suggests that the good reserves are primarily responsible for the high production volume of oil in the northwestern area of Monell Unit.

Waterflood Production

Waterflood in Arch Unit began in October 1964 where a five-spot waterflood pilot was initiated by converting four production wells (Arch wells 6, 7, 8, and 13) to injection wells. A new well, Arch well 79, was drilled as the central production well. In 1967 a major waterflood expansion was undertaken. Most existing production wells at that time were converted into injection wells and new wells were drilled as production wells using a five-spot 80 acres pattern. Compared with its primary production, waterflood recovery in Arch Unit was low.

The decrease of producing gas-oil ratio and the formation of oil banks in both Arch and Monell Unit suggest a proper response to the waterflood. The oil banks were evidenced by the increase of oil production rates followed by the rapid increase of water-oil ratios in production wells (Figs. 5.27 and 5.28). This increase or stabilization of oil rates is caused by the pressurizing of the reservoir through water injection.

Arch Unit. Oil banks were observed before water breakthrough in 12 wells in the eastern region, 3 wells in the northwestern region, and 2 wells in the southwestern region (Fig. 5.29). Oil production rates stabilized in four wells in the eastern region and two wells in the northwestern region during waterfloods. The period of oil bank ranged from 0 to more than 100 months in Arch Unit (Fig. 5.30), indicating a high degree of reservoir heterogeneity in this area. The fast water breakthrough (1 month for Arch well 94, and 8 months for Arch wells 93 and 97, respectively) may be caused by fractures or conductive faults. The oil banks of Arch wells 21, 44, and 46, benefiting from additional pressure maintenance through water injection, helped recover more than 50% OOIP from these three wells.

Seven production wells, drilled after the initiation of waterflood in the eastern region, showed a relatively low producing GOR (below 1 MCF/STB). The early initiation of a pressure maintenance program in this area reduced the decline of reservoir pressure so that oil was produced at or close to the solution gas-oil ratio. Five other production wells in the eastern region produced initially at high gas-oil ratios (greater than 1 MCF/STB) which decreased later to less than 1 MCF/STB as the waterflood proceeded. The decrease of producing gas-oil ratio illustrates the effect of reservoir pressure maintenance by the water injection.

The watered-out area in Arch Unit is shown in figure 5.29. Fourteen of 19 watered-out production wells are located in the eastern region. It was also found that the

water-oil ratio increased from seven other producing wells in the eastern region, which corresponds to the good injection/production volume balance in the eastern region. The lack of gas cap and the early initiation of waterflood in the eastern region explain the fast response of production to the water injection. However, the gas cap in the western edge of Arch Unit results in a decrease of producing gas-oil ratio and a relatively slow response in water production to water injection. The majority of wells in the northwestern and southwestern regions have been producing at low water cuts. A significant amount of injection water is required to fill up the gas cap, evidenced by the low ratio of cumulative injection volume to cumulative production volume in the northwestern and southwestern regions, for pressurizing the reservoir and flooding the oil out. Therefore the continued injection of water in areas of low water cut is needed.

Figure 5.31 shows a high contrast in water breakthrough times. It took from less than one month to more than 100 months to obtain the water breakthrough. The fast breakthrough might be related to a high water saturation (Arch well 94) or injection channeling between injection and production wells. The long breakthrough times for Arch wells 21, 30, 44, and 46 are associated with large gas saturations contributed by the gas cap.

Waterflood recovery is poor in Arch Unit ranging from 7 (Arch well 94) to 288 MBBL (Arch well 79) because of the fast water breakthrough (less than 10 months for 3 wells) and short periods of oil bank. The mean and median of waterflood recovery from 39 Arch wells are 62.7 and 53.3 MBBL, respectively. This corresponds to about 15% OOIP and about one-half of primary recovery of Arch wells. The cumulative oil production since the initiation of waterflood is shown in figure 5.32. It ranged from 2.25 to 221 MSTB in Arch Unit.

A high degree of heterogeneity in Arch Unit is suggested by following observations:

1. The large range of water breakthrough times from less than 1 month for well 94 to more than 100 months for wells 91, 95, and 108. The water-oil ratio exceeded 1 before the gas-oil ratio was reduced to 1 MCF/STB for four of 22 five-spot patterns in Arch Unit. This suggests early breakthrough due to severe water channeling in the gas phase in high-permeability zones.
2. Overall poor waterflood production in Arch Unit indicates a poorer sweep efficiency and lower waterflood recovery than in the Monell Unit. Over 50% of the five-spot patterns in Arch Unit produced less than 150 MSTB from waterflood, whereas less than 20% of the five-spot patterns in Monell Unit produced less than 150 MSTB.
3. The thickness of UA-5 sand varies significantly from well to well. This drastic change in pay thickness and fluid saturations indicate sand discontinuity or compartments.

Monell Unit. A relatively uniform waterflood performance among five-spot patterns was observed in the Monell Unit. After approximately 18 months of water injection, the reservoir was pressurized and the producing GOR reduced to 1 MCF/STB. Water breakthrough occurred between 70 and 90 months of water injection

(Fig. 5.31). The waterflood production period (oil bank) for most Monell wells ranged from 50 to 75 months in contrast to an average of 36 months in Arch Unit (Fig. 5.30). The breakthrough time (50 to 75 months) in the Monell Unit is equivalent to a flow rate of 0.88 to 0.59 ft per day in the 40-acre spacing well pattern. The gradual changes of oil bank periods and water breakthrough times from well to well in Monell Unit indicate a longer spatial correlation length, or a less heterogeneous reservoir, in this area than that in Arch Unit.

A higher gas saturation was observed in the northern area than in the rest of Monell Unit. This is evidenced by the higher initial producing GOR which exceeds 1 MCF/STB from Monell wells 9, 19, 20, and 21. It also took 20 months or more to reduce the producing GOR to less than 1 MCF/STB in the northern area in contrast to 10 to 20 months required in the central and the southern areas of Monell Unit. Because Patrick Draw Field dips to the east or southeast, the high gas saturation in the northern and northeastern areas was not contributed from the gas cap at the western part of Monell Unit. Thus, this suggests possible compartments in northeastern Monell Unit.

The waterflood production ranged from 50 (Monell well 119) to 1366 MSTB (Monell well 38) oil (Fig. 5.32) with a mean of 321.7 MSTB and a median of 244.4 MSTB in Monell Unit. This is comparable to the primary recovery (average 290.7 MSTB per well) and equivalent to a recovery of approximately 18% OOIP. Oil production decreases from the northwest area of good OOIP toward the southeast part with poor OOIP (Fig. 5.32). The smooth decrease in oil production is due to a gradual decrease of pay thickness and oil saturation. The relatively homogeneous formation in Monell Unit may be the most important reason for a better waterflood recovery (18% OOIP) in Monell Unit in comparison to that (15% OOIP) in Arch Unit.

Most Monell wells recovered 10 to 30% OOIP from waterflood (Fig. 5.33). The low waterflood recovery (<10%) wells are located on the edge of Monell Unit. The rock quality generally deteriorates as the reservoir approaches its boundary. Figure 5.34 shows the good recovery efficiency of wells produced from both primary and secondary operations. Seven Monell wells (Monell wells 6, 7, 8, 17, 18, 27, and 38) have been producers since the initiation of primary production in 1960. These seven wells have never been converted into water injectors.

The water injection volume (Fig. 5.35) is related to waterflood production in Monell Unit (Figs. 5.33 and 5.34). The pore volume injection ranged from 15 to 60% PV for most Monell wells in contrast of 10 to 40% PV for most Arch wells. Large PV's of water were injected into wells near the gas cap to increase production in that area. More than 60% PV of water injected into Monell wells 34, 45, and 55 in the central part of Monell Unit helped Monell wells 95, 104, and 116 produce more than 20% OOIP from waterflood. Wells of low injection PV (<15%) matched those of low waterflood recovery (<10%).

Recovery Efficiency and Residual Oil Saturation

Oil recovery efficiency and remaining oil saturation after waterflood were calculated for each well pattern (Fig. 5.36). Monell Unit has recovery efficiency ranging from 20% to more than 50% OOIP indicating a good oil recovery. Arch unit has a relatively poor recovery efficiency (less than 30% OOIP) except for the northern area and the area immediately western to the low-permeability, thin pay.

Arch Unit. Arch wells showed a large contrast in distribution of recovery efficiency (Fig. 5.36). The best recovery wells are found in the area immediately west of the NW-SE trending low-permeability, thin pay in Arch Unit. These wells are located at the bottom of the oil column which was created by the structural dip and a low-permeability, thin, pay. Gas cap expansion and water injection maintained well pressure, and therefore, resulted in a recovery efficiency of more than 50% OOIP for Arch wells 21, 22, 30, 44, 45, and 46. Two wells (well 15 and 44) produced more than one million barrels in the Arch Unit because of large oil reserves and the gas cap expansion.

A poor waterflood recovery in the Arch Unit was evidenced by the fact that 12 out of 22 infill-drilled wells produced less than 100 thousand barrels of oil from five-spot waterflooding. Arch well 94 produced only 7 thousand barrels of oil, while the surrounding wells produced from 26 to 270 thousand barrels of oil per well. The available data based on current well spacing are not sufficient to construct a deterministic reservoir model in this area for simulation and prediction purposes.

Arch Unit has a scattered distribution of ROS after waterflood (Fig. 5.37). The actual ROS's of wells adjacent to the gas cap may not be as high as shown in figure 5.37 because a significant amount of oil associated with such wells was flooded out of the drainage area and produced by neighboring wells. The poor production and relatively high ROS in the southeastern corner of Arch Unit suggest a complex reservoir heterogeneity.

Monell Unit. In the Monell Unit, approximately one half of the wells recovered 20% of OOIP, and majority of the infill-drilled wells produced 10 to 20% OOIP from waterflooding. No recognizable patterns of recovery efficiency is found in Monell Unit. The northwestern and central area showed a relatively higher residual oil saturation (ROS) (Fig. 5.37) than the southeastern area. This is due to high values of initial oil saturation in the northwestern and central area even after successful primary and secondary operations. The ROS's in figure 5.37 were calculated from initial water saturations and productions from both primary and waterflood operations using a volumetric method. In addition to waterflood production, the total production in each inverted five-spot pattern accounts for one quarter of primary production of the four corner wells before being converted into injectors. Six wells (well 4, 6, 7, 17, 27, and 38) produced more than one million barrels each in the northwestern part of Monell Unit because of large OOIP in relatively thick and continuous Almond Formation sandstones.

Enhanced Oil Recovery Potential

Arch Unit. The fast water breakthrough (less than 10 months) shown from 3 Arch wells indicates fluid flow channeling associated with fractures or permeability thief zones. High values of the Hall plot slope from many wells in the Arch Unit suggest possible compartments or deterioration of pay sand near the injection wells. The short oil bank periods (less than 40 months) from 15 Arch wells might be caused by small drainage areas or poor sweep efficiency. If the ROS in the eastern Arch Unit (Fig. 5.37) based on volumetric and production calculations can be verified, a horizontal well can potentially recover additional oil by overcoming compartments and formation channeling in this area.

Monell Unit. The low variability of petrophysical properties and successful primary and secondary production in the Monell Unit suggest a relatively homogeneous reservoir. Because of its significant ROS (Fig. 5.37) and relative reservoir homogeneity, the northwestern and the central parts of the Monell Unit have the potential for increasing oil recovery from EOR process. The key reservoir parameters of the Monell Unit were compared to technical screening criteria for EOR processes. As shown in Table 5.2, the Monell Unit passed the screening criteria of gas injection and polymer floods.

Among the gas injection methods, CO₂ flooding has better potential than nitrogen and hydrocarbon to improve the displacement efficiency of oil. The approximate initial reservoir pressure of the Monell Unit (1790 psig) was higher than the minimum miscibility pressure (MMP) measured by Core Laboratory for the crude oil at reservoir temperature 121°F. The current reservoir pressure after water flooding is close to or above the initial reservoir pressure in the Monell Unit. This will make injected CO₂ miscible with reservoir crude and improve the displacement of oil by the oil swelling and oil viscosity reduction. Nitrogen generally requires a much higher reservoir pressure to reach miscibility with oil than CO₂. The cost of CO₂ is usually less than that of hydrocarbon gas when a nearby access to CO₂ source is available as is the case with Patrick Draw Field. The CO₂ injection has additional benefits in reduction of interfacial effects and increase in rock permeability. As a rule of thumb CO₂ floods recover approximately 30% of the remaining oil after waterfloods using this rough estimate, the total oil recovery from a CO₂ injection project in the Monell Unit could be 13 MMSTB or 1000 STB per acre-ft. A numerical simulation study of CO₂ floods using a compositional simulator is necessary to quantify potential recovery from a CO₂ project.

Steam flooding is not suitable for the Monell Unit because it requires shallow depth (< 4600 ft), high permeability (> 36 mD), high oil saturation (> 36%), low pressure (< 1790 psi), and high oil gravity (< 43° API). In-situ combustion method is not promising for the Monell Unit either because of requirements in oil saturation (40 - 50%) and oil gravity (10 - 35° API).

The Monell Unit failed to pass the requirements in mean permeability (> 40 mD) for surfactant-polymer injection

and oil gravity (< 30° API) for alkaline flooding, respectively. The reservoir parameters of Monell Unit satisfy requirements of polymer floods. The main function of polymer injection is to improve the sweep efficiency of water floods by reducing its mobility ratio of fluids. Because of the low viscosity (0.52 - 0.75 cP) of oil and the low relative permeability (0.035 at ROS) of water in the Patrick Draw Field, the mobility ratio is less than 1 under reservoir conditions. Sweep efficiency, therefore, was not a serious problem in the production history of the Monell Unit. Hence, the Monell Unit might not be benefited from the injection of polymer.

The potential of microbial flood in the Monell Unit is not clear because it prefers a rock permeability of 150 mD in contrast to 36 mD in the Monell Unit. The search for microorganisms working in an environment of low permeability rock is under investigation.

Hall Plot Analysis

Introduction

Hall plots use existing injection pressure and volume data and provide valuable information at no additional cost. In addition to detecting possible wellbore damage developed during water injection, Hall plots were demonstrated in this study to identify nearby permeability barriers or thin pay and times of fill up of gas space in the reservoir. Disturbance of Hall plot slopes due to operation changes need to be accounted for in order to obtain reliable interpretations.

Numerical simulations of water injection were conducted in a reversed five-spot pattern to understand and analyze Hall plots of Patrick Draw Field. Typical rock-fluid properties in Patrick Draw Field were used in simulations to study the effects of permeability barriers on Hall plots. Influence of distance and orientation of barriers to water injector were calculated using an analytical formula.

Hall Plot Technique

Hall plot analysis is a technique for examining water injectivity by plotting cumulative injection pressure (P_H) versus the cumulative water injection volume (CWI or W_i). The equation (Earlougher, 1977) may be written as:

$$P_H = m_H W_i \quad (3)$$

where

$$P_H = \int_0^t p_{wr} dt - p_{et} = \Sigma P \Delta t$$

$$m_H = \frac{141.2 \mu (p_D + s)}{kh} \quad (4)$$

- P = wellhead pressure, psi
- p_{wf} = bottom-hole flowing pressure, psi
- p_e = formation pressure at reservoir

	boundary, psi
p_D	= $\ln(r_e/r_w)$ for steady state,
	dimensionless pressure term
h	= pay thickness, ft
k	= permeability, mD
r_e, r_w	= radius of drainage area and wellbore, respectively, ft
s	= wellbore skin
t	= water injection time, days
μ	= fluid viscosity, cP

The slope of the Hall plot (m_H) indicates the pressure (psi) required to inject 1 bbl/day. Traditionally the Hall plot is used to detect well damages based on the change of slope after water injection reaches the steady state. In fact, any change of parameters on the right side of equation (4) will change the slope of Hall plot. These parameters include permeability, pay thickness, fluid viscosity, or p_D . Values of p_D are affected by drainage radius and operating practices such as addition or reduction of offset producing wells.

Three Periods of Hall Plot

Hall plots from a total of six five-spot injection patterns in Arch Unit were analyzed for changes of its slopes. The Hall plot of well 8 is illustrated in figure 5.38. Well 8, located in sec. 13, T19N, R99W in the eastern part of Arch Unit, is surrounded by four producers, wells 79, 88, 90, and 92. The slope of the Hall plot with cumulative water injection was included in figure 5.38 to facilitate the analysis.

Three injection periods can be identified from figure 5.38:

(1) Reservoir fill-up. The Hall plot slope increases from 2.4 to 6 psi-day/bbl when cumulative water injection volume increases from 0 to 300 MBBL. This increase of Hall plot slope indicates the increase of injection resistance because of pressurizing of the reservoir through the fill-up of the gas-filled reservoir space with water. The amount of water injected in this period is related to the volume of gas-filled reservoir in the well pattern. The amount of water injected (300 MBBL) is equivalent to 9.5% of the pore volume of well 8 in an 80-acre five-spot pattern.

(2) Steady State injection. The first period is followed by a constant slope value of Hall plot until a cumulative injection volume of 780 MBBL. The constant slope in Hall plot reflects a period of steady state injection and little development of wellbore skin during the waterflood.

(3) Operational change. The Hall plot slope increases with water injection after shut-in of well 79 due to its high water cut. As shown in figure 5.38 the slope of the Hall plot continues to increase with the successive shut-in of wells 88, 92, and 90. The Hall plot slope of 24 psi-day/bbl after shut-in of three surrounding producers is approximately four times the slope during the period of steady state injection. The shut-in of three production wells in well pattern 8 left only a quarter of productivity in this pattern, explaining the four fold increase of slope

value.

The same three periods, reservoir fill-up, steady state injection, and shut-in of surrounding producers, were identified from Hall plots of injection well 5, 7, 9, 26, and 42. The beginning of the steady state in waterflood can be determined from the constant slope in Hall plot. At the late injection stage, rather than indicating wellbore injectivity, the increased slope was a response to purely operational procedures. Sharp increases in the slope of Hall plots at late injection stages were found to correspond to the shut-in dates of surrounding production wells for all six well patterns analyzed. This illustrates that operational activities must be accounted for when interpreting Hall plots for reservoir information.

Numerical Simulations

To help understand and analyze Hall plots of Patrick Draw Field, numerical simulations of water injections were conducted in an inverted five-spot pattern based on typical rock-fluid properties found in Patrick Draw Field: permeability 36 mD, porosity 20%, oil saturation 53%, and 40°API oil. A black oil reservoir model BOAST was used. These simulations assume repeated well patterns in the field so that little influence of pressure or injection/production from wells outside of the studied well pattern is observed. The pressure-volume-temperature (PVT) properties in the reservoir model were derived from published analytical correlations. In the numerical simulation, a single well located in the center of 40-acre field was allowed to produce under pressure depletion for one year. The waterflood was followed by converting the central producer to an water injector and adding four producers at four corners of the field. The injection pressures and volumes of cumulative water injection were monitored during waterflood simulations. The Hall plot developed in this way is shown in figure 5.39. The pore volume of the 40-acre reservoir in numerical simulations is 1,240 MBBL.

Two periods can be identified in the Hall plot of a reversed five-spot which has no barriers in the pattern. The slope of Hall plot increases with the water injection volume at the early injection stage because of fill-up of the gas space left after primary production. This change of Hall plot slope agrees well with those observed in figure 5.38 during the early period before the cumulative water injection reached 300 MBBL. The Hall plot slope reaches a constant value of 9 psi/(bbl/day) after a total injection of approximately 60 MBBL (or 5% of pore volume) of water. In contrast to one year's primary production before waterflood in the numerical simulation, most production wells in Patrick Draw Field produced four years or longer before being converted into water injectors. This explains a relatively short injection volume required in numerical simulation to reach a constant slope in the Hall plot.

An additional simulation run was conducted to investigate the effect of shut-in of surrounding production wells at the late production stage. The slope of Hall plot increases sharply in response to the shut-in of offset production wells as shown in figure 5.39. This explains

the large slope of Hall plots observed at late production stages in Patrick Draw Field, thus the effect of operational change on Hall plots needs to be accounted for in its interpretation.

Drainage Volume

Most injection wells in the Arch Unit have Hall plot slope values around 10 psi/(bbl/d). However, the slopes of injection wells on either side of the low-permeability thin pay or sand pinch out exhibit higher values, ranging from 20 to 30 psi/(bbl/d). This observation was confirmed by numerical reservoir simulations where slope values of about 20 psi/(bbl/d) were calculated for injection wells close to flow barriers.

Simulation Studies Figure 5.40 shows the comparison of simulation results of Hall plot slopes from five-spot waterfloods with and without barriers in the pattern. Rock-fluid properties of Patrick Draw Field were used in simulations. The Hall plot slope increases when a permeability barrier is included in the reservoir model. The closer the barrier, the higher the slope of Hall plot. The increase of Hall plot slope is much more significant for reservoirs with two barriers than those with one barrier near the injection well. In the "two barriers" simulation the injector is located 165 ft away from both two barriers which intersect at an angle of 90°.

Due to the two-phase flow in models all Hall plots in figure 5.40 show a transition period in increasing slope values with cumulative water injection. Low mobility values of water phase (low relative permeability values and high viscosity values compared to those of oil phase) result in a low injectivity and a high injection pressure when water flow is dominated in the model. Thus the Hall plot slope is higher in the late rather than the middle injection stage. The transition of Hall plot slopes is easier to identify for reservoirs with barriers than those without barriers. The smaller drainage area for a "two-barrier" case results in a higher saturation of gas near the wellbore after primary production than in the one-barrier or no-barrier case. Therefore, a better injectivity of "two-barrier" case shows a lower slope value of Hall plot at the early stage than that of other three cases in figure 5.40.

Single-Phase Simulations Hall plot slope is a function of the number of permeability barriers and a function of distance between the injector and barriers. Hall plot slopes in figure 5.41 are simulation results of a single-phase model and a cumulative injection volume of 300 MBBL or 24% pore volume. In the single-phase model PVT properties are the same for both displacing and displaced phases and the relative permeability values are identical to saturation values for either phase. The reservoir model and production and injection strategy are the same as those used in simulations for figure 5.40.

The Hall plot slope increases with the decrease of distance between the barrier and the injector (Fig. 5.41). No variations or transitions of Hall plot slope was observed because of a single-phase flow in the model. The jump of Hall plot slope at the beginning of injection is caused by the low bottomhole pressure right after the

primary production. Since the straight-line relative permeability values in this model are much higher than relative permeabilities used in simulations for Patrick Draw Field (Fig. 5.40), the Hall plot slope values obtained are less than 1 psi/(bbl/day) in contrast to about 10 psi/(bbl/day). Similar to two-phase simulations, the injector located near the corner of two intersected barriers shows a higher slope in the Hall plot than the injector near one permeability barrier.

Analytical Calculations Effects of distance between barrier and injector on injection pressure were studied using an analytical formula. Based on the assumption of repeated well patterns and the image method (Earlougher, 1977), the injection pressure can be calculated by accounting the influence of flow rate q_i from all n wells (including image wells) in the studied pattern:

$$\Phi(x,y) = \Phi_m - \frac{\mu}{4\pi kh} \sum_{i=1}^n q_i \ln[(x-x_i)^2 + (y-y_i)^2]$$

where

$\Phi(x,y)$ = injection potential (or pressure) of the injector located at coordinates (x,y)

Φ_m = average reservoir potential (or pressure)

μ = fluid viscosity

h = pay thickness

k = permeability

x_i, y_i = coordinates of well i (or image well i)

Ratios of injection bottomhole pressure with one or two flow barriers to that without barriers were calculated for a five-spot pattern of 40 acres. In the case of two-barrier calculations the injector was located the same distance from both barriers which intersect at 90°. The calculated ratios were plotted in figure 5.42 as a function of distance of the barrier from the injector. The effect of flow barriers to injection pressure becomes significant when the barrier is less than 400 ft away for two intersecting barriers or less than 200 ft away for a single barrier. As expected the intersecting two-barrier case shows a greater influence on the injection pressure than the single-barrier.

All previous numerical simulations and analytical calculations of the effect of a barrier on injection pressure assumed that barriers within the five-spot pattern are parallel to or perpendicular to lines connecting producers. In other words, barriers intersect lines connecting the injector and corner producers at an angle of 45°. Calculations were done to investigate effects of the orientation of a barrier on the injection pressure. Figure 5.43 shows this effect at four angles (0°, 15°, 30°, and 45°), respectively, between a barrier and the injector-producer line. The barrier orientation shows a minimal influence to the injection pressure for the barrier near to the injector. When the barrier is more than 200 ft away from the injector, the barrier effect decreases with the decrease of

the angle between the barrier and the injector-producer line.

Field Data As shown in formula (4), the Hall plot slope is proportional to the reciprocal of permeability-pay (kh) product. To investigate the effect of flow barriers on the dimensionless pressure term (p_D) and Hall plot slope, a plot of Hall plot slope versus the reciprocal of kh product was constructed for wells with available kh values (Fig. 5.44). This plot normalizes the hall plot slope for pay thickness and permeability so that the relationship between the slope value and reservoir barriers can be seen. Hall plot slope values for the wells in the southwestern Arch Unit are distinctly lower than the other wells analyzed due to the high water injectivity caused by the relatively high gas saturation provided by the nearby gas cap (Fig. 5.44).

Four groups of Hall plot slope were distinguished and superimposed on maps of net pay and fault locations (Fig. 5.45). High hall plot slopes can indicate permeability barriers, reservoir compartments, and lateral changes in reservoir permeability (k) or thickness (h). In general, the wells with high hall plot slopes analyzed in Patrick Draw Field are located either near the low-permeability, thin pay area, a mapped fault, or near the water-oil contact. The water-oil contact serves as a flow barrier for nearby injection wells due to the low compressibility of water, resulting in a high Hall plot slope.

The high or very high Hall plot slopes from wells 12, 13, 23, and 56 are caused by the nearby pay sand thin. The faults near well 12, may also contribute to the very high Hall plot slope. The high slopes in wells 3, 5, 6, 9, 24, 41, and 42 are caused by their proximity to nearby faults. The high slopes of Hall plot from Arch wells 38, 48, and 50 located on the eastern edge of Arch Unit is due to the proximity to the water-oil contact which serves as a flow barrier.

The injectors in the southwestern region of the Arch Unit and well 45 exhibit low Hall plot slope values ranging from 0.5 to 2.5 psi/(bbl/d). The low values are interpreted to be a result of the nearby gas cap on the western edge of the field. Two exceptions are wells 13 and 22 which are located near the low-permeability, pay thin area.

Arch wells 22 and 27 are located right in the area of low permeability barrier. Compared to values of offset wells, the relatively higher slope of Hall plot for well 27 (30 psi/bbl/day) and well 22 (7.3 psi/bbl/day) are due to its low values of kh. The slopes for well 27 and 22 were in the normal to low range after normalizing the slopes for kh values (Fig. 5.44). The lower Hall plot slope in well 22 is due to the high gas saturation from the gas cap.

Conclusions

Conclusions from this chapter on lateral variations in production performance may be grouped into four main areas:

Petrophysical Properties and Oil Recovery

1. The efficiency of waterflood recovery was found to increase with the mean permeability of reservoir rock among 12 five-spot patterns in Monell Unit. The reason for this correlation may be a relatively high ratio of oil relative permeability to water relative permeability (k_{ro}/k_{rw}) for reservoir rocks with higher permeability values in this strongly water wet system.
2. No correlations were found between oil recovery efficiencies and Dykstra-Parsons coefficients in either Arch Unit or Monell Unit, suggesting that the Dykstra-Parsons coefficient is not a good indicator of production performance at Patrick Draw Field.
3. Comparison of the permeability distributions indicate that Monell wells have a lower mean permeability, but a more homogeneous permeability distribution as evidenced by the lower value of Dykstra-Parsons coefficient.
4. Due to a greater pay thickness Monell wells have a larger mean well reserve than Arch wells.

Reservoir Volume Balance Calculations

1. Reservoir volume balance calculations in three regions of Arch Unit show no evidence of loss of injection water to sands other than UA-5 and UA-6 sands. This indicates that no major conduits connect the UA-5, UA-6 sands to other sands. Due to the gas cap in the western edge the western region of Arch Unit showed a smaller ratio of injection to production volume than the eastern region.

Production Analysis

1. The good production area of Patrick Draw Field lies primarily in the area of good oil reserve with a thick pay and a high oil saturation value. The expansion of neighboring gas cap and water injection contributed to its successful production from the southwestern area of Arch Unit and the northwestern area of Monell Unit.
2. Waterflood recovery is poor in Arch Unit ranging from 7 to 288 MBBL because of the fast water breakthrough and short periods of oil bank. The mean and median of waterflood recovery from 39 Arch wells are 62.7 and 53.3 MBBL, respectively. This corresponds to about 6% OOIP and about one-third to one-half of primary recovery of Arch wells.
3. In Monell Unit, oil production decreases from the northwest area of good reserves toward the southeast which has poor reserves. The smooth decrease in oil production is due to a gradual variation of pay thickness and oil saturation.
4. Monell Unit has recovery efficiency ranging from 20% to more than 50% indicating a good oil recovery. Arch unit has a relatively poor recovery efficiency (less than 30%) except for the northern area and the area immediately west of the low-permeability, thin pay area.
5. The water injection volume is proportional to its waterflood production of nearby producers in Monell Unit.

The water injected ranged from 15 to 60% PV for most Monell wells and 10 to 40% PV for most Arch wells.

6. A high degree of reservoir heterogeneity in Arch Unit is evidenced by: a) sand discontinuity or compartments indicated by the drastic change in pay thickness and fluid saturations; b) a poor sweep efficiency and low waterflood recovery compared to that in Monell Unit; and c) the large contrast of water breakthrough times ranged from less than 1 month to more than 100 months.

7. The waterflood production ranged from 50 to 1366 MBBL oil with a mean of 321.7 MBBL and a median of 244.4 MBBL in Monell Unit. This is comparable to the primary recovery (mean 290.7 MBBL per well) and equivalent to a recovery of approximately 23% OOIP.

8. The decrease of producing gas-oil ratio and formation of oil banks indicated by the increase of oil rates in both Arch and Monell Unit suggest a normal response to the waterflood.

9. Decline of reservoir pressure and little water production before the initiation of waterflood suggests an inactive aquifer or poor lateral communication with the Almond Formation aquifer down dip at the oil-water contact.

10. The majority of wells in the western region of Patrick Draw Field have been producing at low water cuts due to communication with the gas cap. A continued injection of water in areas of low water cut can help recover additional oil.

Enhanced Oil Recovery Potential

1. The northwestern and the central parts of the Monell Unit have the potential for the EOR process because it is relatively homogeneous and has a significant ROS in the reservoir. The CO₂ flood is promising in the Monell Unit because: 1) reservoir pressure in the Monell Unit is higher than the MMP for miscible flood; and 2) a nearby source of CO₂ is available.

2. Horizontal well drilling has a potential for recovering additional oil by overcoming compartments and formation channeling in Arch Unit, if the ROS in the eastern Arch Unit based on the volumetric and production calculation can be verified.

Hall Plot Analysis

1. No significant wellbore damages were identified in Hall plots for most of injection wells in Arch Unit. This is evidenced by its constant slope of the Hall plot after the gas space in the reservoir was filled up by water.

2. The Hall plot slope in Arch Unit is related to the flow barrier or deterioration of pay sands. Some sharp increases in the Hall plot slopes during the late injection stage were caused by the shut-in of surrounding production wells.

3. Numerical simulations demonstrate that the slope of Hall plot increases with the number of nearby barriers and with the decrease of the distance between barriers and the injection well.

4. Analytical calculations of injection pressures show a significant increase when one barrier is less than 200 ft away or two intersecting barriers are less than 400 ft away.

5. The effect of the orientation of barriers on injection pressure is not as significant as the distance of barriers from the injector.

References

Earlougher, R. C., Jr., 1977, Advances in well test analysis: *in* Henry L. Doherty series, v. 5, Society of Petroleum Engineers of AIME, Dallas, p. 85-87.

Hirasaki, G. J., 1985, Properties of log-normal permeability distribution for stratified reservoirs: unsolicited SPE paper 13416, p. 18.

Schatzinger, R. A., M. J. Szpakiewicz, S. R. Jackson, M. M. Chang, B. Sharma and M. K. Tham, 1992, Integrated Geological-Engineering Model of Patrick Draw Field and Examples of Similarities and Differences Among Various Shoreline Barrier Systems: DOE Report, NIPER-575, 146 p.

Union Pacific Resources Corp., 1983 Data Sheet.

Wyllie, M. R. J., 1962. Relative Permeability: *in* Frick, T. C. ed., Petroleum Production Handbook, p. 25-1 to 25-14.

Wyoming Geol. Assoc., 1961, Wyoming Oil and Gas Fields, Supplement, p. 542-544.

TABLE 5.1. Statistics of petrophysical properties and productions in Arch and Monell Unit wells.

	Number of wells	Minimum	Maximum	Mean	Median	Std. Deviation
Arch Unit						
Permeability, mD	70	2.9	167	37.65	32.4	25.82
Pay, ft	100	0	38	15.96	16	7.59
Porosity, %	100	11.2	27.3	20.5	20.5	1.68
Water saturation, %	100	18.4	86.2	48.75	50	10.61
Porosity x pay	100	0	8.17	3.3	3.237	1.61
Porosity x pay x S_o	100	0	5.367	1.77	1.597	1.07
Cum. oil production, MBBL	101	0	1152	190.27	110	236.34
Initial oil rate, B/D	100	0	658	193.13	129	172.65
Monell Unit						
Permeability, mD	38	0.5	65.2	26.1	23.85	15.74
Pay, ft	143	0	39	20.32	22	8.72
Porosity, %	143	14	22.8	18.85	18.9	1.21
Water saturation, %	143	16.3	97.2	44.87	43.2	12.17
Porosity x pay	143	0	8.03	3.88	4.13	1.74
Porosity x pay x S_o	143	0	5.615	2.26	2.25	1.19
Cum. oil production, MBBL	134	0	2015	290.68	212.5	323.86
Initial oil rate, B/D	134	0	2322	328.32	260	325.44
Injection water, MBBL	78	19	4644	1156.1	1047	904.42
Injection Water, PV	77	0	1.27	0.43	0.4	0.26
Recovery Efficiency	132	0	0.685	0.17	0.16	0.1

Table 5.2
Comparison of reservoir parameters of Monell Unit, Patrick Draw field with EOR screening criteria

	Formation type	Net thickness ft	Depth ft	Temp °F	Average permeability, md	Porosity %	Oil saturation	P, psi	Gravity °API	Viscosity cp
Patrick Draw Field	sandstone	20	4600	121	36	20	36	1790	43	0.5
Chemical flooding										
polymer	sandstone or carbonate	>10	<9000	<200	>20	≥20	≥10% mobile	-	>25	<100
Surfactant polymer	sandstone	N.C.	<9000	<200	>40	≥20	>30%	-	<30 ²	<40
Alkaline	sandstone	N.C.	<9000	<200	>20	≥20	>Residual	-	>35	<90
Gas injection										
hydrocarbon	sandstone or carbonate	Thin unless dipping	>2000 for LPG to >5000 for gas	N.C.	N.C.	N.C.	>30%	-	>35	<10
Nitrogen and flue gas	Sandstone or carbonate	Thin unless dipping	>4500	N.C.	N.C.	N.C.	>30%	-	>24 >35 for N ₂	<10
Carbon dioxide	Sandstone or carbonate	Thin unless dipping	>2000	N.C.	N.C.	N.C.	>30%	≤MMP ¹	>25	<15
Thermal										
In-situ combustion	Unconsolidated sand or sandstone with high porosity or carbonate	≥20	≤11,500	>150 preferred	≥35	≥20°	>40-50%	≤2000	10-35 ²	≤50,000
Steamflooding	Unconsolidated sand or sandstone or carbonate	≥20	≤3,000 ²	N.C.	>250 ²	≥20°	40-50% ²	≤1500 ²	10-34 ²	≤15,000
Microbial										
Microbial drive	Sandstone or carbonate	N.C.	<8,000	<140	>150 ²	-	N.C.	<3000	>15	-

N.C. = Not Critical.

¹MMP = Minimum miscibility pressure which depends on temperature and crude oil composition, 1400 psig for Patrick Draw Field at 121 °F.

²Criteria failed by the Patrick Draw Field.

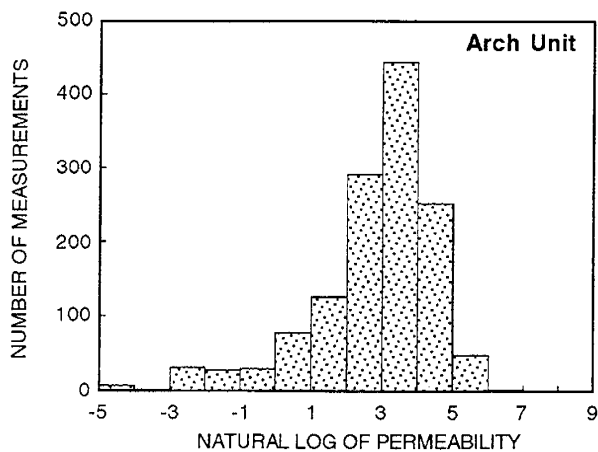


Fig. 5.1. Histogram of sand permeability in Arch Unit, Patrick Draw Field. Histogram is created from 1341 permeability measurements from 70 wells. Arithmetic mean permeability = 39.5 mD, geometric mean permeability = 16.5 mD. Dykstra-Parsons coefficient = 0.825.

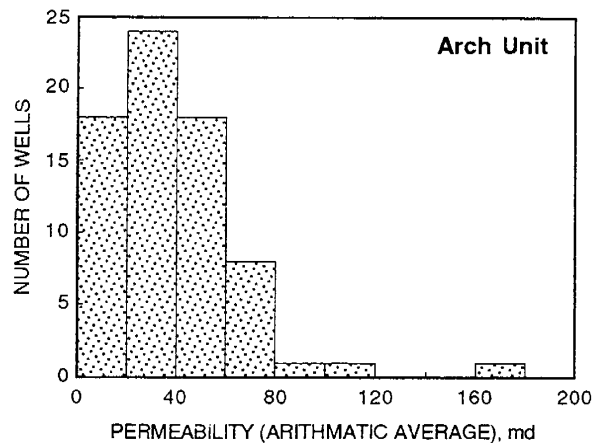


Fig. 5.3. Histogram of mean permeability for 70 wells in the Arch Unit, Patrick Draw Field.

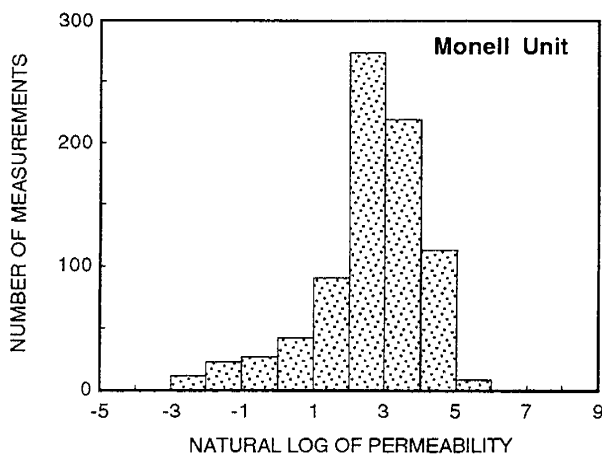


Fig. 5.2. Histogram of sand permeability in Monell Unit, Patrick Draw Field. Histogram is created from 811 permeability measurements from 38 wells. Arithmetic mean permeability = 27.7 mD, geometric mean permeability = 13.3 mD. Dykstra Parson's coefficient = 0.780.

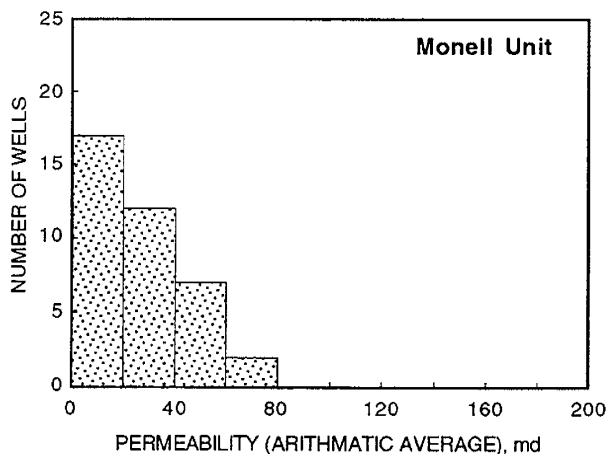


Fig. 5.4. Histogram of mean permeability for 38 wells in the Monell Unit, Patrick Draw Field.

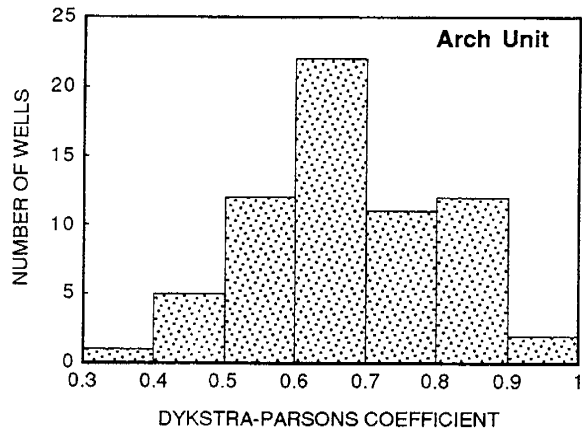


Fig. 5.6. Histograms of Dykstra-Parsons coefficient in 70 Arch Unit wells Patrick Draw Field.

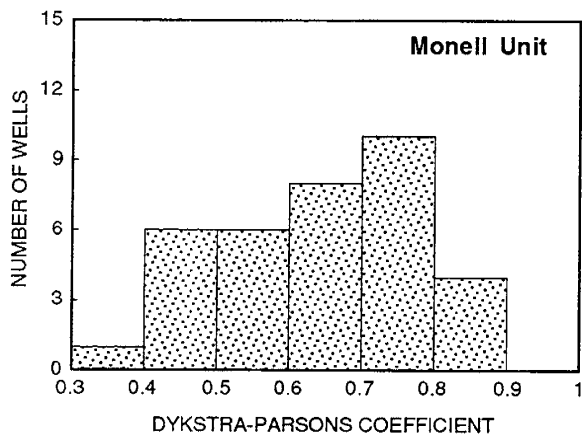


Fig. 5.7. Histogram of Dykstra-Parsons coefficient in 38 Monell Unit wells, Patrick Draw Field.

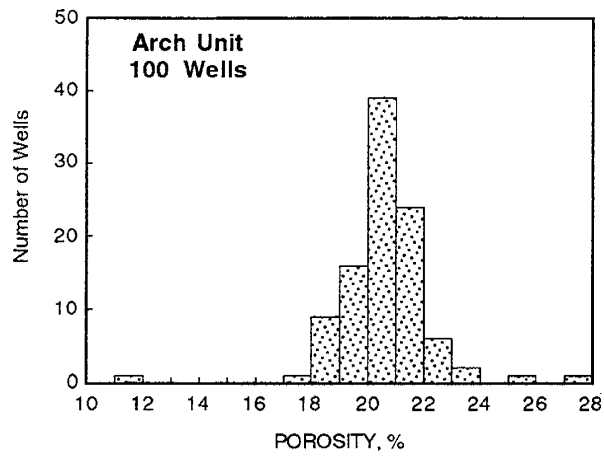


Fig. 5.9. Histogram of sand porosity in Arch Unit, Patrick Draw Field.

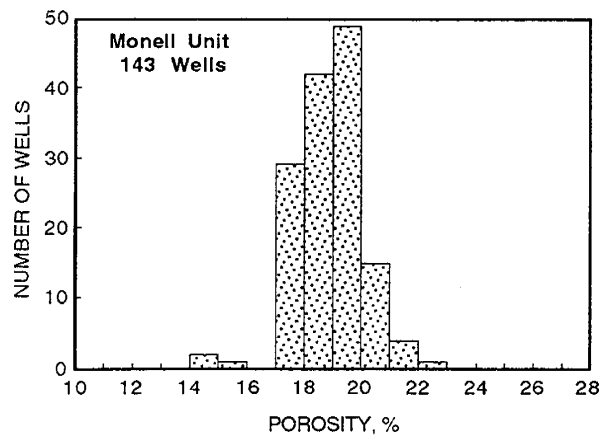


Fig. 5.10. Histogram of sand porosity in Monell Unit, Patrick Draw Field.

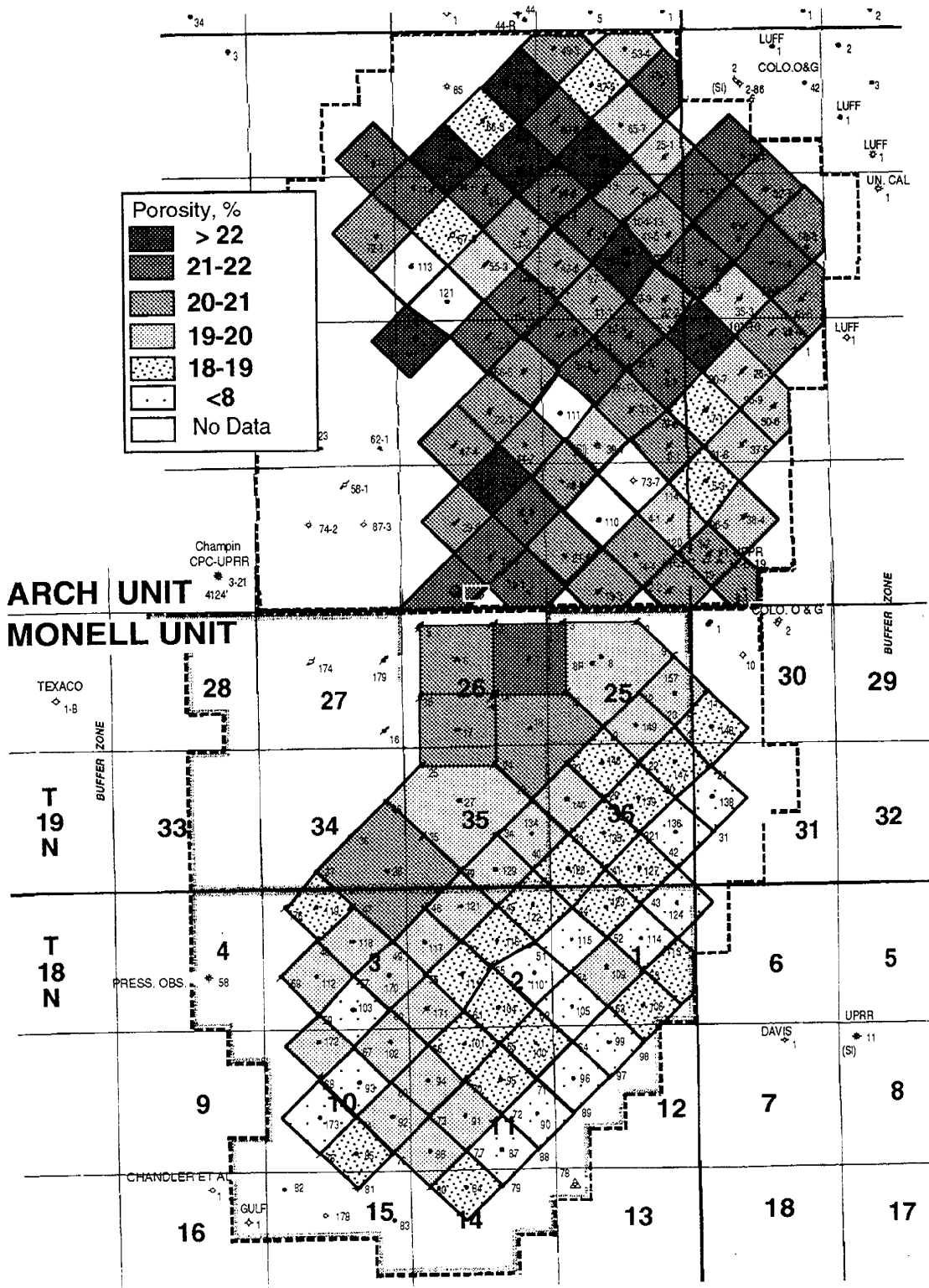


Fig. 5.11. Distribution of average log-derived porosity in Patrick Draw Field. For well numbers, see figure 1.3.

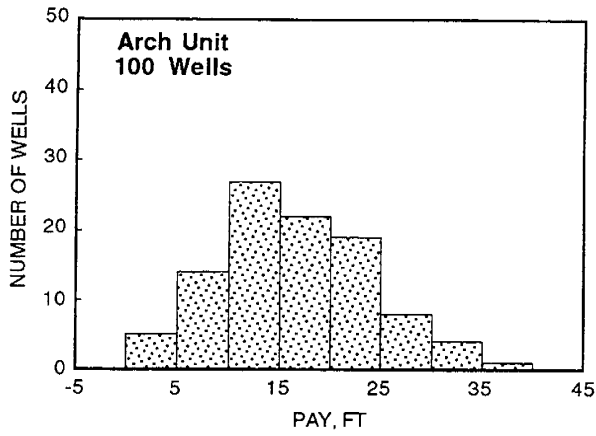


Fig. 5.12. Histogram of pay thickness in the Arch Unit.

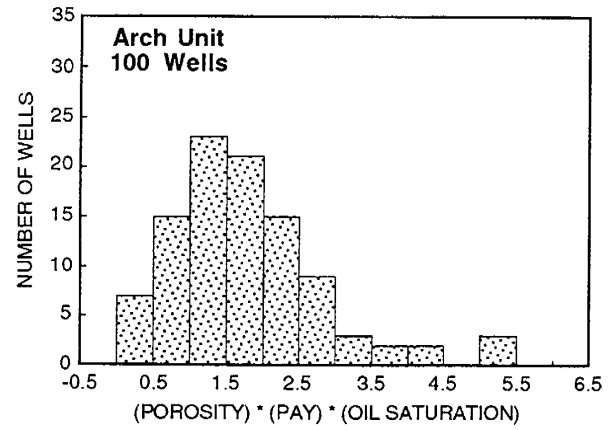


Fig. 5.14. Histogram of product of porosity, pay, and oil saturation in Arch Unit, Patrick Draw Field.

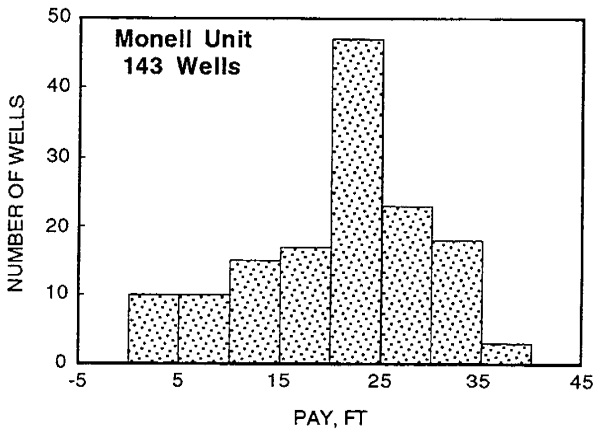


Fig. 5.13. Histogram of pay thickness in Monell Unit, Patrick Draw Field.

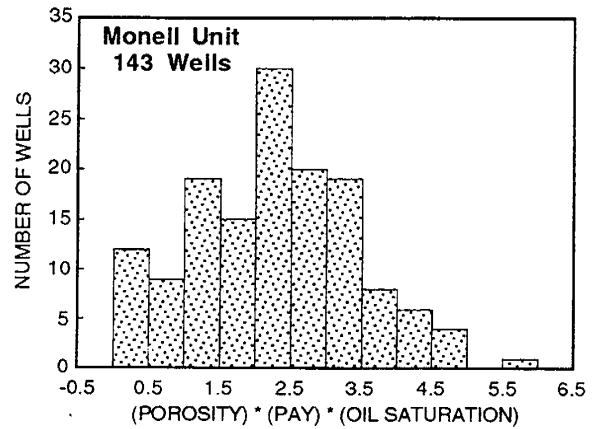


Fig. 5.15. Histogram of product of porosity, pay, and oil saturation in Monell Unit, Patrick Draw Field.

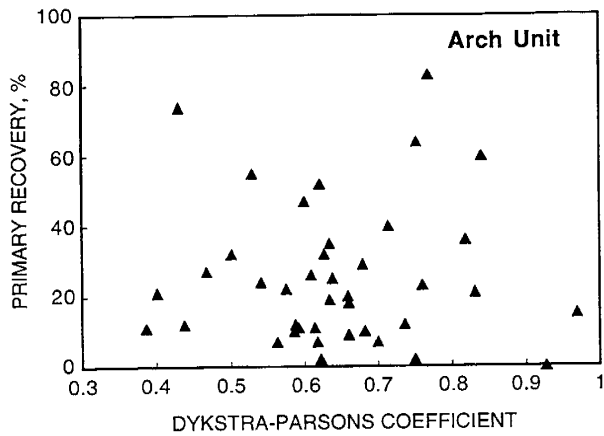


Fig. 5.16. Crossplot of primary recovery efficiency and Dykstra-Parsons coefficient in Arch Unit, Patrick Draw Field.

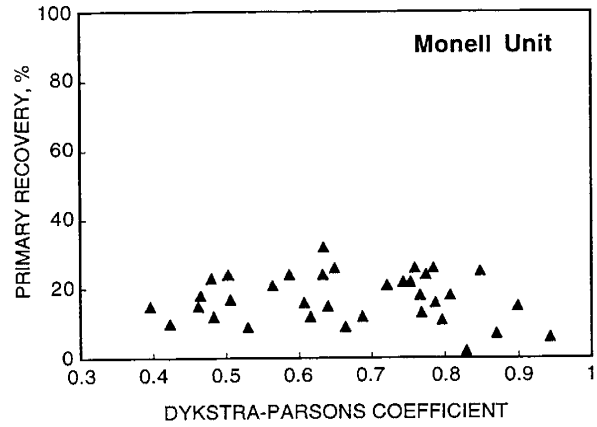


Fig. 5.18. Crossplot of primary recovery efficiency and Dykstra-Parsons coefficient in Monell Unit, Patrick Draw Field.

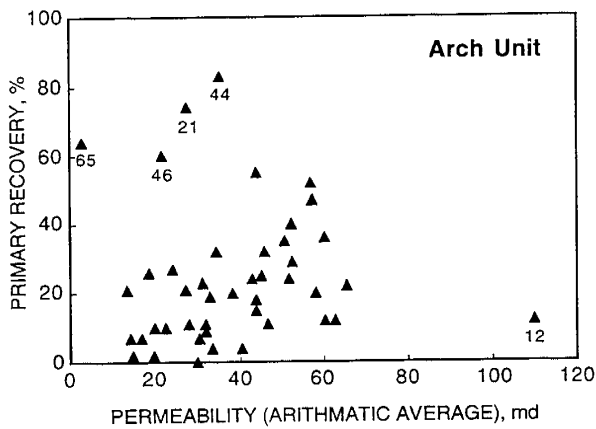


Fig. 5.17. Crossplot of primary recovery efficiency and mean permeability in Arch Unit, Patrick Draw Field.

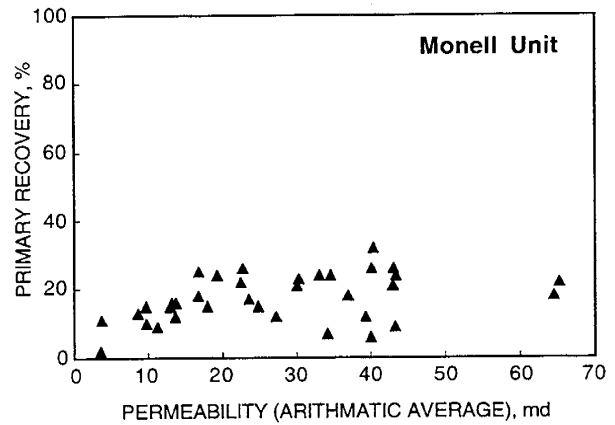


Fig. 5.19. Crossplot of primary recovery efficiency and mean permeability in Monell Unit, Patrick Draw Field.

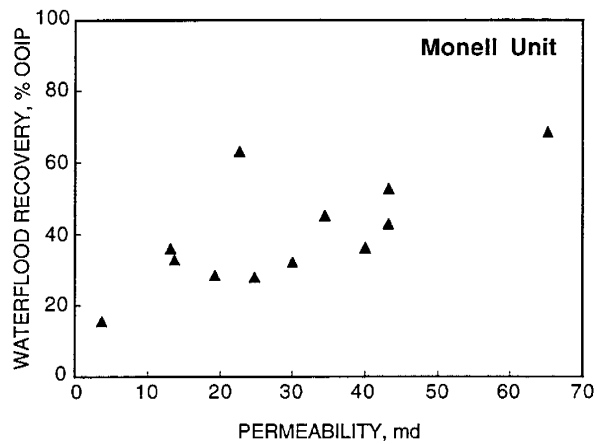


Fig. 5.20. Crossplot of waterflood recovery efficiency and mean permeability in Monell Unit, Patrick Draw Field.

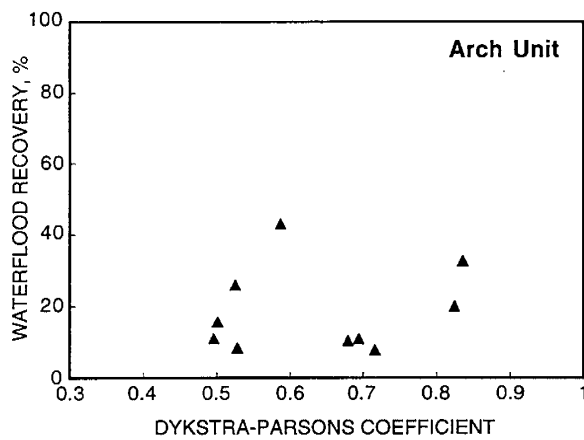


Fig. 5.21. Crossplot of waterflood recovery efficiency and Dykstra-Parsons coefficient in Arch Unit, Patrick Draw Field.

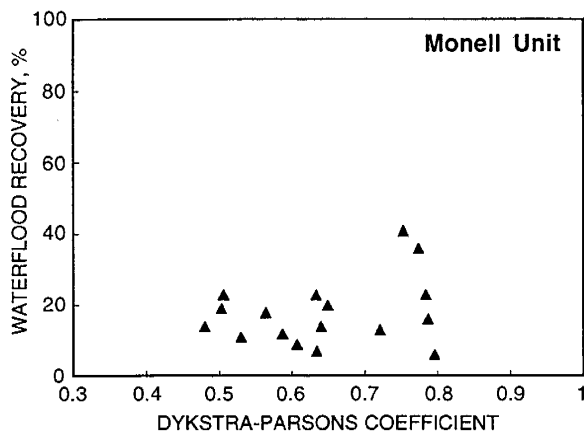


Fig. 5.22. Crossplot of waterflood recovery efficiency and Dykstra-Parsons coefficient in Monell Unit, Patrick Draw Field.

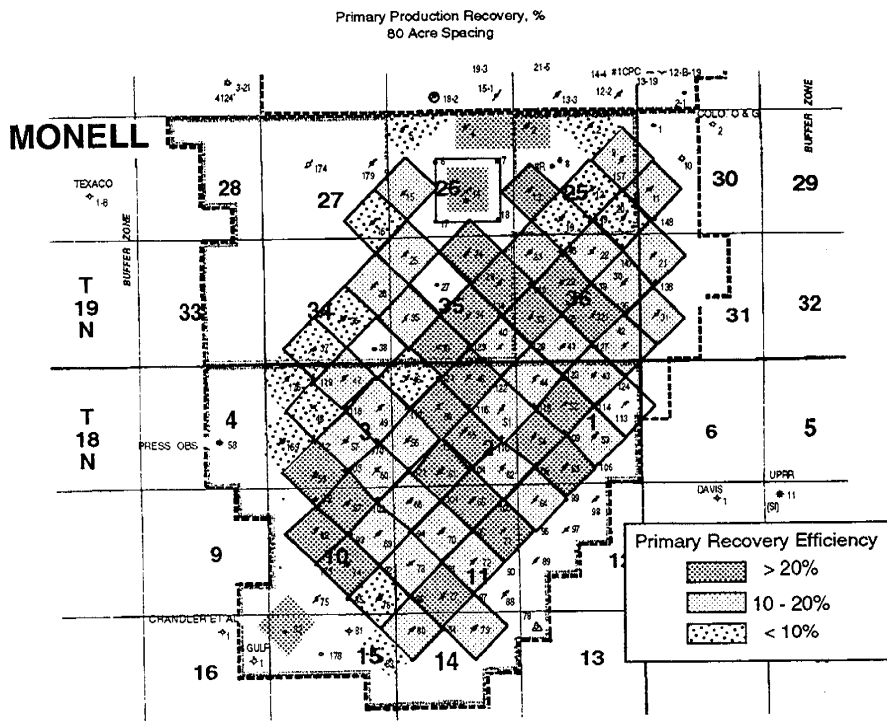


Fig. 5.26. Distribution of recovery efficiency in Monell Unit, Patrick Draw Field for primary production. For well numbers, see figure 1.3.

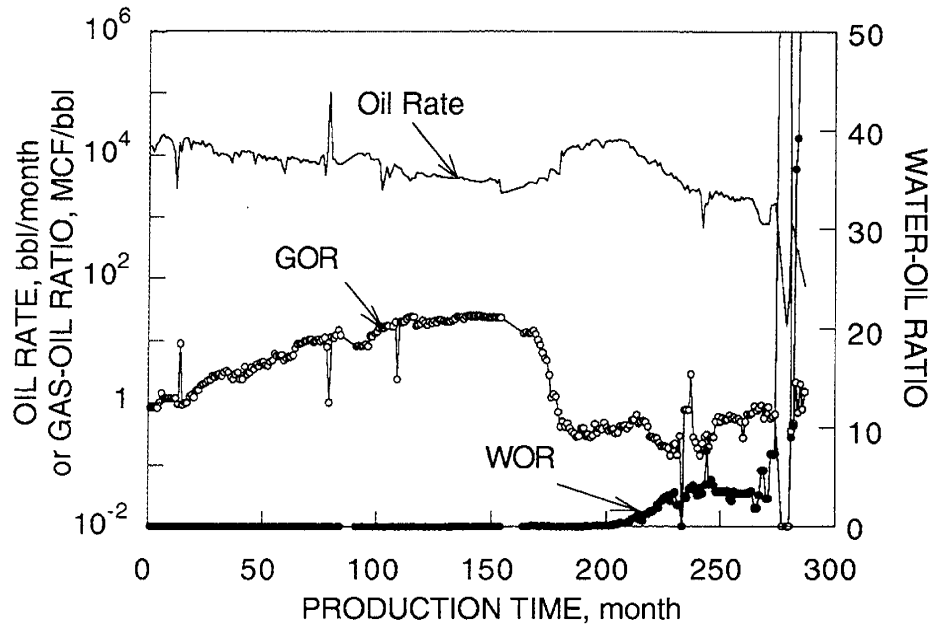


Fig. 5.27. Production history for well Monell 38. Production started in September, 1960.

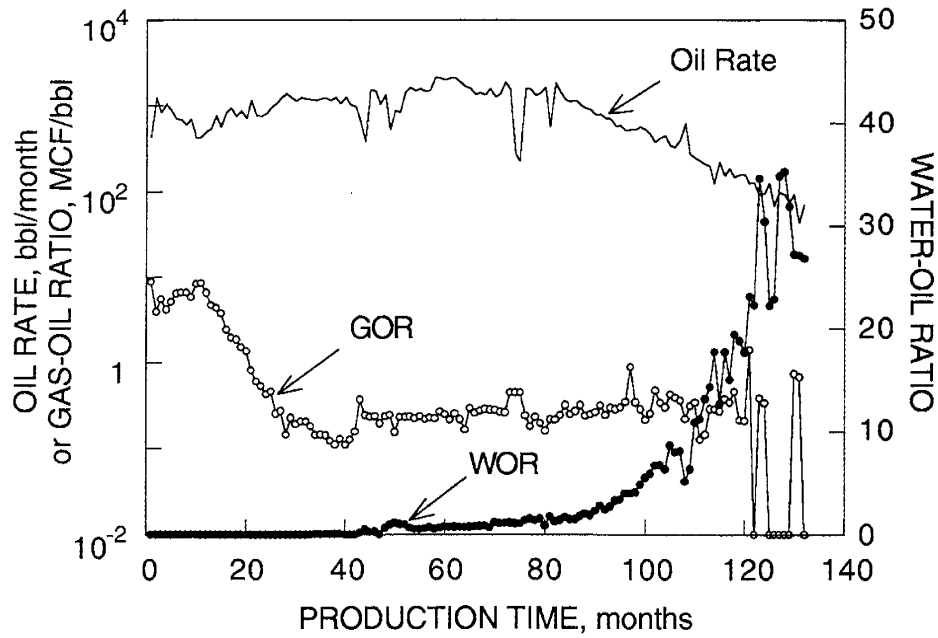


Fig. 5.28. Production history for well Monell 147. Production started in September, 1968.

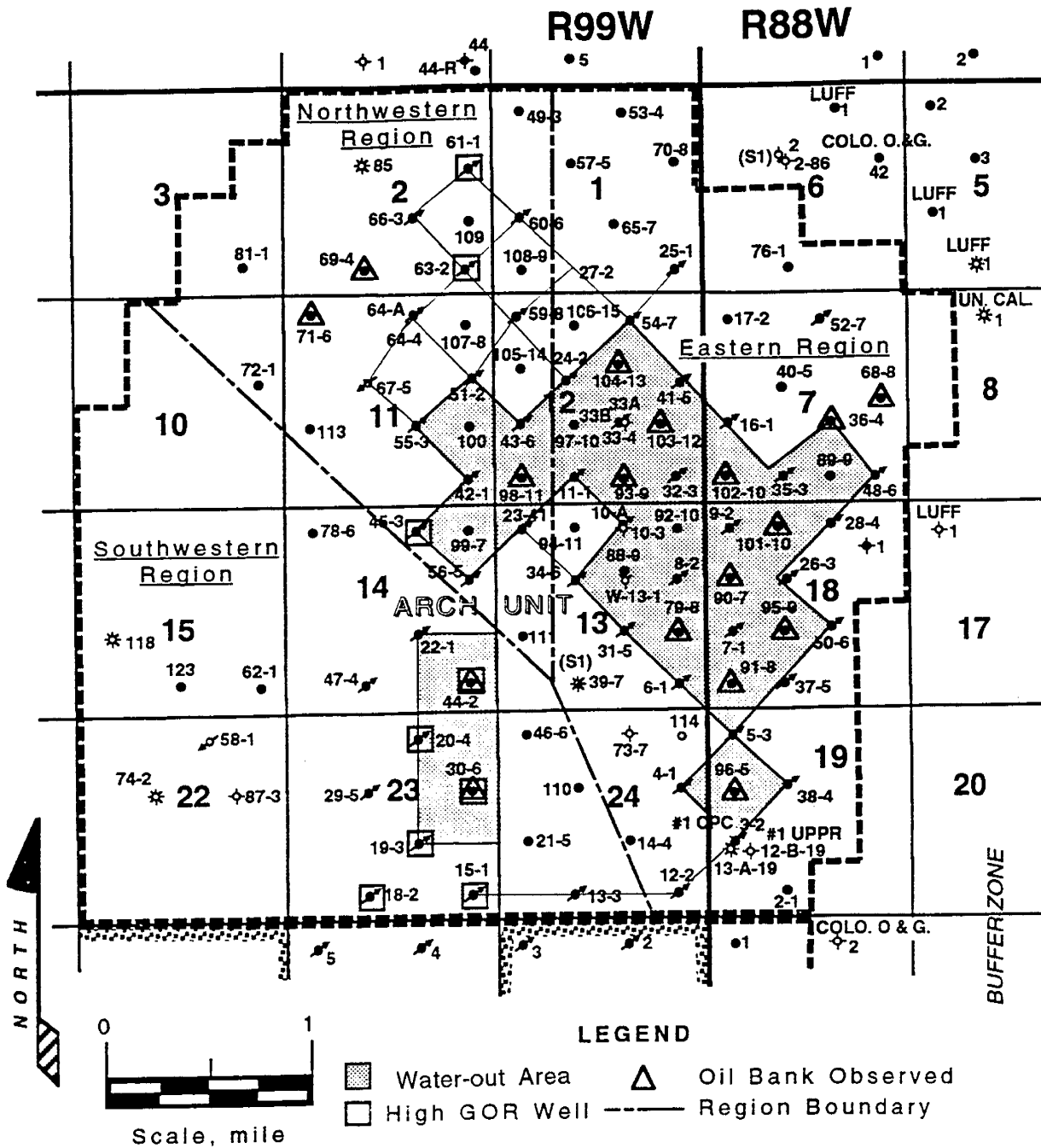


Fig. 5.29. Three regions with different producing characteristics in Arch Unit, Patrick Draw Field. Divisions between the regions correspond to sand thin areas.

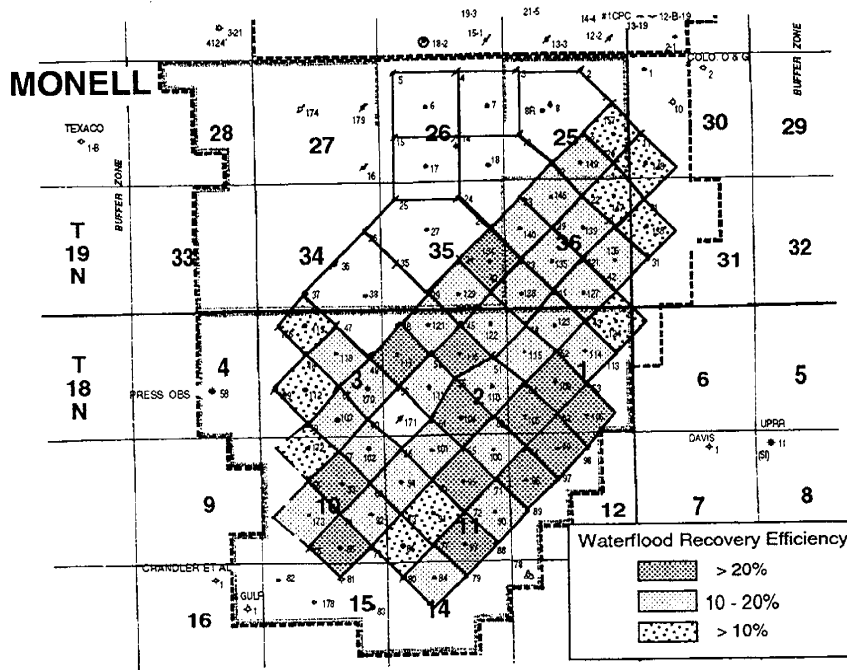


Fig. 5.33. Distribution of recovery efficiency in Monell Unit, Patrick Draw Field for waterflood production. For well numbers, see figure 1.3.

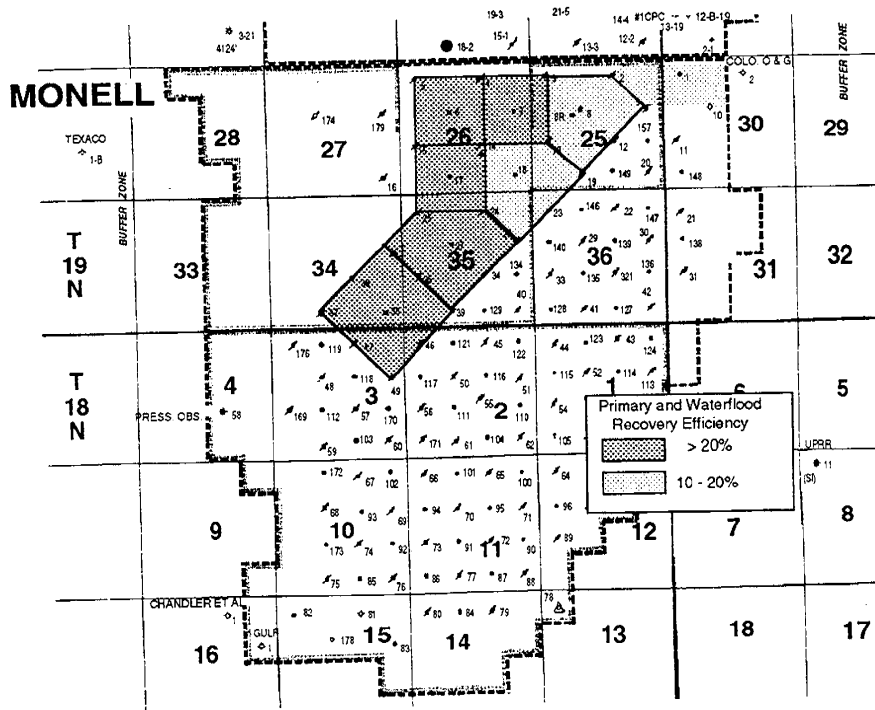


Fig. 5.34. Distribution of recovery efficiency in Monell Unit, Patrick Draw Field for both primary and waterflood productions. For well numbers, see figure 1.3.

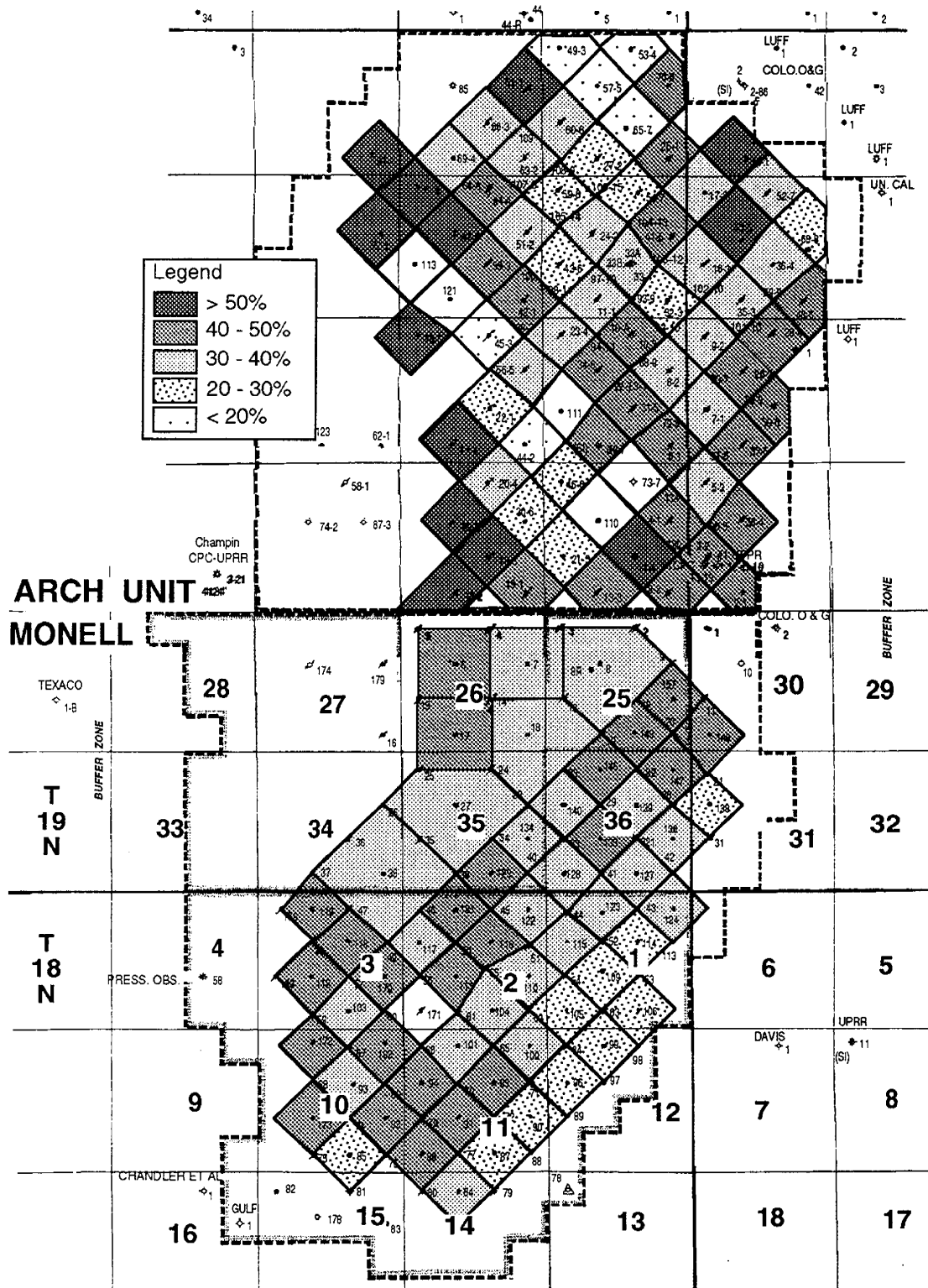


Fig. 5.37. Distribution of remaining oil saturation in Patrick Draw Field. For well numbers, see figure 1.3.

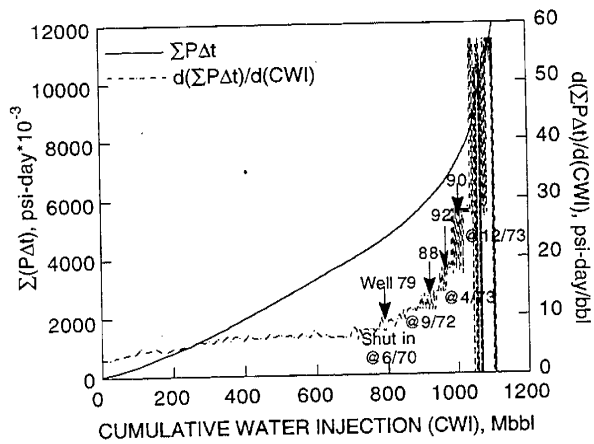


Fig. 5.38. Hall plot from Arch well 8. The shut-in of offset production wells shown by arrows, well number and dates, correspond with an increase in Hall plot slope.

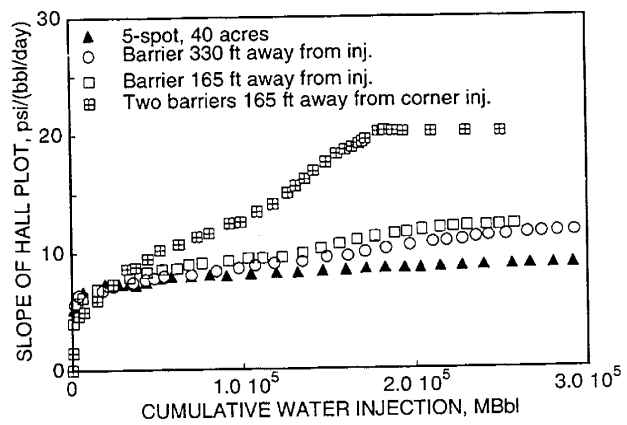


Fig. 5.40. Two-phase simulation results of Hall plots with and without nearby permeability barriers.

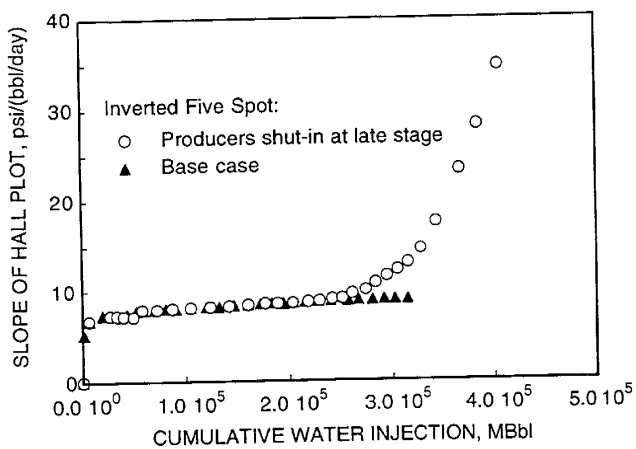


Fig. 5.39. Simulation results of Hall plots with and without shut-in of offset production wells.

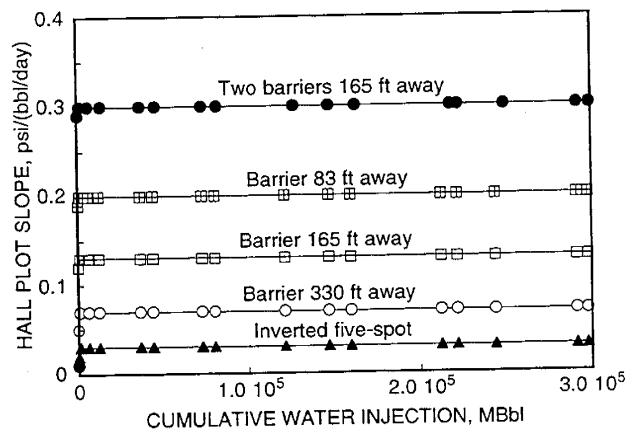


Fig. 5.41. Single-phase simulation results of Hall plots with and without nearby permeability barriers.

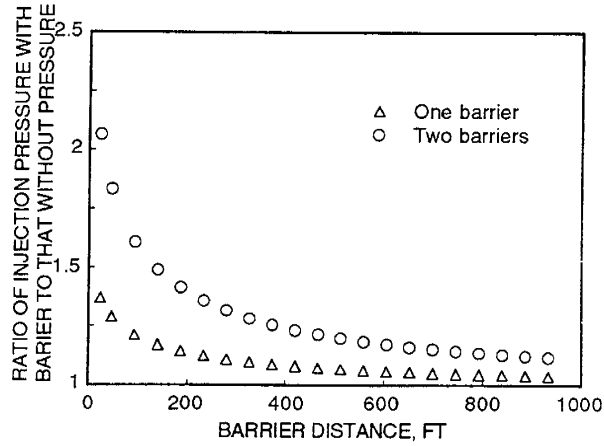


Fig. 5.42. Influence of barrier distance on injection pressure.

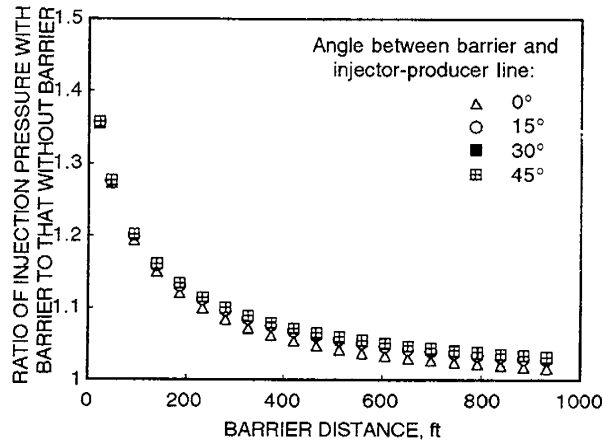


Fig. 5.43. Influence of intersection angle between barrier and injector-producer line on injection pressure.

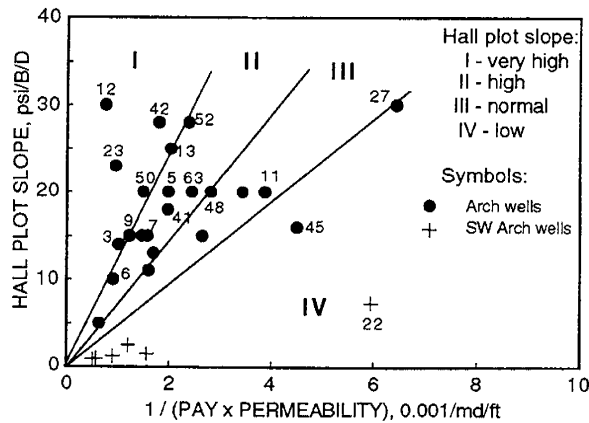


Fig. 5.44. Hall plot slope vs. reciprocal of pay thickness (h) times permeability (k). This plot normalized the hall plot slope for pay thickness and permeability so that the effects of reservoir barriers can be seen.

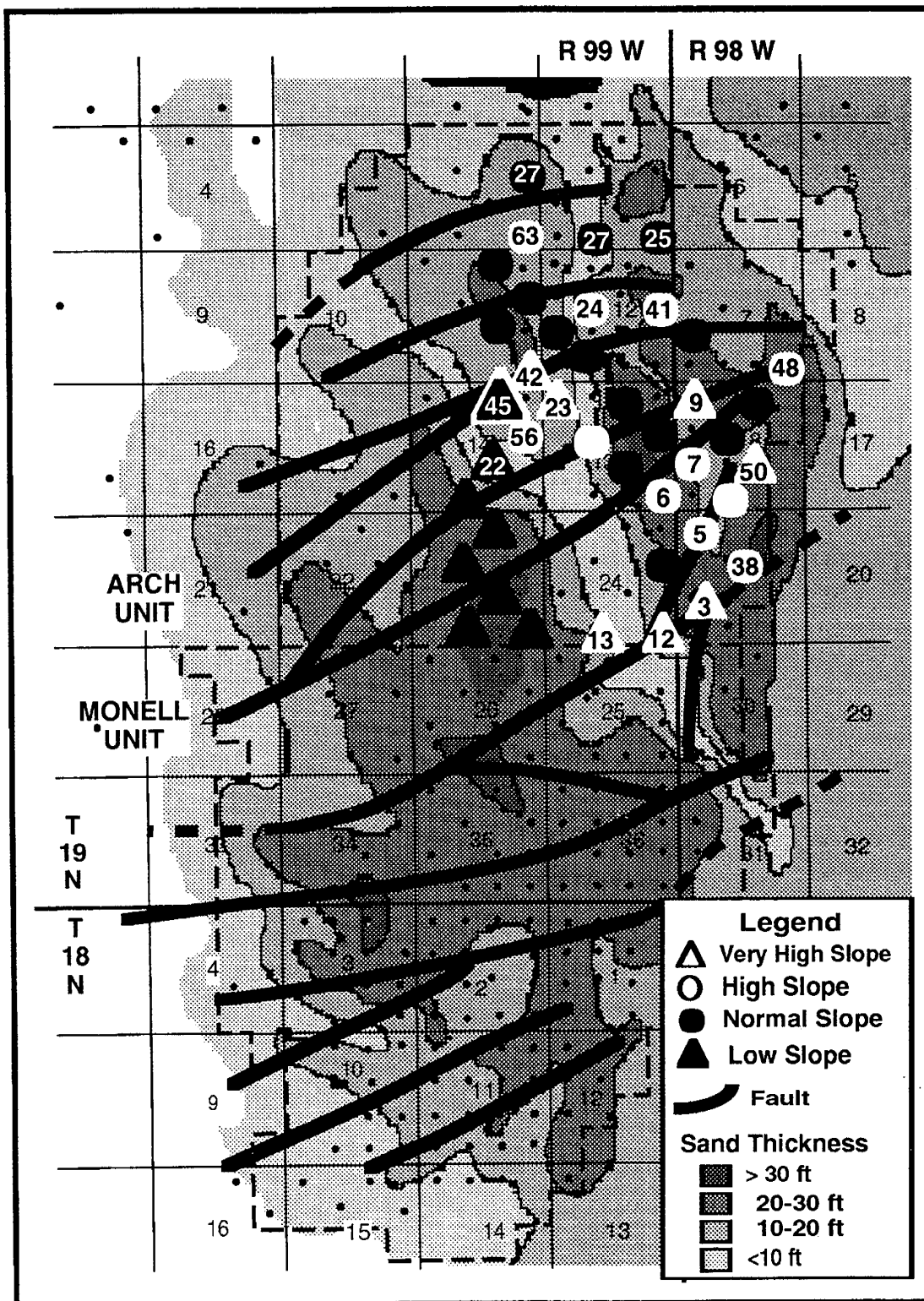


Fig. 5.45 Map showing Hall plot slope values, net pay thickness, and fault locations. In general, wells with high slope values are located either near the low-permeability, thin pay area, a mapped fault, or near the water-oil contact on the eastern edge of the field. Numbers in symbols are well numbers.

